STRUCTURAL AND SPECTROSCOPIC STUDIES OF LYSOZYME

THESIS SUBMITTED FOR THE DEGREE OF

DOCTOR OF PHILOSOPHY IN THE

UNIVERSITY OF OXFORD

MAY, 1976

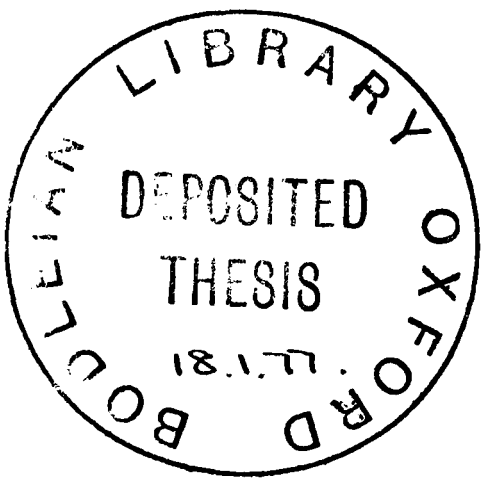

BY

MARVIN WILLIAM MAKINEN

LABORATORY OF MOLECULAR BIOPHYSICS
DEPARTMENT OF ZOOLOGY

MERTON COLLEGE
OXFORD

To Michele

ABSTRACT

The characterisation of productive enzyme-substrate complexes stabilised by sub-zero enzymologic methods in the crystalline state is considered for application of electron spin resonance (ESR) and electron nuclear double resonance (ENDOR) methods. To this end model compounds are investigated as substrate analogues of lysozyme by x-ray diffraction and magnetic resonance methods.

Aromatic-linked mixed disaccharides corresponding in chemical structure to β(aryl)-4-O-(2-deoxy-2-acetamido-D-glucopyranosyl)-D-glucopyranoside are synthesised as substrate analogues of lysozyme to serve as phosphorescent triplet state spectroscopic probes. The stereochemistry and molecular structure of β(1-naphthyl)-D-glucopyranoside-2',3',4',6'-tetra-O-acetate is determined by application of direct methods of structure determination and crystallographic least-squares refinement. The detailed molecular structure of this carbohydrate derivative is compared to that of other glucopyranosides, and the compatibility of the incorporation of the molecular structure of the naphthyl-glucopyranoside moiety only into aromatic-linked mixed disaccharide compounds for purposes of a triplet state spectroscopic probe of lysozyme action is tested by molecular model building studies.

ESR and optical detection of magnetic resonance techniques are employed to evaluate the electronic structure of the phosphorescent substrate analogue of lysozyme. Incorporation of the structural unit of the β(1-naphthyl)-D-glucopyranoside chromophore into a variety of hydrophobic and hydroxylic environments causes readily detectable alterations in the zero-field splitting parameters of the phosphorescent triplet state of the naphthyl group. The zero-field splitting parameters and transitions of the naphthyl-glucopyranoside in these environments are readily distinguishable from those of the expected hydrolysis product α-naphthol. These results indicate that the triplet state properties of phosphorescent aromatic groups are sufficiently sensitive to environmental influences and can be employed as direct spectroscopic probes of enzyme action when suitably incorporated into synthetic substrate analogues.

The spin-label inhibitor of lysozyme β(2,2,6,6-tetramethyl-4-piperidinol-1-N-oxyl)-D-(2-deoxy-2-acetamido-glucopyranoside) is also synthesised as a spectroscopic probe of the active site. ESR and x-ray diffraction studies of single crystals of tetragonal hen egg white lysozyme show that the spin-label is bound in the enzyme crystal. The principal axis corresponding to the g_{zz}-direction is identified by ESR. Application of ENDOR to this orientation results in three types of ENDOR lines arising from interaction of the nitroxide group with nearby hydrogen nuclei. This interaction is analysed in terms of an anisotropic

dipole-dipole mechanism. Interpretation of the ENDOR spectrum suggests that (i) a protein residue is within 3.7 Å of the nitroxide nucleus along the molecular z-axis of the nitroxide group and (ii) the nitroxide group is substantially exposed to the solvent channel or surface of the enzyme. The three-dimensional structure of the spin-label complex is determined by difference Fourier methods. The spin-label binds anomalously across subsites C and B of the lysozyme molecule in a configuration apparently stabilised by binding of the acetamido group in the specificity site in subsite C and by hydrophobic interactions between the methyl groups of the spin-label and Tryp-62 of the enzyme. The structural features of the complex determined by diffraction methods confirm the interpretation of the ENDOR spectrum. Furthermore, the ENDOR results indicate that specific proton sites can be detected in the active site regions of crystalline enzymes as a sensitive means to dilineate stereochemical configurations and structural binding relationships.

Since an enzymatically active form of crystalline lysozyme is prerequisite to further spectroscopic and structural study, the catalytic activity of crystalline human lysozyme is assessed. With use of a p-nitrophenyl-linked mixed disaccharide derivative, human lysozyme in orthorhombic crystals is demonstrated to be enzymatically active only when the crystals are equilibrated with a mixed cosolvent medium containing 2-methyl-pentan-2,4-diol. These solvent conditions have negligible effects on the crystal

structure and are suitable for preserving the crystal structure at cryogenic temperatures at which ESR and ENDOR techniques must be generally applied.

To evaluate conditions appropriate for assaying the enzymatic activity of crystalline enzymes, the catalytic efficiency of crystalline enzymes is analysed mathematically as a function of the diffusion of substrate into crystals and of the kinetic parameters of the enzyme reaction in solution. Relationships are derived to demonstrate that crystal dimensions control the influence of diffusion in measuring the catalytic efficiency of crystalline enzymes and that the critical dimension for onset of rate-limiting diffusion can be predicted on the basis of measurable kinetic parameters of the enzyme reaction in solution and the invariant diffusion coefficient of the substrate. The catalytic efficiency of crystalline enzymes reported hitherto in the literature is analysed on the basis of these mathematical relationships. Except for the case of papain, it is concluded that the results of all other studies are reported for conditions of rate-limiting diffusion of substrate and are consequently inconclusive in comparing the catalytic activity of the enzyme in crystalline and solution states.

In addition, the appropriate chemical conditions are determined for generation and stabilisation of oxymyoglobin in single crystals with use of ferrous D(+)-tartrate in alkaline ammonium sulphate solutions under conditions suitable for high resolution x-ray structural studies.

ACKNOWLEDGMENTS

The completion of my studies at Oxford has been possible only through collaborative studies with others. With considerable pleasure I acknowledge the assistance and collaboration of Dr. N. W. Isaacs in determining the structure of NGTA and of Dr. K. W. Snape in determining the structure of the lysozyme-spin-label complex. Dr. B. A. Coles of the Physical Chemistry Laboratory not only provided cheerful assistance in the use of his ESR spectrometer in experiments which generally required many long hours of effort each but also constructed the necessary modifications for photoexcitation studies at cryogenic temperatures as well as an ENDOR accessory. I am indebted to the kind hospitality of Dr. J. Schmidt, Dr. W. G. van Dorp, and Professor J. H. van der Waals at the Kamerlingh Onnes Laboratorium in Leiden during my visit there. Without the constant assistance of Dr. W. G. van Dorp the optical detection studies could not have been completed within the period of my brief visit. I especially thank Professors J. H. van der Waals and C. A. Hutchison Jr. for helpful discussions on the molecular spectroscopy of triplet state molecules and the theory of ESR and ENDOR of

paramagnetic systems. I thank Professor L. Genzel of the Max-Planck-Institut für Festkörperforschung for his hospitality during an invitation to visit that institute and to participate in low frequency Raman studies of crystalline proteins. Mr. P. S. Rivers assisted in use of the five-circle diffractometer for the low temperature studies of oxymyoglobin.

I thank the National Institutes of Health of the United States Public Health Service for a Special Fellowship (GM 50802) to study at the Laboratory of Molecular Biophysics and the European Molecular Biology Organization for a Short Term Fellowship to carry out magnetic resonance studies in Leiden.

I thank Professor D. C. Phillips for support and assistance during the course of my studies in Oxford and for encouragement in developing new spectroscopic methods to investigate enzyme-substrate interactions.

Miss M. J. Masuga cheerfully provided helpful assistance in typing the manuscript.

TABLE OF CONTENTS

LIST OF TABLES

LIST OF ILLUSTRATIONS

GLOSSARY OF SYMBOLS

Symbol	Definition	Page
$\underline{a}$, $\underline{b}$, $\underline{c}$, α, β, γ	Crystallographic unit cell parameters	73
$\hat{\underline{a}}$, $\hat{\underline{b}}$, $\hat{\underline{c}}$	Vectors defining the unit cell of a crystal	78
$\hat{\underline{a}}^*$, $\hat{\underline{b}}^*$, $\hat{\underline{c}}^*$	Vectors defining the unit cell of the reciprocal lattice	249
$\underline{\underline{A}}$	Electron spin-nuclear spin hyperfine interaction tensor	165
$\underline{\underline{A}}_k$	Hyperfine interaction tensor for proton k in the nearby vicinity of a nitroxide group	237
Ab	Antibody	154
$AB^{\ddagger}$	Activated complex of chemical reaction A + B	15
Asp	Aspartic acid residue incorporated into the polypeptide chain of a protein, generally followed by a number indicating its sequence position	66
BPGTA	β(p-bromophenyl)-D-glucopyranoside-2',3',4',6'-tetra-O-acetate	184
CPK	Corey-Pauling-Kortum, employed with reference to space filling atomic models	129
CuK	Source of x-ray radiation due to the L → K and M → K transitions of a Cu atom	78

d	Diameter of a spherical or cylindrical crystal	36
$\underline{d}$	Minimum interplanar spacing for set of collected x-ray diffraction data	248
D, E	Zero field splitting parameters of a triplet state molecule	164
$D_{\underline{c}}$	Calculated density of a crystal . .	77
D_i	Invariant diffusion coefficient of a substrate molecule in a crystal	32
$D_{\underline{m}}$	Measured density of a crystal . . .	77
DMF	N,N-dimethylformamide	6
DMSO	Dimethylsulfoxide	6
E	Enzyme	19
e	Catalytic efficiency of an enzyme in its crystalline state	34
E_A	Arrhenius activation energy	15
(E_t)	Total enzyme concentration	19
$\|E\|$, $\|E_{hk\ell}\|$	Normalised structure factor amplitude, subscripts $hk\ell$ indicate the Miller indices of the corresponding crystal plane	79
E_1, E_{-1}	Arrhenius activation energy corresponding to reaction with rate constant k_1, k_{-1}, ...	23
EG	Ethylene glycol	6
ENDOR	Electron nuclear double resonance	55
EP	Enzyme-product complex	19
ES	Michaelis enzyme-substrate complex	15

ES_1, ES_2	Intermediate complexes of an enzyme catalysed reaction; subscript refers to the sequential linear order of appearance of the complex in the reaction . .	22
(ES)	Concentration of ES	15
ESR	Electron spin resonance	55
$\|\underline{F}_c\|$	Calculated structure factor amplitude	88
$\|\underline{F}_o\|$	Observed structure factor amplitude	88
$\|\underline{F}_p\|$	Structure factor amplitude of the native lysozyme structure	257
$\|\underline{F}_{SL}\|$	Structure factor amplitude of the lysozyme plus β(TEMPO)-GlcNAc spin-label inhibitor complex . . .	257
$\underline{g}$	Gerade (even)	79
g	Electron g-value	163
$\underline{\underline{g}}$	Electron g-value matrix	226
g_{xx}, g_{yy}, g_{zz}	Diagonal components of the g-value matrix corresponding to the x, y, z molecular axes	227
g_e	Effective value of $\underline{\underline{g}}$	236
Glc	D-glucose	69
GlcNAc	N-acetyl-D-glucosamine	66
$(GlcNAc)_n$	Oligomer of GlcNAc of β(1→4) linkage where n indicates the number of GlcNAc units	64
GlcNAc-Glc	4-O-(2-deoxy-2-acetamido-β-D-glucopyranosyl)-D-glucopyranoside	247
(GlcNAc-MurNAc)	Oligomer of GlcNAc and N-acetylmuramic acid in alternating β(1→4) glycosidic linkage	66

MPD	2-methyl-pentan-2,4-diol	10
n_i	Direction cosine of the electronic dipole moment of a nitroxide with respect to the molecular axis system	237
NAG	GlcNAc	69
NGTA	β(1-naphthyl)-D-glucopyranoside-2',3',4',6'-tetra-O-acetate . . .	74
NGN	GlcNAc-Glc-naphthyl	139
NNNGN	Analogous mixed saccharide substrate to NGN except with three GlcNAc units linked in a β(1→4) glycosidic bond distal to the glucose moiety	139
NGP	GlcNAc-Glc-p-nitrophenyl	148
nm	Nanometer	139
NMR	Nuclear magnetic resonance	200
OD	Optical density	156
ODMR	Optical detection of magnetic resonance	184
P	Product of enzyme catalysed reaction	19
Q_{10}	Factor indicating the relative change in reaction rate produced by a change in temperature of 10°C	285
r	Radius of a spherical or cylindrical crystal	35
$\underline{r}_p$	Positional vector of a proton site from the nitrogen nucleus of a nitroxide group	235
R	Universal gas constant	14
$\underline{r}_{ij}$	Positional vector of the electron i with respect to electron j in a triplet state	162

S	Substrate	19
(S)	Substrate concentration	19
(S_0)	Concentration of substrate in solution outside of an enzyme crystal	33
$\underline{\hat{S}}$	Spin angular momentum operator	162
$\underline{S}$	State of total orbital angular momentum with $L=0$	226
$\hat{S}_i$	Operator for the i^{th} component of the spin angular momentum . .	163
$\langle S \rangle$	Average concentration of S within a crystal as a result of diffusive flow	34
$\langle \underline{S} \rangle_{\pm}$	Expectation value of S due to the point-dipole of an electronic magnetic moment	236
S_0	Ground state singlet system . . .	159
S_1	Lowest excited singlet system . .	159
$S_i(I)$	Standard deviation of the measured intensity I of reflection i	92
T	Temperature in degrees Kelvin . .	14
T_0	Lowest excited triplet state system	159
$\underline{\underline{T}}$	Zero-field splitting tensor of an excited triplet state system	162
TEMPO	2,2,6,6-tetramethyl-4-piperidinal-1-N-oxide	204
Tryp	Tryptophan residue incorporated into the polypeptide structure of a protein	275
$\underline{u}$	Ungerade (odd)	79

U_{ij}	Anisotropic thermal parameter of a nonhydrogen atom in terms of mean square amplitude of vibration in Ångstroms	98
U_{iso}	Isotropic thermal parameter of a hydrogen atom in terms of mean square amplitude of vibration . .	99
v	Velocity of enzyme catalysed reaction	19
$\underline{v}$	Volume of unit cell	77
(v/v)	Volume of a solvent dissolved per 100 ml total volume of solution, generally expressed as a percentage	143
w, w_i	Statistical weighting factor assigned to the observed structure amplitude of reflection i for purposes of crystallographic least-squares refinement	89
(w/v)	Weight in grams per 100 ml volume of solution, generally expressed as a percentage	145
x, y, z	Molecular axes chosen with reference to elements of structural symmetry	161
$\underline{x}$, $\underline{y}$, $\underline{z}$	Fractional crystallographic atomic coordinates	97
$\hat{x}$, $\hat{y}$, $\hat{z}$	Axes of an electron density map corresponding to the $\underline{\hat{a}}$, $\underline{\hat{b}}$, and $\underline{\hat{c}}$ crystal axis directions	258
X, Y, Z	Zero-field energies of a triplet state system	163
$\underline{z}$	Number of molecules per unit cell	73
ZFS	Zero field splitting	188
β_e	Bohr magneton	163
β_n	Nuclear magneton	226

$(\frac{\partial S}{\partial t})$	Time dependent change in concentration of substrate S 32
$\Delta\nu_k$	ENDOR shift of proton k 238
ΔOD	Change in optical density 154
ξ	Central reflection of a quintuplet of reflections of the accessible range of the linear diffractometer 255
γ_e	Magnetogyric ratio of the electron 102
λ_c	Critical thickness in cm or microns of a crystal for demonstrating maximum enzymatic efficiency . . . 34
λ_c'	Critical thickness in cm or microns of a crystal for demonstrating a maximum second order rate constant in the binding of a ligand 38
$\mu(CuK_\alpha)$	Calculated absorption coefficient of a crystal for CuK_α radiation . . 77
$\langle\underline{\mu}\rangle_{\pm}$	Expectation value of the electronic dipole moment 236
ν_{ENDOR}	Frequency of an ENDOR transition 237
ν_p	Free proton frequency 238
ω	One of the four rotation axes of a four-circle diffractometer corresponding an an orienter axis of the crystal 78
ϕ	One of the four rotation axes of a four-circle diffractometer corresponding to an orienter axis head taken through the base of the goniometer 249
σ	Calculated standard deviation of a bond length or angle 106
$\sigma(I_o)$	Mean standard deviation of the observed I_o intensity of a reflection 87

τ_P	Total phosphorescence emission lifetime in seconds	188
θ	Bragg angle of a crystal plane	78

Chapter I

INTRODUCTION

A. The Nature of Intermediate States of Enzyme Reactions

Enzyme reactions generally have transient, short-lived intermediate states. Consequently, molecular enzymology, as the study of the structural and stereochemical basis of enzyme catalytic function, has been developed largely on circumstantial evidence about the probable nature of intermediate states of reactions through x-ray diffraction studies of crystalline enzymes and enzyme-inhibitor complexes. Structural evidence in support of a proposed mechanism of enzyme action obtained through x-ray studies is for this reason of an indirect nature. Moreover, structural relationships of enzyme-inhibitor interactions determined through x-ray studies cannot be expected to be precisely identical to those associated with the binding of true substrates in catalytically productive modes.

Binding of a substrate to an enzyme in a catalytically productive mode is expected for a variety of enzymes to require alteration of the detailed geometry of the substrate, causing significant distortion of bond angles and bond lengths from their normal values (Blow and Steitz,

1970; Jencks, 1969; Lienhard et al., 1971). Furthermore, perturbed electronic states have been associated with substrates in certain intermediate enzyme-substrate complexes (Charney and Bernhard, 1967; Yagi, 1965; Bernhard and Lau, 1971; Stauffer and Zeffren, 1970), indicating rearrangement of the chemical bonding structure of the substrate upon binding productively in the active site region. It is consequently readily apparent that detailed spectroscopic investigation of the reacting catalytic portions of the enzyme and of the substrate in intermediate complexes of enzyme catalysed reactions is required in conjunction with high resolution x-ray diffraction studies to delineate the nature of perturbed stereochemical and electronic configurations. Investigation of such perturbed states would permit a detailed assessment of structure-function and structure-reactivity relationships and would afford a means of determining the mechanistic importance of factors responsible for bond-making and bond-breaking processes in enzyme reactions. The results of such studies would be able to provide fundamental insight into the structural chemistry of enzyme active site surfaces and, in addition, could provide valuable contributions to related areas of study of the structural chemistry of heterogeneous chemical processes.

An important step towards better understanding the catalytic basis of enzyme action was put forth in a hypothesis by Pauling (1946) in which he suggested that enzymes bind substrates more tightly in their transition-state

configurations than in their ground state configurations. He further postulated that the tighter binding of the transition-state configuration served to lower the activation energy of the reaction, explaining the kinetic enhancement observed for enzyme catalysis. Numerous studies (Wolfenden, 1969 and 1972; Lienhard et al., 1971), for which transition-state analogues of substrates have been synthesised, have demonstrated, indeed, that the binding of substrates to enzymes is consistent with this hypothesis and that the active site regions of enzymes appear to provide a surface stereochemically complementary to the transition-state configuration of its substrates. Thus, the binding of a substrate to an enzyme in a catalytically productive mode progressing to formation of its transition-state configuration and finally to products would be expected to require alteration of the detailed geometry of the substrate even prior to completion of all bond-making and bond-breaking processes. These stereochemical changes would be expected, furthermore, to force concomitantly alterations in the chemical bonding structure of the substrate. In addition, comparably strained stereochemical and electronic perturbations may obtain simultaneously in the catalytic residues or prosthetic group of the enzyme.

B. Stabilisation of Intermediate States of Enzyme Reactions under Sub-zero Temperature Conditions

It is not possible to expect to stabilise for physical characterisation the true transition-state species or activated complex of a chemical reaction. However, a more complete understanding of the molecular basis of enzyme action would be achieved by characterisation of the normally transient intermediate complexes of enzyme reactions which are detectable through kinetic studies and from which the true transition-state species must be formed. Although stabilisation of such transient enzyme-substrate complexes in catalytically productive modes has not yet been unambiguously demonstrated in the crystalline state, there is ample chemical evidence to support the notion that such complexes can be formed in the crystal state with lifetimes sufficiently long for characterisation and analysis by ordinary diffraction and spectroscopic techniques.

Investigations by Douzou and co-workers (Douzou, 1971a, 1971b, and 1973) have demonstrated for a variety of enzymes that the reaction between enzyme and substrate in solution can be slowed down according to the Arrhenius equation with stabilisation of reaction intermediates. In these investigations, a decrease in the catalytic rate constant of the enzymatic reaction is achieved by lowering the temperature of the reaction medium with use of binary or ternary organic-aqueous cosolvent mixtures of low freezing points.

A list of enzymes to which these methods have been successfully applied and the corresponding intermediate complexes stabilised at low temperatures given in Table 1 indicates the general widespread applicability of low temperature enzymologic methods to enzymes. These methods provide a means of stabilising intermediates of enzyme reactions which are normally transient at room and body temperatures and are difficult to detect by ordinary structural and spectroscopic techniques.

Stabilisation and characterisation of corresponding intermediate states of enzyme reactions in crystals clearly requires the application of comparable sub-zero temperature methods to suitable crystalline forms of enzymes. It would be expected that such studies could be carried out through one of two methods of approach: (1) crystallisation of the enzyme-substrate complex under the appropriate cosolvent and sub-zero temperature conditions, as in the case of luciferase (Douzou, personal communication), or (2) diffusion of the substrate into crystals of the enzyme, as carried out in general for difference Fourier studies, under conditions where catalysis is inhibited and the crystals have been equilibrated with an appropriate organic-aqueous cosolvent mixture. The latter method is probably the most generally applicable, allowing ready access to enzyme crystals formed through normal laboratory procedures; it requires, however, crystals of enzymes which have retained their characteristic catalytic properties in the solid state after the introduc-

TABLE 1

INTERMEDIATE STATES OF ENZYME AND PROTEIN REACTIONS STABILISED AT SUB-ZERO TEMPERATURES IN ORGANIC-AQUEOUS COSOLVENT MIXTURES

Enzyme or Protein	Complex Stabilised	Solvent	Reference
horse radish peroxidase	compounds I, II, and III	DMF-H_2O	Douzou et al., 1970
carbonmonoxy-liganded haemoglobin	fast reacting compound (Hb*) upon flash photolysis	MeOH-H_2O	Banerjee et al., 1968
cytochrome P-450	ferrocytochrome P-450	EG-H_2O	Debey et al., 1973
D-amino acid oxidase	semiquinone and "intermediate" form; benzoic acid complex	EG-H_2O	Shiga et al., 1968
α-chymotrypsin	Michaelis complex with esteratic substrates;	EG-H_2O	Kraicsovits & Douzou, 1974
	acyl-enzyme intermediate	DMSO-H_2O	Fink, 1973
trypsin	Michaelis complex with peptidase substrates	EG-H_2O	Debey, 1970
xanthine oxidase	oxycomplex with luminol	EG-H_2O	Sireix et al., 1970
lysozyme	lysozyme + chitohexose	EG-H_2O	Hui Bon Hoa et al., 1975
luciferase	luciferase + luciferin	EG-H_2O	Laval & Michelson, 1970

tion of the solvent mixture. That crystalline enzymes with catalytic activity in the solid state can be obtained is readily indicated in Table 2. This provides a list of enzymes and proteins which are catalytically active or exhibit functional reactivity in the crystalline state. In certain instances, notably in the case of papain (Sluyterman and de Graaf, 1969), and ribonuclease S (Doscher and Richards, 1963; Sluyterman and de Graaf, 1969), enzymologic studies indicate that the mechanism of action must be similar in both crystalline and solution states.

The organic-aqueous cosolvent mixtures generally employed for stabilisation of enzyme reaction intermediates at sub-zero temperatures are indicated in Table 3. These solvent mixtures are suitable for enzymologic and physical characterisation of enzyme catalysed reactions by virtue of their depressed freezing points and the absence of deteriorative structural effects on proteins through changes in solvent structure. Moreover, a variety of enzymes and proteins have been crystallised from comparable organic-aqueous cosolvent mixtures. As indicated in Table 4, numerous crystalline enzymes and proteins have been employed for high resolution x-ray diffraction studies crystallised from such solvents. Furthermore, x-ray diffraction studies of crystals of dog-fish lactic dehydrogenase equilibrated with 3 M sucrose solutions (Haas and Rossmann, 1970) and of glutaraldehyde cross-linked crystals of orthorhombic lysozyme (Haas, 1968) indicate that their respective

TABLE 2

ENZYMES WITH CATALYTIC REACTIVITY IN THE CRYSTALLINE STATE DEMONSTRATED BY ENZYMOLOGIC STUDIES

Enzyme	Crystalline Form and Solvent	Substrate	Reference
α-chymotrypsin	space group $P2_1$, 50% ammonium sulphate	acetyl-L-tyrosine hydrazide	Kallos, 1964
		β(3-indole)acryloyl histidine	Rossi and Bernhard, 1970
carboxypeptidase A_α	space group $P2_1$, glutaraldehyde cross-linked, 1 M sodium chloride	carbobenzoxyglycyl-L-phenylalanine	Quiocho and Richards, 1966
carboxypeptidase A_γ	space group $P2_1$, glutaraldehyde cross-linked, 1 M sodium chloride	carbobenzoxyglycyl-L-phenylalanine	Lipscomb, 1973; Quiocho, McMurray, and Lipscomb, 1973
cytochrome c peroxidase	space group (unknown), distilled water	hydrogen peroxide	Yonetani, et al., 1966
elastase	space group $P2_12_12_1$, 1.2 M sodium sulphate	N-benzoyl-L-alanine methyl ester	Shotton, et al., 1971
papain	space group $P2_12_12_1$, 20% sodium sulphate	acetylglycine ethyl ester	Sluyterman and de Graaf, 1969
ribonuclease S	space group C2, 40% ammonium sulphate	uridine-2',3'-phosphate	Doscher and Richards, 1963
ribonuclease A	space group $P2_1$, 75% methylpentanediol	cytidine-2',3-'phosphate	Bello and Nowoswiat, 1965
triosephosphate dehydrogenase	space group (unknown), 80% ammonium sulphate	(not stated)	Murdock, 1967

TABLE 3

REPRESENTATIVE ORGANIC-AQUEOUS COSOLVENT MIXTURES FOR LOW TEMPERATURE ENZYMOLOGIC STUDIES*

Organic Cosolvent	Concentration (v/v)	Temperature (°C) at which D = 80 esu.	Freezing Point (°C)
methanol	40%	-20	-37
methanol	70%	-75	-115
ethylene glycol	50%	-20	-44
1,2-propanediol	40%	-20	-38
glycerol	40%	-10	-29
2-methyl-pentan-2,4-diol	50%	-42	-48
N,N-dimethylformamide	70%	-60	-83
dimethylsulphoxide	50%	+10	-41
dimethylsulphoxide	80%	-30	-38

*Compiled from Travers and Douzou, 1970 and 1974.

TABLE 4

STABLE CRYSTALLINE ENZYMES AND PROTEINS IN ORGANIC-AQUEOUS COSOLVENT MIXTURES IN STRUCTURAL STUDIES

Protein or Enzyme	Cosolvent Mixture and Concentration (v/v)	Reference
chymotrypsinogen	EtOH:H_2O (10:90)	Freer et al., 1970
cytochrome c peroxidase	MPD:H_2O*	Larsson et al., 1970
deoxyhaemoglobin (human)**	MPD:H_2O (70:30)	Arnone, 1972
lactic dehydrogenase	3 M sucrose (in presence of ammonium sulphate)	Haas and Rossmann, 1970
liver alcohol dehydrogenase	EtOH:H_2O (10:90)	Zeppezauer et al., 1967
lysozyme (hen egg white) orthorhombic, high pH form	EtOH:H_2O (55:45)	Haas, 1968
papain	MeOH:H_2O (60:40)	Drenth et al., 1971
ribonuclease A	EtOH:H_2O (40:60)	Carlisle et al., 1974
	MPD:H_2O (75:25)	Bello and Nowoswiat, 1965
staphylococcal nuclease	MPD:H_2O (30:70)	Arnone et al., 1969
superoxide dismutase	MPD:H_2O (57:43)	Richardson et al., 1972

*Concentration not indicated.

**Stable for several days upon transfer from ammonium sulphate solution.

diffraction properties at the temperature of liquid nitrogen are comparable to those under more normal temperatures. Consequently their structural properties in the crystal can be expected to be similar under intermediate temperature conditions. Furthermore, a variety of crystalline proteins and enzymes can be equilibrated with cosolvent mixtures and exhibit diffraction to high resolution at sub-zero temperatures (Petsko, 1975). These observations lead to the inescapable conclusion that introduction of organic-aqueous cosolvent mixtures to crystalline enzymes and proteins can be carried out for structural and spectroscopic studies over a wide sub-zero temperature range with little or no significant alteration of protein and crystal structure.

Since numerous enzymes in crystalline form retain catalytic efficiency without apparent alteration in mechanism of action, application of low temperature enzymologic methods to crystalline enzymes would be expected to provide a means of stabilising reaction intermediates in the crystalline state. Application of low temperature solvent methods (Douzou, 1973; Hui Bon Hoa and Douzou, 1973; Travers and Douzou, 1970 and 1974) to enzymes in the crystalline state, thus, should make possible the detailed characterisation of the molecular structure, stereochemistry and electronic structure of intermediate complexes of enzyme-substrate reactions by ordinary crystallographic and spectroscopic methods. This manner of structural

investigation would then serve as an incisive step towards further elucidating the molecular basis of enzyme action.

It is precisely with the objective of characterising low-temperature stabilised intermediates of enzyme reactions in single crystals by combined x-ray diffraction and spectroscopic methods that the studies outlined in this thesis were undertaken. The following parts of this thesis will be directed, therefore, towards a description of the series of experimental findings and their implications on the feasibility of investigating detailed stereochemical and electronic perturbations of stabilised intermediate reaction complexes of enzymes and substrates. To this end, the potential application of photoexcited triplet state molecules as substrates is explored as a probe of enzyme-substrate interactions in low-temperature stabilised reaction intermediates, with particular reference to the lysozyme catalysed reaction. Also, conditions for stabilisation of crystalline oxymyoglobin suitable for x-ray diffraction studies are outlined.

Chapter II

ENZYME CATALYSED REACTIONS AND THE CATALYTIC EFFICIENCY OF CRYSTALLINE ENZYMES

A. Treatment of Enzyme Catalysed Reactions According to the Arrhenius Equation and Transition State Theory

The modification of molecules in chemical reactions takes place in a manner in which the rate and effectiveness of these transformations are influenced by the availability of the reactants. As the transformation occurs, the original concentration of the reactants must be replenished in order for the chemical process to continue. The net attainable speed of the reaction will consequently depend upon the relative competition of reactivity and of the capability for diffusive flow in the system. With respect to enzyme catalysed reactions we can inquire into the balance between reactivity and replenishment of reactants on two levels: (1) those kinetic factors which control the forward and backward rates of the series of transformations intrinsically inherent to an enzyme catalysed reaction, and (2) those factors which define the influence of availability of reactants on the chemical reactivity. In particular, we shall emphasise the integration of these factors to assess the intrinsic

reactivity and catalytic efficiency of enzymes in the crystalline state and how they may determine conditions under which intermediate states of enzyme catalysed reactions subsequently can be stabilised and characterised in crystals.

1. The General Nature of the Activated Complex

For an enzyme catalysed reaction which involves a series of intermediate states, it is instructive first to consider briefly the various types of intermediate complexes which can be stabilised in the solution state under appropriate solvent and chemical conditions. We then would expect that comparable intermediates can be stabilised for catalytically productive enzymes in the crystalline state. For enzyme reactions the individual rate constants, as for chemical reactions in general, can be conveniently interpreted (cf. Laidler and Bunting, 1973) in terms of the Arrhenius equation

$$k = Ae^{-E_A/RT}. \qquad (2.1)$$

The quantity E_A, the activation energy, is interpreted in terms of potential-energy surfaces, and A is the frequency factor, as developed through transition-state theory (Eyring, 1935; Wynne-Jones and Eyring, 1935), R and T having their usual meanings. The basic idea of transition-state theory is that the rates of reactions are governed exclusively by the situation at the activated state: Once the system has reached this state it is bound to pass into products. A

diagrammatic illustration of the corresponding energy changes in a chemical reaction is provided in Figure 1. From this diagram it becomes apparent that the individual rate constant is a measure of the height of the energy barrier which the system must surmount to pass from reactants to products.

Furthermore, we see that the activation energy can be estimated by determination of the rate constant at more than one temperature since

$$\frac{\partial \ln k}{\partial (1/T)} = - \frac{E_A}{R} . \qquad (2.2)$$

Furthermore, decreasing the temperature of the reaction mixture will ultimately reach a point of a vanishingly negligible reaction rate. Since the probability of a molecule being in a state of energy E_i (associated with a statistical weight g_i) is proportional by the Boltzmann law to $g_i e^{-E_i/kT}$, we cannot expect to "stabilise" for detection by low temperature methods a sufficiently large population of the true transition-state or activated complex $AB^{\ddagger}$ represented by the small region δ on the energy barrier curve. We consequently expect that lower temperatures favour formation of the molecular entity just prior to the transition-state complex, i.e., the ES or Michaelis complex, of the reaction coordinate diagram. With these simple considerations in mind, it is of value to consider the types of enzyme-substrate complexes which could be stabilised under appropriate low-temperature conditions. While our discussion pertains to relatively

Figure 1.--Schematic activation diagram for a reaction between A + B yielding products X + Y. The small region indicated by δ illustrates the region of the course of energy changes where the activated complex $AB^{\ddagger}$ is formed and the reaction is bound to yield the products of the reaction The suggestions of Lovrien (1969) in illustrating activation diagrams have been followed.

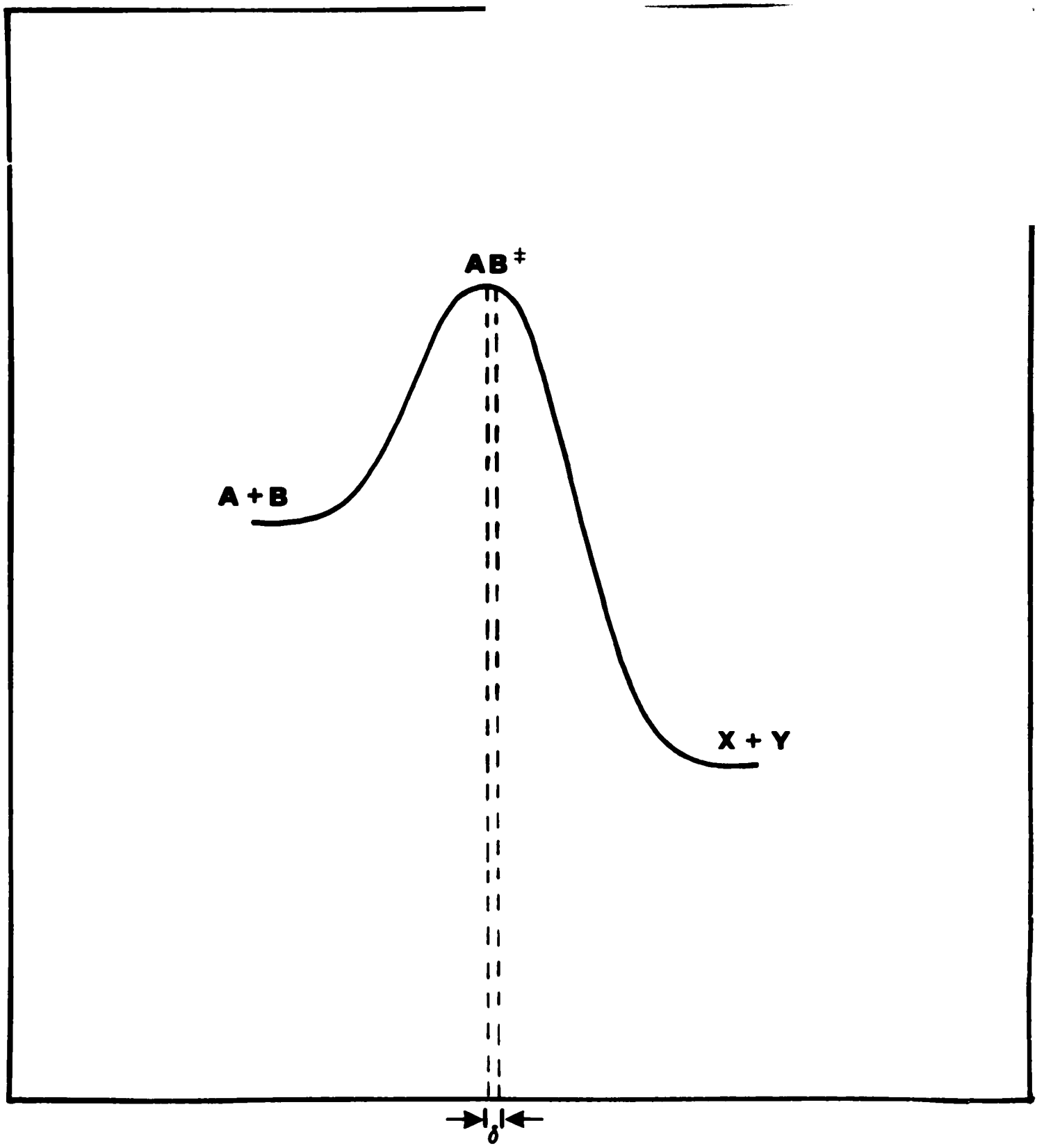
G°
AB‡
A + B
X + Y
δ
Reaction Coordinate

simple and uncomplicated reaction schemes, it serves to illustrate the nature of reaction intermediates which we might expect to be stabilised for physical characterization.

2. Intermediate States of Enzyme Reactions

For any enzyme catalysed reaction the rate law involves at least three kinetic constants. The temperature may be expected to effect these individually, and each constant will be observed to follow the Arrhenius equation, provided the constants can be separated and estimated individually by kinetic studies (Laidler and Bunting, 1973; Laidler, 1972). However, few enzyme catalysed reactions have been investigated in detail for this purpose through kinetic studies, and determination of the temperature dependence of individual kinetic constants, in general, has not always been done. We shall, therefore, limit our discussion to those cases where the temperature dependence of the composite rate constants can be expected to follow the Arrhenius equation and can provide information about the nature of reaction intermediates.

a. Enzyme Reactions with One Intermediate

As the simplest example of an enzyme catalysed reaction, a schematic illustration of the energetic changes and intermediates for an enzyme reaction which follows a true Michaelis-Menten scheme,

$$E + S \underset{k_{-1}}{\overset{k_1}{\rightleftharpoons}} ES \xrightarrow{k_2} E + P \qquad (2.3)$$

is given in Figure 2. For this reaction scheme, it can be shown that at sufficiently high substrate concentrations the rate of reaction upon attaining steady state conditions is

$$v = k_2(ES) = \frac{k_2(E_t)(S)}{K_M + (S)} \qquad (2.4)$$

where (ES), (E_t) and (S) are the concentrations of complex, total enzyme, and substrate respectively and K_M the Michaelis constant is equal to $(k_{-1} + k_2)/k_1$. On the basis of the preceding part we should expect that only the Michaelis complex ES could be stabilised by temperature lowering. Since the energy barrier for formation of the transition-state $EX^{\ddagger}$ complex is greater than that for formation of products from the EP molecular species, formation of the $EX^{\ddagger}$ molecular species is expected to proceed directly to the reaction products and stabilisation of the EP species cannot be achieved directly through reaction with substrates. However, in the case that an enzyme reaction may be associated with some measurable degree of reversibility, the EP complex could be stabilised upon temperature lowering of a reaction mixture of enzyme and product P.

There are few enzyme reactions for which the kinetic constant k_1 for a bimolecular interaction between enzyme and substrate has been determined at more than one temperature.

Figure 2.--Schematic activation diagram for a simple enzyme reaction which follows a Michaelis-Menten scheme. The free energy of activation of the enzyme-substrate complex to the transition state complex prior to release of products is Y kcal/mole and is determined by measurement of k_2. Binding of the substrate is illustrated as a separate process requiring an increase in free energy of X kcal/mole. This quantity is related to the Michaelis constant. If the same transition state were conserved for a reaction without binding of substrate, the free energy of activation would be (X + Y) kcal/mole above free substrate. The free energy of release of the product is also indicated as W kcal/mole while the ΔG° of the reaction is indicated by Z kcal/mole. The reaction pathway for an uncatalysed reaction would require a much greater free energy of activation suggesting that a different transition state obtains in the uncatalysed reaction if the reaction pathways are compared under the assumption that catalysed and uncatalysed reactions proceed from the same ground state of the substrate.

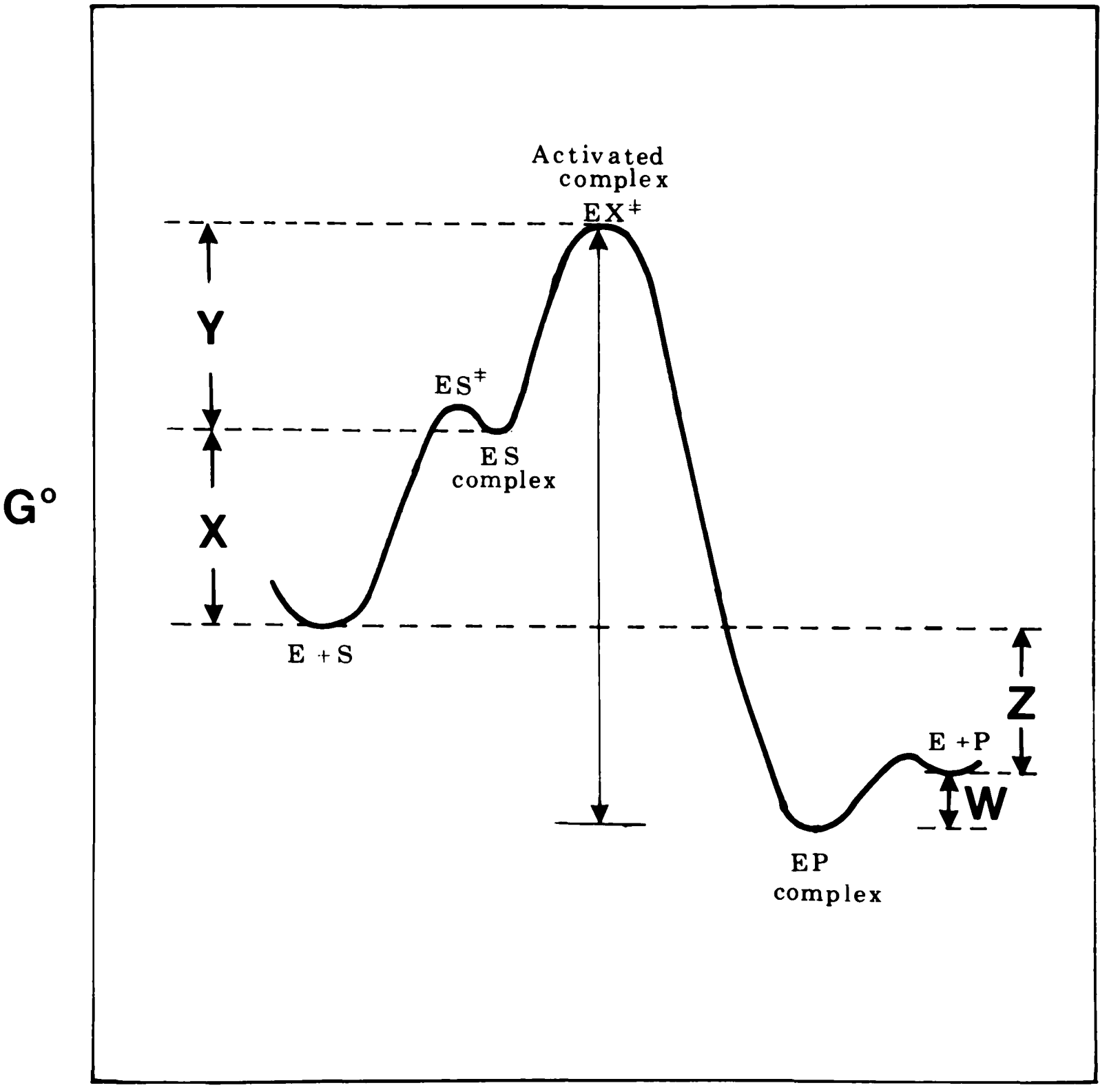
G°
Activated complex
EX‡
Y
ES‡
ES complex
X
E + S
Z
E + P
W
EP complex
Reaction Coordinate

A requirement for estimating the activation energy of the reaction is to determine the temperature dependence of k_2 under conditions for which the individual rate constants are separated as far as possible. This has been done in enzymologic investigations only infrequently. Few enzymes, furthermore, follow a true Michaelis-Menten scheme.

b. Enzyme Reactions with Two Intermediates

Enzyme reactions frequently exhibit more complicated behaviour than that described above, and for a considerable number of enzymes a large body of kinetic and physical evidence indicates that a second intermediate is formed after the initial addition complex. Such a reaction described by the reaction scheme

$$E + S \underset{k_{-1}}{\overset{k_1}{\rightleftharpoons}} ES_1 \underset{X}{\overset{k_2}{\searrow}} ES_2 \xrightarrow{k_3} E + P \qquad (2.5)$$

is associated with release of product X to form the second intermediate ES_2, as often is the case with proteolytic enzymes in formation of the acyl-enzyme complex. For such a mechanism the second-order rate constant

$$k_0 = \frac{k_1 k_2}{k_{-1} + k_2} \qquad (2.6)$$

governs the reaction rate at low substrate concentrations (Laidler and Bunting, 1973). Clearly, the Arrhenius law will not necessarily apply directly to a composite constant.

There are, however, two special cases where the composite constant will obey the Arrhenius law:

(i) When $k_2 \gg k_{-1}$. In this case $k_0 \simeq k_1$ and the rate constant for the overall reaction at low substrate concentrations is that for the formation of the enzyme-substrate addition complex. In this case the corresponding activation energy will be E_1, that for initial complex formation, as illustrated in Figure 3. Since the activation energy barrier E_1 which must be overcome to form the addition complex is greater than that for formation of ES_2, we cannot expect to stabilise the first complex ES_1 directly by low temperature techniques. It may be possible, however, again in the case of reversible catalysis, to stabilise any of the complexes as diagrammatically illustrated by reaction of enzyme with product. Stabilisation of EP will, however, depend upon the nature of the barrier to formation of ES_2 from EP, and this is implied to be small by the limiting conditions.

(ii) When $k_{-1} \gg k_2$. In this case $k_0 \simeq k_1 k_2 / k_{-1}$ and k_1/k_{-1} is simply the equilibrium constant for complex formation:

$$E + S \underset{k_{-1}}{\overset{k_1}{\rightleftharpoons}} ES.$$

The temperature dependence of the equilibrium constant would be given by

$$\frac{k_1}{k_{-1}} = \frac{A_1}{A_{-1}} \cdot \frac{e^{-E_1/RT}}{e^{-E_{-1}/RT}} = Ae^{-\Delta E/RT} \qquad (2.7)$$

Figure 3.--Schematic activation diagram for an enzyme system with more than one intermediate in which the composite rate constant follows the Arrhenius law under the condition that $k_2 \gg k_{-1}$. See text for discussion.

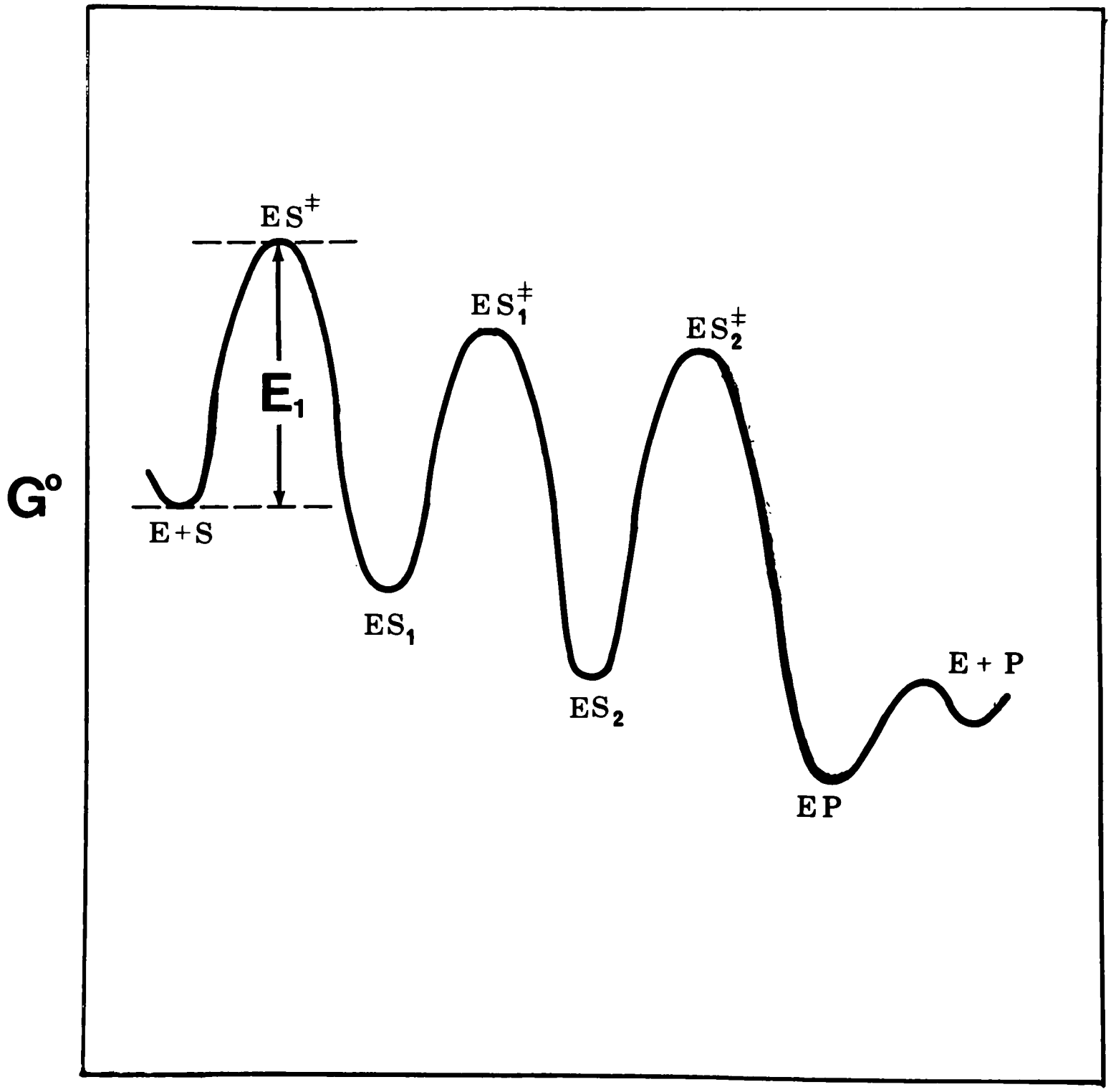
G°
$ES^{\ddagger}$
$ES_1^{\ddagger}$
$ES_2^{\ddagger}$
E_1
E+S
ES_1
ES_2
E + P
EP
Reaction Coordinate

where A_1 and A_{-1} remain essentially temperature invariant. Since k_2 should also follow an Arrhenius-like temperature dependence,

$$\frac{k_2 k_1}{k_{-1}} = \frac{A_2 A_1}{A_{-1}} e^{-(\Delta E + E_2)/RT}$$

and the Arrhenius law will apply to the composite constant. The activation energy determined by its temperature dependence will not correspond accordingly to a single step of the reaction. The energetic changes are illustrated in Figure 4. However, in this case if the temperature dependence of k_1 can be obtained by other methods, appropriate conditions could be applied to stabilise the addition complex ES_1, since the energy barrier to its formation is less than that of ES_2. Correspondingly, ES_2 could be subsequently stabilised through an appropriately determined heating-cooling cycle.

When an enzyme catalysed reaction corresponds to none of these situations, the plot of log k_0 *vs.* 1/T will not necessarily be linear. Activation energies can be obtained, however, from the slope at any one temperature, and it can be shown (Laidler and Bunting, 1973) that the overall activation energy E_A is the weighted mean of E_1 and $(E_1 + E_2 - E_{-1})$ for the extreme cases of (i) and (ii) above. It is of interest to note in this context that for a number of enzyme catalysed reactions studied by Douzou and co-workers (Douzou *et al.*, 1970; Douzou, 1973), several

Figure 4.--Schematic activation diagram for an enzyme system with more than one intermediate in which the composite rate constant follows the Arrhenius law under the condition that $k_{-1} \gg k_2$. See text for discussion.

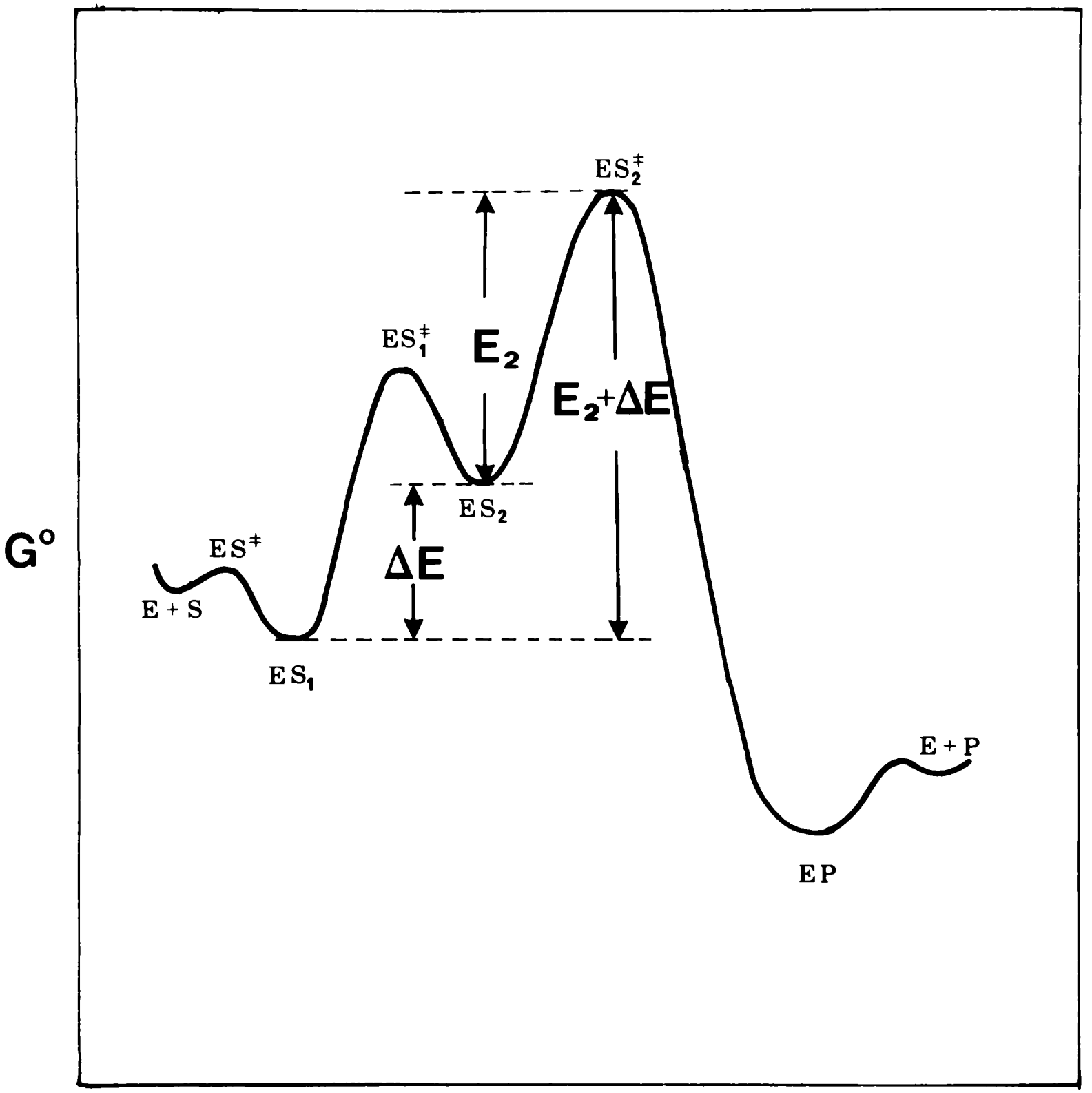
G°
$ES_2^{\ddagger}$
$ES_1^{\ddagger}$
E_2
$E_2+\Delta E$
ES_2
$ES^{\ddagger}$
ΔE
E + S
ES_1
E + P
EP
Reaction Coordinate

exhibited non-linear regions of the Arrhenius plots as low temperatures with a vanishingly small k_0 were approached. These results may indicate conditions where the composite rate constants cease to follow a strict Arrhenius law temperature dependence because the relationships required for the special cases have ceased to remain valid in the low-temperature region.

B. Functional Reactivity of Enzymes and Proteins in the Crystalline State

1. Simultaneous Chemical and Diffusion Processes

Since x-ray crystallographic studies of proteins and enzymes are based on crystalline material and most reactions are studied in solution, there has been an implicit assumption that the reactivity of the crystalline material is identical to that of the protein in solution. Nonetheless, the conformation of a crystalline enzyme can be expected to be considerably more constrained than in solution because of the lattice forces exerted through intermolecular contacts. These contacts may prevent the full expression of conformational changes required for catalysis. Consequently an important requirement of investigating intermediate states of enzyme catalysed reactions in the crystalline state is to demonstrate that not only is the enzyme catalytically active despite its lattice environment but also that the conformational states accessible to the crystal are compatible with its mechanism of action as assessed by other physical

measurements, especially in the solution state. These requirements have been demonstrated rigorously and unambiguously for few proteins and enzymes. Moreover, the efficiency of reactions catalysed by crystalline enzymes is essentially unknown since the concentration of active sites in the crystal that participate in a reaction during its measurement generally has not been directly estimated.

Table 2 in Chapter I provided a list of enzymes and proteins which are catalytically active or exhibit functional reactivity in the crystalline state. In contrast to reactions in organic solids studied by x-ray methods (Lonsdale, 1972; Gougoutas, 1971), crystalline enzymes and proteins demonstrate catalytic or functional reactivity in the same "crystalline" phase. This occurs by virtue of the remarkable characteristic of protein crystals in having large solvent channels and spaces which permit diffusion of substrates and ligands from the mother liquor to the active site region of the molecule (Crick and Kendrew, 1957; Bishop and Richards, 1968).

Diffusion is the physical process by which substrate molecules are transported from the surrounding liquid medium of an enzyme crystal to the active site region of the enzyme incorporated into the periodic crystal lattice and is the process by which replenishment of reactants occurs during their chemical transformation. The detection of enzymatic activity and eventual characterisation of intermediate reaction states can be thus regarded as a problem in diffusion

in which some of the diffusing substrate becomes immobilised as diffusion proceeds or as a problem in chemical kinetics in which the rate of reaction depends on the rate of supply of the substrate by diffusion. Both types of diffusion problems have been treated mathematically (Crank, 1956). We shall investigate here those parameters of enzyme kinetics which may be expected to effect the diffusion process and concentration of participating active sites in the crystal lattice and develop the relationships for crystals approximated as a plane sheet of material. Corresponding relationships derived for cylindrical and spherical crystals are also indicated. Other investigators (Doscher and Richards, 1963; Hoogenstraaten and Sluyterman, 1969) have previously considered the problem of diffusion related to catalytic efficiency of crystalline enzymes. In these studies, however, the interdependence of simultaneously occurring chemical and diffusion processes has not been analysed in mathematical terms. We provide here a general, simple treatment of the steady state condition for substrate binding only and substrate turnover in enzyme crystals. More complex reaction schemes can be treated in an analogous manner.

Case I. Simultaneous Diffusion and Enzyme Catalysis Occurring at Comparable Rates. In the most general and simple manner we consider a one substrate enzyme-catalysed reaction with a single intermediate as given by Equation 2.3 and assume that under steady-state conditions diffusion and enzyme reactions are carried out at comparable rates. The

steady-state condition is simply expressed as

$$\left(\frac{\partial S}{\partial t}\right)_{reaction} + \left(\frac{\partial S}{\partial t}\right)_{diffusion} = 0 \qquad (2.8)$$

where $\left(\frac{\partial S}{\partial t}\right)$ represents the time dependent change in concentration of the substrate S. In the case of simultaneous diffusion and reaction processes of comparable rates, the general diffusion equation must be modified to account for the depletion of diffusing substance by both forward and backward reactions of the simultaneously occurring chemical reaction (Crank, 1956). The equation of diffusion, when considered with respect to the chemical reaction of Equation 2.3., then has the form

$$\left(\frac{\partial S}{\partial t}\right) = D_i \frac{\partial^2 S}{\partial x^2} - \frac{\partial (ES)}{\partial t} \qquad (2.9)$$

where D_i is the invariant diffusion coefficient of substrate S inside the crystal, x is the distance from the middle of the crystal a substrate molecule is transported in time t, and (ES) is the concentration of the reaction intermediate. We know from elementary considerations of enzyme kinetics that

$$\frac{\partial (ES)}{\partial t} = k_1(E)(S) - (k_{-1} + k_2)(ES) \qquad (2.10)$$

where (E) and (S) are the concentrations of free enzyme and substrate in the crystal participating in the reaction. The rate constants are indicated for the appropriate steps of Equation 2.3 such that the Michaelis constant K_M is defined by

$$K_M = \frac{k_{-1} + k_2}{k_1} . \qquad (2.11)$$

Since

$$D_i \frac{\partial^2 S}{\partial x^2} - k_1(E)(S) - (k_{-1} + k_2)(ES) = -\left(\frac{\partial S}{dt}\right)_{reaction}$$

and the velocity of the reaction

$$v = -\frac{dS}{dt} = k_2(ES) ,$$

we see that Equation 2.9 leads to the relation

$$D_i \frac{\partial^2 S}{\partial x^2} = k_1(E)(S) - \frac{k_{-1}}{K_M}(E)(S)$$

and

$$\frac{\partial^2 S}{\partial x^2} = \frac{k_2(E)}{D_i K_M}(S) . \qquad (2.12)$$

By a different approach, Hoogenstraaten and Sluyterman (1969) have derived an expression identical to Equation 2.12. The solution of Equation 2.12 gives under the boundary conditions $S = S_0$, $x = \pm 1/2\ d$ at $t = 0$; and $S = 0$, $x = 0$ at $t = 0$

$$(S) = (S_0)\frac{\cosh(\alpha d)}{\cosh(1/2\alpha d)} \qquad (2.13)$$

where $\alpha^2 = k_2(E)/D_i K_M$. The analysis of Hoogenstraaten and Sluyterman (1969) provides from here further insight into how these relationships can be applied to the determination of catalytic efficiency of crystalline enzymes.

We can expect that the catalytic efficiency of a crystalline enzyme is a maximum when the substrate concentration and supply is not diffusion limited. Furthermore, under the assumption that the kinetic constants of enzyme reactions measured in the solution state can be applied to the enzyme in its crystalline lattice environment, the catalytic efficiency can be expected to be at least as great as that in solution whenever $(S) \tilde{=} (S_0)$. The average substrate concentration throughout the crystal $\langle S \rangle$ can be shown to be calculated as

$$\langle S \rangle = (S_0) \frac{\tanh(1/2\,\alpha d)}{(1/2\,\alpha d)} . \qquad (2.14)$$

If, accordingly, enzymatic efficiency of the crystals is defined as

$$e = \frac{\langle S \rangle}{(S_0)} , \qquad (2.15)$$

this ratio approaches 1.0 in the limit of thin crystal plates, at small values of αd, since then $\tanh(1/2\,\alpha d) \tilde{=} 1/2\,\alpha d$. Thus, the critical thickness of a platy crystal for demonstrating maximum enzymatic efficiency is

$$\lambda_c = \pm \frac{1}{\alpha} = \sqrt{\frac{D_i K_M}{k_2(E)}} . \qquad (2.16)$$

This condition is adhered to only if (E) is independent of x. This condition is observed when $(S) \ll K_M$ making $(E) = (E_t)$ where (E_t) is the total concentration of enzyme

in the crystal reaction system. If $(S) = (S_0)$ everywhere in the crystal; i.e., a steady state condition has been reached, the substitution

$$(E) = \frac{K_M(E_t)}{(S) + K_M}$$

can be made into Equation 2.16 yielding

$$\lambda_c = \pm \sqrt{\frac{[(K_M + (S_0)]D_i}{k_2(E_t)}} . \qquad (2.17)$$

This expression serves as a good approximation (Hoogenstraaten and Sluyterman, 1969) for correcting activities for crystal size up to $\lambda/\lambda_c = 40$ and $(S)/K_M = 70$. In Case III below we shall demonstrate how this expression is derived under conditions of rate-limiting diffusive flow.

Comparable expressions can be derived for a cylindrical or spherical crystal of radius r. The equations relating diffusion and catalytic activity then become

$$\frac{\partial^2 S}{\partial r^2} + \frac{1}{r}\frac{\partial S}{\partial r} - \frac{k_2(E)}{D_i K_M}(S) = 0 \qquad (2.18)$$

and

$$\frac{\partial^2 S}{\partial r^2} + \frac{2}{r}\frac{\partial S}{\partial r} - \frac{k_2(E)}{D_i K_M}(S) = 0 \qquad (2.19)$$

for the cylindrical and spherical cases respectively. These equations have more complicated solutions obtained by use of Bessel functions and are considerably more cumbersome in application than in the case of Equations 2.12 and 2.16 For instance, Equation 2.18 has the solution

$$(S) = AI_0\left\{ r\sqrt{\frac{k_2(E)}{D_i K_M}} \right\} + BK_0\left\{ r\sqrt{\frac{k_2(E)}{D_i K_M}} \right\}$$

where I_0 and K_0 are imaginary zero-order Bessel functions of the first and second kind respectively and A and B are constants to be evaluated by the boundary conditions. Inspection of the complicated expressions describing the time-dependent supply of a chemical substance into cylindrical and spherical crystals in the presence of a simultaneously occurring chemical reaction (Roughton, 1952; O'Sullivan, 1955) indicate that no easily applied solution would be extracted comparable to Equation 2.16.

We can readily dispense with this problem, however, by a simple assumption: Consider a plane sheet of crystal to be comprised of a single layer of cylindrical or spherical crystals of radius r arranged in an orderly fashion adjacent to each other with their diameter d defining the thickness of the sheet. The maximum thickness of the plane sheet will be the diameter d or rather 2r, and the solution of the steady state equation will take the form of Equation 2.12 with x substituted by r. Obviously, in this case diffusion of substrate molecules in a direction parallel to the thickness of the hypothetical plane sheet but not through the centre of a crystal; i.e., along a secant, results in transport of substrate along a distance less than the critical distance of λ_c required by Equation 2.16. The

catalytic process under these conditions clearly remains not diffusion limited, and we can expect that the solution for the case of a platy crystal of thickness 2x will be rigorously applicable to cylindrical or spherical crystals of diameter 2r.

Case II. Simultaneous Diffusion and Substrate Binding Only Occurring at Comparable Rates. In consideration of sub-zero temperature conditions where enzyme catalysis is inhibited but substrate binding, nonetheless, occurs, it is also useful to examine the interdependence of diffusion and binding processes. Although the following discussion using the notation applied earlier is then directed towards the binding of a substrate without catalysis; i.e., $k_2 \simeq 0$ in Equation 2.3, the model applies in general to the binding of any ligand by a crystalline protein or enzyme, including the binding of prosthetic groups, co-enzymes, haem ligands, as well as inhibitors of enzyme action.

Again we consider the case of simultaneous diffusion and reaction processes of comparable rates; i.e., the diffusion process is not rate limiting. Beginning with Equation 2.9 and the simple equilibrium condition

$$E + S \underset{k_{-1}}{\overset{k_1}{\rightleftharpoons}} ES \qquad K_{eq} = k_1/k_{-1}$$

we consider that the diffusion process supplies a ligand which binds to the crystalline protein molecule and that the rate of chemical reaction is measured as the disappearance

of the original form of the protein in the crystal. Thus, in analogy to Case I,

$$D_i \frac{\partial^2 S}{\partial x^2} - k_1(E)(S) + k_{-1}(ES) = k_1 (E)(S) \qquad (2.20)$$

where k_1 is the second order rate constant of the binding reaction with velocity

$$v = -\frac{dE}{dt} = k_1(E)(S).$$

The diffusion equation then becomes

$$\frac{\partial^2 S}{\partial x^2} = \frac{k_1}{D_i}(E)(S) \qquad (2.21)$$

for which the solution remains analogous to that of Equation 2.12 with

$$(\alpha')^2 = \frac{k_1(E)}{D_i}.$$

The relationships for the critical thickness of a crystal under which $(S) \simeq (S_0)$ everywhere in the crystal is given by

$$\lambda_c' = \pm\frac{1}{\alpha'} = \sqrt{\frac{D_i}{k_1(E)}}. \qquad (2.22)$$

For crystals of dimensions $\leq \lambda_c'$ one can expect that kinetic measurement of the second order rate constant characteristic of the protein in its crystal environment can be made without interference from rate limiting diffusion processes.

Case III. Rate Limiting Diffusion Process Occurring Simultaneously with a Chemical Reaction. Although the conditions under which diffusion of substrate into catalytically active enzyme crystals becomes rate-limiting are unsuitable for determining enzymatic efficiency in the crystalline state, it is instructive to examine the effects on the interdependence of reaction and diffusion processes. Rate limiting diffusion can arise not only from crystals with dimensions greater than the critical length λ_c described above, but also from the temperature dependent behaviour of diffusion of small molecules and the increased viscosity of solvents of high ionic strength or with viscous organic cosolvents at low temperatures.

The mathematical treatment (Crank, 1956) of diffusion with simultaneous chemical reactions, in which the reaction proceeds much faster than the diffusion process and local equilibrium can be assumed to exist between free and immobilized substrate, differs from that given in Cases I and II where the two processes occur at comparable rates. According to Crank (1956) and using the notation developed above for enzyme reactions as previously, beginning with Equation 2.9 where

$$K_M = \frac{(E)(S)}{(ES)} \text{ and } \frac{\partial(ES)}{\partial t} = \frac{(E)}{K_M}\frac{\partial S}{\partial t}$$

the diffusion equation acquires the form

$$\frac{\partial S}{\partial t} = \left[\frac{D_i K_S}{K_M + (E)}\right]\frac{\partial^2 S}{\partial x^2} . \qquad (2.23)$$

This derivation is carried out under the assumption that in the usual expression for the Michaelis constant of the enzyme reaction described by Equation 2.3, $k_{-1} \gg k_2$ and $K_M \simeq k_{-1}/k_1$ and that the concentration of bound substrate is linearly proportional to the free substrate concentration; i.e.,

$$(S) = K(ES) \text{ or } (S) = \frac{K_M(ES)}{(E)}.$$

Under the assumption that the chemical reaction process can be observed, however slight, and that the relationship

$$\left(\frac{\partial S}{\partial t}\right)_{\text{diffusion}} + \left(\frac{\partial S}{\partial t}\right)_{\text{reaction}} = 0$$

remains valid, Equation 2.23 then leads to the following expression

$$\frac{\partial^2 S}{\partial x^2} = \left[\frac{K_M + (E)}{D_i K_M}\right] \cdot \left[\frac{k_2(E_t)(S)}{K_M + (S)}\right] \qquad (2.24a)$$

or

$$\frac{\partial^2 S}{\partial x^2} = \frac{k_2(E)}{D_i K_M}\left[1 + \frac{(E)}{K_M}\right](S). \qquad (2.24b)$$

In analogy to Case I we have the expression

$$\frac{\partial^2 S}{\partial x^2} = \{\alpha^2 + \text{constant}\}(S) = \beta^2(S)$$

where $\alpha^2 = \frac{k_2(E)}{D_i K_M}$ as in Case I and

$$\beta^2 = \alpha^2 \left[1 + \frac{(E)}{K_M} \right] .$$

We see that as the ratio $(E)/K_M$ tends towards small values, $\beta^2 \rightarrow \alpha^2$. It is of interest to note that Hoogenstraaten and Sluyterman (1969) have pointed out that in the measurement of the catalytic efficiency of crystalline enzymes, conditions favouring low $(E)/K_M$ ratios; i.e., high substrate concentrations converting free enzyme to ES complex, and high K_M values can be utilised to increase λ_c.

Similarly it is readily shown from Equation 2.24a that

$$\frac{\partial^2 S}{\partial x^2} = \frac{k_2(E_t)(S)}{D_i[K_M + (S)]} \cdot \left[\frac{K_M + (E)}{K_M} \right] .$$

We again see that under conditions where $K_M >> (E)$ the value of $\left[\frac{K_M + (E)}{K_M} \right]$ tends towards unity and we obtain the result in Equation 2.17, namely

$$\lambda_c = \pm \sqrt{\frac{[K_M + (S_0)]D_i}{k_2(E_t)}} .$$

In this manner we observe that this mathematical treatment of the interdependence of crystalline enzyme reactivity and diffusion provides selfconsistency and indicates the general correctness of the approach.

The analogous expression in the case of ligand binding only, i.e., Case II, limited by diffusion is

$$\frac{\partial^2 S}{\partial x^2} = \frac{k_1(E)}{D_i}\left\{1 + K_M(E)\right\}(S). \qquad (2.25)$$

Again a low affinity of the enzyme for the ligand or high ligand concentrations favours a similar relationship between Equations 2.25 and 2.21 as between Equations 2.24 and 2.12. Although the solution to Equations 2.24 and 2.25 do not provide the mathematical tools of choice for evaluation of crystal kinetic data, the treatment outlined in the case of a rate-limiting diffusion process supports the validity of the general principles deduced in Cases I and II and provides some insight into the mathematical consistency of the physical processes described.

It is evident by the simple mathematical treatment provided above that accurate estimation of catalytic efficiency and reactivity of crystalline enzymes and proteins and the determination of conditions for stabilisation of reaction intermediates requires the use of crystals of no greater than the critical dimensions defined in Cases I and II. The choice of the limits of crystal dimension is dictated, however, by the accuracy of estimates of the kinetic and equilibrium constants as well as of the temperature and viscosity dependence of the diffusion coefficients of the substances used. Since such data are not generally available for most substrates employed in enzymologic studies, any detailed investigation of crystalline enzyme systems requires a major physical chemical investigation of the substrates and solvents to be used.

2. A Brief Review of Studies of the Reactivity of Crystalline Enzymes and Proteins

The preceding inquiry into the catalytic reactivity of crystalline enzymes essentially incorporates a mathematical solution analogous to the application of the Thiele modulus (Thiele, 1939; Weisz, 1973) in analysing the interaction between reactivity and diffusive flow in porous industrial catalyst particles. Application of this analytic method is consequently useful to those studies in which the chemical reactivities of crystalline enzymes and proteins have been compared to their dissolved counterparts. Table 5 provides a comparison of the reactivity of a number of enzymes and proteins in crystalline and solution states. For this comparison the diffusion constant was estimated as suggested by Sluyterman and de Graaf (1969) to account for the effect of salt components on diffusion, and the K_M and k_{cat} values for each substrate were those provided in the crystal studies or in related enzymologic investigations. Those constants were always employed whenever possible for the solvent conditions under which reactivity of the crystalline protein had been measured.

Of special importance in Table 5 is the comparison of the calculated values of λ_c or λ_c' and that extracted from the description of the experimental details of the studies reported. Only in the case of papain has the influence of interaction of chemical reactivity and diffusive flow been quantitatively estimated, and in this case it

TABLE 5

COMPARISON OF REACTIVITIES OF ENZYMES AND PROTEINS
IN CRYSTAL AND SOLUTION STATES

Enzyme or Protein	Substrate or Ligand	Relative Activity Solution : Crystal	Concentration of Enzyme in Crystal (moles/liter)	λ_c (μ)	$\lambda_{Experimental}$ (μ)	References
α-chymotrypsin	acetyl-L-tyrosine hydrazide	1:0.18	0.0311	6.6	crystals of up to 0.2-0.8 mm dimensions used, thickness not stated	Kallos, 1964
carboxypeptidase A_α	carbobenzoxyglycyl-L-phenylalanine	1:0.33	0.0450	6.0	300-15	Quiocho and Richards, 1966
carboxypeptidase A_γ	carbobenzoxyglycyl-L-phenylalanine	1:0.003	0.0450	6.0	not stated	Lipscomb, 1973
elastase	N-benzoyl-L-alanine methyl ester	1:0.46	0.0294	0.83	0.5^+	Shotton, et al., 1971
papain	acetylglycine ethyl ester	1:1.34	0.0279	8.0	1-6	Sluyterman and de Graaf, 1969

ribonuclease S	cytidine-2',3'-phosphate	active in crystal; ratio not stated	0.0596	0.39	50+	Doscher and Richards, 1963
ribonuclease A	cytidine-2',3'-phosphate	1:1-1:10	0.0056	1.3	0.02*	Bello and Nowcswiat, 1965
liver alcohol dehydrogenase	NADH	1:0.001#	0.0080	0.16	> 1	Theorell, et al., 1966
sperm whale metmyoglobin	azide anion	1:0.048#	0.0493	0.90	2-9	Chance, et al., 1966
horse methaemoglobin	azide anion	1:0.4-1:0.045#	0.0382	0.27	1	Chance and Ravilly, 1966
fast reacting deoxyhaemoglobin (horse Hb*)	CO	1:1	0.0382	0.11	< 1, (but CO already in crystal after flash photolysis)	Parknurst and Gibson, 1967

+average crystal thickness stated by authors

*estimated crystal thickness

#ratio of second order rate constants for binding process

appears that the overall rate constant for the hydrolysis of the ester substrate is similar for both crystalline and soluble enzyme. Similarly, the reactivity of crystalline ribonuclease A appears comparable to that of the dissolved enzyme. However, in this case the mean thickness of the crystals employed in the enzymologic assays was indirectly estimated and may consequently be in considerable error. For crystalline enzymes and proteins, it is obvious that for no other study have sufficiently small crystals been employed to be certain that the influence of diffusion is negligible. Furthermore, in none of these cases can the claim for diminished reactivity of the crystalline protein or enzyme be supported unambiguously. Indeed, each case should be reinvestigated with use of crystals of dimensions at least less than those estimated through Equations 2.16 and 2.22. The comparisons provided through Table 5 thus serve to underline in a most emphatic manner the need to accurately determine the critical crystal dimensions before comparison of the reactivity in solution and crystalline states can be made on a meaningful basis.

3. Determination of the Concentration of Participating Active Sites in the Chemical Reaction

A crystalline enzyme or protein that has been rendered insoluble by its incorporation into a periodic lattice structure is surrounded by a microenvironment that is defined by the solvent composition within the solvent

channels of the crystal and the intermolecular contacts which define its crystal structure. Understanding the mode of action of catalytically reactive enzymes in the crystalline state consequently requires not only establishing a correlation between enzyme activity and the flow of substrate but also investigating the effect of the solvent contents and of the conformational or configurational constraints imposed by intermolecular contacts on catalytic reactivity. Since x-ray structures are determined from crystalline molecules and most enzyme and protein reactions are generally studied in solution, there has been generally an implicit assumption that the reactivity of the crystals is identical to that of the dissolved material. Indeed, although general similarities have been well documented, the need to compare molecules in crystal and solution under as nearly the same solvent environment as possible cannot be overemphasised (Rupley, 1969). Only in this manner can the reactivities in solution and crystalline states be properly assessed and differences in reactivity analysed according to (1) reduced rates of diffusion, (2) solvent contributions, or (3) specific interactions between neighbouring molecules resulting in alterations in motility or conformation. The first has been analysed in mathematical terms and assessed in preceding parts of this chapter. The second can be properly assessed only by comparing the reactivity of the enzyme in crystalline and solution states in the same solvent medium (Rupley, 1969; Sluyterman and

de Graaf, 1969). The third requires more detailed, critical evaluation since subtle alterations in conformation or motility could lead to a change in the catalytic efficiency of the enzyme in its crystalline form or possibly to a change in the concentration of participating active sites in the chemical reaction as well as to a combination of both effects.

In order to provide some conceptual basis of how intermolecular interactions within the lattice structure could lead to a change in the number of participating active sites, it is of value to briefly inquire into the results of x-ray crystallographic studies of α-chymotrypsin. This enzyme crystallises in space group $P2_1$ with a crystallographic asymmetric unit consisting of two molecules related to each other approximately by a noncrystallographic axis of two-fold symmetry (Sigler et al., 1966). A detailed investigation with use of difference Fourier methods has indicated, however, that changes in tertiary structure in the active site region of the α-chymotrypsin molecule can be induced by alterations in pH (Mavridis et al., 1974). Although structural transitions in pH conformers appear to be associated with known pH values of different ionizable groups in the protein, one conformer in particular shows large asymmetrical changes whereby one molecule in the asymmetric unit undergoes a severe reorganization in tertiary structure in the active site region while the other remains essentially unchanged. Such changes leading to different environments

of ionizable groups are concluded to result in slightly different pK values of two independent residues (Mavridis et al., 1974). In the event that the ionizable residues were of catalytic importance, the pH dependence of the concentration of participating residues in the crystal would clearly not be identical for each molecule in the asymmetric unit, and the pH profile of the activity of the crystalline enzyme would not be necessarily parallel to that of the enzyme in solution even in the same solvent medium.

Since the asymmetrical changes in tertiary structure have been observed by x-ray methods in other proteins such as insulin (Blundell et al., 1971) in an analogous manner to those described for α-chymotrypsin (Mavridis et al., 1974), the possibility of intermolecular contacts altering reactivity and the concentration of participating active sites must be considered in investigations and comparisons of enzyme reactivity in crystalline and solution states. For instance, such asymmetrical changes resulting in a reduced reactivity or concentration of participating binding sites may have been of importance in the kinetic investigations of Theorell et al., (1966) on the binding of NADH and other ligands by horse liver alcohol dehydrogenase. The change in space group from $C222_1$ of the apoenzyme having two subunits related by a crystallographic axis of two-fold symmetry (Bränden, 1965) to a monoclinic space group for the binary complex of the enzyme with NADH (Zeppezauer et al., 1967) suggests a loss of exact symmetry of the enzyme molecule with one molecule of bound coenzyme.

For the investigation of reactivity of crystalline enzymes and proteins listed in Table 5, the concentration of participating active sites was simply considered on the combined basis of the number of molecules of protein per unit volume in the crystal and the amount of crystalline protein added to the reaction mixture or on the basis of its equivalent measured as the concentration of protein upon dissolving the crystals of an aliquot of the crystal suspension. This procedure assumes that the effective concentration of participating active sites is equal to the concentration of the protein in the crystal, for instance, as could be calculated from crystallographic data.

In view of the preceding discussion on the need to determine the concentration of participating active sites in the chemical reaction, it is of value to compare several general methods to achieve this objective. In this manner, one may consider the problem analogous to the determination of site densities of catalytic reaction centres of catalyst particles of heterogeneous chemical reactions (Maatman, 1970 and 1973).

a. Chemical Methods

Favourable conditions may make possible the estimation of the concentration of reacting sites by direct measurement.

The concentration of reacting enzyme molecules incorporated into the crystalline lattice of suspended crystals may be readily estimated by spectrophotometric means

and compared to that for the bound form. A suitable example of this would be found in studies of the ligand binding properties of crystalline haem enzymes since the extinction coefficients of the initial reactant haem derivative and of the liganded form are generally well characterised (Eaton and Hochstrasser, 1968; Makinen and Eaton, 1973 and 1976; Smith and Williams, 1970).

In a similar manner the concentration of participating active sites of a crystalline enzyme suspension can be estimated by measurement of the binding of an inhibitor under comparable conditions to those employed in the measurement of enzymatic activity. In this instance, the inhibitor must exhibit specific tight binding in the active site only. It should preferentially bind to similar residues in the active site region as the true substrate and be of comparable molecular volume in order to induce tertiary structural changes associated with substrate binding which may result in intermolecular interactions and asymmetrical conformational alterations. A suitable example of this method would be found in the study of Davis and Hess (1974) in which the binding of indole by crystalline α-chymotrypsin was followed by radioisotope methods. Comparable examples to determine the concentration of participating active sites with use of spectrophotometric methods would be the binding of proflavin by α-chymotrypsin (Brandt, Himoe and Hess, 1967) and its displacement upon formation of the Michaelis complex (Gutfreund and Sturtevant, 1956; Kraicsovits and Douzou,

1974) as well as the binding of Biebrich scarlet by lysozyme (Holler, Rupley, and Hess, 1975). In these cases the binding of the chromophoric dye by the crystalline enzyme and its subsequent displacement by substrate binding should be followed under identical solvent conditions used to evaluate catalytic activity of the crystalline state.

The most direct method of estimating through chemical means the concentration of participating active sites in the enzyme crystal is probably by use of a suitable chromophoric substrate or substrate-like substance which reacts with the enzyme by a comparable mechanism. In this respect the chromophoric properties of slowly reversible, covalent bound inhibitors employed in the active site titration of proteolytic enzymes (Kèzdy and Kaiser, 1970) may be of potential interest. Since such substances are employed to determine the concentration of active enzyme in the solubilised state in the presence of other protein or enzymic contaminants, their application in the case of crystalline serine proteases may be possible. In a comparable manner, the use of rapidly reversible, covalently bound substances such as p-nitrophenyl ester substrates of α-chymotrypsin (Kèzdy and Kaiser, 1970) may also be suitable. In this case the absorbance change observed as an initial rapidly formed burst upon addition of substrate to enzyme serves as a stoichiometric estimate of the concentration of active sites. Since such substrates as well as the reversible, covalently bound inhibitors must diffuse through

the crystal solvent channels, these chemical methods may provide the most appropriate means to determine the concentration of participating active sites in the crystal lattice under the solvent conditions employed.

b. Kinetic Methods

In analogy to the determination of site densities in industrial catalyst particles (Maatman, 1973), in principle every parameter in the rate law can be determined and often one of these parameters may contain the density of active sites as a factor. Under these conditions the assumption must be made that for the reaction

$$\text{substrate} + \text{immobilized enzyme} \rightarrow \text{products}$$

the rate-determining step is the chemical change of the bound substrate. The rate law can be expressed based on Equation 2.1 as

$$k_{cat} = \frac{kT}{h} e^{-E/RT} .$$

Since the reaction velocity is given by the relation

$$v = k_{cat}(ES)$$

the overall rate can be shown to be given by the relation

$$v = c_a \frac{kT}{h} e^{-E/RT} \qquad (2.26)$$

where c_a is the concentration of participating active sites or the site density and $\underline{k}$ and h are the Boltzmann and Planck constants. Since the activation energy E_A remains essentially temperature independent, comparison of the overall reaction rate as a function of temperature should provide an indication of a significant change in concentration of participating active sites. Evaluation of this parameter clearly acquires importance in investigation of enzyme catalysed reactions in the crystalline state at low temperatures. On this basis a change in reaction mechanism may be detected on the basis of a change in the slope of the Arrhenius plot or a temperature dependence of the diffusion constant may be detected which could contribute to the apparent reduced catalytic activity of the crystalline enzyme.

Chapter III

PRELIMINARY INVESTIGATIONS FOR THE DEVELOPMENT AND APPLICATION OF PARAMAGNETIC PROBES OF LOW TEMPERATURE STABILISED ENZYME-SUBSTRATE COMPLEXES: CRYSTALLOGRAPHIC AND CHEMICAL STUDIES

A. A Combined Spectroscopic and Crystallographic Approach to Low Temperature Stabilised Enzyme-Substrate Complexes

1. Phosphorescent Triplet State Molecules as Probes of Enzyme Action

A remarkably sensitive spectroscopic technique in assessing the perturbing influence of environment and stereochemical distortions on the electronic structure of small molecules is electron spin resonance (ESR) and electron nuclear double resonance (ENDOR) of the phosphorescent triplet state of aromatic molecules. These methods have been widely applied to determine alterations in the symmetry and distribution of spin density over the molecular nuclear framework and the nature of small stereochemical distortions of aromatic molecules induced through changes in the environment (McGlynn et al., 1969; Hutchison, 1967 and 1971). Moreover, the methods are most suitably applied to the investigation of molecules sub-

stitutionally incorporated into the lattice matrix of a host crystalline material, and generally require cryogenic temperatures for detection of the paramagnetism of the photoexcited triplet state.

Such methods applied to the investigation of enzyme-substrate interactions in single crystals would appear to offer a comparably sensitive means to determine with precise quantitation the influence of alterations in the environment of a triplet state substrate molecule placed in the active site region. As the enzyme-substrate reaction is allowed to progress through each low temperature stabilised intermediate of the enzyme reaction, as is in principle possible with heating-cooling cycles, small stereochemical distortions of the substrate, difficult to detect by x-ray methods, can be expected to be induced by the various catalytically productive modes of binding. The judicious placing of the photoexcited triplet state residue as a reporter group on the substrate molecule at or adjacent to the point of enzymatic attack would consequently provide a direct monitor of the influence of the enzymic active site region on bond-making and bond-breaking processes. The influence of stereochemical distortions on electronic structure associated with these processes could then be evaluated on the basis of the paramagnetic resonance properties of the triplet state probe. Furthermore, application of ENDOR methods measuring the nuclear magnetic resonance absorption of protons in the vicinity of the paramagnetic site could

be carried out to determine alterations in local structure of residues near the bound substrate of the triplet state probe as well as alterations in electronic structure of the molecular probe. This stereochemical information would then enhance the assessment of structural relationships derived from x-ray studies. The physical theory underlying these methods is discussed more completely in Chapter IV.

The investigation of the triplet state of phosphorescent aromatic molecules by ESR and ENDOR has generally been carried out on solutions of the triplet state molecule substitutionally doped into the host matrix of an inert crystalline substance maintained at cryogenic temperatures ($< 80°$ K). An oriented single crystal system of this type provides the most generally informative results through analysis of the anisotropic magnetic interactions with reference to the various sets of crystal, molecular, and magnetic axes. In typical organic crystals the concentration of triplet state molecules as dope sites in the host crystal lattice is generally only of the order of $10^{-3} - 10^{-2}$ M, as in the case of naphthalene in the host crystal of durene (Hutchison and Mangum, 1959). Enzyme crystals, on this basis, compare favourably since relatively large crystals can often be grown, generally containing of the order of $10^{-2} - 10^{-3}$ M concentration of active sites. Suitable equilibration of enzyme crystals with substrates to form low temperature stabilised intermediate complexes could result in a sufficiently high concentration of oriented enzyme-bound substrate

molecules for detection by ESR and ENDOR techniques, providing large crystals, generally at least as large as those required for x-ray studies, are available for use. Such methods could be especially suitable for study of enzyme-substrate interactions since enzyme crystals in cosolvent mixtures can be readily frozen at cryogenic temperatures without severe structural damage. Under these conditions the cosolvent mixture remains a solid transparent glass, permitting photoexcitation of chromophores within the crystal.

Of the spectroscopic probes developed for general investigation of enzyme and protein structure-function relationships, few have been synthesised which serve as substrates for enzymes. Even these, however, cannot be readily employed to investigate and quantitatively assess the influence of structural and environmental perturbations on the electronic structure of the substrate. On the other hand, a wide variety of substrates have been employed in enzymology which contain an aromatic group serving as a chromophoric monitor of enzyme activity. Of importance among these synthetic substrates or related derivatives with respect to their potential use as spectroscopic probes is that they are readily turned over by enzyme action and have come to serve in numerous cases as standard materials for enzyme assays despite their nonphysiologic origin. Furthermore, the aromatic group, often a p-nitrophenyl derivative, is adjacent to the point of enzymatic attack and can be

substituted by an aromatic group with well characterised triplet state properties. This aromatic group can be expected consequently to experience those electronic and structural perturbations which underlie the basis of enzyme activity. A list of enzymes with substrates of this type is given in Table 6. In particular, substrates are listed for some of the enzymes which are known to exhibit catalytic activity in the crystalline state and for which intermediate complexes have been stabilised in organic-aqueous cosolvent mixtures.

For the application of such substrates as triplet state probes, it is essential that a probe be employed for which the triplet state energy level above the ground state level is less than that of tryptophan residues in order to prevent depletion of excited state species by transfer of energy into protein residues. In this respect it is evident from Table 6 that a number of such synthetic substrates, e.g., naphthalene derivatives (cf. McGlynn et al., 1969), already possess an aromatic residue released by the enzyme which could serve as a suitable triplet state probe for investigation of enzyme-substrate interactions. Furthermore, while the nitrophenyl derivatives would serve as poor triplet state molecular probe systems primarily because of their low phosphorescence intensity and short phosphorescent lifetime (McGlynn et al., 1969), substitution of this aromatic group could often be made with a naphthalene, azanaphthalene or pyrazine derivative which would be more suitable for

TABLE 6

COMPARISON OF ENZYME CATALYSED REACTIONS WITH SUBSTRATES CONTAINING AROMATIC RESIDUES AT THE SITE OF ENZYMATIC ATTACK

Enzyme	Substrate	Reaction Catalyzed	Reference
alcohol dehydrogenase	benzaldehyde* β-naphthaldehyde*	reduction to alcohol	Jacobs et al., 1974
alkaline phosphatase	p-nitrophenylphosphate β-naphthylphosphate*	phosphate ester hydrolysis	Garen and Levinthal, 1960 Levine et al., 1969
aromatic hydroxylase	acetanilide	hydroxylation of aromatic group	Hayaishi, 1963
arylsulfatase	p-nitrophenylsulfate	sulfate transfer	Robbins, 1962
carbonic anhydrase	p-nitrophenylesters	ester hydrolysis	Pocker and Storm, 1968
chymotrypsin (and other serine proteases)	p-nitrophenylacetate p-nitrophenyl-N-methyl-tryptophan β(3-indole)acryloylimidazole*	ester and peptide hydrolysis	Bender, 1962 Rossi and Bernhard, 1971
cytochrome P-450	benzpyrene*	hydroxylation of aryl hydrocarbon	Nebert and Kon, 1973

glyceraldehyde-3-phosphate dehydrogenase	benzaldehyde* p-methoxybenzaldehyde β-(2-furoyl)acryloyl-phosphate	oxidation and oxidative phosphorylation	Fife, et al. 1971 Malhotra and Bernhard, 1968
β-glucosidase	β(p-nitrophenyl)-D-glucose β(1-naphthyl)-D-glucose*	glycoside hydrolysis	Fink and Good, 1974 Seligman et al., 1949
3-hydroxyanthranilate oxygenase	3-hydroxyanthranilate*	oxygenase	Hayaishi, 1963
p-hydroxybenzoate hydroxylase	p-hydroxybenzoic acid	hydroxylation of p-hydroxy-benzoic acid	Howell and Massey, 1971
naphthalene hydroxylase	naphthalene*	hydroxylation of aromatic ring	Booth and Boyland, 1958
peroxidase	salicylic acid*	hydroxylation of aromatic ring	Hayaishi, 1963
phenylalanine hydroxylase	phenylalanine	oxidation of aromatic ring	Kaufman, 1963
tryptophan oxygenase	L-tryptophan*	oxidation of indole ring	Hayaishi et al., 1957

*Substrates with long-lived phosphorescent triplet states.

spectroscopic purposes and may allow retention of substrate turnover. Application of such spectroscopic molecular probe systems could consequently be made to a wide variety of enzyme systems which would serve as direct monitors of bond-making and bond-breaking processes in the active site region. In addition, the application of these ESR and ENDOR methods to naturally occurring phosphorescent prosthetic groups in enzymes such as flavins (Lhoste et al., 1966) and pyridoxal-phosphate groups (Wampler and Churchich, 1969), aromatic triplet state probes of membrane structure (Naqvi et al., 1974), and triplet state probes of nucleic acid structure (Lalitha and Haug, 1972) illustrates the general potential usefulness of photoexcited triplet state systems in the investigation of the structural and electronic basis of macromolecular function.

2. Triplet State Probes for Study of Lysozyme-Substrate Interactions

Development and application of triplet state probes of enzyme-substrate interactions require in initial studies a suitable crystalline enzyme with numerous favourable characteristics: (i) it must exhibit catalytic activity in the crystalline state, especially upon introduction of the aromatic triplet-state substrate; (ii) its native structure must be characterised to high resolution by x-ray methods; (iii) its crystal lattice must remain stable in a suitable organic-aqueous cosolvent mixture and (iv) its enzymatic properties in solution should be well characterised,

preferentially under conditions in which cosolvent mixtures have been employed. Satisfying these conditions would appear to be necessary in initial studies for successfully demonstrating that such triplet state molecules are useful probes of enzyme function.

Although this objective has not been achieved with complete satisfaction in this thesis, reasonable progress towards this goal has been made. For these initial studies a series of substrates were synthesized as potential triplet state probes of lysozyme action and employed in structural and spectroscopic investigations. The reasons for selection of lysozyme as a model enzyme system were several-fold. The mechanism of action of lysozyme in solution has been investigated in detail through chemical studies (Johnson et al., 1968; Imoto et al., 1972). Recent investigations in this laboratory (Banyard, 1973) on the high resolution structure of human lysozyme indicate that the active site cleft is not sterically blocked by intermolecular contacts as in the case of tetragonal hen egg-white (HEW) lysozyme (Blake et al., 1967). The HEW and human enzymes have similar mechanisms of action (Dahlquist et al., 1969). Consequently, crystalline human lysozyme would appear as a suitable system for the development and application of triplet state probes. Of particular importance in this respect is that mixed disaccharide substrate analogues with hydrolysable aromatic residues have been employed to investigate structure requirements of the substrate for catalysis (Rand-Meir et al., 1969).

Furthermore, molecular orbital calculations of the catalytic effect of lysozyme (Loew and Thomas, 1972) suggest that a redistribution of electron density around the glycosidic oxygen should occur upon positioning the hemiacetal group of the substrate into the vicinity of the general acid catalyst group of Glu-35 as required for hydrolysis, a condition resulting in an alteration of the electronic structure of the aglycone residue. In addition, low temperature enzymologic studies indicate that an enzyme-substrate complex can be stabilised in cooled cosolvent mixtures (Hui Bon Hoa *et al.*, 1975).

The active site of lysozyme can accommodate six units of an oligomeric substrate, of which the $\beta(1\rightarrow4)$-linked hexasaccharide of N-acetylglucosamine $(GlcNAc)_6$ is probably the best known. The mechanism of action proposed for lysozyme (reviewed by Imoto *et al.*, 1972) which has been deduced from crystallographic and solution studies is schematically illustrated in Figure 5. This mechanism accounts for the catalytic rate enhancement of substrate hydrolysis primarily as resulting from (1) distortion (Phillips, 1967; Ford *et al.*, 1974) associated with binding of the saccharide ring that contains the glycosidic oxygen, (2) the general acid catalyst properties of Glu-35, and (3) the resultant stabilisation of a carbonium ion. However, a major complication in the study of the mechanism of lysozyme action through solution studies has been that most substrates form a variety of nonproductive complexes, undergo hydrolytic cleavage of oligomeric sub-

Figure 5.--Schematic illustration of the lysozyme active site cleft with bound substrate and mechanism of action. In the upper portion of the figure (Part A) an oligomeric molecule of (GlcNAc-MurNAc) linkage is schematically illustrated in the active site cleft across subsites A-F. The positions of the catalytic carboxylic acid side chains are shown in subsite D with the distorted carbohydrate ring just proximal to the glycosidic C-O bond that is hydrolysed. The lower portion of the figure (Part B) illustrates the probable bond rearrangement steps involved in the mechanism of lysozyme action producing an enzyme bound carbohydrate ring in subsite D with a stabilised carbonium ion at the C1 position. Distortion of the carbohydrate ring is not illustrated in the lower portion of the figure. (Part A from Laidler and Bunting, 1973; Part B from Imoto et al., 1972).

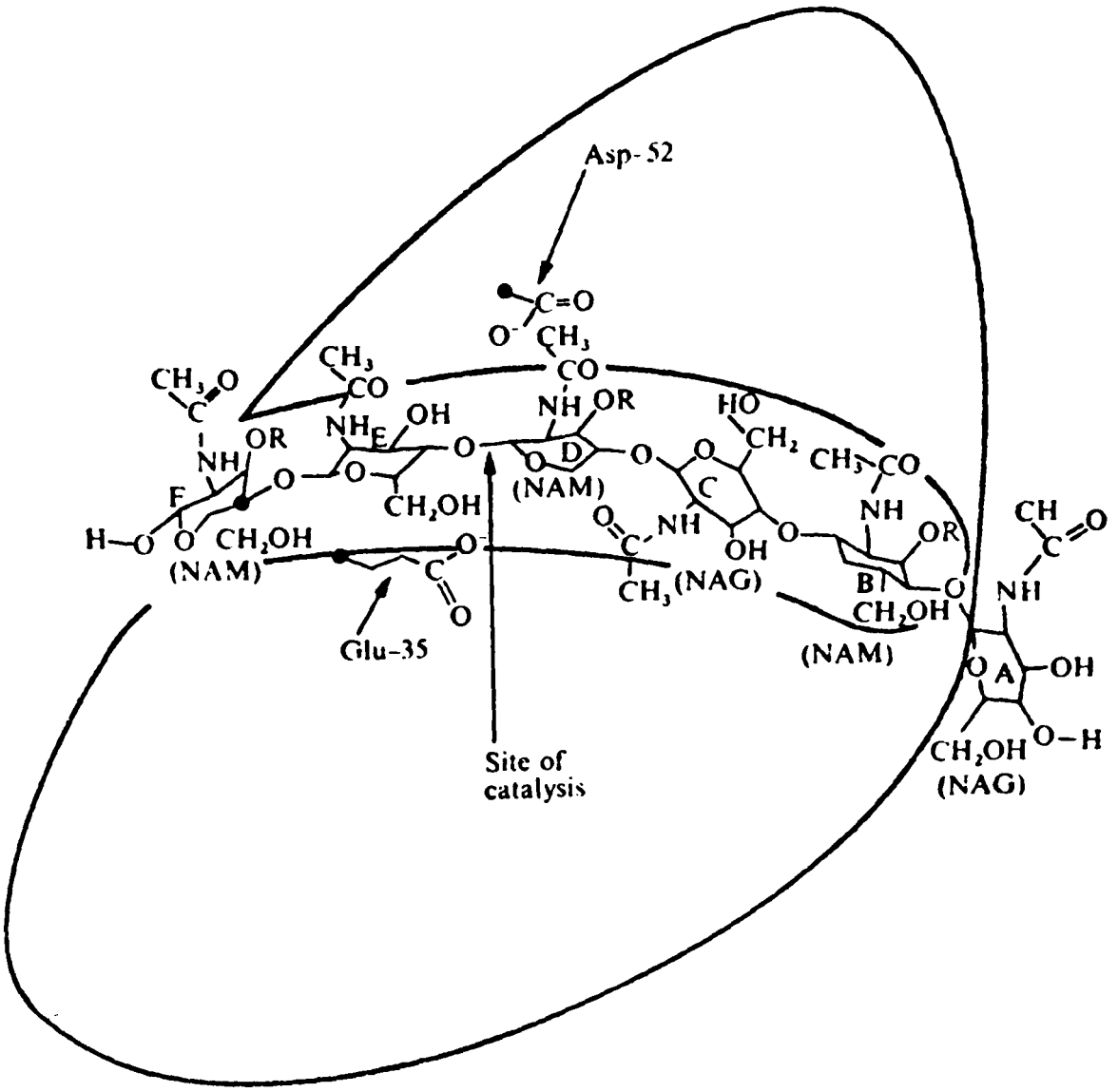
Asp-52
Glu-35
Site of catalysis
(NAM)
(NAG)
(NAM)
(NAG)

A

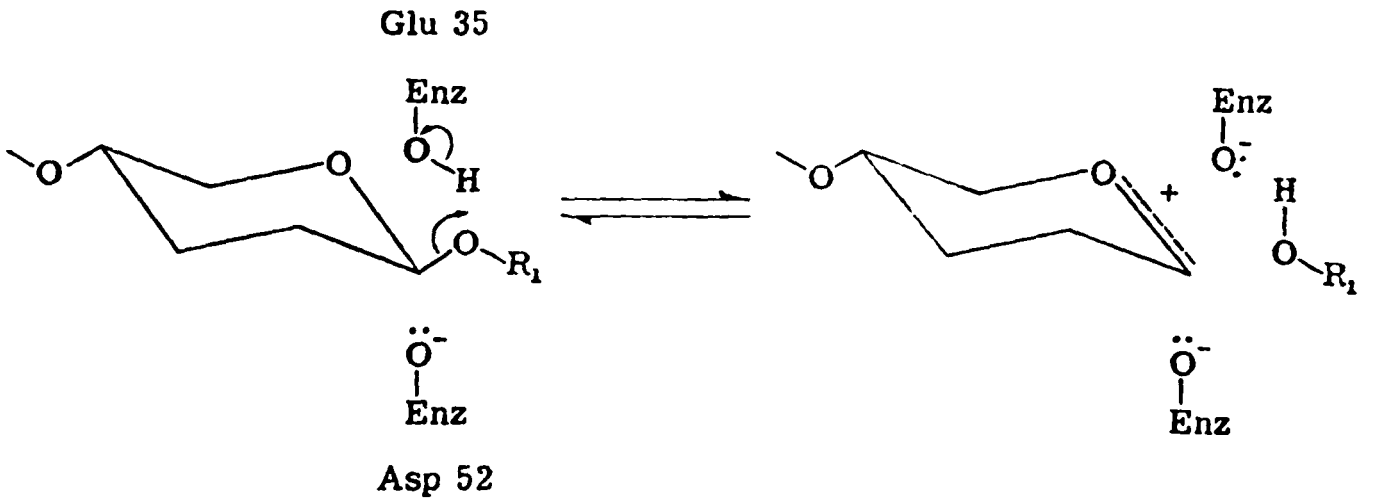
Glu 35
Enz
Enz
Enz
Asp 52

B

strates according to more than one pattern, or undergo transglycosylation reactions (Sharon and Seifter, 1964; Raftery and Rand-Meir, 1968) preventing ready identification of a unique productive enzyme-substrate complex.

However, a series of aryl-linked disaccharide substrates have been synthesised by Raftery and co-workers (Dahlquist et al., 1969; Rand-Meir et al., 1969) which contain an aryl-glucoside moiety covalently linked to one or more units of GlcNAc through a $\beta(1 \rightarrow 4)$ glycosidic bond. The chemical structure of these substrates is illustrated in Figure 6. These substrates are bound by the enzyme with exclusive cleavage of the aryl-glucosidic bond and resultant formation of a carbonium ion intermediate. No evidence of transglycosylation at the C1 position of the glucose ring has been observed (Dahlquist et al., 1969).

In order to develop the use of a triplet state probe of lysozyme action, synthetic substrates were made patterned after those employed by Raftery and co-workers. In this chapter their structures are described, and the chemical methods employed to determine the catalytic properties of crystalline human lysozyme are outlined. Also, conditions under which the enzyme crystals remain stable for low temperature studies are briefly discussed. In Chapter IV the spectroscopic investigations are outlined on the use of triplet state aromatic-linked disaccharide substrates with crystalline lysozyme.

Figure 6.--Schematic illustration of the comparison of binding modes of oligosaccharides and glycosides to lysozyme. The enzyme is regarded as having six binding subsites, each accommodating a 2-acetamido-pyranose ring in the active site cleft. Subsites A, B, and C form tight complexes with GlcNAc units while the other rings do not. The relative positions of GlcNAc units in the subsites A-F is illustrated in the lower part of the diagram. The oligosaccharide NAG-NAG-NAG represents chitotriose $(GlcNAc)_3$ and the glycoside NAG-GLUC-R represents the aryl-linked mixed disaccharide substrate GlcNAc-Glc-phenyl or β(phenyl)-4-O-(2-acetamido-2-deoxy-β-D-glucopyranosyl)-D-glucopyranoside. The structure of this mixed disaccharide substrate and cleavage point during enzyme catalysed hydrolysis is illustrated in the upper part of the figure. [Based on Figure 1 of Rand-Meir *et al*. (1969).]

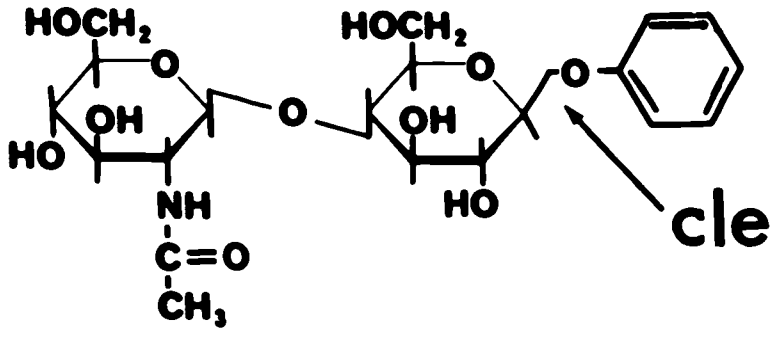

A	B	C	D	E	F

NAG-NAG-NAG

NAG-NAG

NAG-$CH_3(\beta)$

NAG-GLUC—R

B. The Structure of Mixed Saccharide Substrates with a β-linked Aromatic Group

1. Synthesis and Crystallography of β(Aryl)-D-glucopyranosides

To provide fundamental stereochemical information about the aryl-glucosidic moiety as well as to provide a suitable host matrix system to investigate the triplet state properties of the aromatic chromophore, a series of related aryl-linked glucopyranosides were synthesised and characterised crystallographically. The phenyl, p-methoxyphenyl, p-bromophenyl, 1-naphthyl, and 2-naphthyl derivatives of β(aryl)-D-glucopyranoside-2',3',4',6'-tetra-O-acetate were synthesised according to the method of Bretschneider and Beran (1949) with use of BF_3 as a catalyst. The parent phenolic compounds were of analytical reagent grade (BDH Chemicals, Ltd.), and β-pentaacetyl-D-glucose was obtained from Sigma Chemical Co., Ltd. The reaction products were recrystallised several times from 95% ethanol. Chemical composition was established by elemental analysis, mass spectrometry*, melting point determination, or gas-liquid chromatography* for the 1-naphthyl, phenyl, and p-bromophenyl derivatives. The pertinent data are compared in Table 7. The synthesis of other derivatives for which chemical analyses were not performed was assumed to proceed in an analogous manner.

---

*Kindly performed by Dr. J. D. Priddle of the Laboratory of Molecular Biophysics.

TABLE 7

COMPARISON OF CHEMICAL ANALYSES OF TETRAACETYLATED β-(ARYL)-D-GLUCOPYRANOSIDES

Aryl Group in β-glycosidic Linkage	Formula	Mol. Wt.	Elemental Analysis % Composition	Theor.	Exptl.	Melting Point (Uncorrected) (°C)
phenyl	$C_{20}H_{24}O_{10}$	424.41	C	56.60	56.67	125
			H	5.70	5.85	
p-bromophenyl	$C_{20}H_{23}O_{10}Br$	503.31	Mass spectrometric analysis* indicated presence of a tetra-acetylated glucose derivative only			128
p-methoxyphenyl	$C_{21}H_{26}O_{11}$	454.42	(None performed)			112
1-naphthyl	$C_{24}H_{28}O_{10}$	476.49	C	60.50	60.36	175
			H	5.92	5.85	
2-naphthyl	$C_{24}H_{28}O_{10}$	476.49	(None performed)			132

*Kindly performed by Dr. J. D. Priddle of the Laboratory of Molecular Biophysics.

Single crystals of all of the purified derivatives were prepared by slow evaporation of a saturated solution of each glucopyranoside derivative in DMSO. Description of the crystals is given in Table 8. Suitable single crystals were mounted on a glass fibre with Eastman E109 Adhesive for crystallographic studies for use with diffractometer or photographic methods.

Since the triplet state of the naphthyl group lies lower than that of protein residues (McGlynn *et al.*, 1969), it is evident that the naphthyl group would be the most generally suitable type of derivative for use as a triplet state probe. Therefore, the other glycoside derivatives were synthesised in efforts to find a convenient host matrix for carrying out magnetic resonance studies of the 1-naphthyl derivative. Well formed single crystals of only the *p*-bromophenyl derivative as host matrix could be obtained upon co-crystallisation with less than 0.01 mole fraction of the 1-naphthyl, 2-naphthyl, and phenyl analogues. Weissenberg photographs indicated no change in unit cell parameters of crystals of the *p*-bromophenyl glucopyranoside derivative as the host matrix for other glycosides.

TABLE 8

COMPARISON OF CRYSTALLOGRAPHIC DATA OF TETRAACETYLATED β(ARYL)-D-GLUCOPYRANOSIDES CRYSTALLISED FROM DMSO

Aryl Group in β-glycosidic Linkage	Crystal Description	Unit Cell Parameters by Weissenberg Methods
phenyl	long, prismatic crystals, orthorhombic by microscopic examination	—
p-bromophenyl	short, prismatic crystals, space group $P2_1$	a = 14.57 Å, b = 13.94 Å, c = 5.73 Å, β = 91.3°; z = 2.0 ± 0.08 by method of Kempster and Lipson (1972)
p-methoxyphenyl	platy, diamond shaped crystals, monoclinic by microscopic examination	—
1-naphthyl	short, prismatic crystals, space group $P2_12_12_1$	a = 16.50 Å, b = 21.8 Å, c = 6.85 Å; z = 4.0 ± 0.3 by method of Kempster and Lipson (1972)
2-naphthyl	short, prismatic crystals, orthorhombic by microscopic examination	—

2. The Crystal and Molecular Structure of β(1-naphthyl)-D-glucopyranoside-2',3',4',6'-tetra-O-acetate

a. Experimental Procedures

(1) Crystal Data and Data Collection

A schematic drawing of the structure of β(1-naphthyl)-D-glucopyranoside-2',3',4',6'-tetra-O-acetate (hereafter referred to as NGTA) and the labeling scheme of the constituent atoms are shown in Figure 7. Determination of the space group and initial approximation of the unit cell parameters were carried out by Weissenberg and oscillation film techniques. The space group of $P2_12_12_1$ was determined by characteristic systematic extinctions. The most precise unit cell parameters were obtained from a least-squares refinement of the diffractometer measured setting angles of fourteen general reflections. The unit cell volume suggested 4.0 ± 0.3 formula units according to the empirical correlation of Kempster and Lipson (1972). The calculated density (Stout and Jensen, 1968) for four formula units per unit cell is 1.28 g/cm^3. The approximate density of the crystal was observed to lie in the range of 1.23 - 1.33 g/cm^3 with use of ammonium sulphate solutions of known density prepared by Mrs. S. Cutfield. A summary of pertinent crystal data is given in Table 9.

A crystal measuring 0.5 x 0.15 x 0.1 mm was mounted for diffraction studies on a glass fibre with the rotation axis parallel to the long axis of the crystal and, thus,

Figure 7.--Schematic drawing of the structure of β(1-naphthyl)-D-glucopyranoside-2',3',4',6'-tetra-O-acetate. The labeling of the atomic positions employed in the text is indicated.

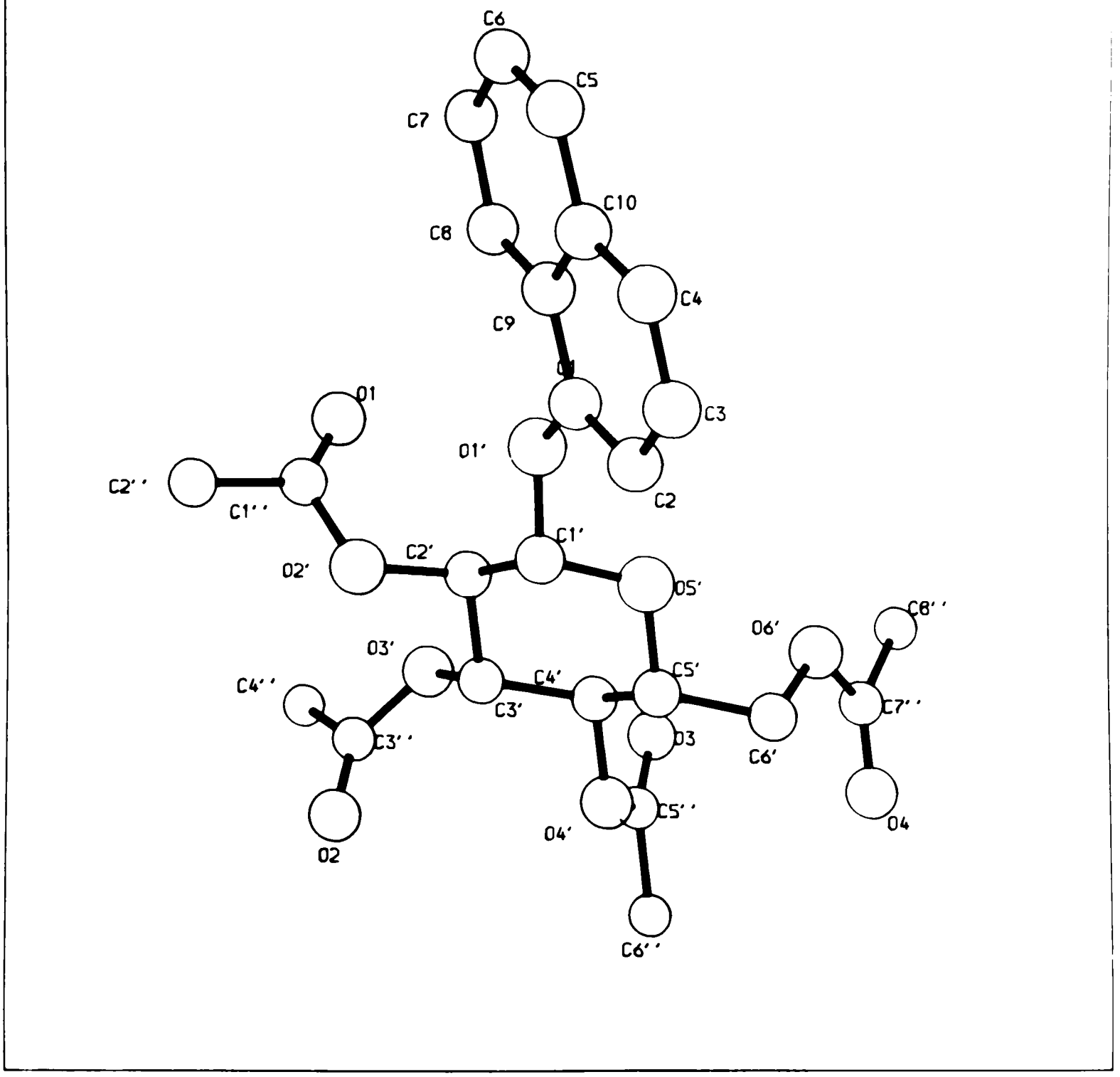
C6
C5
C7
C10
C8
C4
C9
C3
O1
O1'
C2''
C2
C1''
C1'
C2'
O2'
O5'
C8''
O6'
O3'
C4'
C5'
C4''
C3'
C7''
O3
C3''
C6'
C5''
O4'
O4
O2
C6''

TABLE 9

FUNDAMENTAL CRYSTAL PROPERTIES OF NGTA CRYSTALLISED FROM DMSO

β(1-naphthyl)-D-glucopyranoside-2',3',4',6'-tetra-O-acetate, $C_{24}H_{28}O_{10}$, M. W. 476.49, orthorhombic, space group $P2_12_12_1$ from systematic absences for $(h00)$, $(0k0)$, (00ℓ) when h, k, or $\ell = 2n+1$.

Parameter	Observed Value*
a	16.423(2) Å
b	21.832(3) Å
c	6.876(2) Å
v	2465.4 Å^3
z	4
D_m	1.23 - 1.33 g/cm^3
D_c	1.28 g/cm^3
F_{000}	1008
μ(CuKα)	8.535 cm^{-1}

*The numbers in parentheses are the standard deviations referred to the last decimal position.

parallel to the $\hat{c}$ axis. X-ray intensity data were collected on a PDP-8 computer controlled Hilger and Watts four-circle diffractometer with nickel filtered CuK radiation and a scintillation counter. The ω-2θ step-scan technique was used. The scan range of 0.80° in θ was sampled in 40 equal steps with a counting time of 1.0 sec per step. An ordinate analysis method was used to determine integrated peak and background intensities. The same number of equivalent reflections were measured in two different octants of the reciprocal lattice. Of the 7743 reflections measured with $\theta \leq 72°$, 2891 were unique. Of these, 2018 reflections with $I_o \geq 3\sigma(I_o)$ were used in subsequent calculations [$\sigma(I_o)$ being the standard deviation determined by counting statistics]. The agreement between measurements of equivalent reflections was 5.1% (based on I). Three monitor reflections of moderate intensity measured ca. every four hours showed no signs of radiation damage over the period of data collection. Data were corrected for Lorentz and polarisation effects. The empirical absorption correction of North, Phillips and Mathews (1968) was applied. The highest correction factor was 1.037.

(2) Determination of the Structure

(a) Solution of the Structure by Direct Methods

The structure was solved by application of direct methods using a multi-solution tangent formula technique following the procedure described by Kennard et al. (1971).

Normalised structure factors were calculated after the structure amplitudes had been corrected for thermal motion using an overall temperature factor derived from a Wilson plot (Wilson, 1942), and the data were scaled so that $\langle|E|^2\rangle = 1.00$. The $|E|$ statistics obtained are compared with theoretical values in Table 10.

Σ_2 interaction pairs were calculated for 137 reflections with $|E| \geq 1.8$ to select a suitable set of origin and enantiomorph defining phases. A starting set of phases were chosen of the type $g0u$, $0ug$, $uu0$ and $0gu$ to define the origin and enantiomorph. The fourth is linearly dependent on the previous three and defines the enantiomorph (Hauptman and Karle, 1956). One additional reflection was added to the starting set of phases on the basis of Σ_1 relationships. In space group $P2_12_12_1$ the Σ_1 relationships are of the form

$$sE_{2h2k0} \sim s\Sigma_{\ell}(-1)^{\ell+h}(|E_{hk\ell}|^2 - 1)$$

$$sE_{2h02\ell} \sim s\Sigma(-1)^{k+\ell}(|E_{hk\ell}|^2 - 1)$$

$$sE_{02k2\ell} \sim s\Sigma(-1)^{h+k}(|E_{hk\ell}|^2 - 1)$$

where s means sign of (Karle and Karle, 1964). The probability $P_+(E_{2h})$ that the 066 reflection had a phase of 0 was calculated to be 0.83 where

$$P_+(E_{2h}) = 1/2 + 1/2 \tanh \sigma_3 |E_{2h}| \Sigma_1 / 2\sigma_2^{3/2}.$$

TABLE 10

STATISTICAL AVERAGES AND DISTRIBUTIONS OF NORMALISED STRUCTURE FACTORS OF NGTA

	Experimental	Theoretical*	
		Centrosymmetric	Noncentro-symmetric
$\langle\|E\|\rangle$	0.888	0.798	0.886
$\langle\|E\|^2 - 1\rangle$	0.758	0.968	0.736
$\langle\|E\|^2\rangle$	1.000	1.000	1.000
$\|E\| > 1$	33.0%	32.0%	37.0%
$\|E\| > 2$	2.7%	5.0%	1.8%
$\|E\| > 3$	0.1%	0.3%	0.01%

*From Karle, Dragonette, and Brenner (1965).

Σ_1 is the appropriate sum in the above expression, and

$$\sigma_n = \sum_{j=1}^{N} Z_j^n$$

Z_j being the atomic number of the jth atom in a unit cell containing N atoms. Pertinent data for the starting set of phases are provided in Table 11.

The choice between reflections for the starting set was made on the basis of their high |E| values and the number of Σ_2 interactions they held with other reflections of high |E| value. This latter property is given more weight in the selection of a starting set of phases and is assessed in Table 11 according to the number of triplet relationships for each reflection and the corresponding value of K where

$$K = \sigma_3 \sigma_2^{-3/2} |E_h| \Sigma |E_k| |E_{h-k}|.$$

In addition to the five reflections mentioned, three additional reflections were included as symbolic phases. The symbolic phases were systematically assigned values of $\pm\pi/4$, $\pm\pi/2$ except for the 401 reflection. This reflection belongs to the centrosymmetric class for this space group and is restricted to have a phase of $\pm\pi/2$. This combination of phases with use of the 401 reflection reduces to 32 the total number of possible phase sets to be calculated in extension of the phases by the tangent formula.

Beginning with the phases assigned to the starting set, the phases of the other reflections were calculated and

TABLE 11

DATA FOR SELECTION OF ORIGIN AND ENANTIOMORPH DEFINING REFLECTIONS AND SYMBOLIC REFLECTIONS

Reflection and Type	|E|	NT*	$K = \sigma_3\sigma_2^{-3/2}\|E_h\|\Sigma\|E_k\|\|E_{h-k}\|$	K/NT		Φ Initial
(g 0 u) 6 0 5	3.27	21	50.77	2.42	π/2	
(0 u g) 0 15 4	3.26	25	62.59	2.50	π/2	Fixed for origin definition
(u u 0) 5 1 0	2.46	40	79.97	1.99	π/2	
(0 g u) 0 18 3	2.40	14	28.66	2.05	0	Fixed for enantiomorph definition
			Σ_1 relationships			
0 6 6	3.57	15	40.97	2.73	0	
			Symbolic reflections			
9 2 2	2.67	26	55.86	2.15	±π/4, ...	Systematically assigned values
5 15 3	2.65	20	40.60	2.03	±π/4, ...	
4 0 1	2.30	34	75.55	2.22	±π/2	

*Number of triplet relationships.

refined by the tangent formula (Karle and Karle, 1966). For these calculations 218 reflections with $|E| \geq 1.6$ were used. In the iterative series of calculations, the acceptance of new phases for the next cycle of refinement was based on the phase satisfying the following criteria:

(1) Its value did not change by more than a specified amount ($\pi/2$) from cycle to cycle;

(2) $t > t_{min}$ set at 0.25 where

$$t = (A^2 + B^2)^{1/2} / \Sigma |E_k| \cdot |E_{h-k}| \quad (0 < t < 1)$$

for which the values of A and B are defined by the relationships

$$A = \sum_k |E_k| \cdot |E_{h-k}| \cos(\phi_k + \phi_{h-k})$$

$$B = \sum_k |E_k| \cdot |E_{h-k}| \sin(\phi_k + \phi_{h-k});$$

and

(3) $\alpha > \alpha_{min}$, specified as 2.5 to give a standard deviation of $\simeq 40°$ (Karle and Karle, 1966) where

$$\alpha = 2\sigma_3 \sigma_2^{-3/2} |E_h| (A^2 + B^2)^{1/2}$$

the σ_n being defined earlier.

In the tangent formula calculations the 80 reflections with the highest $|E|$ values were refined for five cycles, the 150 highest for 10 cycles, and finally all reflections for 10 cycles. For each phase set calculated an R-value is calculated defined as

$$R_K = \frac{\sum_k \left| |E_h|_{obs} - |E_h|_{calc} \right|}{\sum_k |E_h|_{obs}}$$

where $|E_h|_{calc} = (A^2 + B^2)^{1/2}$ and is scaled so that $\Sigma|E_h|_{obs} = \Sigma|E_h|_{calc}$. Of the 32 phase sets calculated one had a significantly low R_K value (0.231) with 207 of the 218 data phased. This conforms closely to the criteria of Karle and Karle (1966) for indicating the most probably correct phases.

An E map was calculated using the phased |E| values determined for this set as coefficients. Of the 40 highest peaks contoured, 25 corresponded to clearly recognisable structural features of either the glucose ring and side chains or the naphthyl ring and were selected for the initial structure factor calculations on the basis of their calculated bond lengths and angles. At this stage the C-C bond lengths ranged from 1.20 - 1.55 Å and the C-O bond lengths from 1.10 - 1.35 Å. Atoms not included in this initial set (with reference to Figure 7) were O1, O3 and O4; C7 and C9, and C1", C2", C4" and C6". Figure 8 shows the contoured E map projected along the $\underline{\hat{c}}$ axis with the final least squares refined structure of the molecule superimposed.

A structure factor calculation based on these 25 atoms (19 carbon, 6 oxygen) gave a conventional reliability factor defined as

Figure 8.--Illustration of the contoured E map of NGTA projected along the $\underline{\hat{c}}$ axis with the final least squares refined structure of the molecule superimposed. The positions of the constituent atoms can be recognised by comparison of the molecule to that in Figure 7. Distinguishably separate peaks were not considered sufficiently well resolved or sufficiently prominent for the atoms O1, O3, O4, C7, C9, C1", C2", C4" and C6" to include the positions of these atoms in the initial structure factor calculation.

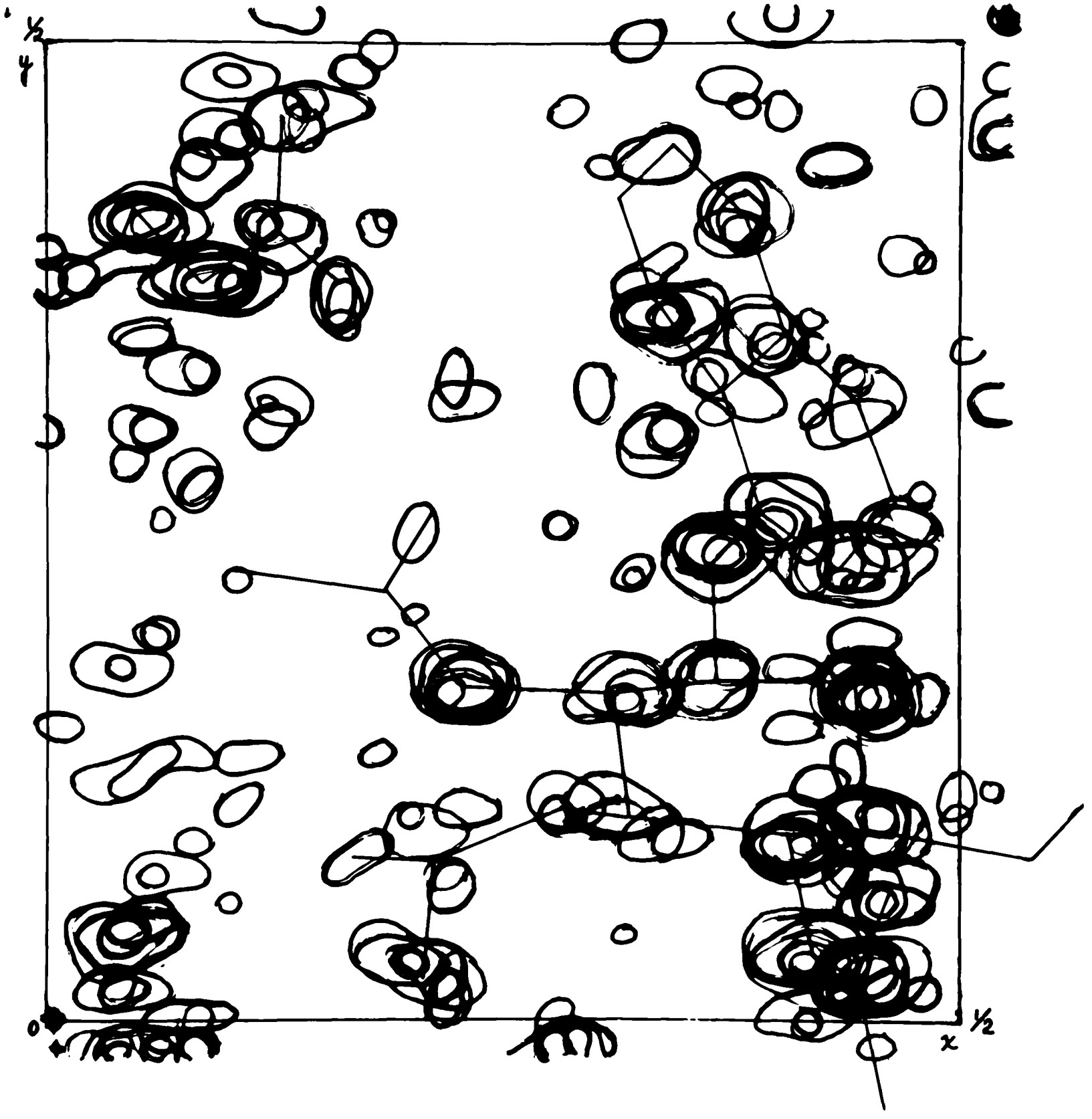
½
½
0
x
½

$$R = \frac{\sum_i \left| |F_{o_i}| - |F_{c_i}| \right|}{\sum_i |F_{c_i}|}$$

of 0.408 for the set of 2018 reflections with $I_o \geq 3\sigma(I_o)$. Calculation of an F_{obs} map based on this initial phased set from 25 atoms yielded the positions of the remaining 9 atoms of the molecule with no indication of solvent molecules in the asymmetric unit. At this stage, however, the carbonyl oxygen atom and methyl carbon atom of the acetyl side chains could not be distinguished from each other and the scattering contribution of each acetyl group in the subsequent structure factor calculation was considered as that fromthree carbon atoms. A structure factor calculation based on 34 atoms (28 carbon, 6 oxygen) gave an R-value of 0.261. Calculation of bond lengths allowed the carbonyl oxygen and methyl carbon atoms to be distinguished only for the C2', C4' and C6' side chains (C-C $\simeq$ 1.5 Å, C=O $\simeq$ 1.2 Å). A third structure factor calculation based on 25 carbon atoms and 9 oxygen atoms gave a conventional R-value of 0.233 but the ambiguity of the carbon and oxygen atoms of the C3' acetyl group still could not be resolved on the basis of bond lengths.

(b) Refinement of the Structure

Although the ambiguity in the C3' acetyl group could not be resolved, full matrix least squares refinement was started using the structure factors at an R-value of 0.233 calculated with 25 carbon atoms and 9 oxygen atoms. Three

cycles of refinement with individual isotropic temperature factors and unit weights reduced the R-value to 0.176. Calculation of bond distances and angles indicated that one of the bond lengths of the ambiguous acetyl group was 1.61 Å and the other 1.07 Å, the longer bond distance was assumed to correspond to the C-C bond, and the shorter to the C=O bond. A fourth cycle of full matrix refinement brought the R-value to 0.172.

Conversion to a least squares refinement with individual anisotropic temperature factors and unit weights with diagonal block approximation indicated only a slow decrease in the R-value which converged at ~0.12. A difference electron density map indicated that only 5 of the 7 aromatic hydrogen atoms and 4 of the 7 glucose hydrogen atoms could be identified with certainty. In addition, while all bond lengths for the non-hydrogen atoms were within ±0.05 Å of their expected values, the C=O bond distance of the C3' acetyl group remained at 1.14 Å while the corresponding distance for the other acetyl groups ranged from 1.19 - 1.22 Å. Inspection of the list of structure factors indicated that approximately 90 reflections of moderate to high intensity differed significantly in values for $|\underline{F}_o|$ and $|\underline{F}_c|$. Of these reflections, for approximately 70 reflections for which more than one measurement had been made, the $|\underline{F}_o|$ value was readjusted by removing the contribution from measurements with significant disagreement from the $|\underline{F}_c|$ value.

Least squares refinement with anisotropic temperature factors and unit weights was consequently reinitiated with the set of 2018 unique reflections. Three cycles of refinement using a diagonal block approximation scheme reduced the R-value to 0.117. Significantly, the highly questionable C=O bond length of the C3' acetyl group had lengthened to 1.17 Å while the other three C=O bonds remained at 1.18 - 1.20 Å. Calculation of a difference electron density map allowed identification of the aromatic and glucose C1' through C5' hydrogen atoms. These atoms, introduced at their calculated positions with isotropic temperature factors equal to those of the atoms to which they were bonded, were included into the structure factor calculation but were not refined. Further least squares refinement reduced the R-value to only 0.11, however, while the weighted R-value (Hamilton, 1965) defined as

$$R_W = \left[\frac{\sum_i w_i (|\underline{F}_{o_i}| - |\underline{F}_{c_i}|)^2}{\sum_i w_i |\underline{F}_{o_i}|^2} \right]^{1/2}$$

was 0.15.

An agreement analysis and inspection of the list of calculated and observed structure factors indicated that a number of reflections of high intensity appeared to be underestimated by experimental measurement. Of these reflections 21 which disagreed by more than 10% and had an $|\underline{F}_o|$ value >50 were consequently removed from the list of

structure factors and assumed to be underestimated through secondary extinction effects (Pinnock, Taylor, and Lipson, 1956). These reflections belonged to the group of 90 for which significant disagreement in $|\underline{F}_o|$ and $|\underline{F}_c|$ values had been earlier noted. This final set of 1997 independent reflections was employed for all further refinement calculations. A subsequent cycle of anisotropic least squares refinement with unit weights brought the conventional and weighted R-factors only to 0.10 and 0.135.

A weighting scheme for further refinement was fitted with a three parameter Chebyshev polynomial (Rollett, 1965). This scheme determined the weight for each reflection by the relationship

$$w = 1/[30.516\, T(0)'\,(X) + 41.777\, T(1)'\,(X) + 13.155\, T(2)'\,(X)].$$

In this calculation the above coefficients of a Chebyshev series in $T(I)'\,(X)$ with $X = F_o/F_{max}$ are determined by a least squares procedure which minimises $\Sigma w(|\underline{F}_o| - |\underline{F}_c|)^2$ over all reflections. This weighting scheme thus assigns approximately equal weights to reflections of high and low intensity with little disagreement in $|\underline{F}_o|$ and $|\underline{F}_c|$ but weights down reflections for which the disagreement is greater.

Refinement was continued thereafter with a block-diagonal least squares procedure using a two-block scheme. The scale factor and individual anisotropic temperature factors were included in one matrix block and the coordinates

of the non-hydrogen atoms in the second. Two cycles of refinement brought the conventional R-value to 0.085 and the weighted R-value to 0.115. A difference electron density map based on structure factors calculated for non-hydrogen atoms indicated the positions of all of the glucose, aromatic, and acetyl methyl hydrogens, except for the hydrogen bonded to the C2' atom. Addition of the hydrogen atoms at their observed positions to the structure factor calculation reduced the conventional R-value to 0.0705 and the weighted R-value to 0.0953 after three further cycles of refinement. No change in the atomic coordinates or in the R-values was observed by introducing all hydrogen atoms at their calculated positions into the calculation of structure factors. A difference electron density map calculated with structure factors for the fully refined non-hydrogen atoms only indicated no spurious electron density peaks. All peaks on the difference electron density map with density greater than 0.30 - 0.50 e/$\mathring{A}^3$ were found to correspond to the calculated positions of hydrogen atoms.

For comparative purposes refinement of the structure was carried out using a weighting scheme based on the counting statistics of reflections. The standard deviation for each unique reflection was calculated by the relationship

$$\sigma_i = \left(\frac{\sum_i w_i S_i (I)^2}{\sum_i w_i} \right)^{1/2}$$

where w_i is a weight assigned to each contributing measurement in data reduction based on a Gaussian distribution and $S_i(I)$ is the standard deviation of the measured intensity estimated as

$$S_i(I) = (N_{Background} + N_{Peak})^{1/2}.$$

The refinement calculations with this weighting scheme were initiated with the atomic parameters obtained after convergence of the full matrix refinement with individual isotropic temperature factors. For these calculations the set of reflections with $I_o \geq 3\sigma(I_o)$ were used, those influenced by secondary extinction having been dropped. Three cycles of refinement using a two-block scheme with block approximation as for the Chebyshev polynomial weights brought the conventional R-value to 0.082 and the Hamilton weighted value to 0.105. Introduction of the hydrogen atoms at their calculated positions into the structure factor calculation as for the previous refinement scheme brought the series of iterative calculations to convergence after four more cycles. The final values for the conventional and Hamilton weighted R-value were 0.0677 and 0.0743 respectively. A difference electron density map calculated with nonhydrogen atoms only showed no spurious electron density features and was similar in all respects to that obtained by the Chebyshev weighting scheme. Introduction of hydrogens at the observed positions caused no change in the R-values.

The stereochemical data presented in this discussion are those obtained by refinement based on counting statistics. The final stereochemical values of the refined structures agreed closely for the two refinement schemes. Bond lengths and angles agreed closely in all cases within $1-2\sigma$, where σ is the estimated standard deviation of the bond length or angle. The most important differences were in the bond length of the glucose C5'-C6' bond and in the naphthyl ring. For refinement based on counting statistics, the C5'-C6' bond was slightly longer by 0.008 Å. Also, the bond lengths associated with the naphthyl ring were in closer general agreement with those values expected for naphthalene (Cruickshank and Sparks, 1960) and showed better agreement for two-fold symmetry of the ring structure along the C9-C10 bond. Upon convergence of the refinement calculations, one further cycle of refinement was carried out for which the C5'-C6' was constrained to be that of the average C-C bond lengths in the glucose ring. No change in the R-values was observed. Consequently the shortening of this bond is considered to have origin in systematic errors and not to reflect an intrinsic stereochemical perturbation in the crystal. This aspect is discussed later.

The complete list of observed and calculated structure factors is provided in Appendix III. This list contains the reflections not used in the refinement calculations as "unobserved" $[I_o < 3\sigma(I_o)]$ as well as those underestimated through extinction effects. In the refinement

process the atomic scattering factors of the non-hydrogen atoms were those given in International Tables for X-ray Crystallography, Vol. III (1962), and the hydrogen scattering factors were those of Stewart, Davidson and Simpson (1965). Also a list of computer programs employed in the structure determination and refinement are indicated in Appendix III.

b. Description of the Molecule

(1) The Glucose Ring

(a) Stereochemical Data for Bond Lengths and Bond Angles

A stereoscopic view of the molecule is provided in Figure 9.

In Tables 12 and 13 are given the fractional coordinates of the non-hydrogen atoms and their anisotropic temperature factors. In Table 14 the unrefined fractional coordinates and isotropic temperature factors of the hydrogen atoms are provided. The unrefined bond lengths for the observed hydrogen positions were all 1.00 ± 0.15 Å. In Tables 15 and 16 are listed the intramolecular bond distances and angles with standard deviations and these are illustrated in Figure 10. The mean standard deviations are 0.009 for C-C bonds, 0.007 for C-O bonds, and 1.2° for the valence angles for the molecule as a whole. In Table 17 are listed respectively the deviations of the carbon atoms of the naphthyl ring from the calculated least squares plane. The deviation of the glycosidic oxygen O1' from this plane

Figure 9.--Stereoscopic view of β(1-naphthyl)-D-glucopyranoside-2',3',4',6'-tetra-O-acetate. The positions of hydrogen atoms are not shown. The constituent carbon and oxygen atoms are drawn in approximate accordance to their relative atomic radii. The absolute configuration of NGTA was not determined. Since the absolute configuration of D-glucose is known by x-ray structural studies using the anomalous scattering of its oxygen atoms (cf. Strahs, 1970), the structure of NGTA was calculated to conform to this configuration.

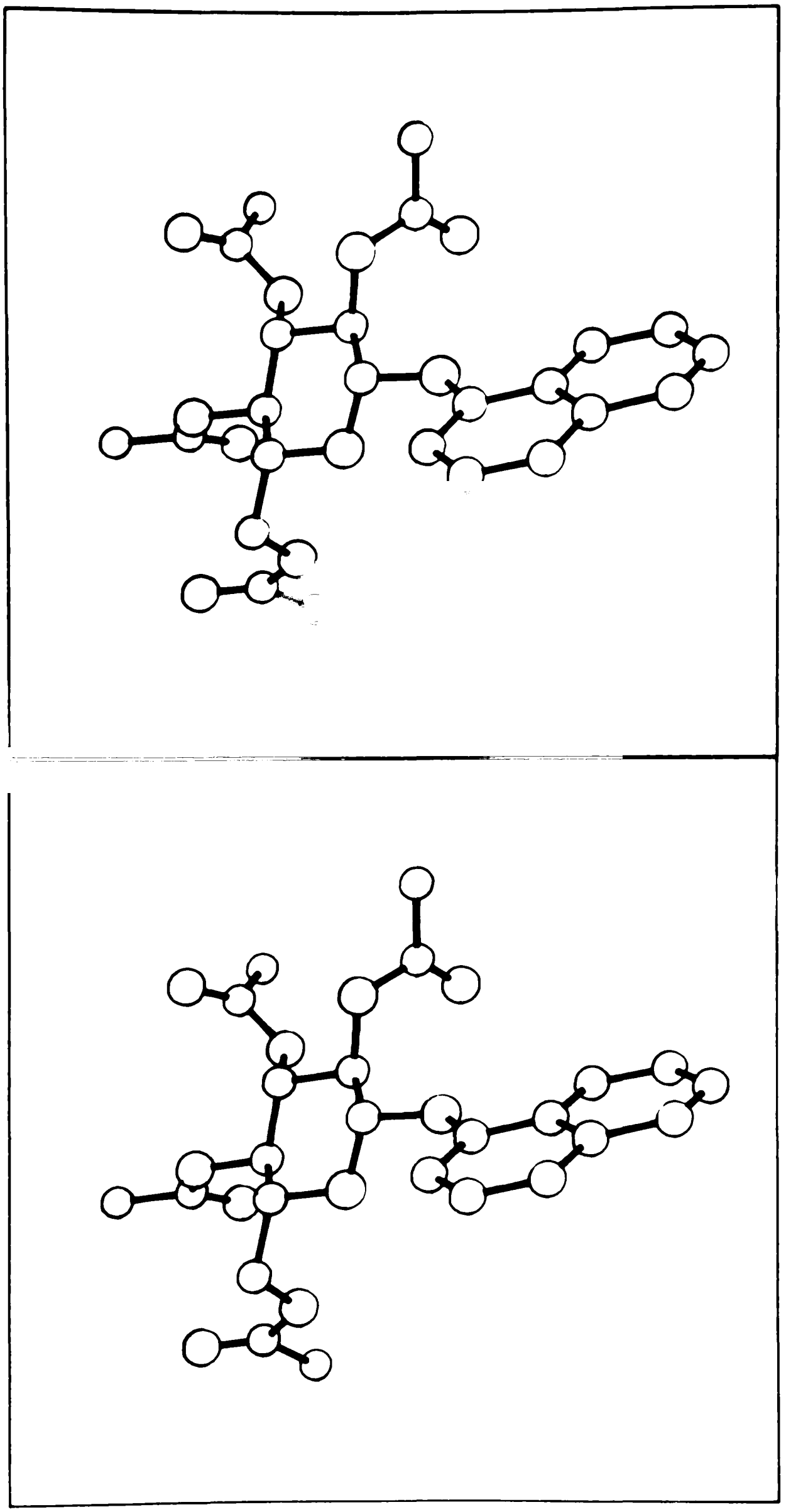

TABLE 12

FRACTIONAL ATOMIC COORDINATES* OF A UNIQUE MOLECULE OF NGTA

Atom	x	y	z
O1	0.2132(5)	0.2605(4)	0.2855(16)
O2	0.2082(4)	0.0249(3)	0.1657(12)
O3	0.4621(4)	0.0665(2)	-0.1156(7)
O4	0.6330(4)	0.0367(3)	0.1321(10)
O1'	0.3685(3)	0.2419(2)	0.5858(7)
O2'	0.2312(3)	0.1741(2)	0.4491(8)
O3'	0.2803(3)	0.1093(2)	0.1020(7)
O4'	0.4231(3)	0.0324(2)	0.1773(7)
O5'	0.4512(3)	0.1638(2)	0.4973(7)
O6'	0.5859(3)	0.1223(2)	0.2676(8)
C1	0.3965(4)	0.2645(3)	0.7641(10)
C2	0.4391(5)	0.2304(3)	0.8975(11)
C3	0.4631(6)	0.2584(4)	1.0686(13)
C4	0.4453(6)	0.3176(4)	1.1097(14)
C5	0.3816(6)	0.4160(3)	1.0050(17)
C6	0.3436(6)	0.4488(3)	0.8668(17)
C7	0.3199(5)	0.4232(4)	0.6858(16)
C8	0.3358(5)	0.3625(3)	0.6511(13)
C9	0.3772(4)	0.3266(3)	0.7900(11)
C10	0.4018(5)	0.3532(3)	0.9718(13)
C1'	0.3709(5)	0.1784(3)	0.5489(10)
C2'	0.3148(4)	0.1690(3)	0.3763(11)
C3'	0.3242(4)	0.1061(3)	0.2863(10)
C4'	0.4131(4)	0.0947(2)	0.2475(10)
C5'	0.4600(4)	0.1010(3)	0.4366(10)
C6'	0.5484(5)	0.0870(3)	0.4222(11)
C1"	0.1878(6)	0.2230(4)	0.3903(18)
C2"	0.1060(6)	0.2223(5)	0.4853(21)
C3"	0.2206(5)	0.0682(4)	0.0705(13)
C4"	0.1749(6)	0.0855(5)	-0.1110(17)
C5"	0.4492(5)	0.0245(3)	-0.0089(11)
C6"	0.4594(6)	-0.0421(4)	-0.0566(14)
C7"	0.6258(5)	0.0900(4)	0.1308(13)
C8"	0.6592(6)	0.1333(5)	-0.0216(17)

*The estimated standard deviations of the fractional coordinates are given in the parentheses. They refer to the last decimal positions of the respective values.

TABLE 13

ANISOTROPIC THERMAL PARAMETERS* FOR CARBON AND OXYGEN ATOMS OF NGTA

Atom	U_{11}	U_{22}	U_{33}	U_{23}	U_{13}	U_{12}
O1	0.1185(56)	0.1509(72)	0.1855(96)	0.1006(76)	0.0345(62)	0.0539(55)
O2	0.1117(48)	0.0977(42)	0.1032(49)	0.0215(43)	-0.0272(44)	-0.0408(37)
O3	0.1300(50)	0.0707(30)	0.0403(24)	0.0077(25)	0.0101(31)	-0.0036(34)
O4	0.1159(48)	0.0784(35)	0.0890(40)	-0.0082(35)	0.0319(41)	0.0056(34)
O1'	0.0888(32)	0.0470(22)	0.0560(26)	-0.0034(21)	-0.0074(28)	0.0081(22)
O2'	0.0615(24)	0.0601(24)	0.0650(28)	0.0067(25)	0.0031(25)	0.0082(21)
O3'	0.0723(28)	0.0626(25)	0.0518(25)	-0.0021(23)	-0.0100(23)	-0.0128(23)
O4'	0.0816(30)	0.0468(21)	0.0482(23)	0.0024(20)	0.0104(24)	0.0009(21)
O5'	0.0693(26)	0.0512(20)	0.0507(24)	-0.0054(20)	-0.0036(23)	0.0030(20)
O6'	0.0689(26)	0.0576(24)	0.0724(31)	0.0086(26)	0.0039(27)	0.0038(21)
C1	0.0671(36)	0.0551(33)	0.0414(32)	-0.0027(30)	-0.0035(30)	-0.0027(30)
C2	0.0810(47)	0.0495(32)	0.0682(40)	0.0012(32)	-0.0014(39)	-0.0074(33)
C3	0.0876(51)	0.0634(40)	0.0669(48)	0 0018(40)	-0.0145(47)	-0.0103(39)
C4	0.0948(55)	0.0718(43)	0.0764(54)	-0.0117(45)	-0.0103(52)	-0.0065(42)
C5	0.0894(56)	0.0576(38)	0.1224(75)	-0.0198(50)	-0.0050(60)	-0.0052(39)
C6	0.0898(54)	0.0520(36)	0.1198(73)	-0.0205(48)	0.0082(59)	-0.0028(37)
C7	0.0769(48)	0.0556(40)	0.1169(73)	0.0062(50)	-0.0059(56)	0.0005(37)
C8	0.0658(42)	0.0558(36)	0.0843(50)	-0.0017(40)	0.0064(43)	0.0062(33)
C9	0.0601(35)	0.0558(32)	0.0630(42)	-0.0004(34)	0.0046(35)	-0.0085(31)
C10	0.0704(40)	0.0529(31)	0.0823(47)	-0.0127(36)	0.0074(40)	-0.0061(31)
C1'	0.0742(42)	0.0471(29)	0.0455(31)	-0.0037(29)	-0.0034(34)	0.0054(31)
C2'	0.0641(39)	0.0582(29)	0.0553(39)	-0.0017(32)	-0.0000(36)	0.0001(31)
C3'	0.0685(37)	0.0573(32)	0.0487(36)	0.0013(31)	-0.0117(33)	-0.0042(29)
C4'	0.0664(36)	0.0395(24)	0.0484(33)	-0.0023(27)	0.0060(33)	0.0016(25)
C5'	0.0701(37)	0.0506(31)	0.0499(32)	0.0062(29)	-0.0059(32)	0.0087(30)
C6'	0.0775(43)	0.0630(38)	0.0598(36)	0.0074(33)	-0.0052(37)	0.0083(35)
C1"	0.0871(52)	0.0827(56)	0.1179(80)	0.0234(62)	-0.0008(60)	0.0230(48)
C2"	0.0816(55)	0.1190(72)	0.1264(98)	0.0193(81)	0.0171(66)	0.0353(56)
C3"	0.0811(47)	0.0693(44)	0.0733(53)	-0.0098(47)	-0.0038(46)	0.0000(40)
C4"	0.0977(61)	0.0900(60)	0.1051(76)	-0.0093(60)	-0.0384(61)	-0.0119(51)
C5"	0.0761(45)	0.0601(34)	0.0594(39)	-0.0132(34)	0.0060(39)	0.0036(34)
C6"	0.0957(59)	0.0656(41)	0.0763(53)	-0.0138(43)	0.0135(54)	0.0058(42)
C7"	0.0665(39)	0.0821(52)	0.0742(47)	0.0094(46)	0.0038(40)	0.0042(39)
C8"	0.0812(55)	0.1259(72)	0.1010(71)	0.0317(67)	0.0124(59)	-0.0047(54)

*The estimated standard deviations are given in the parentheses and refer to the last decimal positions of the respective values. The expression for the general temperature factor is

$$\exp[-2\pi^2(U_{11}\,{}^2a^{*2} + U_{22}\,{}^2b^{*2} + U_{33}\ell^2c^{*2} + 2U_{12}\;a^*b^* + 2U_{13}\;\ell a^*c^* + 2U_{23}\;\ell b^*c^*)]$$

where the U_{ij} are the thermal parameters expressed in terms of mean-square amplitudes of $_{ij}$ vibration in Ångstroms.

TABLE 14

FRACTIONAL UNREFINED ATOMIC POSITIONS
AND ISOTROPIC THERMAL PARAMETERS
OF HYDROGEN ATOMS OF NGTA

Atom	x	y	z	U_{iso}
H2	0.4526	0.1865	0.8713	0.080
H3	0.4947	0.2339	1.1659	0.090
H4	0.4555	0.3458	1.2219	0.090
H5	0.4027	0.4246	1.1391	0.120
H6	0.3315	0.4930	0.8924	0.120
H7	0.2921	0.4490	0.5853	0.120
H8	0.3249	0.3337	0.5405	0.080
H1'	0.3569	0.1536	0.6664	0.070
H2'	0.3266	0.2006	0.2750	0.060
H3'	0.3022	0.0723	0.3691	0.070
H4'	0.4337	0.1235	0.1456	0.070
H5'	0.4377	0.0717	0.5350	0.070
H6'	0.5753	0.0973	0.5485	0.080
H6'	0.5555	0.0423	0.3944	0.080
H2"	0.0741	0.2589	0.4417	0.130
H2"	0.1131	0.2240	0.6301	0.130
H2"	0.0765	0.1842	0.4490	0.130
H4"	0.1303	0.0550	-0.1343	0.110
H4"	0.2129	0.0856	-0.2240	0.110
H4"	0.1505	0.1272	-0.0944	0.110
H6"	0.4787	-0.0456	-0.1937	0.100
H6"	0.5004	-0.0607	0.0337	0.100
H6"	0.4060	-0.0635	-0.0408	0.100
H8"	0.6890	0.1093	-0.1231	0.130
H8"	0.6976	0.1629	0.0414	0.130
H8"	0.6134	0.1563	-0.0832	0.130

TABLE 15

INTRAMOLECULAR BOND LENGTHS OF CARBON AND OXYGEN ATOMS OF NGTA

Atom(i)	Atom(j)	L(ij)*
C1	C2	1.373(9)
C2	C3	1.383(9)
C3	C4	1.354(9)
C4	C10	1.420(10)
C10	C5	1.430(9)
C5	C6	1.343(12)
C6	C7	1.418(12)
C7	C8	1.373(9)
C8	C9	1.410(9)
C9	C1	1.404(8)
C9	C10	1.436(10)
C1	O1'	1.399(7)
O1'	C1'	1.410(6)
C1'	C2'	1.516(8)
C2'	C3'	1.513(8)
C3'	C4'	1.505(8)
C4'	C5'	1.517(8)
C5'	O5'	1.440(6)
O5'	C1'	1.403(7)
C5'	C6'	1.486(9)
C2'	O2'	1.466(7)
C3'	O3'	1.460(7)
C4'	O4'	1.453(6)
C6'	O6'	1.450(8)
O2'	C1"	1.347(8)
O3'	C3"	1.347(8)
O4'	C5"	1.361(8)
O6'	C7"	1.345(8)
C1"	O1	1.167(10)
C3"	O2	1.168(8)
C5"	O3	1.192(7)
C7"	O4	1.169(7)
C1"	C2"	1.494(12)
C3"	C4"	1.505(11)
C5"	C6"	1.501(9)
C7"	C8"	1.515(11)

*The estimated standard deviation is given in parentheses and refers to the last decimal positions of the respective values.

TABLE 16

INTRAMOLECULAR BOND ANGLES OF CARBON AND OXYGEN ATOMS OF NGTA*

Atom(i)	Atom(j)	Atom(k)	Angle(ijk)
C1	C2	C3	118.3(1.2)
C2	C3	C4	122.6(1.2)
C3	C4	C10	119.4(1.4)
C4	C10	C5	122.4(1.2)
C4	C10	C9	120.1(1.1)
C10	C5	C6	120.4(1.3)
C5	C6	C7	122.6(1.3)
C6	C7	C8	118.7(1.2)
C7	C8	C9	120.7(1.3)
C8	C9	C10	120.1(1.1)
C8	C9	C1	124.0(1.2)
C1	C9	C10	116.0(1.3)
C9	C10	C5	117.5(1.4)
C9	C1	C2	123.6(1.0)
C9	C1	O1'	112.2(1.2)
C2	C1	O1'	124.2(1.0)
C1	O1'	C1'	119.7(0.8)
O1'	C1'	O5'	107.2(1.2)
O1'	C1'	C2'	104.9(1.2)
C1'	C2'	C3'	112.4(1.1)
C2'	C3'	C4'	108.8(1.2)
C3'	C4'	C5'	109.0(1.1)
C4'	C5'	O5'	106.4(1.2)
C5'	O5'	C1'	112.6(0.9)
C1'	C2'	O2'	107.0(1.2)

C2'	C3'	O3'	105.2(1.2)
C3'	C4'	O4'	108.9(1.2)
C4'	C5'	C6'	111.8(1.2)
O2'	C2'	C3'	107.7(1.1)
O3'	C3'	C4'	109.5(1.2)
O4'	C4'	C5'	108.2(1.1)
O5'	C1'	C2'	107.2(1.2)
C6'	C5'	O5'	108.3(1.3)
C2'	O2'	C1"	116.9(1.1)
C3'	O3'	C3"	117.9(1.0)
C4'	O4'	C5"	117.8(1.0)
C6'	O6'	C7"	116.2(1.1)
O2'	C1"	O1	123.5(1.3)
O3'	C3"	O2	125.3(1.1)
O4'	C5"	O3	122.5(1.0)
O6'	C7"	O4	124.4(1.2)
O2'	C1"	C2"	109.7(1.8)
O3'	C3"	C4"	109.3(1.6)
O4'	C5"	C6"	111.3(1.2)
O6'	C7"	C8"	109.5(1.5)
O1	C1"	C2"	126.8(1.3)
O2	C3"	C4"	125.4(1.2)
O3	C5"	C6"	126.2(1.0)
O4	C7"	C8"	126.5(1.3)

*The standard deviation in degrees is given in parentheses.

TABLE 17

DEVIATIONS OF THE CARBON ATOMS FROM THE CALCULATED LEAST-SQUARES PLANE* OF THE NAPHTHYL GROUP

Atom of Naphthyl Group**	Deviation from Best Plane in Angstroms
1	0.027
2	-0.006
3	-0.030
4	-0.007
5	0.030
6	-0.009
7	-0.031
8	0.000
9	0.010
10	0.017

*Equation of Plane:

$$14.30493x + 5.87517y - 2.825z = 5.093.$$

**The glycosidic oxygen atom O1' is not included into the set of atoms defining the plane of the aromatic ring. Its deviation from the least squares plane is 0.056 Å.

Figure 10.--Schematic illustration of the least squares refined bond distances and angles of NGTA. The stereochemical data are those obtained by least squares refinement based on counting statistics. The standard deviations of the refined bond distances and angles are provided in Tables 15 and 16. The bond lengths are indicated in Ångstroms in the upper part of the diagram and the valence angles in degrees in the lower part.

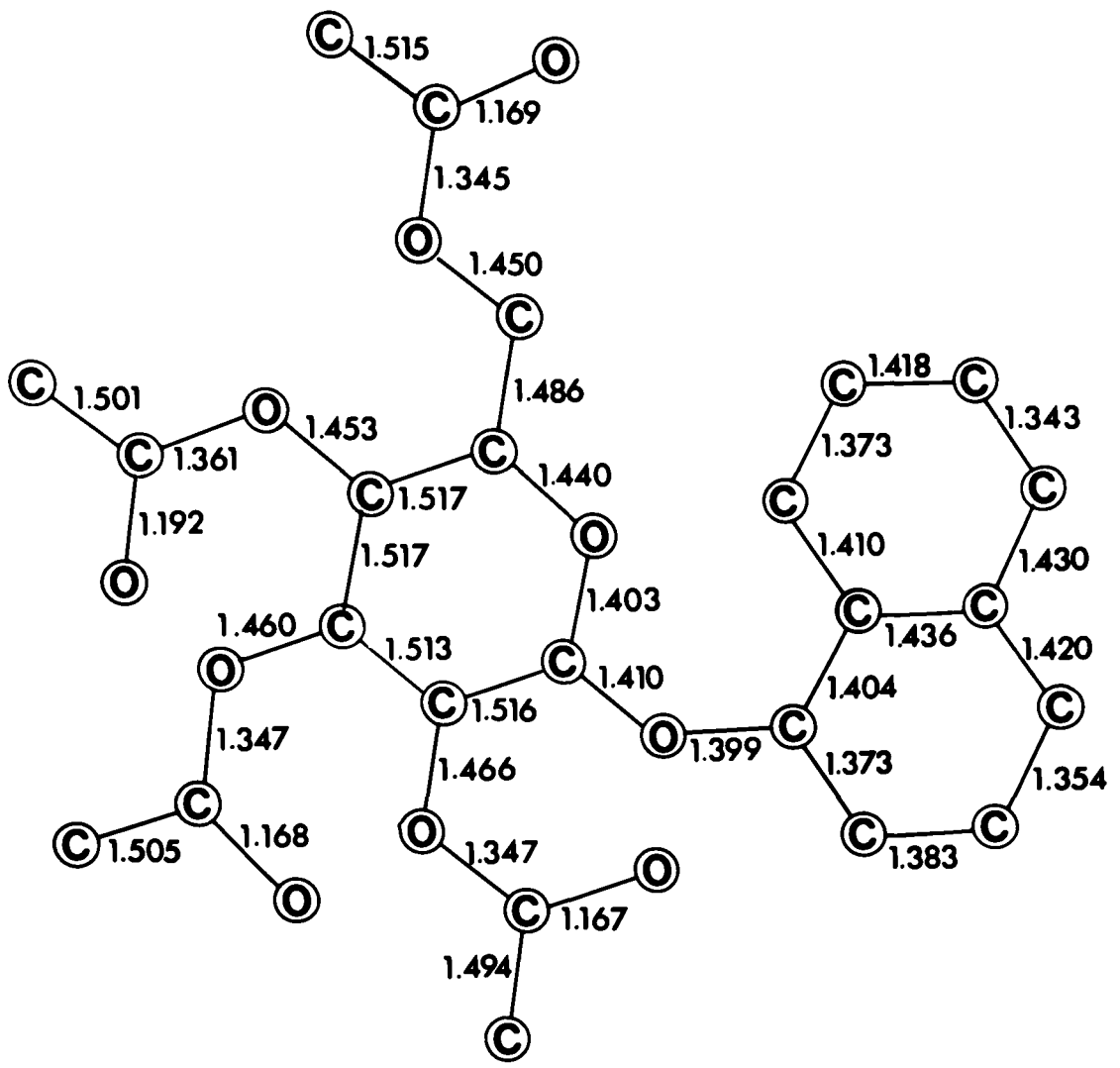
C 1.515 O
C 1.169
1.345
O 1.450
C
1.486
C 1.501
O 1.453
C 1.361
C 1.517
C 1.440
1.192
O
1.517
O
1.403
1.460 C 1.513
O
C 1.410
C 1.516
1.347
O 1.399
1.466
C 1.505 1.168
O
O 1.347
O
C 1.167
1.494
C
C 1.418
C 1.343
1.373
C
C
1.410
1.430
C 1.436
C 1.420
1.404
C
C 1.373
1.354
C 1.383
C

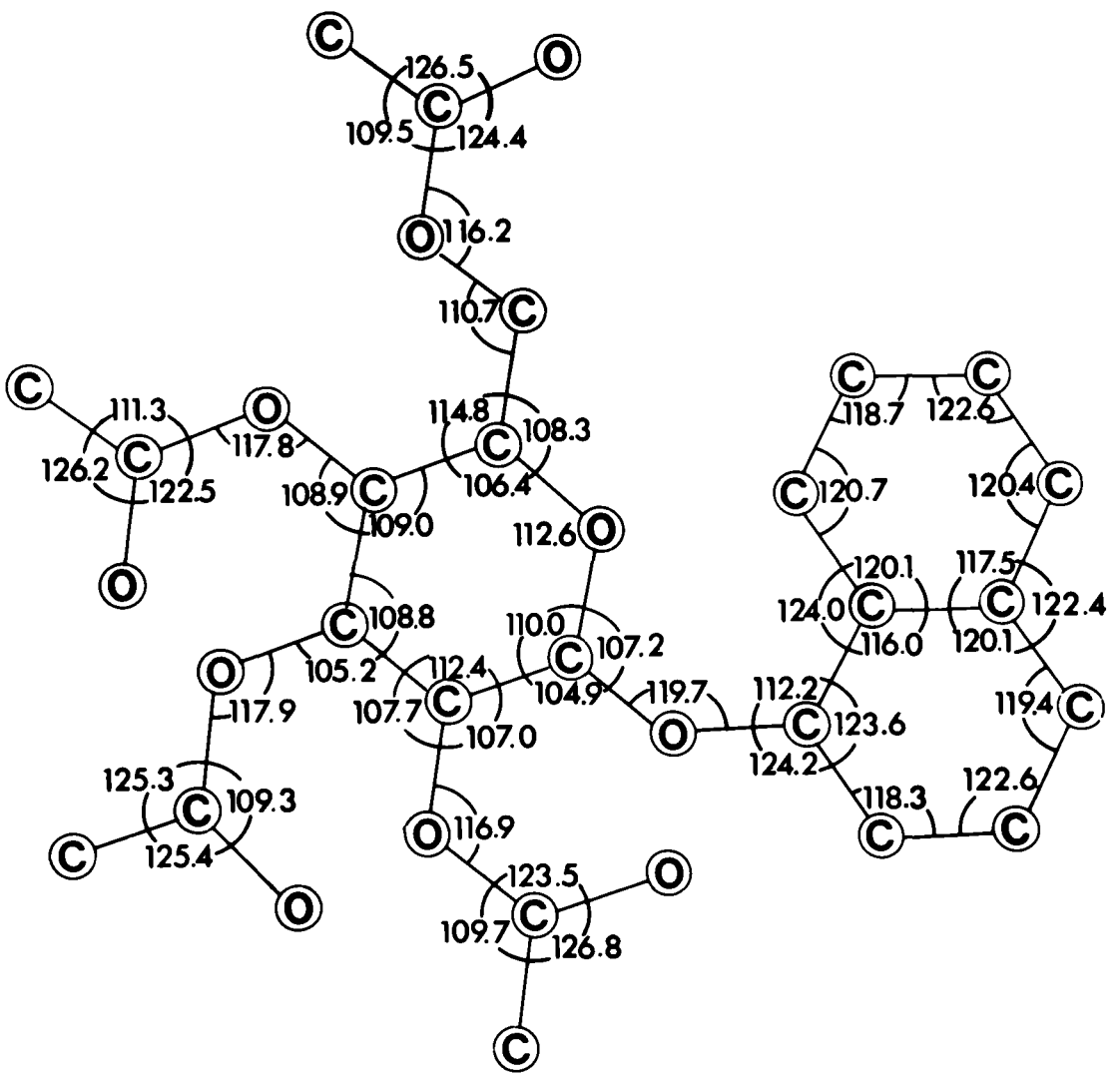
C 126.5 O
C
109.5 124.4
O 116.2
110.7 C
C
111.3
O
114.8
C 108.3
117.8
126.2 C
C 108.9
C 106.4
122.5
109.0
O
112.6
O
C 108.8
110.0
O
105.2
112.4
C 107.2
117.9
107.7 C
104.9
119.7
O
107.0
125.3
C 109.3
O 116.9
C
125.4
O
123.5 O
109.7 C 126.8
C
C 118.7 122.6 C
C 120.7
120.4 C
120.1
117.5
124.0 C
C 122.4
116.0
120.1
112.2
C 123.6
119.4 C
124.2
118.3
122.6
C
C

is also indicated. In Table 18 are listed the deviations of the four non-hydrogen atoms of each esterified side-chain from its calculated least squares plane. Table 19 provides a list of the deviations of the non-hydrogen atoms from the calculated least squares plane which defines the "seat" of the glucosidic chair configuration. An angle of 6.15° was calculated between the normals to the two planes defined by the C1', C2', O5' and the C3', C4', C5' atoms respectively.

The stereochemistry of the glucose ring and side chains is best compared to that of several closely related carbohydrate structures. If the C5'-C6' bond length is excluded (*vide infra*) the mean glucose C-C bond length (with a maximum deviation of 0.012 Å) for atoms defining the ring, is 1.513 Å ($\sigma = 0.008$) in close agreement with the mean value of 1.520 Å ($\sigma = 0.0018$) and 1.522 Å ($\sigma = 0.0016$) for β-D-glucose and cellobiose respectively (Chu and Jeffrey, 1968). The corresponding value for β(*p*-nitrophenyl)-D-(2-acetamido-2-deoxy)-glucopyranoside (hereafter called GlcNAc-PN), as the only other example of a β(aryl)-linked glucopyranoside is 1.531 Å ($\sigma = 0.009$) (Brehm and Moult, 1975). It is also of interest to note that a mean C-C bond length of 1.519 Å ($\sigma = 0.01$) has been reported through a preliminary publication for α-chloro-glucopyranoside-2',3',4',6'-tetra-O-acetate refined to a conventional R-value of 0.073 (James and Hall, 1969). On the other hand, the mean C-C bond length of the four acetyl groups, while uniformly shorter than those of the C-C bonds, is 1.504 Å ($\sigma = 0.011$) differing by less than

TABLE 18

DEVIATIONS OF NON-HYDROGEN ATOMS FROM CALCULATED LEAST-SQUARES PLANE OF EACH ESTERIFIED SIDE CHAIN OF NGTA

Ring Position	Atom of Side Chain	Deviation(Ångstroms)
C2'	C2"	0.003
	O1'	0.005
	C1"	-0.011
	O2'	0.003
Equation of plane:	5.91031x + 11.3361y + 5.33053z = 5.730	
C3'	C4"	0.003
	O2	0.005
	C3"	-0.012
	O3'	0.004
Equation of plane:	10.38719x - 11.77398y - 3.82300z = 1.231	
C4'	C6"	-0.001
	O3	-0.001
	C5"	0.002
	O4'	-0.001
Equation of plane:	15.57586x + 0.79873y + 2.16530z = 6.999	
C6'	C8"	0.000
	O4	0.000
	C7"	0.000
	O6'	0.000
Equation of plane:	13.91167x + 1.95619y + 3.60200z = 9.353	

TABLE 19

DEVIATIONS OF CARBON AND OXYGEN ATOMS
FROM LEAST-SQUARES PLANE* OF
GLUCOPYRANOSE RING OF NGTA

Atom	Deviation in Angstroms
O6'	1.890
C6'	0.472
C5'	-0.044
O5'	0.046
C1'	-0.635
O1'	-0.361
C2'	-0.043
O2'	-0.944
C3'	0.042
O3'	0.877
C4'	0.726
O4'	0.703

*The plane is defined by the atoms C5', O5', C2' and C3'.

Equation of plane:

$$6.15276x + 7.95832y - 5.86182z = 1.119.$$

1σ from the mean ring C-C bond. The corresponding C-C bond length of the acetyl group in GlcNAc-PN (Brehm and Moult, 1975) is 1.503 Å (σ = 0.009).

The length of the carbohydrate C-O bonds, excluding the ring oxygen and anomeric carbon atoms, is 1.457 Å (σ = 0.007) compared to the corresponding mean C-O bond length of 1.425 Å (σ = 0.0021) and 1.420 Å (σ = 0.0017) for β-D-glucose and cellobiose (Chu and Jeffrey, 1968) and 1.428 Å (σ = 0.008) for GlcNAc-PN (Brehm and Moult, 1975). The difference with respect to glucose at a significance level of 4σ undoubtedly reflects the incorporation of the alcoholic oxygen atom into an ester linkage. A more appropriate comparison, therefore, is to the corresponding bond length of carboxylic acid ester derivatives. Such a comparison unfortunately is less precise, for a survey of the published reports of ester derivatives indicates that the structures are not as precisely refined as in the present study. However, the CH_3-O bond length of methyl p-bromocinnamate (Leiserowitz and Schmidt, 1965) is 1.46 Å. In this comparison the methyl carbon atom is considered as chemically more analogous to the glucose ring carbon atom since both retain a tetrahedrally bonded configuration.

The average C=O bond length of 1.174 Å (σ = 0.008) and the average C-O bond length of 1.352 Å (σ = 0.008) between the carbonyl carbon atom of the acetyl group and the alcoholic oxygen of the glucose ring are consistent with corresponding values in esters and anhydrides. In succinic anhydride the

C=O bond distance is reported as 1.19 Å ($\sigma = 0.01$) and the carboxylic C-O bond distance is 1.375 Å ($\sigma = 0.01$) (Ehrenberg, 1965) while in methyl p-bromocinnamate the corresponding values are 1.19 Å and 1.32 Å respectively (Leiserowitz and Schmidt, 1965). Values of 1.18 Å ($\sigma = 0.01$) and 1.36 Å ($\sigma = 0.01$) have been similarly reported for the C=O and carboxylic C-O bonds in acetylsalicylic acid (Wheatley, 1964). These values are generally consistent with the less precisely refined stereochemical data of a variety of ester derivatives (cf. Mathieson and Welsh, 1965).

It is well established that each carbon atom in a crystalline sugar molecule has a unique environment of adjacent bonds which could account for the differences between bond lengths larger than their standard deviation (Berman, Chu, and Jeffrey, 1967). In this respect the C5'-C6' bond of the glucose ring must be examined closely. In NGTA the unconstrained bond length was observed to be 1.486 Å ($\sigma = 0.009$), shorter than the average ring C-C bond distance by 2.3σ. No change in the bond length was observed by changing the position of hydrogen atoms bonded to the C5' and C6' atoms from those observed in a calculated difference electron density map to those assumed on the basis of an idealised calculated geometry at a C-H distance of 1.00 Å. Ham and Williams (1970) have observed that the corresponding C-C bond length is shortened in the methyl β-cellobioside methanol complex as well as in a variety of carbohydrate structures. To this end the C-C bond distances reported for glucopyranose structures

have been compared in Table 20. The variation in the extent of shortening as indicated by the significance of the difference between the mean ring C-C bond and the C5'-C6' bond distance may reflect the different crystal environments of the side chain. However, in this study after convergence of the refinement, a cycle of refinement with a constrained C5'-C6' bond length at 1.513 Å had no effect on the R-values. For this calculation no change was observed for bond lengths and angles in the rest of the molecule. A comparable test of the significance of the apparent shortening has not been applied in the study of Ham and Williams (1970). In the present study, there is no obvious chemical reason why the bond length should be shortened. It is consequently likely that the apparent shortening is a result of systematic errors in the data especially in view of the lack of effect on R-values by constraining the bond length in a cycle of refinement.

(b) The Geometry of the Glucose Ring and Side Groups

The configuration of the atoms defining the carbohydrate ring illustrates a minimally distorted ring system. The deviations of the atoms which define the plane of the glucose ring corresponding to the "seat" portion of the chair are uniformly equidistant from the calculated mean best plane (Table 19) such that the diametrically opposed atoms find themselves on the same side of the plane. Furthermore, the angle of 6.15° between the normals to the planes

TABLE 20

COMPARISON OF SHORTENED C-C BOND LENGTHS OF GLUCOPYRANOSE RINGS

	Average Ring C-C	Range Ring C-C	C5'-C6'	Significance*
NGTA	1.513 Å	1.505-1.517 Å	1.486(9) Å	2.2
Methyl β-cellobioside (Ham and Williams, 1970)				
Primed ring	1.530	1.526-1.535	1.515(6)	2.3
Unprimed ring	1.525	1.513-1.533	1.505(6)	3.0
β-D-glucose (Chu and Jeffrey, 1968)	1.521	1.511-1.529	1.513(5)	1.5
Cellobiose (Chu and Jeffrey, 1968)				
Unprimed ring	1.528	1.520-1.534	1.519(5)	1.9
Primed ring	1.523	1.514-1.530	1.501(5)	3.8
Methyl α-D-glucoside (Berman and Kim, 1967)	1.523	1.509-1.531	1.506(4)	3.8
α-D-glucose (Brown and Levy, 1965)	1.526	1.519-1.534	1.510(3)	4.8
Methyl β-malto-pyranoside (Chu and Jeffrey, 1967)				
Primed ring	1.518	1.514-1.533	1.513(9)	0.4
Unprimed ring	1.524	1.510-1.525	1.526(9)	-0.2
GlcNAc-PN (Brehm and Moult, 1975)	1.528	1.523-1.536	1.516(9)	0.9

*Significance is expressed as the average C-C bond length in the ring minus the C5'-C6' bond length divided by the σ of this difference where $\sigma = (\sigma_1^2 + \sigma_2^2)^{1/2}$.

defined by the C3', C4', C5' and C2', C1', O5' groups of atoms indicates that these planes are nearly parallel. The C-O bonds and C=O bonds of each acetylated side chain are in a cis-configuration, this relationship corresponding to the configuration of least strain in an ester linkage (Mathieson and Welsh, 1965).

The carbon-oxygen bond lengths involving the ring oxygen and anomeric carbon atoms deserve special consideration in glucopyranoside derivatives since these bonds form the characteristic acetal group and give rise to much of the variety in carbohydrate chemistry in aqueous solution. For this reason, the C-O bond distances involving the ring and glycosidic oxygen atoms of NGTA are compared to those of other glucopyranosides in Table 21. In NGTA the C1'-O1' bond length is 1.410 Å ($\sigma = 0.006$) significantly shorter (5σ) than the mean C-O value of 1.457 Å ($\sigma = 0.007$) for the other equatorially displaced C-O bonds. It is also shorter (1.9σ) than the mean equatorial C-O bond lengths not involving the ring and glycosidic oxygen atoms in β-D-glucose and cellobiose (Chu and Jeffrey, 1968), GlcNAc-PN (Brehm and Moult, 1975), and methyl β-maltopyranoside (Chu and Jeffrey, 1967). As pointed out by Chu and Jeffrey (1967), the anomeric C1'-O1' bond length in β-D-glucosides is significantly shorter ($2\text{-}7\sigma$) than the mean C-O bond length not involving the anomeric carbon atom or the ring oxygen atom. In NGTA the C5'-O5' bond length of 1.440 Å ($\sigma = 0.006$) is more nearly equivalent in length to the equatorial C-O bonds

TABLE 21

COMPARISON OF BOND LENGTHS AROUND THE GLYCOSIDIC OXYGEN AND ANOMERIC CARBON ATOMS OF β-D-GLUCOPYRANOSIDES

Compound	Configuration at C1'	Bond Length C1'-O1'	Bond Length of Ring C-O Bonds C1'-O5'	C5'-O5'	Bond Length Distal to Glycosidic O	Glycosidic Group
NGTA	equatorial	1.410(6) Å	1.403(7) Å	1.440(6) Å	1.399(7) Å	naphthyl
β-D-glucose[a]	equatorial	1.383(4)	1.433(4)	1.437(4)	—	H
Cellobiose[a]						
Primed ring	equatorial	1.381(5)	1.435(4)	1.437(4)	—	H
Unprimed ring	equatorial	1.397(4)	1.425(4)	1.436(4)	1.446(4)	glucosyl
Methyl β-maltopyranoside[b]						
Primed ring	equatorial	1.375(8)	1.427(7)	1.430(7)	1.425(11)	methyl
Unprimed ring	axial	1.416(7)	1.408(7)	1.440(7)	1.438(7)	glucosyl
Methyl β-celloboise[c]						
Primed ring	equatorial	1.379(5)	1.434(5)	1.432(5)	1.435(6)	methyl
Unprimed ring	equatorial	1.390(5)	1.432(5)	1.430(5)	1.437(5)	glucosyl
GlcNAc-PN	equatorial	1.399(7)	1.409(7)	1.442(8)	1.377(8)	p-nitrophenyl

[a] Chu and Jeffrey, 1968

[b] Chu and Jeffrey, 1967

[c] Ham and Williams, 1970

[d] Brehm and Moult, 1975

while the C1'-O5' bond length at 1.403 Å ($\sigma = 0.007$) remains significantly shorter (5.4σ) than the other ring C-O bond. Moreover, in GlcNAc-PN (Brehm and Moult, 1975), the only other known example of an aromatic substituted β-glucopyranoside, parallel relationships are observed, including a shortening of the glucosidic C1'-O1' bond length.

Chu and Jeffrey (1967) have discussed the acceptance criteria of shortened C-O bond lengths involving the ring and glycosidic oxygen atoms in pyranose structures. The following "rules" heretofore have been characteristic of glucosides:

(1) An axial glycosidic bond is short only when the hydrogen atom on O1' is unsubstituted.

(2) An equatorial glycosidic C1'-O1' bond is short irrespective of whether the hydrogen atom on O1' is substituted or not.

(3) When there is a shortening of the C1'-O1' bond length, no significant differences have been observed in the ring C-O bond lengths.

(4) If the C1'-O1' bond is not significantly short, the two ring C-O bond lengths are possibly different with that adjacent to the glycosidic linkage being the shorter.

For the β-aryl substituted glucoside described here, in contrast we observe shortening of the glycosidic C1'-O1' bond with a significant difference in the ring C-O bond lengths. The stereochemical relationships involving

the glycosidic carbon and oxygen atoms in aromatic substituted glucopyranosides consequently do not conform simply to the rules previously outlined for other glucopyranosides but with substituted aliphatic aglycone residues (Chu and Jeffrey, 1967). The different stereochemical relationships observed for aromatic substituted derivatives undoubtedly reflect the chemical properties of aromatic substituted glucosides as compared to aliphatic substituted glucosides with an equatorial glucosidic linkage (Feather and Harris, 1965).

In contrast to the C-O bond length distal to the glycosidic oxygen of aliphatic substituted β-glucopyranosides (Table 21), in NGTA the corresponding bond length is 1.399 Å ($\sigma = 0.007$) consistent with the aromatic C-O bond length of 1.38 Å ($\sigma = 0.01$) observed in 1,2-diphenoxyethane (Yasuoka, Ando, and Kurijabashi, 1967), of 1.371 Å ($\sigma = 0.01$) for an ether linkage involving an unsaturated carbon atom in the photolysis product of N-chloroacetylmescaline (Karle and Karle, 1970), and of 1.377 Å ($\sigma = 0.008$) for the corresponding aryloxy bond length in GlcNAc-PN (Brehm and Moult, 1975).

In NGTA the valence bond angle at the glucosidic oxygen is 119.7° ($\sigma = 0.8°$) compared to that of 120.0° ($\sigma = 0.5°$) in GlcNAc-PN (Brehm and Moult, 1975), and agrees closely with the valence bond angle of 116.1° at the glyco-

sidic oxygen atom between the two glucopyranose rings of cellobiose (Chu and Jeffrey, 1968) and of 115.8° in methyl β-cellobioside (Ham and Williams, 1970). Ham and Williams (1970) have pointed out that bulky substituents of the glycosidic oxygen both increase the valence bond angle observed with a methyl group (~113°) and increase the length of the glycosidic bond by about 0.011 Å. The valence angle of the ring oxygen is 112.6° (0.9°) in close agreement to that of 112.8° (0.4°) in GlcNAc-PN (Brehm and Moult, 1975).

The carbon valence bond angles interior to the glucose ring average 109.3° ($\sigma = 1.1°$) with a spread of 6.0°. The corresponding average values of methyl β-cellobioside are respectively 110.0° and 6.5° (Ham and Williams, 1970) and for cellobiose 110.0° and 4.0° (Chu and Jeffrey, 1968). The carbon valence bond angles exterior to the ring in NGTA average 108.2° ($\sigma = 1.2°$) with a spread of 9.9°. For methyl β-cellobioside the corresponding values are 109.8° and 9.9°, and for cellobiose 109.5° with a spread of 8.2°. Although the mean carbon valence bond angle exterior to the ring is less than for other glucopyranose derivatives, the difference in average value and spread does not appear to be significant. In methyl β-maltopyranoside (Chu and Jeffrey, 1967) the exterior ring valence angles range from 115.2° to 107.1°.

The individual conformation angles (Reeves, 1950) of NGTA are listed in Table 22 and compared to those of β-D-glucose (Chu and Jeffrey, 1968). The conformation

TABLE 22

CONFORMATION ANGLES* OF NGTA

Bond	Compound	
A. Within pyranose ring	NGTA	β-D-glucose**
C1' → C2'	+51.9°	+53.7°
C2' → C3'	-51.0	-50.8
C3' → C4'	+57.2	+53.4
C4' → C5'	-63.9	-59.8
C5' → O5'	+66.8	+66.3
O5' → C1'	-60.5	-62.8
B. Outside pyranose ring		
C1-[O1' → C1']-C2'	+163.7°	—
C1-[O1' → C2']-O5'	-79.4	—
O5'-[C1' → C2']-O2'	+169.9	+175.0°
O1'-[C1' → C2']-O2'	-75.1	-69.2
C1'-[C2' → C3']-O3'	-168.2	-170.5
O2'-[C2' → C3']-O3'	+74.2	+68.9
C2'-[C3' → C4']-O4'	+175.0	+173.1
O3'-[C3' → C4']-O4'	-70.6	-67.5
C3'-[C4' → C5']-C6'	+176.3	+179.0
O4'-[C4' → C5']-C6'	+58.1	+59.6
C6'-[C5' → O5']-C1'	-169.3	-169.6
C5'-[O5' → C1']-O1'	-174.1	-179.4
O5'-[C5' → C6']-O6'	-66.0	-60.4

*The conformation angle of a directed bond C(i) → C(j) is defined as the angle, measured counter-clockwise that the projection of the C(i-1) - C(i) bond makes with respect to the projection of the C(j) - C(j+1) bond. The angle is positive if it is measured clockwise (Klyne and Prelog, 1960).

**Calculated from Chu and Jeffrey (1968).

angles within the pyranose ring range from 51.0 to 66.5°. The same angles in β-D-glucose range from 50.8 to 66.3°. There is also close agreement for corresponding conformation angles involving the side groups outside of the ring.

In view of the general paucity of precise stereochemical data for bond lengths and angles of ester groups, the four side chains in NGTA are of added interest. The acetyl side chains attached to the alcoholic ring oxygen atoms exhibit a remarkably low degree of variation in bond lengths and valence bond angles involving either the alcoholic oxygen or the carboxylic carbon atoms (see Figure 7). The mean values of bond distances and angles of the four ester groups are illustrated in Figure 11. In view of the cis-configuration of the ester linkage common to each side chain and the absence of perturbing hydrogen bonding networks, these values may serve as characteristic stereochemical values for an ester group. As pointed out above, the bond lengths, in general, are consistent with corresponding values of less precisely refined ester derivatives.

(2) The Naphthyl Group

Table 17 gives a list of the calculated deviations of the carbon atoms from the calculated least-squares plane of the naphthyl group. The bridging glycosidic oxygen atom is observed to deviate from the mean best plane by 0.056 Å and consequently cannot be considered coplanar with the naphthyl ring. While the constituent atoms of the ring

Figure 11.--Schematic illustration of the mean values of bond distances and angles of the esterified side chains of NGTA. The mean standard deviations are indicated in parentheses. For bond distances they refer to the last decimal positions. For angles they are indicated in degrees. C_{gluc} represents the generalised glucose carbon atom at the point of attachment of the esterified side chain.

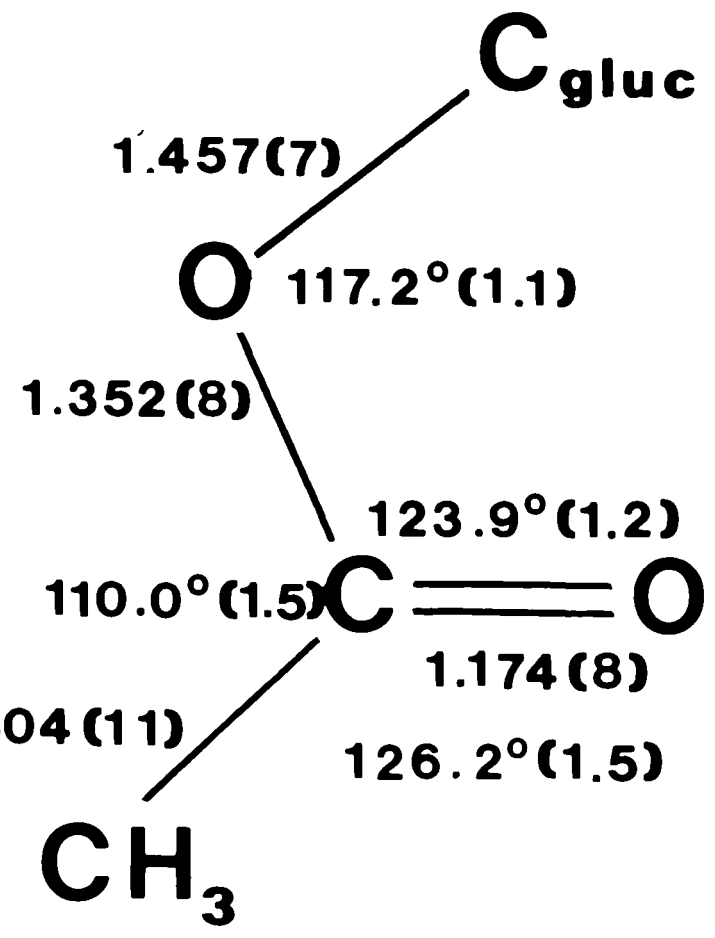
C gluc
1.457(7)
O
117.2°(1.1)
1.352(8)
123.9°(1.2)
110.0°(1.5)
C
O
1.174(8)
1.504(11)
126.2°(1.5)
CH3

deviate only slightly from the calculated least squares plane, they cannot be considered strictly planar on the basis of the test ratio $\sum_{\underline{m}} d_{\underline{m}}/\sigma_{ref}$ (Stout and Jensen, 1968), where $d_{\underline{m}}$ is the perpendicular distance of an atom $\underline{m}$ from the calculated least squares plane and σ_{ref} is the mean-square value of the uncertainty in the refined coordinate position.

No other mono-substituted naphthalene derivative has been characterised to comparable precision. In contrast to the stricter orthorhombic ($D_{2\underline{h}}$) symmetry of naphthalene (Cruickshank and Sparks, 1960), this Cl-substituted derivative exhibits in the group theoretical sense only $C_{\underline{S}}$ symmetry, that is, symmetry only with respect to the plane of the ring. However, upon consideration of the standard deviations of the C-C bond lengths, the naphthyl group can be considered to exhibit two-fold symmetry with respect to the long and short axes of the planar ring structure perpendicular and parallel to the C9-C10 bond respectively. Of further interest is that the deviations of the carbon atoms from the calculated least squares plane (Table 17) closely exhibit two-fold symmetry about an axis perpendicular to the plane. The effect of an electro-negative substitution at the C1 position is thus observed to be negligible stereochemically. No naphthalene derivative with a substituent at the C2 position has been characterised to comparable precision. Therefore, the relative distortions of both types of derivatives cannot be compared.

(c) The Crystal Structure and Intermolecular Contacts

The intermolecular contact distances between adjacent molecules less than 3.50 Å are listed in Table 23 and are illustrated in Figure 12 projected along the $\hat{c}$ axis. There are nine such distances which appear to be slightly less than the sum of the van der Waals radii based on the values of Bondi (1968) for the chemical groups involved. Of these all intermolecular contacts involving only carbon atoms are between the aromatic ring and methyl groups of the acetyl side chains, and those involving carbon and oxygen atoms, except for one, are between methyl or aromatic carbon atoms and carbonyl oxygen atoms. The distances for carbon-carbon contacts are significantly less than 4.0 Å as the estimated sum of the van der Waals radii (Bondi, 1968). Of the oxygen-carbon intermolecular contacts only the O1-C8" interaction can be considered significantly less than 3.5 Å, the estimated sum of the respective van der Waals radii. There are thus two intermolecular contacts involving hydrophobic groups only and one C-H···O interaction which appear to provide stability to the crystal lattice. In this respect the crystal structure of NGTA differs markedly from those of other carbohydrates which are all characterised by intermolecular hydrogen bonds with concomitant stereochemical perturbations on the glucose ring and side chains (Strahs, 1970). On this basis, especially since the O1' and O5' atoms are not involved in intermolecular

TABLE 23

INTERMOLECULAR CONTACT POINTS IN NGTA CRYSTAL WITH INTERATOMIC DISTANCES* LESS THAN 3.5 ÅNGSTROMS

Atom(i)	Atom(j)	Distance(ij)	S	Tx	Ty	Tz
O1	C8"	3.074(11)	3	-1	0	0
O2	C4"	3.443(12)	4	1	0	0
	C6"	3.371(11)	4	1	0	0
C4	C6	3.473(10)	3	0	0	1
	C7	3.394(10)	2	1	-1	0
	C7	3.428(10)	3	0	0	1
O4'	C4"	3.366(9)	4	0	0	0
C7	C7"	3.440(10)	3	-1	0	1
C7"	C7	3.463(7)	3	0	0	1

*Standard deviations of the intermolecular distances are given in parentheses and refer to the last decimal positions of the respective values. The symbols S, Tx, Ty, and Tz indicate the nth molecule of the unit cell and the translational operations with respect to molecule 1 required to produce the intermolecular contacts.

Figure 12.--Schematic illustration of the crystal structure of NGTA projected along the $\hat{c}$ axis. The structurally significant intermolecular contacts listed in Table 23 indicated by broken lines can be identified with reference to the labeling scheme given in Figure 7.

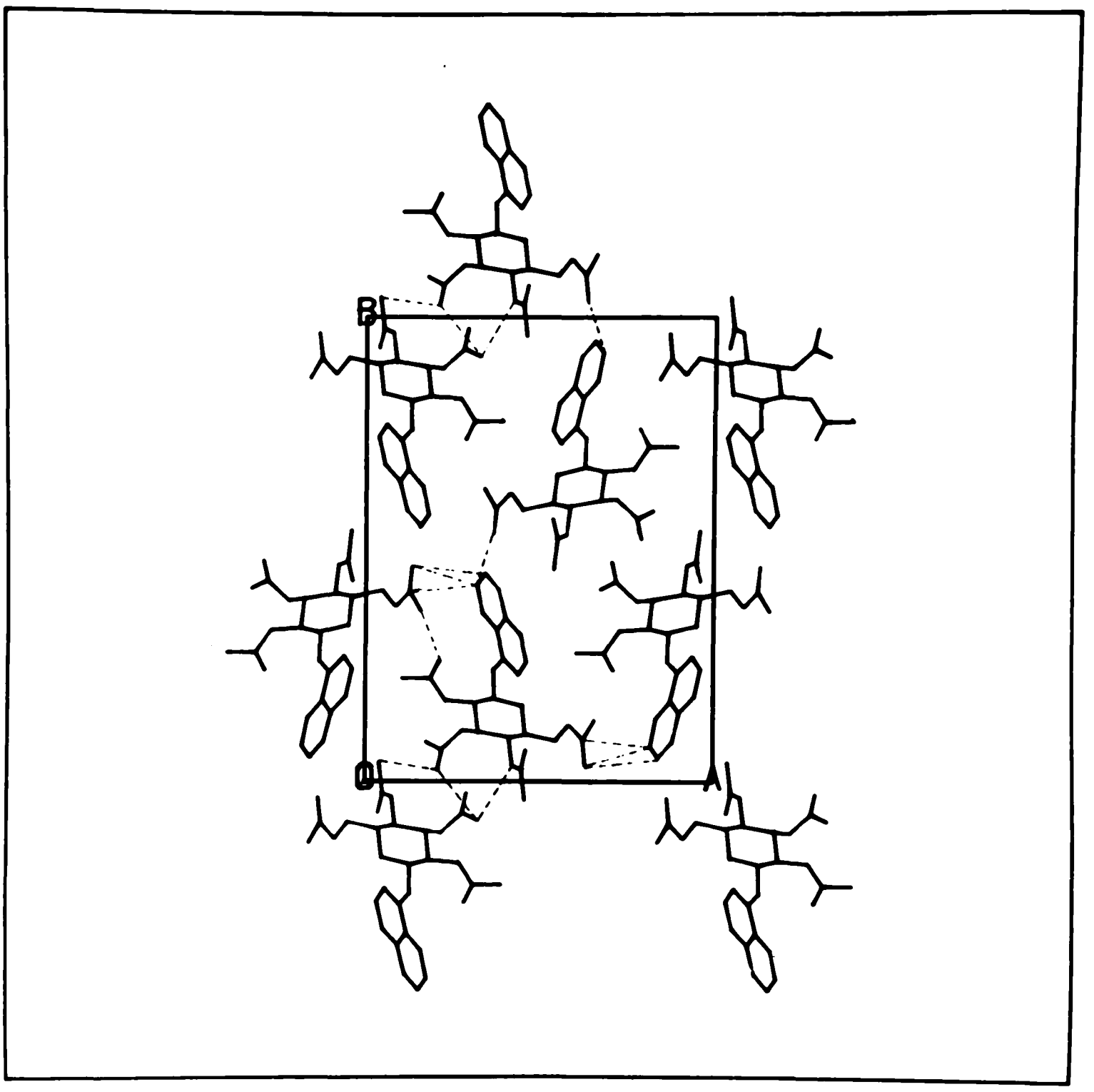
B

contacts, the ring structure of the glucose moiety can be considered as negligibly perturbed by its environment.

In connection with structural studies on polyproline and related polymers, there has been considerable discussion on the possibility of intermolecular C-H···O bonds (Ramachandran et al., 1967; Krimm et al., 1967). This interaction is estimated (Poland and Scheraga, 1967) as approximately 0.9 kcal/mole and is a weak hydrogen bond because of the absence of an electrostatic contribution. For this estimate the closest distance of approach between the hydrogen and oxygen atoms is $r_{H...O} = 2.05$ Å (Poland and Scheraga, 1967), suggesting that to this extent only the O1-C8" interaction may be energetically significant in the NGTA crystal since the other oxygen-carbon interactions are longer. Nonetheless, at least for this one oxygen-carbon interaction, we have observed to our knowledge for the first time structural evidence of such predicted intermolecular hydrogen bonds, and the data lend credence to the existence of such interactions in other molecules.

(d) The Molecular Structure of NGTA and Related Glucopyranosides

It is of importance, furthermore, to point out some salient features of the molecular structure of NGTA observed in the crystal to that of an unacetylated derivative, particularly as the glucosidic portion of a mixed disaccharide substrate analog of lysozyme. Model building studies of the tetraacetylated and free aromatic-linked

glycosides indicate no added steric hindrance by the acetyl groups to the rotation of the naphthoxy-group about the glycosidic oxygen atom. A minimum potential energy calculation to determine the configuration of the naphthyl group with respect to the glucose ring suggests identical coinciding minimum potential energy configurations for the two derivatives, precisely for that configuration observed here crystallographically (W. D. S. Motherwell, personal communication). In addition, as discussed above with respect to the stereochemical relationships of the hemiacetal group, the molecular structure of GlcNAc-PN is closely similar (Brehm and Moult, 1975). This is of particular importance in view of the chemical behaviour of hemiacetals in acid-catalysed reactions (Feather and Harris, 1965).

We can expect, therefore, that the relative configuration of the naphthyl and glucose moieties in the molecular structure of NGTA is at least one of the configurations which obtains for the molecule in solution and which may be of importance in binding to the active site cleft of lysozyme. Model building studies indicate that an aromatic-linked disaccharide substrate for either a phenyl or naphthyl analog can be accommodated into the active site cleft of lysozyme as can the more usual GlcNAc oligomers. Figures 13 and 14 illustrate the fit observed with use of CPK space filling models for the substrate and nearby protein residues of both a phenyl and naphthyl disaccharide substrate analog. Furthermore, the fitting of both disac-

Figure 13.--Colour photograph of the fitting of a molecular model of a phenyl-linked mixed disaccharide substrate in the active site cleft of lysozyme. The laboratory atomic model of lysozyme constructed to a scale of 1 Å/2 cm was modified by substituting CPK space filling components for the amino acid residues in the active site cleft. The fit of a molecular model of the β(phenyl)-linked substrate GlcNAc-Glc-phenyl constructed of CPK components was then tested. By incorporating the acetamido specificity contacts in subsite C and the corresponding hydrogen bonding contacts for carbohydrate hydroxyl groups in subsites C and D expected for catalytically productive binding (Imoto et al., 1972), a fit of the molecular model could be obtained only by allowing distortion of the acetal group and glycosidic linkage of the glucose moiety in subsite D. The model fitting illustrates that binding of the disaccharide substrate is sterically compatible with structural requirements of productive substrate binding and catalysis. The aromatic group is seen as a dense black hexagonal structure in the lower part of the front of the molecule.

Figure 14.--Colour photograph of the fitting of a molecular model of naphthyl-linked mixed disaccharide substrate in the active site cleft of lysozyme. All conditions are described in Figure 13. The aromatic group is seen as a dense structure in the lower part of the front of the molecule as in Figure 13.

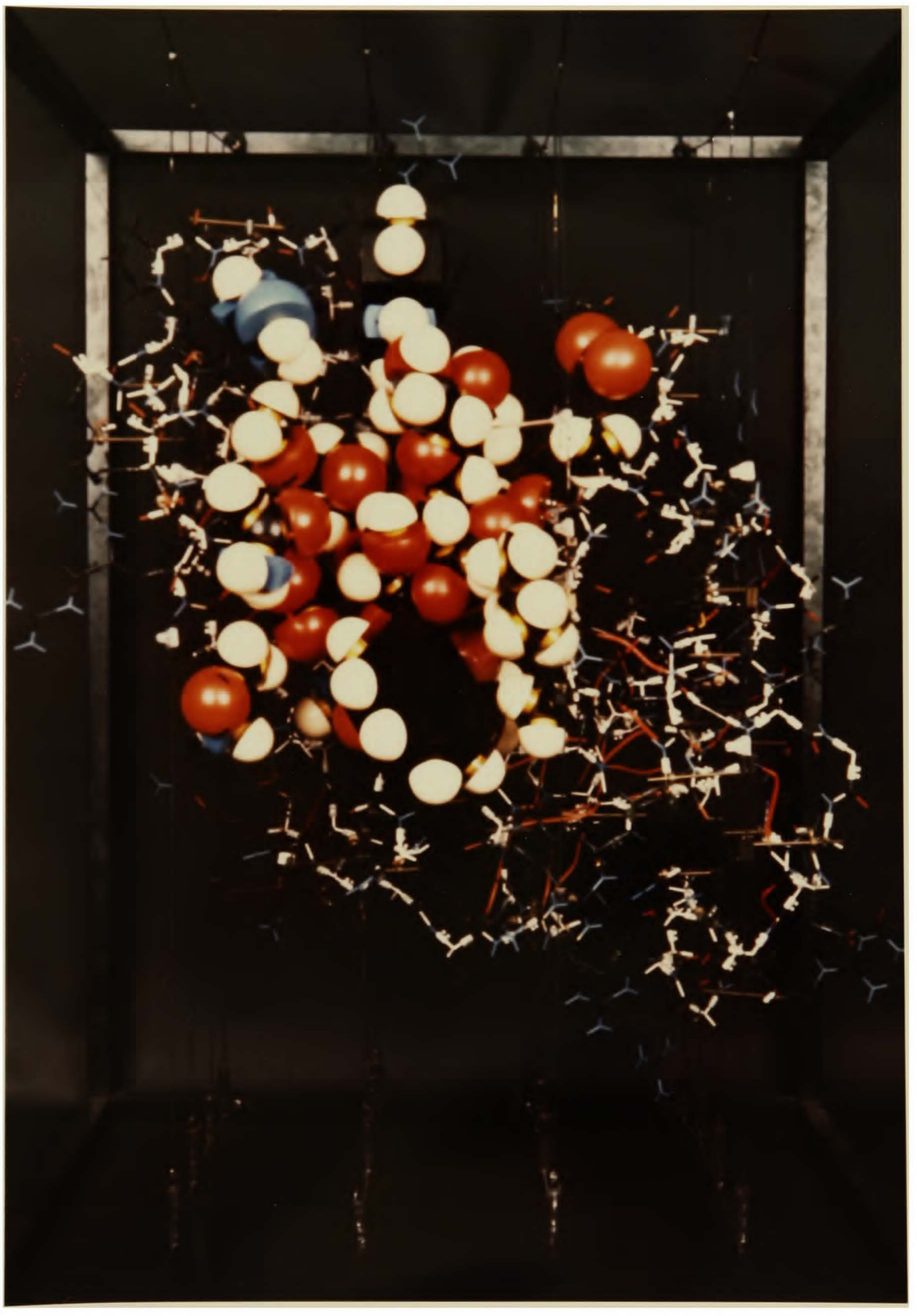

charide substrate models required distortion of the glucose residue in subsite D for accommodation into the active site cleft.

C. Synthesis of Substrate Analogues and Preparation of Crystals of Lysozyme

1. Chemical Synthesis of Substrate Analogues

a. Purification of Acid Hydrolysis Products of Chitin

Chitin oligosaccharide mixtures were prepared by hydrolysis of crustacean shell chitin (BDH Chemicals, Ltd.) in concentrated HCl at 40°C as described by Rupley (1964). The hydrolysate was cooled to below 20°C and slowly neutralised with NaOH at this temperature. The neutralised solution was filtered on a Büchner funnel and treated with activated charcoal until colourless. The pH was then adjusted to neutrality, and oligosaccharide products from 10 g of hydrolysed chitin were separated on a 4 x 108 cm column of Bio-Gel P-2 (Raftery *et al.*, 1969) with 0.1 M NH_4HCO_3 as solvent. Approximately 12 ml fractions were collected. Fractions under each peak were pooled, concentrated by evaporation *in vacuo*, and lyophilised. More highly purified oligosaccharide material was obtained by rechromatography with use of a 2 x 170 cm column of Bio-Gel P-4 (Beddell, 1970) with 0.1 M NH_4HCO_3 as solvent. The use of NH_4HCO_3 as solvent for separation of oligosaccharides in addition to satisfying ionic strength requirements for chromatography on Bio-Gel (Raftery *et al.*, 1969) retarded bacterial growth

in the effluent. Furthermore, since lyophilisation served to completely sublime the salt leaving behind the dry, hydrolysed product only, the use of NH_4HCO_3 also served to circumvent the costly application of ion-exchange resins to remove NaCl otherwise necessary for purification of oligosaccharides (Raftery et al., 1969; Beddell, 1970).

Chromatography of a partial acid hydrolysate on Bio-Gel P-2 gave the separation shown in Figure 15. Identification of oligosaccharides was carried out by descending paper chromatography in butanol : acetic acid : water : pyridine solvent (20:6:24:20) on Whatman 3 MM paper (Sharon and Seifter, 1964). Purified samples of chitobiose, chitotetraose, and chitohexose obtained from Dr. J. A. Rupley were used as controls.

b. Synthesis of β(aryl)-4-O-(2-acetamido-2-deoxy-β-D-glucopyranosyl)-D-glucopyranoside Substrate Analogues of Lysozyme

Conditions for synthesis of β-phenyl-linked mixed disaccharide substrates of lysozyme by the transglycosylation reaction have been described by Raftery and co-workers (Rand-Meir, et al., 1969; Dahlquist et al., 1969). Comparable conditions were employed to synthesise the 1-naphthyl, 2-naphthyl, p-bromophenyl, and 4-methyl-umbelliferyl derivatives in addition to the phenyl, and p-nitrophenyl analogues previously reported by Raftery and co-workers.

The synthesis of β(p-bromophenyl)-D-glucopyranoside tetraacetate is described in Section III.A.2. Deacetyla-

Figure 15.--Chromatography on a column of Bio-Gel P-2 of the partial acid hydrolysis mixture of crustacean shell chitin. The Roman numerals I-VI represent the peaks identified with each oligomer of GlcNAc from (GlcNAc) to $(GlcNAc)_6$. Fractions were approximately 11 ml in volume. The transmission of the effluent was monitored at 220 nm in a 0.1 cm flow cuvette, and fractions were monitored after the collection of the void volume of the column. Details of the chromatography conditions are provided in the text.

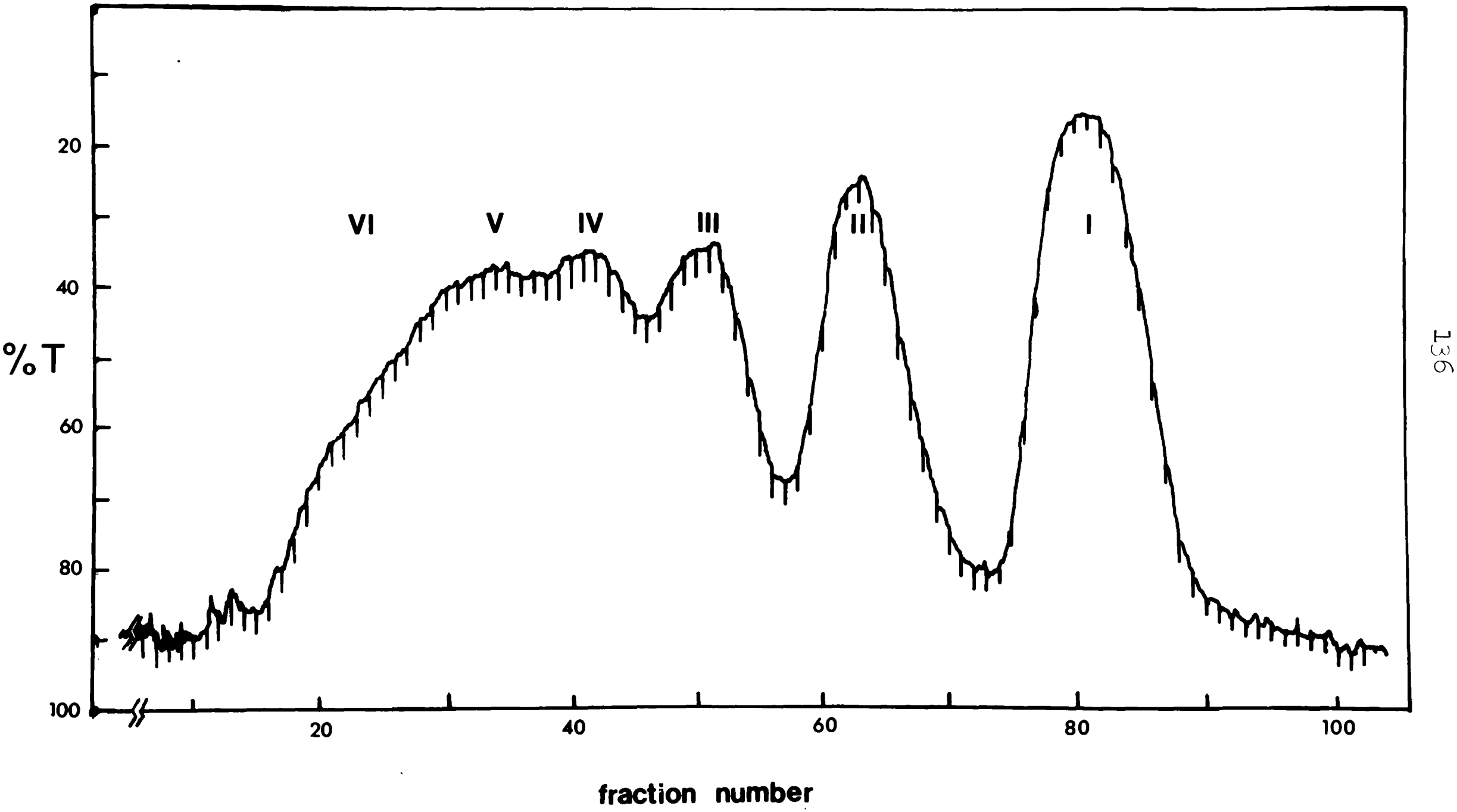
VI
V
IV
III
II
I
20
40
%T
60
80
100
20
40
60
80
100
fraction number

tion of the β(p-bromophenyl)-D-glucopyranoside-tetra-acetate derivative was carried out with use of barium methoxide in methanol at 0°C as described by Dahlquist et al. (1969). Barium ions were removed with Amberlite monobed MB-3 ion exchange resin, and the methanol solution of the deacetylated material was concentrated and evaporated in vacuo to dryness. This material was used in the transglycosylation reaction without further purification. Synthesis of other β-aryl-linked substrates was carried out with use of the corresponding purified β-aryl-D-glucopyranoside obtained commercially (Koch-Light Laboratories, Ltd.). The transglycosylation reaction method was found to give comparable yields of disaccharide products starting either from equivalent weights of purified chitotetraose and chitobiose or from mixtures of chitohexose, chitopentose, and chitotetraose. Consequently oligosaccharide materials in peaks IV-VI (Figure 15) were not further purified before use in transglycosylation catalysed syntheses.

The reaction mixture containing enzyme, products, and unreacted starting materials was neutralised and applied to a 4 x 180 cm Bio-Gel P-2 column with 0.1 M NH_4HCO_3 as solvent. Separation of products was monitored at an appropriate wavelength for each derivative with a Beckman DB spectrophotometer. A flow-cell with a path-length of 0.1 cm was used. A typical chromatogram for the separation of the β(1-naphthyl)-4-O-(2-acetamido-2-deoxy-

β-D-glucopyranosyl)-D-glucopyranoside derivative is shown in Figure 16. Fractions under each peak were pooled and lyophilised. Further purification of lyophilised products from unreacted oligosaccharides was achieved with a 2 x 50 cm column of Sephadex LH-20 using a 1:1 (v/v) mixture of methanol and water. This procedure served to separate efficiently the β(aryl)-disaccharide (Peak II, Figure 16) from the unreacted β(aryl)-glucopyranoside (Peak I, Figure 16) as well as from unreacted chitobiose.

Chemical identification of purified mixed saccharide substrate analogues was obtained by elemental analysis and mass spectrographic analysis. These are summarised in Table 24, wherein the results for the p-nitrophenyl derivative confirm those of Rand-Meir et al. (1969). On the basis of these results the separation pattern of other aryl-linked substrates was assumed to be analogous. Higher oligomers of the β(aryl)-linked substrate analogues (Peaks III and IV, Figure 16) were also readily separated from each other by molecular weight. Mass spectrographic analysis of the purified oligosaccharides indicated the absence of unreacted oligomers and served to establish the chemical composition of purified reaction products. For a typical reaction mixture containing 0.5 g lysozyme (Sigma Chemical Co., Ltd.), 0.5 g oligosaccharide and 0.5 g β(aryl)-D-glucopyranoside, approximately 0.025 g of the purified disaccharide product was obtained. Smaller yields of higher molecular weight β-aryl-glucopyranosyl oligomers

Figure 16.--Chromatography on a column of Bio-Gel P-2 of a reaction mixture of HEW lysozyme and β(1-naphthyl)-D-glucopyranoside and oligomers of GlcNAc. E refers to the fractions containing lysozyme. The peaks labeled I, II, III, etc. represent fractions found to contain respectively unreacted glucoside naphthyl-glucopyranoside, GlcNAc-Glc-naphthyl (NGN), and higher molecular weight oligomeric mixed saccharide substrates with two or more GlcNAc units linked distally to the glucose moiety at the C4' position (NNGN, etc.). The material in each series of pooled fractions corresponding to the separate peaks was identified by mass spectrometry. The transmission of the effluent was monitored at 285 nm in a 0.1 cm cuvette. Spectrophotometric monitoring of the fractions began at the beginning of the collection of the void volume of the column. Details of the chromatography conditions are provided in the text.

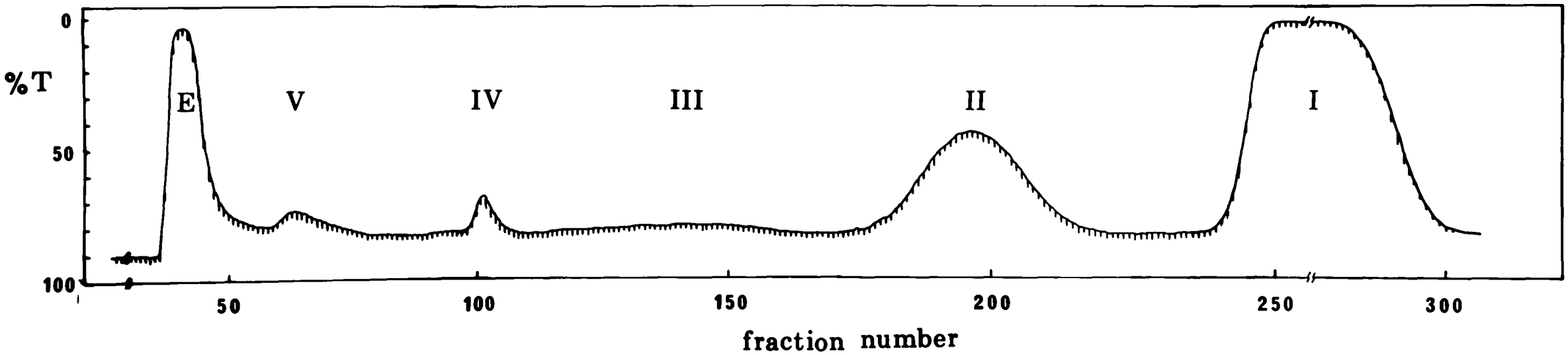
0
%T
50
100
E
V
IV
III
II
I
50
100
150
200
250
300
fraction number

TABLE 24

COMPARISON OF CHEMICAL ANALYSES OF β(AROMATIC)-LINKED MIXED SACCHARIDE SUBSTRATES OF LYSOZYME

Compound*	Chemical Formula	Mol. Wt.	Elemental Analysis % Composition	Theor.	Exptl.	Comments
GlcNAc-Glc-p-nitrophenyl	$C_{20}H_{28}O_{13}N_2$	504.44	C	47.61	48.13	Mass spectrographic analysis+ identified molecular ions of GlcNAc-Glc and GlNAc moieties only.
			H	5.59	6.32	
			N	5.55	3.13	
GlcNAc-Glc-(1-naphthyl)	$C_{24}H_{31}O_{11}N$	509.50	C	56.57	52.80	Mass spectrographic analysis+ identified molecular ions of GlcNAc-Glc and GlNAc moieties only.
			H	6.13	6.07	
			N	2.74	3.67	
$(GlcNAc)_3$-Glc (1-naphthyl)	$C_{40}H_{57}O_{21}N_3$	915.88	C	52.45	49.80	Mass spectrographic analysis+ identified molecular ions of GlcNAc, $(GlcNAc)_2$, $(GlcNAc)_3$, and $(GlcNAc)_3$-Glc moieties only.
			H	6.27	6.59	
			N	4.58	4.49	

*GlcNAc ≡ N-acetylglucosamine residue; Glc ≡ glucose residue.

+Kindly performed by Dr. J. D. Priddle of the Laboratory of Molecular Biophysics.

were obtained corresponding to peaks III and IV in Figure 16. These were shown by mass spectrometry to correspond to oligomers containing respectively two and three residues of GlcNAc distal to the glucose ring.

2. Preparation of Lysozyme Crystals for Low Temperature Studies

a. Crystallisation of Hen Egg White and Human Lysozyme

Lysozyme was obtained as a thrice-crystallized and lyophilized product from Sigma Chemical Co., Ltd., and used without further purification. Tetragonal crystals of hen egg white lysozyme were prepared from solutions containing 5-7% (w/v) protein, 5% NaCl (w/v), and 0.02 M sodium acetate, pH 4.7, at ambient temperature as described by Moult (1970). These crystals belong to space group $P4_32_12$ with unit cell parameters of $\underline{a} = \underline{b} = 79.1$ Å, $\underline{c} = 37.9$ Å (Blake *et al.*, 1967).

Crystals of human lysozyme purified from urine of leukemic patients by Dr. E. Osserman were obtained from Dr. C. C. F. Blake in connection with previous x-ray studies (Blake and Swan, 1971; Banyard, 1973). These crystals were obtained from solutions containing 2% protein in 7 M NH_4NO_3 buffered with 0.02 M sodium acetate at pH 4.7. The crystals belong to space group $P2_12_12_1$ with unit cell parameters of $\underline{a} = 57.1$ Å, $\underline{b} = 61.0$ Å, $\underline{c} = 33.0$ Å and $z = 4$ molecules/unit cell (Banyard, 1973). However, since aggregate and multiply twinned crystals are predominantly formed, other methods of crystallisation were sought.

Human lysozyme was chromatographed on a 4 x 180 cm of Bio-Gel P-2 column in 0.1 M NH_4HCO_3. Fractions of the protein only in the first peak appearing immediately after collection of the void volume were pooled. The protein was lyophilised and redissolved for crystallisation as described by Banyard (1973). Crystals appeared after a period of approximately one year but with identical morphology and multiply twinned forms. In contrast to crystallisation of the cruder protein provided from Dr. Osserman's laboratory, solutions of the chromatographed protein contained no precipitated amorphous material and were considerably less discoloured.

b. Effect of Organic-Aqueous Co-solvents on Crystalline Lysozyme

Attempts to crystallize lysozyme (5-20% w/v) directly from solutions of 50% (v/v) ethylene glycol saturated with sodium chloride at pH 4.7 failed to produce crystals at either ambient or sub-zero (-20°C) temperatures. Crystals of lysozyme were consequently stabilised for sub-zero temperature studies by slow equilibration with high concentrations of MPD.

Crystals were transferred in their mother liquor to separate vials and freed of excess solvent by gentle removal of adherent drops of solvent with strips of filter paper. An aliquot of a solution of MPD, buffered with 0.02 M acetate at pH 4.7 and precooled to 0°C, was gently layered on the crystals and the vial placed on ice for

overnight equilibration. Crystals could then be brought to ambient temperatures with no harmful effects. For tetragonal hen egg white lysozyme, 80% (v/v) MPD was sufficient to prevent dissolution of the crystals, and for human lysozyme a 90% (v/v) concentration was necessary. Crystals prepared in this manner exhibited no change in birefringence properties under examination in the polarising microscope. In addition to 0.02 M sodium acetate at pH 4.7 the mixtures contained 0.005 M NaCl or NH_4NO_3 to retard possible loss of the protein bound anion.

In Figure 17 the HK0 view of a precession photograph of a crystal of tetragonal lysozyme equilibrated with 80% (v/v) MPD is compared to that of the native enzyme. No change in unit cell parameters was observed. Furthermore, multiple freeze-thaw cycles of crystals treated with MPD resulted in no change in either the clarity or distribution of intensity of the diffraction pattern. Comparable results have been also reported by Petsko (1975).

Comparison of the MPD treated crystal to that of the native enzyme indicates, however, noticeable alteration in the distribution of diffracted intensity by introduction of the organic solvent. These changes are presumed to arise from two separate sourses. Low order reflections are expected to be sensitive to changes in the solvent composition in the crystal (Bragg and Perutz, 1952). Furthermore, a variety of alcoholic and polyol

Figure 17.--HKO precession photographs of tetragonal HEW lysozyme. Photograph A illustrates the diffraction pattern of a crystal of lysozyme equilibrated with 8% (w/v) sodium chloride buffered to pH 4.7 with 0.02 M sodium acetate. Photograph B illustrates the corresponding diffraction pattern of a crystal equilibrated at 0°C with an 80% (w/v) aqueous mixture of 2-methylpentane-2,4-diol buffered to pH 4.7 with 0.02 M sodium acetate. The pattern observed in photograph B remained unchanged with repeated freeze-thaw cycles of a crystal dipped into liquid nitrogen. Both HKO and HOL views indicate no significant alteration in unit cell parameters upon equilibration with the organic cosolvent mixture. Limiting resolution of photographs is 2.5 Å.

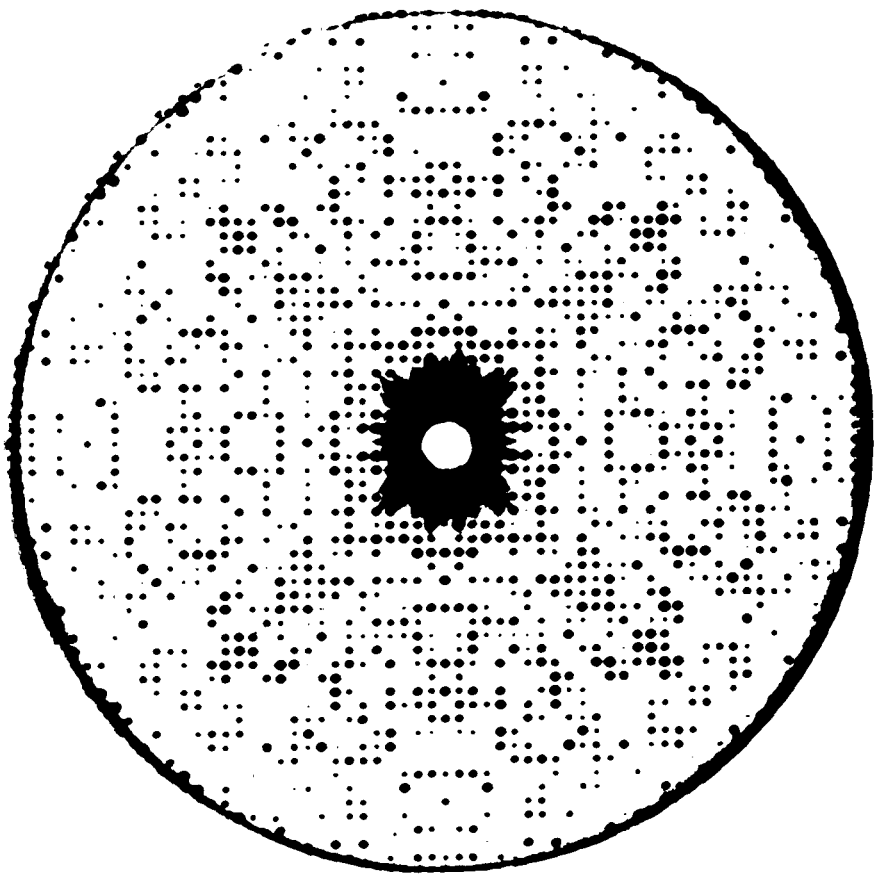

A

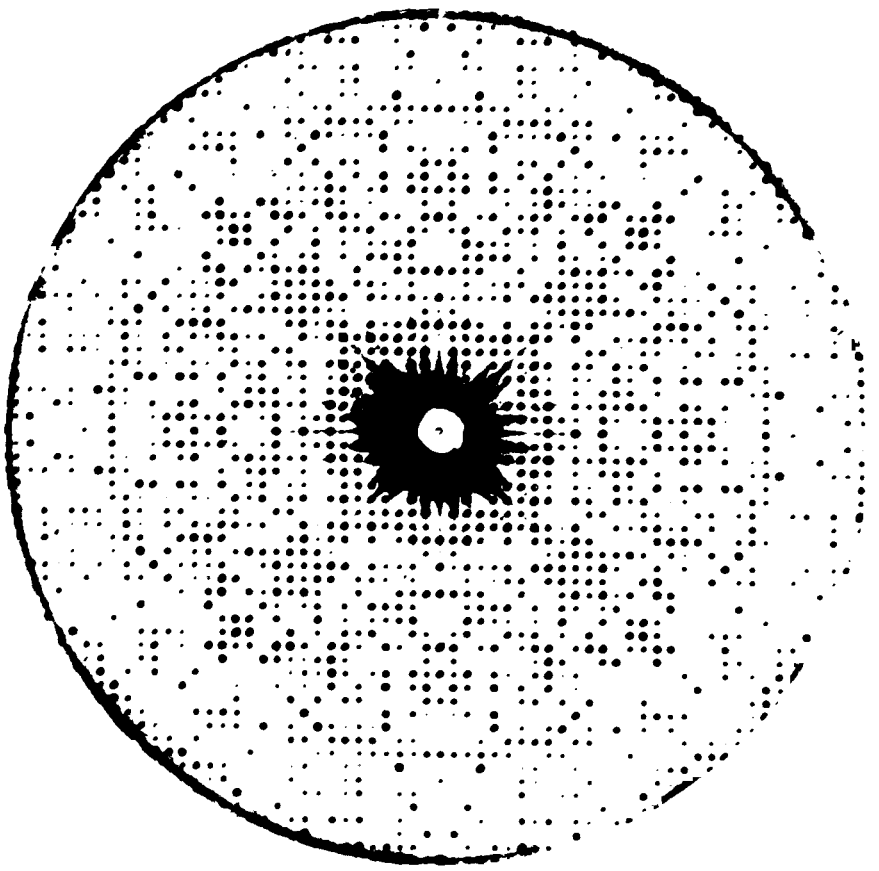

B

substances have weak binding affinities to residues in the active site cleft, presumably those residues involved in binding the carbohydrate hydroxyl groups of the substrate molecule (Ikeda and Hamaguchi, 1970). The high concentration of MPD is, thus, consistent with weak binding of the cosolvent molecules to the enzyme and could be reflected on this basis in the diffraction pattern. The weakly bound cosolvent molecules should be readily displaced upon introduction of oligomeric substrates even at low concentrations (Kuramitsu, Ikeda, and Hamaguchi, 1973). Comparable treatment of human lysozyme crystals in 90% MPD results in no loss of crystallinity and no change in unit cell dimensions, as determined by diffractometer data for crystals at sub-zero temperatures (G. A. Petsko, D. C. Phillips, and P. S. Rivers, unpublished observation).

Crystals of tetragonal lysozyme were also observed to remain stable in mixtures of buffered 70% (v/v) ethanol at 0°C. Under these conditions, however, the lysozyme crystals did not remain stable upon introduction to ambient temperatures.

3. Enzymatic Activity of Crystalline Human Lysozyme

Rand-Meir *et al*. (1969) have observed that the activity of lysozyme towards mixed aromatic linked disaccharide substrates is significantly lower than against oligomers of GlcNAc. We have similarly observed comparable activity with use of the *p*-nitrophenyl and phenyl-

linked mixed disaccharide substrates. Hydrolysis of the β(1-naphthyl) and of the β(4-methyl-umbelliferyl) derivatives was observed with human lysozyme in solution, but the rate of the reaction appeared even lower than that with the p-nitrophenyl derivative and consequently was not further quantitated. Consequently, in view of the difficulty of otherwise readily assaying the hydrolysis of a substrate which can diffuse into enzyme crystals and in view of the intense absorptivity of p-nitrophenolate as the hydrolysis product of the p-nitrophenyl-disaccharide, this substrate analogue appeared suitable to determine whether crystalline human enzyme is catalytically active.

Human lysozyme crystals with multiply twinned and aggregated forms unsuitable for x-ray studies had been previously equilibrated overnight at 0°C in 90% (v/v) MPD buffered with 0.02 M acetate at pH 4.7 in connection with low temperature x-ray and spectroscopic studies. These crystals ranged in size from microscopic to $\leq$ 0.1 mm in their largest dimension. Since the crystals employed were the only remaining crystals in the laboratory at that time and their weight in MPD could not be readily estimated, they were separated into three approximately equal aliquots under microscopic examination. One aliquot was reequilibrated with 8 M ammonium nitrate buffered with 0.02 M acetate at pH 4.7. The supernatant was removed and to this aliquot of crystals 1.0 ml of a 0.004 M NGP solution in the same solvent was added. For the other two aliquots,

the supernatant cosolvent mixture was then removed, and to each aliquot of crystals was introduced 1.0 ml of an MPD:H_2O solution containing 0.004 M NGP. The ammonium nitrate containing mixture and one of the MPD containing mixtures were maintained at 37°C while the other MPD mixture was incubated at 20°C over a roughly two week period with frequent, gentle daily stirring of the suspensions. No further deterioration of the crystals was observed microscopically over this period. Aliquots of the supernatant of each mixture were removed at approximately 24 hr. intervals and diluted 1:10 with 0.05 M NaOH and the optical density recorded at 400 nm. Figure 18 illustrates a plot of the change in optical density with time. It is evident that hydrolysis of the substrate was observed as a continuous function of time only with the sample maintained in MPD at 37°C. No activity was observed in the ammonium nitrate mixture, and no activity was observed in the MPD mixture at 20°C until it was transferred to an environment at 37°C.

Although there were not sufficient crystals to quantitatively estimate the rate of hydrolysis as a function of crystal weight and estimated crystal surface area, it remained necessary to determine whether the hydrolysis of the substrate by crystalline lysozyme at 37°C was due entirely to molecules on the surface of the crystals or whether the substrate had penetrated into the crystals to be hydrolysed. To this end immunoglobulin with antihuman

Figure 18.--Illustration of the time dependent change in optical density at 400 nm of mixtures of human lysozyme crystals with the substrate GlcNAc-Glc-(p-nitrophenyl). Aliquots of the supernatant were removed from the reaction mixture and diluted with 0.01 M sodium hydroxide. Curve A represents the OD change of a mixture of crystals equilibrated in 90% (v/v) MPD buffered at pH 4.7 and kept at 37°C. Curve B illustrates the OD change of a mixture of crystals similarly equilibrated with 90% MPD maintained at 20°C. A slow increase in OD was observed when this mixture was brought to an environment of 37°C (OD increase is not shown). Curve C illustrates the OD change of a mixture of crystals equilibrated with 8 M ammonium nitrate at 37°C. Details of the hydrolysis assay are given in the text.

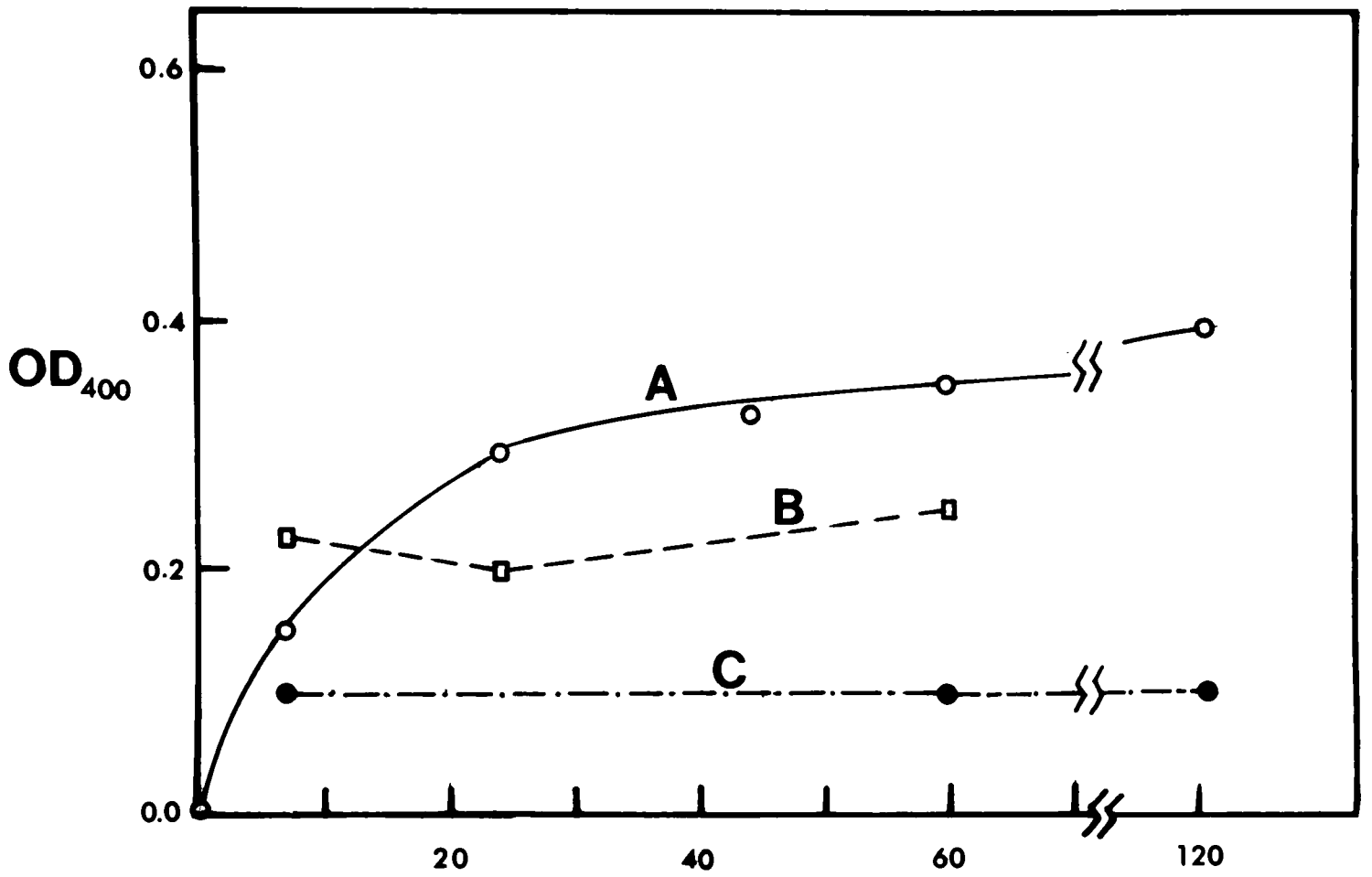
0.6
0.4
0.2
0.0
OD400
A
B
C
20
40
60
120
REACTION TIME IN HOURS

lysozyme activity was induced in rabbits and purified by Miss E. G. Press of the Department of Biochemistry. This anti-lysozyme antibody preparation was observed to have an inhibitory effect on lysozyme activity. Figure 19 illustrates a plot of the loss of lysozyme activity as estimated by lysis of a suspension of M. lysodeicticus cells (Shugar, 1952). The inhibitory effect on the change in light scattering of bacterial cells was observed in the presence of specific immunoglobulin only. On this basis, approximately 0.50 ml of the immunoglobulin solution was sufficient to completely inhibit the activity of 1 mg of human lysozyme. Assuming that a lysozyme molecule at the crystal surface occupies an area no less than 20 x 20 $Å^2$, this is sufficient antibody to coat approximately 1673 cm^2 of crystal surface area.

Since the immunoglobin preparation was precipitated in the presence of high concentrations of MPD, the immunoglobulin solution was made 8 M with respect to ammonium nitrate and 0.005 M in sodium phosphate of pH 6.5. Crystals from the mixture incubated at 37°C were washed several times with buffered 90% MPD over several days, and the excess solvent removed. The crystals were re-equilibrated first with 8 M ammonium nitrate at pH 6.5 and then incubated overnight with 5 ml of the immunoglobulin solution containing 8 M ammonium nitrate. No dissolution of the crystals was observed upon the antibody treatment. The crystals were then freed of excess solvent and

Figure 19.--Graphical illustration of the inhibitory effect of anti-human lysozyme antibody on lysozyme activity. Lysozyme activity was estimated on the basis of lysis of a suspension of M. lysodeicticus cells (Shugar, 1952). A 0.05 ml aliquot of purified human lysozyme (2% w/v) was first diluted in 0.95 ml of a 0.05 M sodium acetate solution at pH 4.7 into each of several tubes. To each was then added an aliquot of the purified rabbit antibody mixture as indicated in the graph. The mixture was then brought to 2.00 ml in volume and a 2.00 ml aliquot of M. lysodeicticus cells was added to each reaction mixture. The optical density at 450 nm was then monitored with a Zeiss PMQII spectrophotometer. The OD at 450 nm of a suspension of 2.00 ml of cells diluted to 4.00 ml with buffer and antibody only was 1.50 and remained constant. The results in the graph on the resultant ΔOD values after a 65 min reaction period. A parallel behaviour were observed for the reaction mixtures after a 1, 3, 5, 15, and 35 min reaction period. The extrapolated value for total loss of lysozyme activity is indicated in terms of the volume of antibody solution required to produce 100% loss of activity. Since the antibody preparation contains a mixture of nonspecific rabbit antibody proteins in addition to anti-lysozyme antibody, the equivalence of this value in terms of the quantity of specific anti-lysozyme antibody is not known.

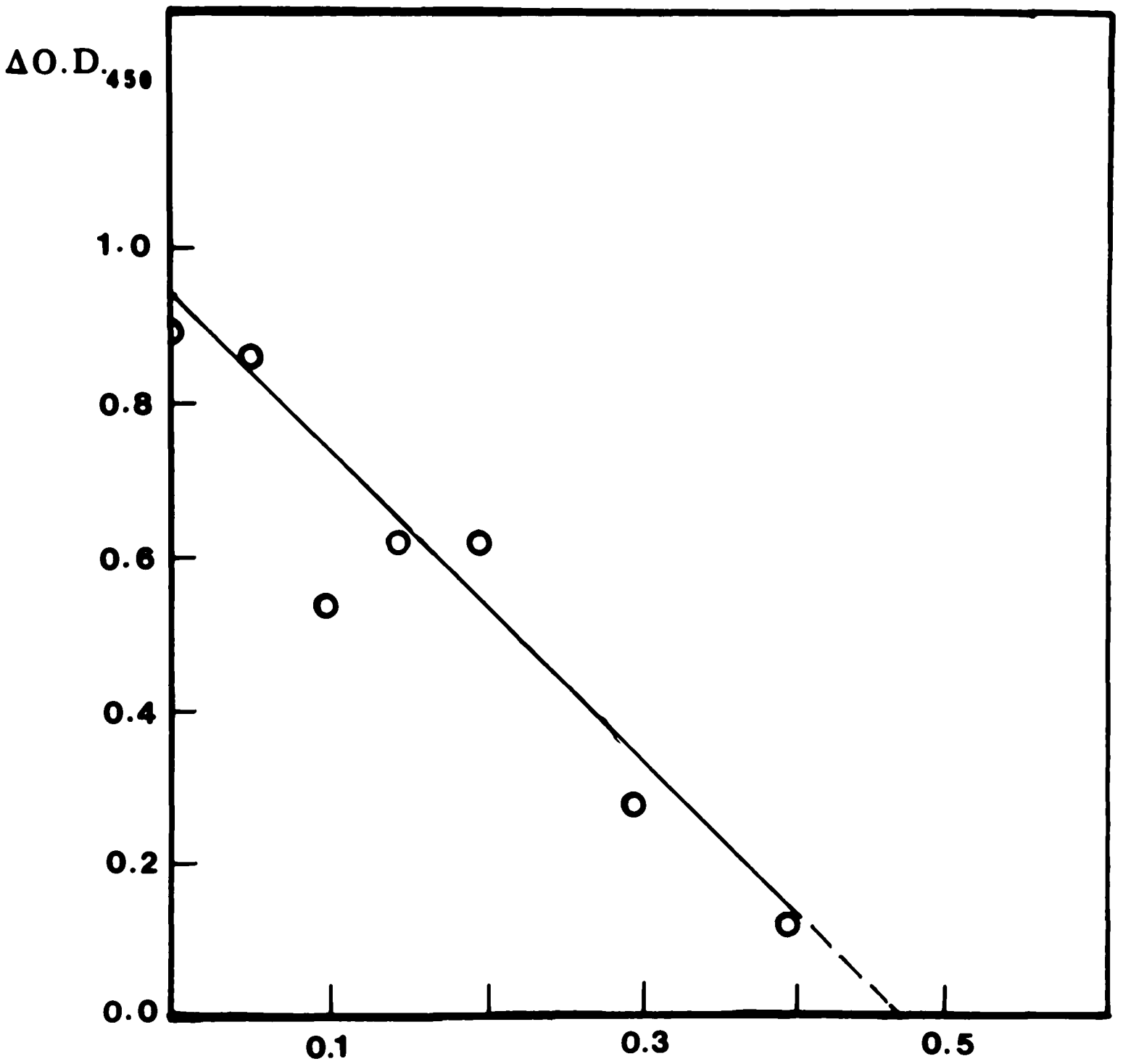
ΔO.D.450
1.0
0.8
0.6
0.4
0.2
0.0
0.1
0.3
0.5
ml IgG fraction
with anti-human lysozyme Ab

reequilibrated with 90% MPD at pH 4.7 containing 0.004 M NGP as previously. A series of control reaction mixtures was also carried out, and all solutions were incubated at 37°C. Aliquots of the reaction mixtures were removed as previously described, and the optical density at 400 nm recorded. The results are tabulated in Table 25.

Hydrolysis of the substrate was observed only in the presence of the antibody treated crystalline human lysozyme or in the presence of solubilised lysozyme in the absence of specific antibody. Since the immunoglobulin was precipated in solutions containing more than 50% (v/v) MPD, antilysozyme antibody adherent to the crystal surface would not be expected to become solubilised in the incubation mixture for the crystals.

While this result does not unambiguously demonstrate that the crystal surface molecules were inhibited by adherent anti-lysozyme antibody, the marked inhibitory effect of the specific immunoglobulin preparation and the general high affinity of antibodies for specific antigenic sites suggest that the activity of the surface molecules should have been inhibited. That the hydrolysis of the substrate is probably catalysed by molecules in the inner regions of the crystals is also suggested in consideration of the estimated λ_c for this substrate according to Equation 2.16. With use of the kinetic constants estimated for this substrate in aqueous solution by Rand-Meir et al. (1969) and an estimated range of D_i from 10^{-6} to

TABLE 25

COMPARISON OF ENZYMATIC ACTIVITY OF HUMAN LYSOZYME AND IMMUNOGLOBULIN MIXTURES

Composition of Reaction Mixture*	Observation of Increase in OD at 400 nm from Hydrolysis of NGP after Two Weeks at 37°C
Human lysozyme crystals after treatment with specific antilysozyme immunoglobulin in 90% MPD at pH 4.7	++
1 mg human lysozyme + 0.50 ml specific antilysozyme antibody in 40% MPD at pH 4.7	-
1 mg human lysozyme in 40% MPD at pH 4.7	+
1 mg human lysozyme + 0.50 ml nonspecific rabbit immunoglobulin (equal in protein concentration to antilysozyme antibody solution) in 40% MPD at pH 4.7	+
0.50 ml nonspecific rabbit immunoglobulin in 40% MPD at pH 4.7	-

*NGP concentration = 0.004 M; 40% MPD solutions were employed for solubilised proteins to prevent precipitation of immunoglobin. Total reaction volume = 2.0 ml.

10^{-8} cm^2/sec for the substrate, the calculated λ_c has limits of 0.8 to 0.2 mm. These are well above the largest dimensions of the crystals employed. We consequently conclude that the observed hydrolytic activity of the crystalline human lysozyme in MPD solvent at 37°C (Figure 18) had its origin not only from molecules on the crystal surfaces but also from molecules within the crystals. These results demonstrate that substrate molecules can be diffused into crystals of human lysozyme to be hydrolysed. Providing a substrate can be employed with a sufficiently high overall rate of hydrolysis, one can, furthermore, expect that application of low temperature mixed solvent methods can provide a means to stabilise a productive enzyme-substrate complex in crystals for investigation by spectroscopic and x-ray diffraction techniques.

Chapter IV

PRELIMINARY INVESTIGATIONS FOR THE DEVELOPMENT AND APPLICATION OF PARAMAGNETIC PROBES OF LOW-TEMPERATURE STABILISED ENZYME-SUBSTRATE COMPLEXES: APPLICATION OF MAGNETIC RESONANCE TECHNIQUES

A. Triplet State of the Phosphorescent Molecules

In Chapters I and III the need for spectroscopic probes of low temperature stabilised enzyme-substrate complexes has been discussed with particular emphasis on the objective of describing perturbed stereochemical and electronic configurations of the substrate molecule. The potential applicability of phosphorescent triplet state probes of enzyme-substrate interactions and the sensitivity of detection of perturbations expected through use of ESR and ENDOR techniques provide support to consider preliminary experiments to test their general suitability. To this end a variety of paramagnetic resonance studies were carried out on model compounds and lysozyme-substrate systems to evaluate the necessary conditions for detecting the paramagnetism of phosphorescent substrates. We describe here the results of these studies and provide a brief introduction into the basic theory of the spectroscopic measurements and their interpretations. Appropriate

references for the derivation of the equations of the spin hamiltonian are indicated.

After the pioneering studies of Lewis and Kasha (1944, 1945) who first recognised the phosphorescence of organic molecules as coming from the lowest triplet state, numerous investigations have confirmed the existence of a metastable paramagnetic state of phosphorescent molecules. Photoexcitation with ultraviolet light at cryogenic temperatures of a molecule diluted in a crystalline matrix or inert glassy solvent causes a one-electron promotion from the ground state S_0 into the singlet system. The molecule may return to its ground state from the S_1 singlet state with emission of fluorescence or may undergo the spin-forbidden process of intersystem crossing into the lowest triplet state T_0. As a molecule with a well characterised triplet state system, this is schematically illustrated for naphthalene in Figure 20. From the lowest triplet state the molecule may relax to the ground state with emission of phosphorescence or decay into the ground state by a nonradiative process. This phosphorescent state is paramagnetic, for there are two parallel unpaired electrons with resultant triplet spin multiplicity $[(2S + 1) = 3]$. The triplet manifold is consequently comprised of three spin components.

In the absence of an external magnetic field, the three spin components designated by the quantum numbers $M_s = 1$, 0, and -1 need not be degenerate for molecules of

Figure 20.--Energy diagram of the lowest excited singlet and triplet states of naphthalene. In the upper part of the diagram, the choice of molecular axes is indicated. The molecule is excited to the first excited singlet state S_1 by x-polarised absorption of ultraviolet light. Through intersystem crossing (ISC) the spin-forbidden process of singlet to triplet conversion occurs. The excess of vibrational energy is lost by radiationless processes and the molecule arrives in one of the three components of the lowest triplet state T_0. In the case of naphthalene the upper state is mostly populated, and radiation resulting from decay of the molecule to its ground state level S_0 is green and z-polarised.

In the right hand part of the figure the effect of introduction of a magnetic field parallel to the y-axis is illustrated. The upper and lower states of the T_0 system are mixed while the middle one remains unaffected. At three different magnetic field strengths ESR transitions occur as described in the text. These can be detected by monitoring the absorption of incident microwave power on the sample placed in the laboratory magnetic field or by monitoring the phosphorescence emission intensity in the presence of microwave irradiation (optical detection of magnetic resonance). See text for further discussion. [Figure from van Egmond (1973).]

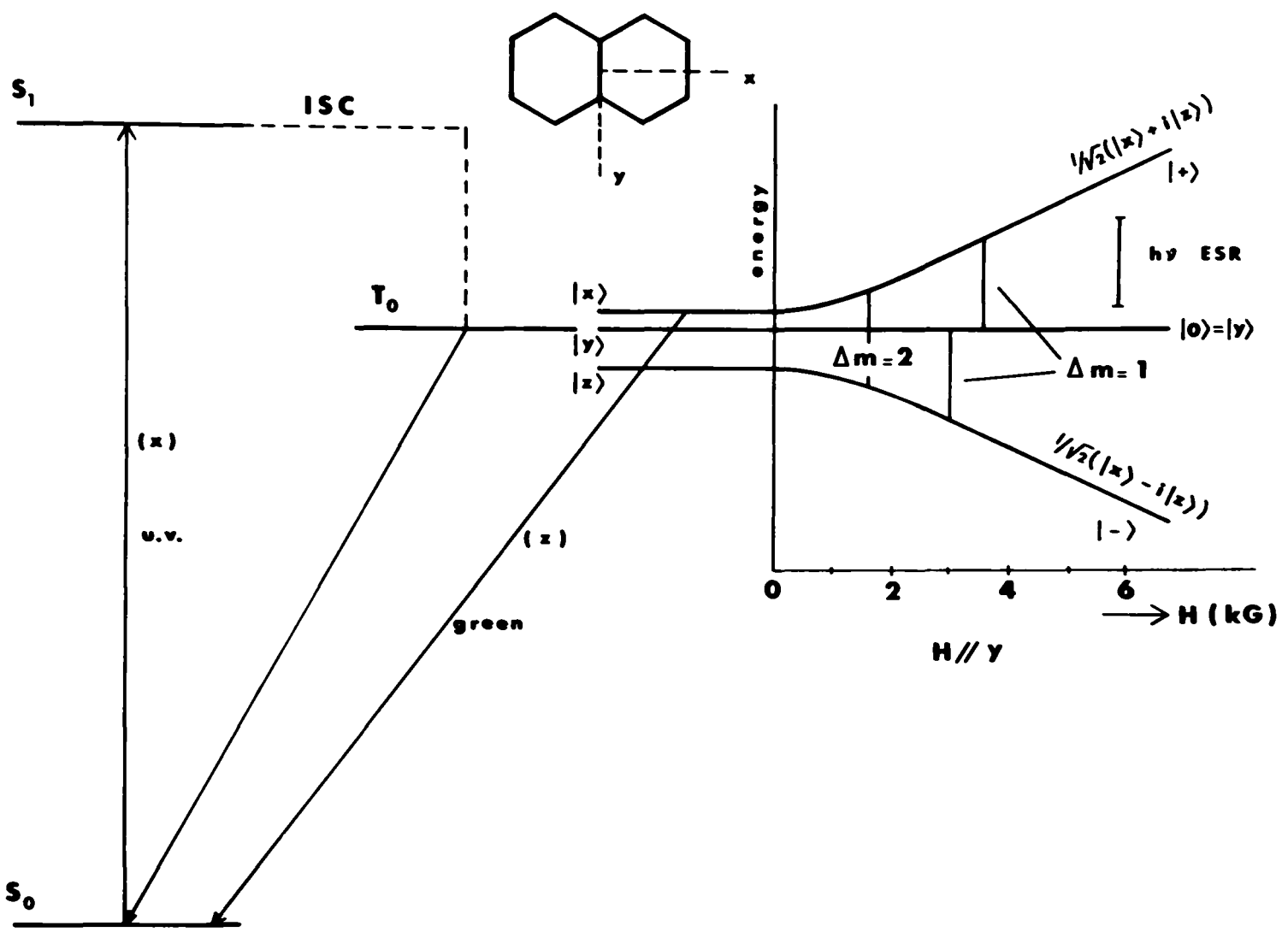
S1
ISC
x
y
T0
|x⟩
|y⟩
|z⟩
energy
1/√2(|x⟩+i|z⟩)
|+⟩
hν ESR
|0⟩=|y⟩
Δm=2
Δm=1
1/√2(|x⟩-i|z⟩)
|-⟩
0
2
4
6
H (kG)
H // y
(x)
u.v.
(z)
green
S0

low symmetry. Consequently a zero-field splitting can be observed between the substates of the triplet manifold. This splitting is determined by the magnetic dipole-dipole interaction between the two electron spins. The dipole-dipole interaction is given (van der Waals and de Groot, 1959) by the relation

$$\mathcal{H}_{ss} = \gamma_e^2 \left(\frac{h}{2\pi}\right)^2 \sum_{i<j} \left\{ \frac{\underline{s}_i \cdot \underline{s}_j}{r_{ij}^3} - \frac{3(\underline{s}_i \cdot \underline{r}_{ij})(\underline{s}_j \cdot \underline{r}_{ij})}{r_{ij}^5} \right\} \qquad (4.1)$$

where $\underline{s}_i$ and $\underline{s}_j$ are the spin angular momentum operators of electrons i and j, $\underline{r}_{ij}$ gives the position of electron i with respect to electron j, and γ_e is the magnetogyric ratio of the electron. The interaction energy is obtained by integrating over the spatial distribution of the electrons in the phosphorescent state T_0.

Within the triplet manifold the hamiltonian $\mathcal{H}_{ss}$ of Equation (4.1) can be written as a phenomenological spin hamiltonian (cf. Wertz and Bolton, 1972). With the substitution $\underline{\hat{S}} = \sum_i \underline{s}_i$ where $\underline{\hat{S}}$ is the operator for the total spin angular momentum

$$\mathcal{H}_{ss} = \underline{\hat{S}} \cdot \underline{\underline{T}} \cdot \underline{\hat{S}} \qquad (4.2)$$

where $\underline{\underline{T}}$ is the zero-field splitting tensor. Furthermore, the spin system of an organic molecule is weakly coupled to its own anisotropic environment so that spin dependent interactions are different for different orientations of the spin angular momentum with respect to the laboratory

magnetic field. If an axis system, x, y, z is chosen such that $\underline{\underline{T}}$ is diagonal and component terms involving $\hat{S}_x\hat{S}_y$, etc. vanish, $\mathcal{H}_{ss}$ reduces to

$$\mathcal{H}_{ss} = -X\hat{S}_x^2 - Y\hat{S}_y^2 - Z\hat{S}_z^2. \qquad (4.3)$$

If the molecule exhibits at least C_{2v} symmetry, then the principal axes of $\underline{\underline{T}}$ coincide with the molecular axes x, y, z. If the molecule has lower symmetry this need not be the case.

The parameters X, Y, Z are the zero field energies and satisfy the relationship

$$X + Y + Z = 0.$$

In the presence of an external magnetic field as in an ESR experiment, a Zeeman term appears in the spin hamiltonian and in this case the spin hamiltonian acquires the form

$$\mathcal{H} = \mathcal{H}_{ss} + \mathcal{H}_z = -X\hat{S}_x^2 - Y\hat{S}_y^2 - Z\hat{S}_z^2 - \gamma_e \frac{h}{2\pi} \underline{H}_0 \cdot \hat{\underline{S}} \qquad (4.4)$$

where $\underline{H}_0$ is the laboratory magnetic field. This equation can be rewritten in matrix form as

$$\mathcal{H} = g|\beta_e|H_x\underline{S}_x + g|\beta_e|H_y\underline{S}_y + g|\beta_e|H_z\underline{S}_z - X\underline{S}_x^2 - Y\underline{S}_y^2 - Z\underline{S}_z^2,$$

where $|\beta_e|$ is the absolute value of the Bohr magneton and an isotropic g factor is assumed. For this equation the eigenfunctions $|1\rangle$, $|0\rangle$, $|-1\rangle$ are a basis set of the complete hamiltonian. Solution of this equation can be then obtained, for instance, by subtracting W from each diagonal element to produce the determinant

$$\begin{vmatrix} g|\beta_e|H_z - \tfrac{1}{2}Z - W & 0 & -\tfrac{1}{2}(X - Y) \\ 0 & Z - W & \\ -\tfrac{1}{2}(X - Y) & 0 & -g|\beta_e|H_z - \tfrac{1}{2}Z - W \end{vmatrix} = 0$$

whereupon the parameters describing the trace of $\underline{\underline{T}}$ are generally designated as

$$D = -\frac{3}{2}Z \text{ and } E = -\frac{1}{2}(X - Y).$$

The hamiltonian (4.4) then becomes

$$\mathcal{H} = g|\beta_e|\underline{H}_0 \cdot \underline{\hat{S}} + D(\hat{S}_z^2 - \frac{1}{3}\hat{S}^2) + E(\hat{S}_x^2 - \hat{S}_y^2) \qquad (4.5)$$

and the energy levels of the substates of the triplet manifold become

$$\begin{aligned} W_x &= \frac{1}{3}D - E \\ W_y &= \frac{1}{3}D + E \qquad (4.6) \\ W_z &= -\frac{2}{3}D \end{aligned}$$

with axes chosen such that $|D| \geq |3E|$.

An ESR spectrum of a phosphorescent triplet state molecule is obtained by applying a microwave magnetic field to the photo-irradiated sample in the static laboratory magnetic field, and transitions are induced between spin states if their energy separation corresponds to the frequency of the microwave field. In general three ESR transitions are observed: one between the highest and lowest component (van der Waals and de Groot, 1959) generally designated as the $\Delta m = 2$ transition analogous to the atomic

case, and two transitions corresponding to $\Delta m = 1$ (Hutchison and Mangum, 1961). The positions of these lines become stationary when $\underline{H}_0$ is parallel to one of the principal axis directions. This allows one to determine the direction of the spin axes in the molecule and subsequently the zero-field splitting parameters.

The ESR spectra are often split by hyperfine interaction of the electron spin with the nuclear spins. This interaction is described by a term appearing in the spin hamiltonian.

$$\mathcal{H}_{HF} = \underline{\hat{S}} \cdot \underline{\underline{A}} \cdot \underline{\hat{I}}$$

where $\underline{\underline{A}}$ is the hyperfine tensor and $\underline{\hat{I}}$ is the nuclear spin operator. An evaluation of the hyperfine interaction of nuclei with the paramagnetic center leads directly to an estimate of the distribution of spin angular momentum in the system (Hutchison, 1967 and 1971). This evaluation is often simplified and determined most directly by application of ENDOR techniques, and it is on this basis that application of ENDOR methods may prove useful in evaluating the electronic structure of triplet state probes in enzyme-substrate complexes. Although ENDOR experiments were successfully carried out by repeating the results of Hyde (1965) on the tetracene cation in solution and of Ehret and Wolf (1968) on the triplet state of naphthalene in a durene crystal, we have been unable to detect ENDOR of triplet state substrate probes in glassy solvents or in enzyme

crystals. Consequently these studies will not be described further. Application of ENDOR to a nitroxide spin-label inhibitor of lysozyme is discussed in Chapter V.

In the absence of an external magnetic field, transitions between the substates of the triplet manifold can be observed by application of a microwave field of appropriate frequency. These transitions are linearly polarised in x, y, and z directions (as indicated in Figure 20), and the splitting of the electron spin states is independent of the orientation of the molecule. A transition is induced by a component of the microwave magnetic field along the corresponding direction of polarisation in the molecule. Since phosphorescence can result by decay from the triplet state manifold to the ground state and not all substates are associated with radiative decay processes, induction of a zero-field transition can then alter the emission intensity accordingly. On this basis rests the technique of optical detection of magnetic resonance (Schmidt and van der Waals, 1968; Schmidt, 1971; Kwiram, 1972) whereby the most precise determination of the zero-field splitting parameters can be made. These methods were subsequently employed to determine the influence of molecular environment on the electronic structure of a triplet state substrate probe of lysozyme and are discussed below.

B. Experimental Details

1. The ESR Spectrometer

The ESR spectrometer used in these experiments was a custom-built instrument designed and constructed by Dr. B. A. Coles of the Physical Chemistry Laboratory. It is a microwave superheterodyne spectrometer which was operated at a frequency of $9.030 \pm 0.001 \times 10^9$ Hz between 1000 and 5000 G. The cavity is a full wavelength, rectangular gold-plated copper cavity operating in the matched TE_{102} mode. Microwave power levels incident on the matched cavity ranged from 16 to 0.0015 milliwatts. Because of the cavity geometry and the multiple silica inserts employed for tuning, the microwave field amplitude $|\underline{H}_1|$ cannot be calculated. The static laboratory magnetic field was calibrated with use of a proton tracking device (Coles, 1972) between 2000 and 5000 G and with a Hall-effect probe at lower fields.

The temperature of the sample in the cavity for ESR experiments was controlled by use of a Heli-Tran, LTD-3-110 System (Air Products and Chemicals Inc., Allentown, Pennsylvania, U.S.A.) kindly loaned for use by Mr. A. G. Hutchins. The temperature of the sample was monitored by the Heli-Tran thermocouple probe on the heat exchanger at the bottom of the cavity dewar. This was previously calibrated against a second thermocouple at the sample position and indicated the temperature of vapourised helium surrounding the sample to within ±1°K.

For triplet state studies the sample was photo-irradiated with use of a 900 watt high pressure xenon lamp (Wotan XBO 900 W/2) with a 120 B/S (Transformers and Rectifiers, Ltd.) current supply unit. The lamp was mounted to an optical bench and aligned to the cavity of the spectrometer. The optical bench consisted of a water or $CuSO_4$ solution heat filter with a 28 mm path, a Jarrell-Ash 0.25 m single grating monochromator with variable slits, and 3 quartz optical lenses of 200 and 100 mm focal length. The optical bench is diagrammatically shown in Figure 21. Calibration of the monochromator was carried out with use of a low pressure mercury arc placed at the entrance slit while a selenium photodiode plate connected to a Philips microvoltmeter was placed with black electrician tape at the exit slit. The observed peaks of the mercury-emission spectrum were all found to agree to within ±0.5 nm of the known peaks (Harrison, 1939) between 600 and 250 nm.

Irradiation of the sample in the cavity of the spectrometer was accomplished by directing the beam of light through a quartz disc covered slot in the cavity wall directly at the level of the sample. Figure 22 illustrates a picture of the optical bench aligned to the entrance light slit of the cavity of the spectrometer. No variation in ESR signal peak height with time could be detected during steady state photo-irradiation of a sample.

Figure 21.--Diagrammatic illustration of the optical bench employed for photo-irradiation of triplet state molecules in ESR studies. A spherical front surface silvered mirror is adjusted for optimum focussing and attached to the lamp housing (not shown). The xenon arc source is a 900 watt (Wotan XBO 900 W/2) high pressure lamp connected to a current stabilizer and current supply unit. Lens A is of 200 mm focal length while lenses B and C are of 100 mm focal length. All lenses were made from a commercial optical grade of quartz. Between lens B and the entrance slit of the Jarrell-Ash 0.25 m single grating Ebert-type monochromator (indicated as grating) a heat filter of 28 mm in path length was placed. The lens positions were adjusted to achieve maximum throughput of light onto the sample placed in the ESR cavity.

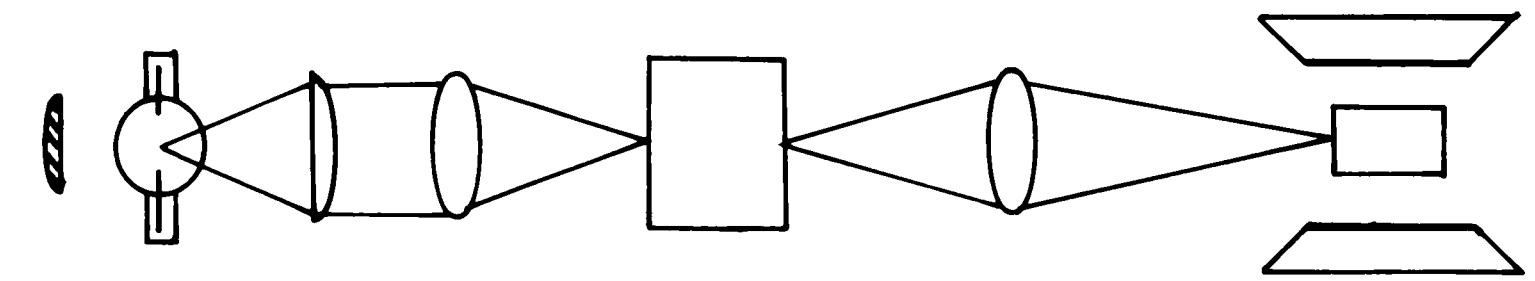
xenon
arc lamp
grating
cavity and
magnet
mirror
lens A
lens B
lens C

Figure 22.--Picture of the optical bench aligned to the ESR cavity in photo-irradiation studies. With reference to Figure 21, the following parts are identified: A, focusable mirror; B, lamp housing of xenon arc source; C, Jarrell-Ash single grating monochromator; D, cavity of ESR spectrometer; E, lens C (distal from the monochromator); the second smaller lens placed proximally had been tested to determine whether the light intensity incident on the cavity could be increased by correcting for spherical aberration of lens C; F, liquid helium transfer line of Air Products Heli-Trans System. Not visible are the xenon arc lamp and lenses A and B with the heat filter between the lamp source and monochromator.

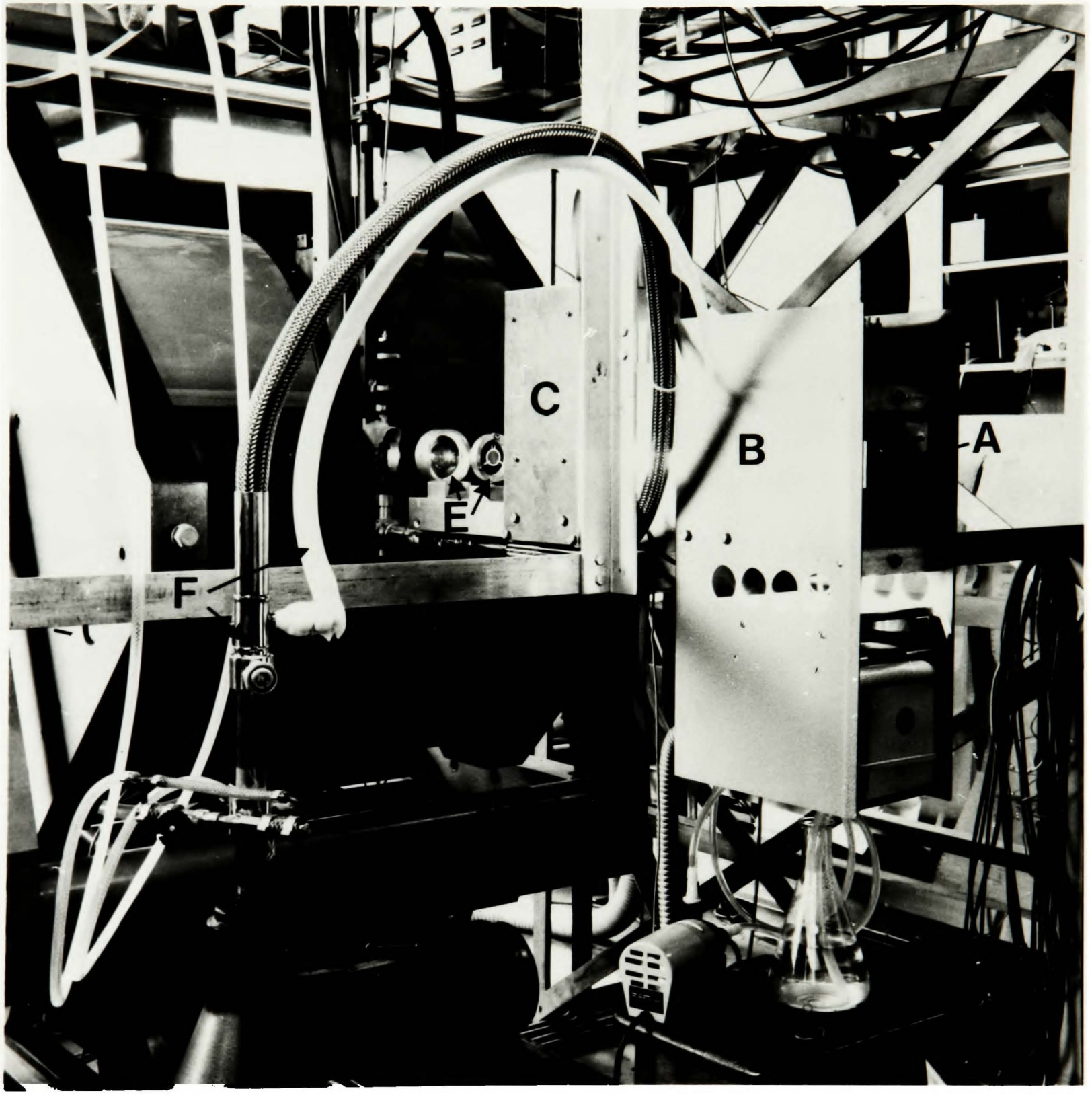
C
B
A
E
F

2. The Zero-Field Spectrometer

Experiments carried out in the laboratory of Professor J. H. van der Waals in the Kamerlingh Onnes Laboratorium at the University of Leiden employed a zero-field spectrometer with optical detection (Schmidt, 1971). This spectrometer has been described in numerous publications from that laboratory (Schmidt and van der Waals, 1968; Schmidt, 1971; Chan et al., 1971; Schmidt, Antheunis, and van der Waals, 1971). A Hewlett Packard HP 8690B sweep oscillator serves as the microwave source, and microwave power is fed through coaxial leads via an adjustable attenuator and a circulator to a helix. The sample is placed at the end of a quartz light pipe projecting into the helix at a position of maximum radiofrequency field. The light source was a Philips SP 1000 watt water-cooled superhigh pressure mercury arc directed at the sample through a heat filter of $NiSO_4$ and $CoSO_4$ (Kasha, 1948) and a glass filter (Schott and Gen. UG-5). The phosphorescence of the sample is detected with an EMI 9524B photomultiplier at the exit slit of a Jarrell-Ash 0.25 m single grating monochromator at the top of the quartz light pipe. Interference filters of suitable transmitting quality were placed at the entrance slit of the monochromator to insure that light from the arc source was excluded. The temperature of the sample for all experiments was in the range 1.3 - 1.5°K.

In steady-state experiments the sample is continuously irradiated as for ESR experiments. The signals were generally obtained with dc detection of the photomultiplier output. In the case of NGTA doped into a host matrix of the β(bromophenyl)-analogue, a "lock-in" amplifier could be used for signal detection.

The photomultiplier detected signal was fed into a Hewlett Packard 5480A storage display unit for improvement of signal-to-noise ratio as necessary. Microwave frequency calibration was carried out with the use of a Hewlett Packard 536A frequency meter.

3. Materials

Organic solvents of spectroscopic quality were used wherever possible. All reagents were otherwise of analytical reagent grade or of the highest grade available. Naphthalene was obtained as a zone-refined product ($\geq$ 99.9% purity) from Aldrich Chemical Co. Tryptophan was obtained from BDH Chemicals, Ltd. Other materials are described in Chapter III.

4. Phosphorescence Spectral Studies

Phosphorescence spectra were determined at the temperature of liquid nitrogen with use of a Perkin-Elmer MPF-2 fluorescence spectrophotometer with a phosphorescence attachment, kindly provided for use by Professor R. R. Porter of the Department of Biochemistry. Excitation and

phosphorescence emission spectra were determined of all materials prior to ESR studies. Phosphorescence lifetimes (τ_p) were determined on samples which had been previously degassed to at least 10^{-4} Torr.

C. Magnetic Resonance Studies of Triplet State Molecules

1. Preliminary ESR Studies of Model Compounds

Figure 23 illustrates the ESR spectrum of β(1-naphthyl)-D-glucopyranoside in ethanol at 5°K. In separate experiments it was determined that no change in peak position or shape occurred up to a concentration of 0.05 M, and that microwave power saturation effects were absent for the conditions indicated. This concentration range corresponds closely to that of naphthalene (Siegel and Goldstein, 1966) for avoiding spectral perturbations due to molecular aggregates and differential solubilities formed by temperature lowering and depolarisation of the high-field transitions through exciton effects. The polarisation of the transitions indicated in Figure 23 determined by the method of magnetophotoselection (El-Sayed and Siegel, 1966) is similar to that of the parent compound naphthalene. Table 26 compares the corresponding line positions of a number of derivatives in frozen alcoholic media. Table 27 provides a comparison of ZFS parameters determined by ESR methods. Comparison of our results for naphthalene with those provided by Wasserman et al. (1964)

Figure 23.--The high field ESR absorption spectrum of the photoexcited phosphorescent state of β(1-naphthyl)-D-glucopyranoside. The glycoside was dissolved to a concentration of 0.01 M in 95% (v/v) ethanol, and the solution was degassed with multiple freeze-thaw cycles during gas evacuation. The sample in a flattened narrow quartz tube was placed in the cavity and photo-irradiated as illustrated in Figure 22 with incident light at 315 nm. The high field spectrum was obtained with 25 decibel attenuation of microwave power (0.052 milliwatts) incident on the cavity. The magnetic field dependence of the ESR absorption intensity is recorded as a first derivative spectrum. The sample temperature is estimated as approximately 5°K. The central portion of the high field spectrum centered at $g = 2$ is not shown since the intense absorption arises from free radicals formed with solvent molecules by photoexcitation.

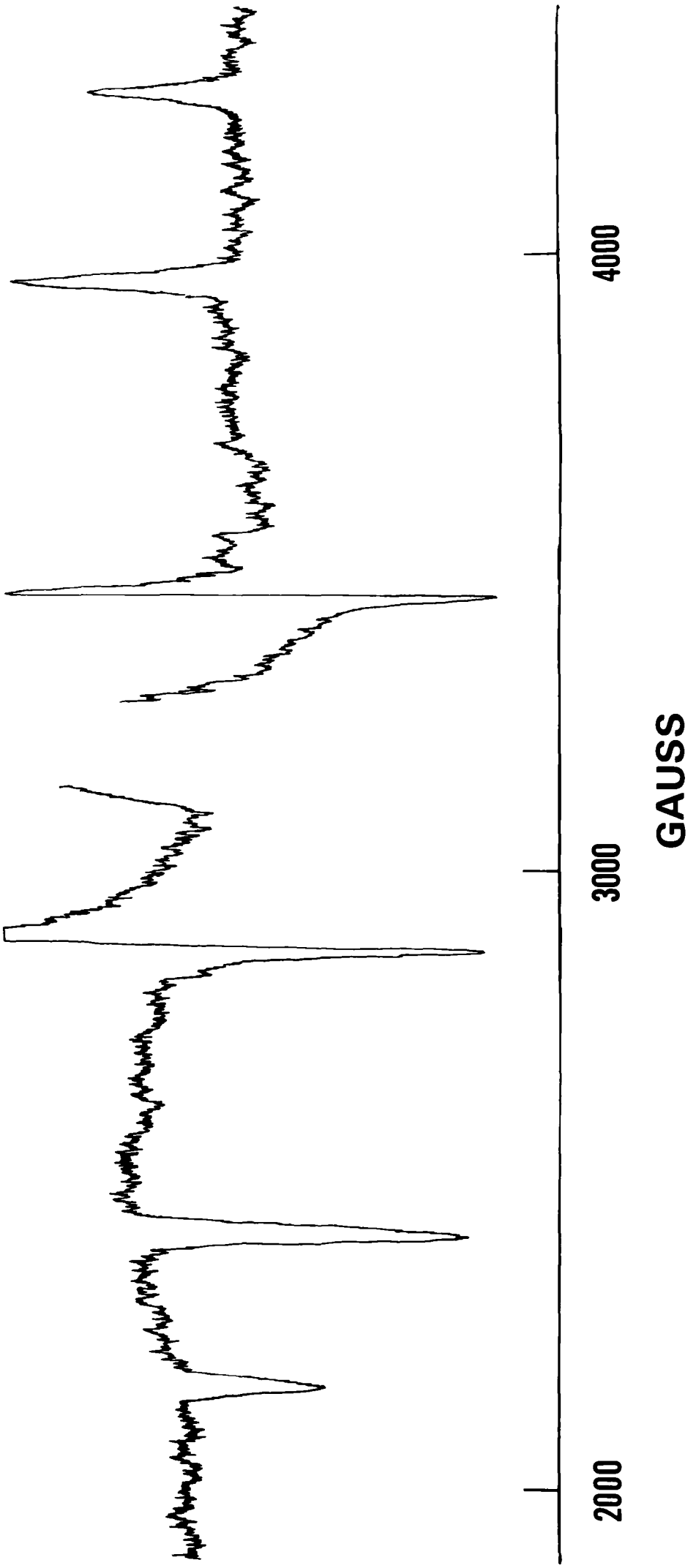
4000
3000
2000
GAUSS

TABLE 26

COMPARISON OF MAGNETIC FIELD POSITIONS OF ESR TRANSITIONS OF TRIPLET STATE MOLECULES IN FROZEN ETHANOLIC GLASSY MEDIA

Compound	τ_P (sec)	Transition* $\Delta m = 2$	$\Delta m = 1$					
		H_{min}	H_{x_2}	H_{x_3}	H_{y_2}	H_{y_3}	H_{z_2}	H_{z_3}
naphthalene	2.0	1469	2848.6	3448.8	2390	3989.4	2129	4308.5
β(1-naphthyl)-D-glucopyranoside	1.8	1472	2881	3453	2420	3956	2176	4264
NGN + lysozyme**	1.8	1476	2880	3453	2419	3960	2172	4264
α-naphthol	1.8	1483	2886	3454	2464	3923	2220	4223
L-tryptophan	4.2	1405	3005	#	2113	4275	2014	4402
β-phenyl-D-chitobioside	1.2	1215+						
phenol	1.2	1310+						

*Labeling of field positions is according to Kottis and Lefebvre (1963). Field positions were determined with samples at 5°K and are given in Gauss to an accuracy of ±1 G.

**At equimolar ratios at ~0.002 M concentration in 50% EG (w/v) at pH 4.7.

#Transition not resolvable because of intense line near g = 2 of photo-induced free radicals.

+Determined at 77°K. The chitobioside was kindly provided by Dr. G. Lowe of the Dyson Perrins Laboratory.

TABLE 27

ZERO-FIELD SPLITTING PARAMETERS* FROM $\Delta m = 1$ TRANSITIONS

Compound	X	Y	Z	$D(=-\frac{3}{2}Z)$	$E(=-\frac{1}{2}(X-Y))$
naphthalene ($C_{10}H_8$)	0.01829	0.04937	0.06789	0.1018	0.01554
perdeutero-naphthalene ($C_{10}D_8$)#	0.01837	0.04948	0.06780	0.1017	0.01556
β(1-naphthyl)-D-glucopyranoside	0.01753	0.04756	0.06511	0.09766	0.01502
α-naphthol	0.01742	0.04509	0.06244	0.09366	0.01384

*Parameters are given in units of cm^{-1}.

#Wasserman, Snyder, and Yager (1964). Results of perdeuterated naphthalene $C_{10}D_8$ in a frozen methyltetrahydrofuran glass at 77°K.

for perdeuterated naphthalene in a comparable glassy matrix is also made in order to indicate the precision of our measurements with reference to those of other investigators.

The ESR spectrum of the substrate analogue NGN in a glass was identical to that of β(1-naphthyl)-D-glucopyranoside in Figure 23 under comparable conditions. The low field signal of NGN could be observed for crystals of tetragonal lysozyme equilibrated with 80% MPD and 0.01 M substrate analogue. No high-field transitions of the substrate analogue under these conditions were observed for packed crystals or for oriented single crystals.

2. Optical Detection of Magnetic Resonance Studies of β(1-naphthyl)-D-glucopyranoside Substrate Analogues

In efforts to determine whether the photoexcited triplet state properties of phosphorescent substrates would be adequately sensitive to small configurational and environmental perturbations induced by binding to the active site of an enzyme, a series of zero-field magnetic resonance experiments were carried out in the laboratory of Professor J. H. van der Waals at the Kamerlingh Onnes Laboratorium of the University of Leiden with the assistance of Mr. W. G. van Dorp. The primary reason for attempting to apply optical detection methods of magnetic resonance in zero-field was that the sensitivity of

optical detection was known to be several orders of magnitude greater than conventional ESR techniques (Sharnoff, 1967; Schmidt, 1971; Kwiram, 1972; Geschwind, 1972) and that the measurement of the zero-field splitting parameters, as a monitor of environmental influences on the electronic structure of a molecule, is far more precisely carried out by zero-field methods (Schmidt, 1971; Kwiram, 1972). Since optical detection of magnetic resonance (ODMR), furthermore, can be carried out on randomly oriented samples, the need for precisely aligned single crystals of an enzyme-substrate complex could be circumvented in preliminary investigations.

In order to determine the extent of the influence of environment on the triplet state properties of a phosphorescent substrate analogue, the basic glycosidic structural unit of the β(1-naphthyl)-D-glucopyranoside molecule was incorporated into the different matrix environments compared in Table 28. These host matrix systems can be expected to provide a means to estimate the influence of the changes in environment of the substrate during the course of the enzyme catalysed reaction. They include the naphthyl-glucopyranoside substrate analogue in the solvent free of enzyme, the naphthyl-glucopyranoside in the solvent channels of enzymatically inactive tetragonal lysozyme crystals where the proximity of protein amine residues could alter the phosphorescent lifetime of the naphthyl chromophore, and the naphthyl-glucopyranoside

TABLE 28

COMPARISON OF MATRIX ENVIRONMENTS OF 1-NAPHTHYL CONTAINING MOLECULES IN ZERO-FIELD STUDIES

Compound	Matrix	Comments
β(1-naphthyl)-4-O-(2-deoxy-2-acetamido-β-D-glucopyranosyl)-D-glucopyranoside ≡ GlcNAc-Glc-naphthyl	Frozen glass of 80% MPD buffered to pH 4.7	Randomly oriented chromophore molecules with completely hydroxylic environment.
GlcNAc-Glc-naphthyl	Tetragonal ($P4_32_12$) HEW lysozyme in 80% MPD buffered to pH 4.7	Randomly oriented molecules in solvent channels of the crystal with no expected change in solvation. Chromophore may experience influence of protein side chain residues.
β(1-naphthyl)-D-glucopyranoside-tetraacetate ≡ NGTA	β(p-bromophenyl)-D-glucopyranoside tetraacetate	1-naphthyl chromophore doped into host crystal lattice may be expected to experience a totally hydrophobic environment.
GlcNAc-Glc-naphthyl	Orthorhombic ($P2_12_12_1$) human lysozyme crystals in 90% MPD buffered to pH 4.7	Active site region is accessible to substrate analogue and chromophore should experience environment of the hydrophobic cleft and catalytic side chains.

molecule doped into the host organic matrix of a structurally similar molecule providing a totally hydrophobic environment which could be considered, therefore, to approximate more closely the influence of the hydrophobic active site region of the enzyme. In addition, the matrix of the enzymatically active crystalline form of human lysozyme was also investigated. Optical detection studies were carried out for each matrix system.

a. ODMR Studies of Molecular Crystals of NGTA

A suitable crystalline host matrix of NGTA was found by crystallographic measurements and cocrystallisation studies (Section III.B.1.) to be that of the structurally similar bromophenyl derivative BPGTA. That the incorporation of NGTA into this host matrix under the crystallisation conditions employed resulted in a periodic substitution of NGTA for BPGTA molecules was first suggested by the phosphorescence emission spectrum of the doped crystals. In Figure 24 the phosphorescence emission spectra of NGTA doped into a BPGTA crystal is illustrated. This spectrum is identical in band shape and band position to that of NGTA in a frozen alcoholic glass. Although the concentration of NGTA in the crystal is not known, it can be expected to be no greater than 0.01 mole fraction by the cocrystallisation conditions. Since the bromophenoxy-residue exhibits some emission intensity of a structureless, broad-banded nature centered at 440 nm, we

Figure 24.--Phosphorescence emission spectrum of NGTA substitutionally doped into a host crystal lattice. The cocrystallisation conditions with use of BPGTA as the host lattice are described in the text. A single crystal was placed in a narrow diameter quartz sample tube and maintained at the temperature of boiling nitrogen in the sample compartment of the phosphorescence attachment of a Perkin-Elmer MPF-2 spectrometer. The incident exciting wavelength was 315 nm, and the emission spectrum was scanned with a constant bandpass of 5 nm. The shape and relative intensities of the bands remained unchanged upon rotation of the sample tube and crystal in the beam of incident unpolarised light. A comparable spectrum was observed in ODMR studies upon introduction of the filter conditions of the incident irradiation as described in the text. The emission at the maximum of the shortest wavelength band was 476 nm and was employed to monitor phosphorescence intensity in ODMR studies of the 1-naphthyl chromophore.

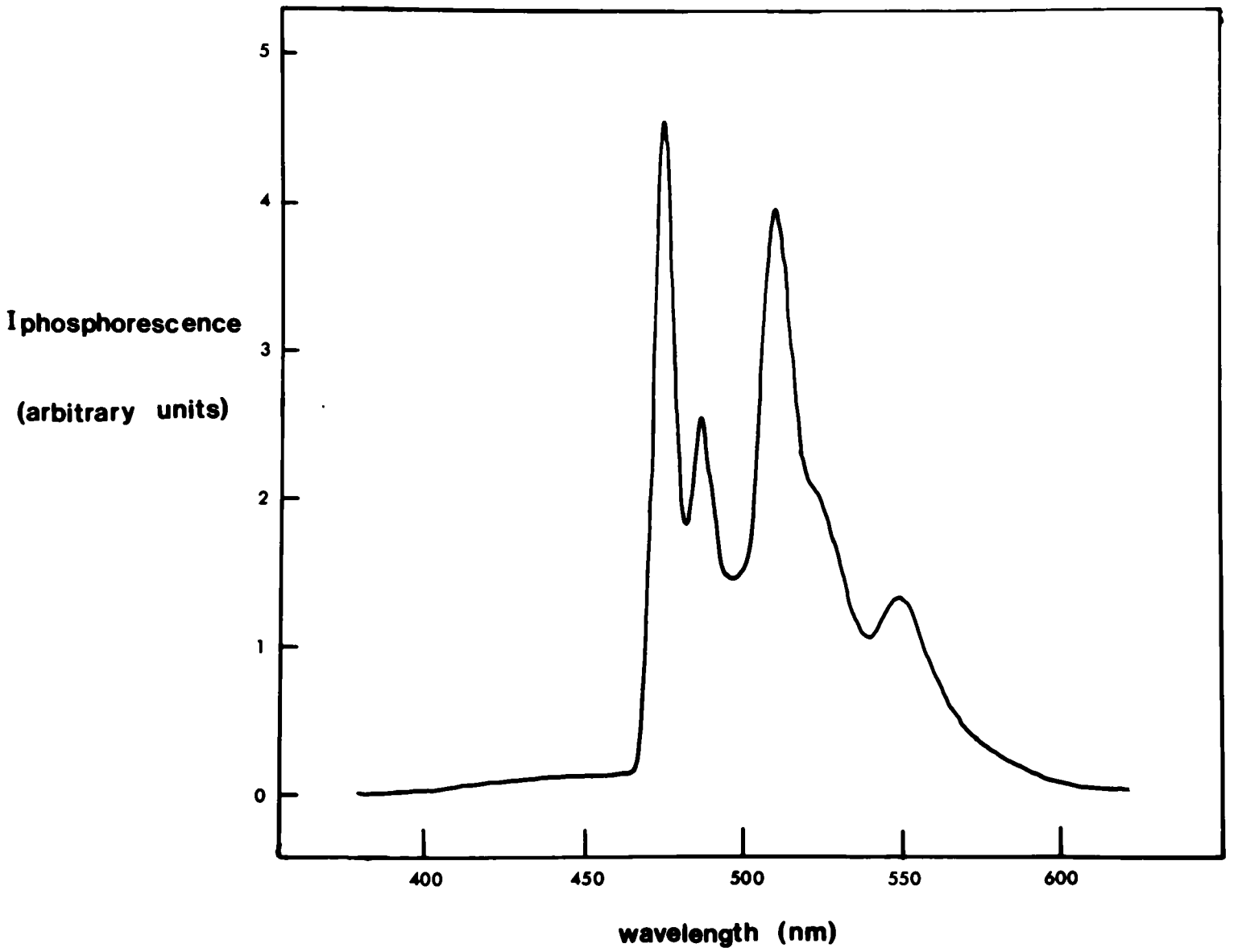
I phosphorescence
(arbitrary units)
5
4
3
2
1
0
400
450
500
550
600
wavelength (nm)

can conclude that in the crystal the naphthoxy residue is brought into an excited state by both direct light absorption and energy transfer from the host molecule. In view of the similar spectrum of the crystal to that of a dilute solution we can conclude that the doped crystal behaves essentially as a periodic lattice collection of electronically noninteracting molecular species and adheres to the criteria for an "oriented gas" of the molecule.

For initial experiments to determine the ZFS parameters of NGTA in a BPGTA host matrix, the super high pressure Hg arc source with only a $NiSO_4$-$CoSO_4$ solution and pyrex glass filter was used first as the exciting radiation. Phosphorescence intensity was monitored as described in Section IV.B.2. This resulted, however, in deterioration of the phosphorescence emission spectrum of the sample indicating that the host matrix was altered by strong light excitation. A prism monochromator with a numerical aperture of f/3.5, therefore, was employed to provide monochromatic light for selective excitation of the guest molecule at 315 nm. This arrangement of photo-excitation with phase sensitive detection of the phosphorescence emission intensity was continued for all further experiments to hinder the photo-induced deterioration of the host crystal lattice and was found satisfactory on the basis of stable phosphorescence emission spectra of the crystal in the cavity of the zero-field spectrometer. Under these conditions the total phosphorescence emission

lifetime (τ_P) was found to be 0.3 sec at 1.3°K. Since the total phosphorescence lifetime of the NGTA in an alcoholic medium is estimated at 77°K to be ~1.8 sec, the decrease in emission lifetime undoubtedly reflects the external spin-orbit coupling influence of the bromine atoms of the host molecule (McGlynn, et al., 1969).

Figure 25 compares the two optically detected zero-field transitions of NGTA in a BPGTA host crystal at 1.2°K. The spectra were recorded with phase sensitive detection of the emission intensity at 476 nm and with amplitude modulation at 20 Hz of the microwave power (estimated at approximately 100 milliwatts). The bands at half-maximum intensity are 2.3 MHz wide and are located at 858.8 and 2487.8 MHz respectively. The third zero-field transition, calculated on the basis of the two transitions in Figure 25 to lie at 3347 MHz was not detectable with lock-in amplification. However, a transition could be observed in the 3-4 GHz region by broad-banded sweeping of the microwave frequency.

b. ODMR Studies of β(1-naphthyl)-4-O-(2-acetamide-2-deoxy-4-O-glucopyranosyl)-D-glucopyranoside in Lysozyme Crystals

In order to assess the influence of environmental changes on the basic structural chromophoric unit of β(1-naphthyl)-D-glucopyranoside, ZFS parameters of the substrate analogue NGN were determined first in a frozen glassy

Figure 25.--The optically detected zero-field transitions of NGTA in a host crystal. The spectra were recorded with amplitude modulation of the microwave power at 20 Hz together with phase sensitive detection of the phosphorescence emission intensity by "lock-in" amplifier techniques. The sweep rate was approximately 0.15 MHz/sec. The sample temperature was 1.2°K. The transition near 2500 MHz, inadvertently illustrated as corresponding to an increase in phosphorescence emission intensity, corresponds to a decrease in phosphorescence emission.

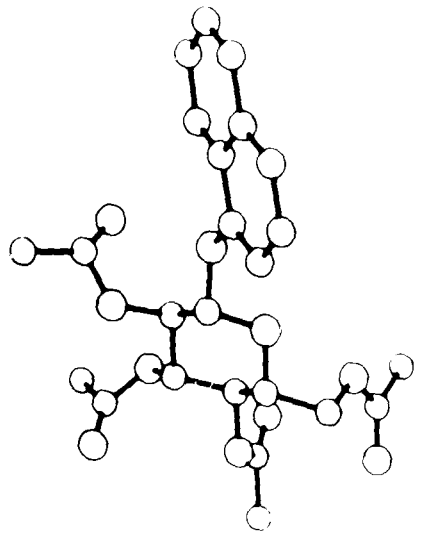

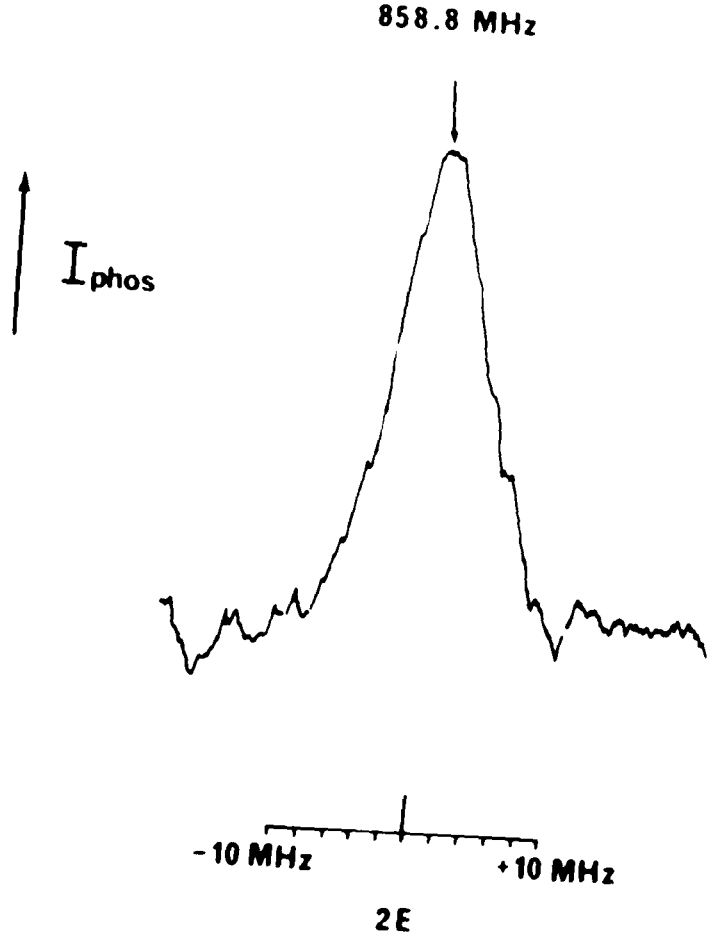
858.8 MHz
I_{phos}
-10 MHz
+10 MHz
2E

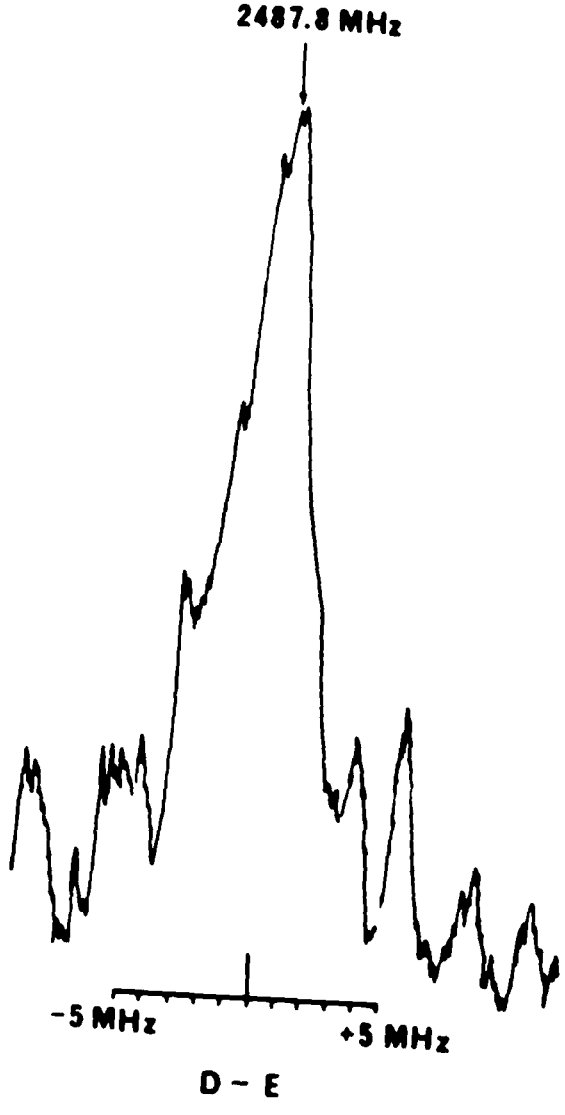
2487.8 MHz
-5 MHz
+5 MHz
D - E

matrix of buffered MPD. The total phosphorescence lifetime of the 1-naphthoxy chromophore under these conditions was determined as ~1.6 sec at 1.2°K, and application of the lock-in amplification technique did not prove feasible for signal detection. Peak positions for the zero-field transitions of NGN corresponding to those in Figure 23 for NGTA were consequently determined by calibrating the microwave frequency at suitable regions bracketing the two most intense zero-field transitions and estimating the line positions by linear interpolation. Under these conditions the change in phosphorescence emission intensity with a long lifetime, induced by approaching resonance with the microwave frequency, is complicated by the decay of the relatively long lived excited triplet state to the ground state as magnetic resonance conditions are approached by sweeping the microwave frequency. This complication was more pronounced for the transition near 2500 MHz for NGN in a hydroxylic frozen glass matrix than for the transition near 900 MHz.

Figure 26 illustrates the zero-field transition near 900 MHz of NGN in a frozen glassy matrix at 1.2°K. The same peak position was observed for 1 sec scans between 800 and 1000 MHz with either increasing or decreasing microwave frequency. The decay of luminescence intensity was not observed to affect the position of maximum emission intensity for scans of increasing or decreasing microwave frequency.

Figure 26.--The optically detected zero-field transition near 900 MHz of GlcNAc-Glc-naphthyl in a hydroxylic glassy matrix. The spectrum was obtained by signal averaging the dc detected emission intensity of 10 separate scans with use of a Hewlett Packard 5480A storage display unit. The spectrum was obtained by linear scans of the microwave frequency with 5 MHz frequency modulation using a sweep rate 200 MHz/sec. The sample temperature was 1.3°K. The spectrum is derived from scans of increasing microwave frequency.

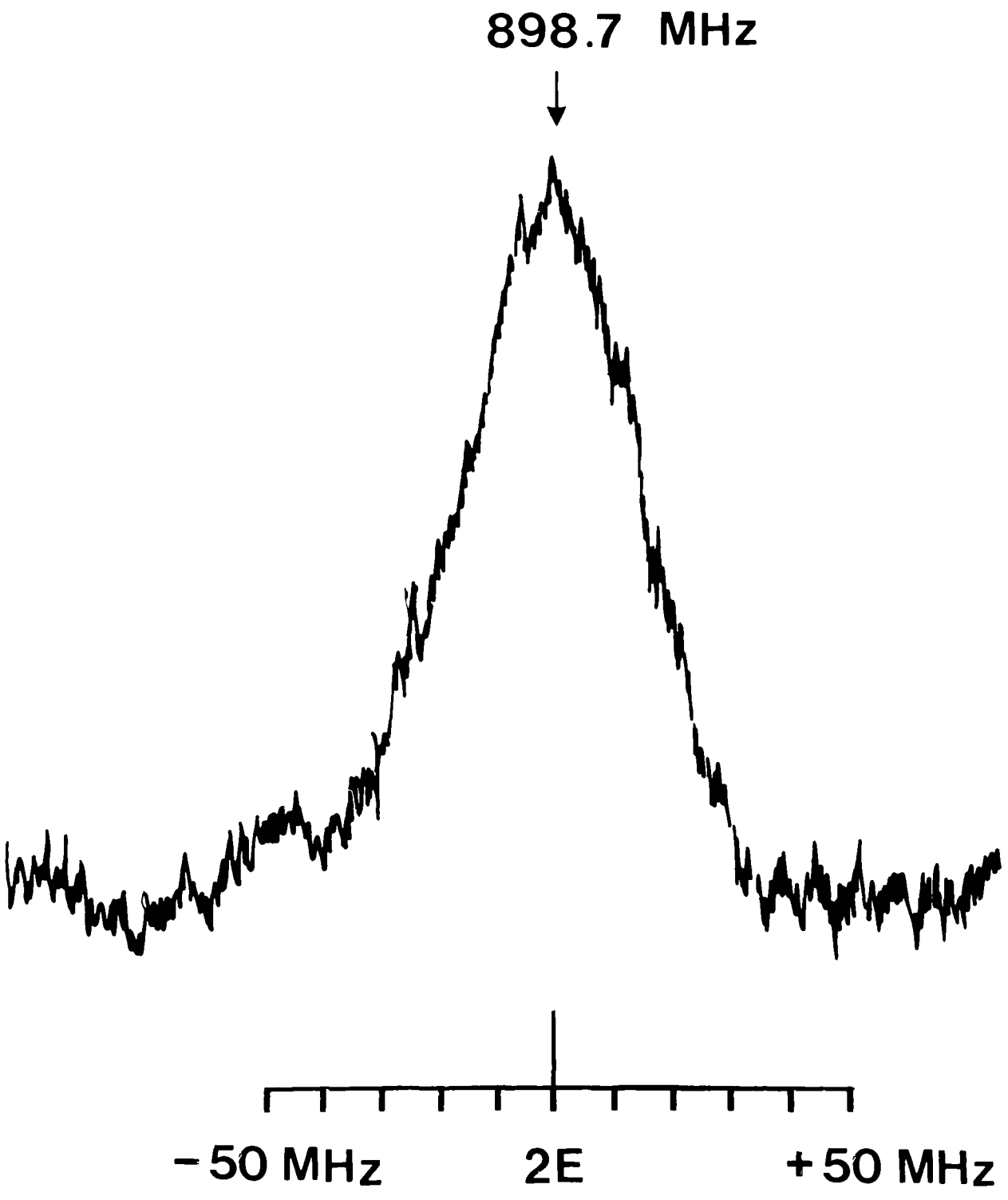
898.7 MHz
−50 MHz
2E
+50 MHz

The bandwidth at half-maximum intensity is estimated as ~36 MHz. On the other hand, the emission intensity changes for the transition near 2500 MHz were less favourable for analysis by this scan technique. The band position was not identical for scans of increasing and decreasing frequency, and the broad-bandedness of the transition and an apparent two-component decay of the phosphorescence emission complicated the graphical interpolation. The cross-over point, however, of the trace of the phosphorescence emission for scans of increasing or decreasing frequency was observed not to vary by more than ±3 MHz between 2400-2600 MHz. An average value of 2485 ± 6 MHz is estimated for the transition.

Comparable methods were employed to detect the zero-field transitions of NGN soaked with tetragonal HEW lysozyme crystals equilibrated with 80% MPD (Section III.C.2.a.). Here, comparable band widths were observed as for NGN in a frozen glassy matrix. Although the bandwidth of the transition near 900 MHz in the case of tetragonal HEW lysozyme crystals was 52 MHz, the band position could be estimated with use of lock-in detection for scans of increasing and decreasing frequency. The results are compared in Table 29 for the β(naphthyl)-D-glucopyranoside chromophore in the three solvent and crystal media.

Since the zero-field studies had no requirement for crystal orientation, the influence of the active site

TABLE 29

COMPARISON OF ZERO-FIELD TRANSITION ENERGIES AND CHARACTERISTICS OF 1-NAPHTHYL CONTAINING MOLECULES DETERMINED WITH USE OF OPTICAL DETECTION METHODS IN THE ABSENCE OF AN EXTERNAL MAGNETIC FIELD

Compound and Matrix	Transition	Transition Energy (in MHz)	Bandwidth at Half-Maximum Intensity (MHz)
naphthalene in ethanol*	2|E|	931.8	
	|D| - |E|	2586.0	
	|D| + |E|	3517.8	
naphthalene in durene single crystal#	2|E|	940	
	|D| - |E|	2601	2-3
	|D| + |E|	3541	
GlcNAc-Glc-naphthyl in frozen glass of 80% MPD	2|E|	898.7±5	36
	|D| - |E|	2485 ± 6	~50
	|D| + |E|	(3384**)	

GlcNAc-Glc-naphthyl in HEW lysozyme crystal in 80% MPD	$2\|E\|$	909 ±5	52
	$\|D\| - \|E\|$	2513	≤95
	$\|D\| + \|E\|$	(3422**)	
NGTA in BPGTA single crystal	$2\|E\|$	858.8 ±0.5	2.3
	$\|D\| - \|E\|$	2487.8	2.3
	$\|D\| + \|E\|$	(3346.6**)	
α-naphthol in ethanolic glass*	$2\|E\|$	829.5	
	$\|D\| - \|E\|$	2394.1	
	$\|D\| + \|E\|$	3223.7	
GlcNAc-Glc-naphthyl in ethanolic glass*	$2\|E\|$	900.3	
	$\|D\| - \|E\|$	2477.5	
	$\|D\| + \|E\|$	3376.9	

*Calculated for comparison on the basis of ESR results presented in Tables 26 and 27.

#From Schmidt (1971) and provided for comparison with ESR results since these ODMR measurements were obtained with the use of the same zero-field spectrometer.

**Calculated since transition was too broad for precise determination of its frequency position.

environment of crystalline human lysozyme on the parameters on NGN was also investigated. For these experiments aggregated and multiply twinned crystals were equilibrated with 90% MPD buffered at pH 4.7 as described in Section III.C.2.a. The crystals were then soaked overnight in the same buffered MPD solvent containing 0.005-0.010 M NGN and in another experiment 0.010 M NNNGN. Soaking of the crystals was carried out at room temperature and at -20°C with identical results. As with the tetragonal HEW lysozyme crystals, the crystals were rinsed once with NGN-free solvent and blotted free of excess solvent before mounting in the sample holder and placed in the cryostat of the spectrometer. No excess solvent adherent to the crystals was present in the sample holder which could have contained a significant detectable quantity of phosphorescent substrate. In the case of human lysozyme crystals, photoexcitation at 315 nm produced only a weak emission band at 476 nm above the broad emission spectrum of the protein. No zero-field transition could be observed with wide microwave frequency sweeps from 100-1000 MHz and a transition could be detected only with broad banded frequency sweeps from 2000-3500 MHz. Its precise width and position could not be determined. No other transition could be observed with sweeps up to 8000 MHz.

In view of the general discoloration which these crystals demonstrated, the lack of detectable zero-field transitions for the substrate analogue was suspected to be

caused by the presence of a quenching agent. This hypothesis was confirmed by comparing later the phosphorescence emission and excitation spectra of the human lysozyme crystals employed in ODMR experiments with those of lyophilised human lysozyme dissolved in the same solvent just prior to spectral studies. In the case of the human lysozyme crystals employed in ODMR studies, a component with light absorption centered near 320 nm was observed which was not present in the solution spectrum of the lyophilised protein. This component appeared to make no contribution to the phosphorescence emission spectrum. The chemical nature of this quenching agent remains unknown, but in view of the severe discoloration which these crystals undergo over long periods of time, it may reflect oxidation of aromatic residues, particularly of tryptophan side chains, in the protein.

In these studies, a test of the influence of the active site on a bound triplet state substrate analogue unfortunately could not be observed directly because of a quenching or energy trapping agent in the protein crystal. However, the ZFS parameters of the β(1-naphthyl)-glucoside were sensitive to environmental changes comparable to those expected during the binding of a substrate into the hydrophobic active site of an enzyme. They were, furthermore, distinguishable from the ZFS parameters and transitions of the expected hydrolysis product α-naphthol. These preliminary studies, thus, did demonstrate that triplet state

molecules appropriately incorporated into substrate analogues can be expected to be sensitive to environmental perturbations during the catalytic process. Stereochemical distortions induced by catalytically productive modes of substrate binding would probably produce alterations in the distribution of spin density over the nuclear framework of the phosphorescent probe which would be more marked than those observed simply for an exchange of a hydroxylic by a hydrophobic environment. Application of such molecular probes of enzyme-substrate interactions with use of highly sensitive optical detection methods of ESR (Schmidt, et al., 1967) and of ENDOR (Chan, Schmidt, and van der Waals, 1969) of triplet state molecules may provide a suitable means of investigating electronic structure and stereochemistry of substrates of low temperature stabilised intermediates of enzyme reactions.

Chapter V

SPECTROSCOPIC AND CRYSTALLOGRAPHIC STUDIES OF THE THREE-DIMENSIONAL STRUCTURE OF A LYSOZYME SPIN-LABEL INHIBITOR COMPLEX

A. Spin-label Nitroxide Radicals as Probes of Lysozyme Structure

Site-directed paramagnetic nitroxide radicals, generally referred to as spin-labels, have been employed for a variety of ESR and nuclear magnetic resonance (NMR) studies of macromolecular structure-function relationships. These compounds have the general structural formula I exhibited in Figure 27 and exist as stable free radicals in solution. In the case of lysozyme, the binding of the inhibitor 4-N-acetamido-2,2,6,6-tetramethyl-piperidine-N-oxide was studied crystallographically at 6 Å resolution (Berliner, 1971), from which investigation two binding sites were observed. These corresponded to subsites C and A as the major and minor binding sites respectively. In this case the nitroxide containing piperidinyl moiety in subsite C did not extend directly into subsite D but appeared to protrude into the solvent channel out of the active site cleft. It was evident that the binding energy presumably derived from the binding of

Figure 27.--Structural formulae of nitroxide spin-label compounds. I represents the generalised structure of the stable tetramethyl nitroxide employed in ESR studies of biological macromolecules. II indicates the structure of the lysozyme inhibitor 4-N-acetamido-2,2,6,6-tetramethyl-piperidine-1-N-oxide, found to bind in subsites A and C of the enzyme (Berliner, 1971). III indicates the structure of the spin-label glycosidic inhibitor of lysozyme β-(2,2,5,5-tetramethyl-3-carbinol-pyrrolidinyl-1-N-oxyl)-4-O-(2-acetamido-2-deoxy-β-D-glucopyranosyl)-(2-acetamido-2-deoxy-β-D-glucopyranoside) employed in NMR studies (Wien, et al., 1972).

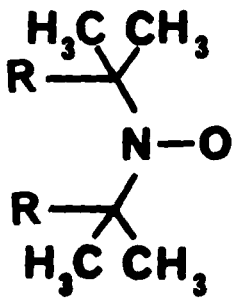

(I)

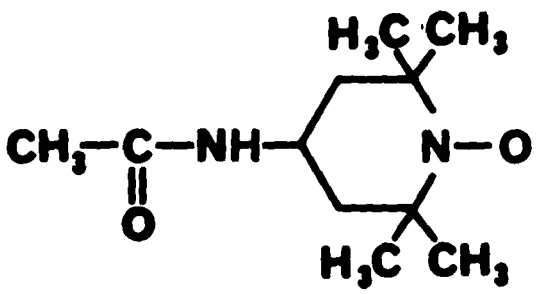

(II)

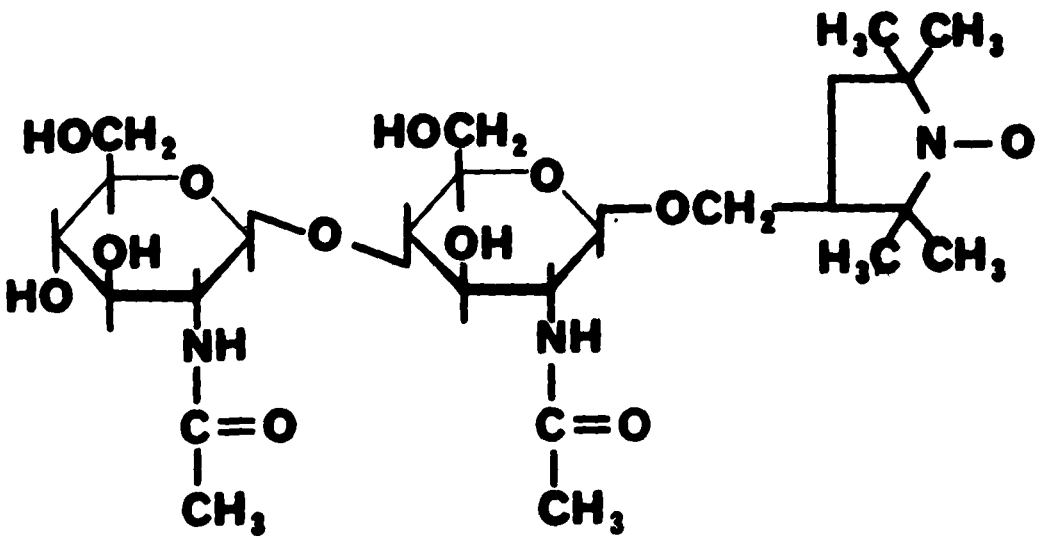

(III)

the acetamido side chain in subsite C, analogous to the binding of a GlcNAc residue, was not sufficient to orient the inhibitor molecule into the catalytic portion of the active site.

Analogous site-directed paramagnetic spin-label inhibitors of lysozyme have also been employed in NMR studies (Wien, Morrisett, and McConnell, 1972) to perturb the nuclear magnetic resonance of specific protons. In this case the spin-label glycoside derivatives of GlcNAc and $(GlcNAc)_2$ also illustrated in Figure 27 were bound to the active site of lysozyme and found to broaden the resonance of the C-2 proton of His-15. In these studies, presumably because of the greater structural similarity between the saccharide inhibitors and small GlcNAc oligomers, binding was assumed to direct the nitroxide moiety into subsite D and the distance of the nitroxide to the histidine ring was estimated on the basis of the broadening effects for both glycosides. That a binding mode truly comparable to that of oligomers of GlcNAc could not have obtained, however, in this study is suggested by the affinity constants determined for the monosaccharide and dissaccharide derivatives. In contrast to the affinity constants of GlcNAc and $(GlcNAc)_2$ to lysozyme of the order of 28 M^{-1} and 2500 M^{-1} respectively (Ikeda and Hamaguchi, 1973), the monosaccharide and dissacharide spin-label inhibitors exhibited constants of 185 and 150 M^{-1} respectively (Wien, et al., 1972). Furthermore, the distance

determined by Wien, et al. (1972), between the nitroxide moiety and the histidine side chain would not be incompatible with other binding configurations, for instance, a configuration whereby the nitroxide ring protrudes more into the solvent or lies in subsite B in an anomalous binding mode.

Although these investigations of lysozyme, as in the case of similar investigations of proteins with doped paramagnetic substituents (Cohn and Reuben, 1971), indicate that specific protons can be selectively perturbed, the assumed binding configuration of such inhibitors to macromolecules may not correspond strictly to that which in fact obtains. In order to mimic as closely as possible true enzyme-substrate interactions with spin-labels, an essential requirement clearly is to incorporate the spin-label derivative into part of a chemical substance that would maintain strict site-directed specificity in analogy to interactions of the enzyme with natural substrates and inhibitors. Such chemical synthesis is obviously not a straightforward or simple objective to achieve. Furthermore, structural studies are required to characterise these binding relationships in order to evaluate the possible influence of the tetramethyl moiety on the structure of the enzyme.

The high resolution structure of the spin-label derivative 2,2,6,6,-tetramethyl-4-piperidinol-1-N-oxide (TEMPO) has been refined with determination of the positions

of hydrogen atoms (Berliner, 1970). This crystallographic investigation has shown that the structure of the six-membered ring is similar in part to that of cyclohexane but with an "out-of-plane" angle of the N-O axis from the plane defined by the C-N-C bonds causing it to resemble in part the half-chair configuration of a cyclohexane ring or the half-chair configuration of the oxycarbonium ion of glucose (Lemieux and Huber, 1965). This structure is illustrated in Figure 28. It would be expected, therefore, that such a structure might more readily mimic the distorted saccharide ring in subsite D of a substrate molecule bound to lysozyme (Phillips, 1967; Ford et al., 1975), providing it could be incorporated into a suitable substrate analogue. The positioning of the nitroxide moiety into subsite D on this basis might then provide a suitable means for magnetic resonance studies to probe the active site for protons of the catalytically active carboxylate groups of Glu-35 and Asp-52.

A molecular model of β(2,2,6,6-tetramethyl-4-piperidinol-1-N-oxyl)-D-(2-acetamido-2-deoxy-glucopyranoside) (β-TEMPO-GlcNAc) the structure of which is illustrated in Figure 29 was constructed with CPK space filling models and its fit into the enzyme active site cleft in subsites C and D was tested. This molecular model building study indicated that the glycoside might be expected to bind with negligible steric hindrance into the active site region and if binding obtained strictly analogous to a

Figure 28.--Structure of 2,2,6,6-tetramethyl-4-piperidinol-1-N-oxide. In part A is a schematic diagram of the molecule indicating the bond lengths and angles determined by least squares crystallographic refinement (Berliner, 1970). In part B is an ORTEP stereophotograph of the nitroxide molecule structure showing the refined positions of the hydrogen atoms and the out-of-plane configuration of the N-O bond. From Berliner (1970).

A

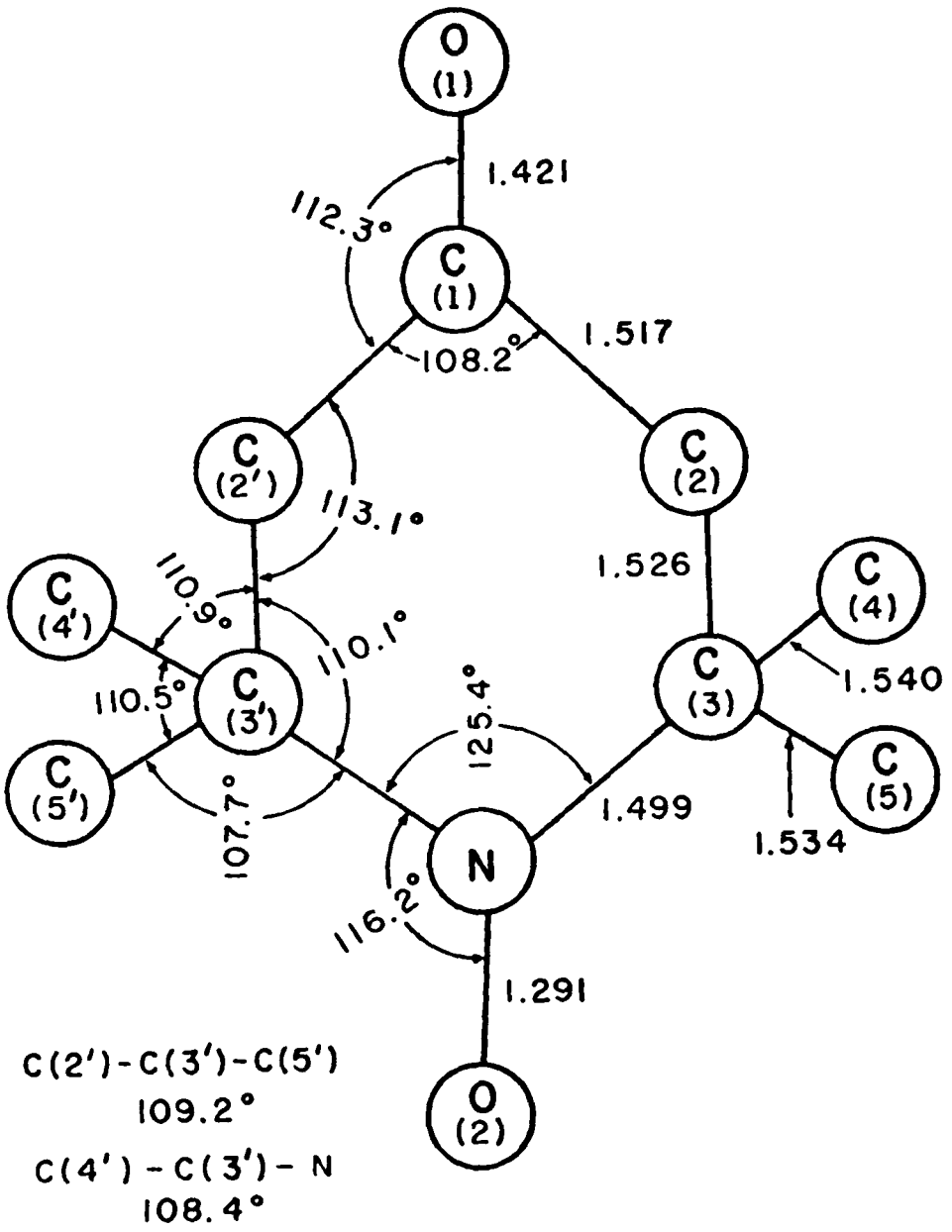
O (1)
1.421
112.3°
C (1)
1.517
108.2°
C (2')
C (2)
113.1°
1.526
C (4')
110.9°
C (4)
110.1°
C (3')
C (3)
1.540
110.5°
125.4°
C (5')
107.7°
1.499
C (5)
1.534
N
116.2°
1.291
O (2)
C(2')-C(3')-C(5')
109.2°
C(4')-C(3')-N
108.4°

B

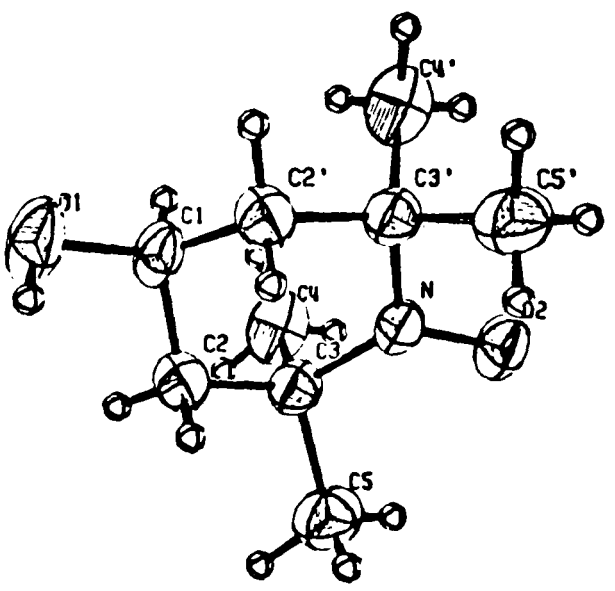
C4'
C2'
C3'
C5'
O1
C1
C4
N
O2
C2
C3
C5

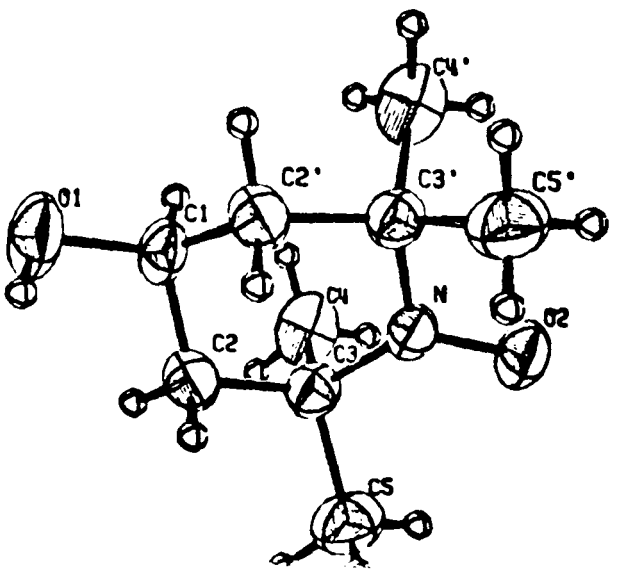
C4'
C2'
C3'
C5'
O1
C1
C4
N
O2
C2
C3
C5

Figure 29.--Structural formula of the spin-label inhibitor of lysozyme β(2,2,6,6-tetramethyl-4-piperidinol-1-N-oxyl)-D-(2-acetamido-2-deoxy-glucopyranoside) synthesised for ESR and ENDOR studies.

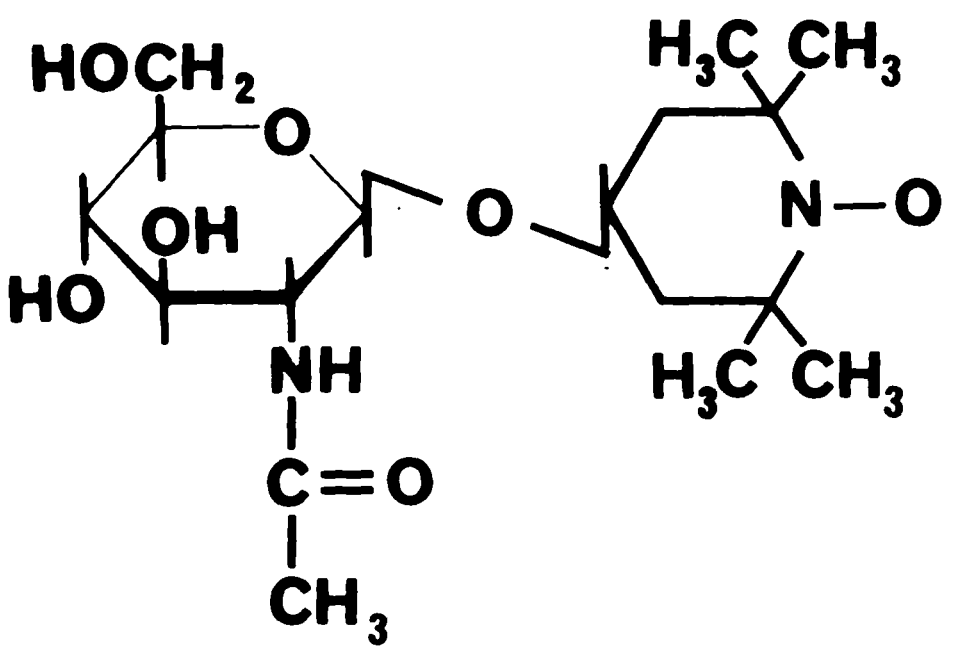
HOCH2
O
OH
HO
NH
C=O
CH3
O
H3C CH3
N—O
H3C CH3

productive binding mode, the nitrogen atom of the nitroxide moiety would be 5-7 Å distant from the carbonyl carbon atoms of the catalytically active carboxylate groups. Since this separation is the optimal distance to which protons in the vicinity of a free radical can be detected by ENDOR techniques (Hyde, Rist, and Eriksson, 1968), a combined ESR and ENDOR investigation of single crystals of HEW lysozyme with the bound inhibitor might be expected to provide a means to detect through physical techniques the presence of the catalytically involved proton from Glu-35 as well as to determine with high precision the relative configuration of the two carboxylate side chains with a bound substrate analogue. To this end the spin-label inhibitor was synthesised and its binding configuration characterised by both spectroscopic and difference Fourier methods.

B. Chemical and Preliminary Crystallographic Studies of β(TEMPO)-GlcNAc Bound to Lysozyme

1. Synthesis of β(TEMPO)-GlcNAc

The synthesis of spin-label inhibitors of lysozyme with a pyrrolinidyl nitroxide unit linked in a β-configuration at the C1 position to a GlcNAc residue has been carried out by direct chemical condensation methods (Wien, et al., 1972). However the piperidinyl derivative could not be synthesised by this method and decomposed in the organic solvents employed [T. Frey, unpublished observation

cited by Wien, et al. (1972), and L. Berliner, personal communication].

Synthesis of the spin-label inhibitor analogue β-(TEMPO)-GlcNAc, therefore, was carried out by means of the transglycosylation reaction of lysozyme in analogy to the use of cyclohexanol as acceptor (Rupley, Gates, and Bilbrey, 1968). To a mixture of 0.5 g HEW lysozyme in 50 ml of 0.05 M citrate at pH 5.0 containing 0.5-1.0 g chitotetraose, 0.5 g of 2,2,6,6-tetramethyl-4-piperidinol-1-oxide (Aldrich Chemical Co., Milwaukee, Wis., U.S.A.) was added. The reaction mixture was gently agitated at 37°C for 48 hours, neutralised, and chromatographed on a 4 x 180 cm Bio-Gel P-2 column equilibrated with 0.1 M NH_4HCO_3. The light transmission of the effluent was monitored at 260 nm with a Beckman DB-G spectrophotometer with a flow rate of 90 ml/hr. The chromatographic separation of reaction products is illustrated in Figure 30. Identification of the parent spin-label compound in fractions 118-150 was made initially by chromatography of unreacted spin-label under identical solvent conditions. Fractions 95-101 and 103-116 were pooled separately, concentrated in vacuo, and lyophilised. ESR signals characteristic of nitroxide spin-labels at $g = 2$ were detected only for the pooled fractions 95-101, 103-116, and 118-150.

The chemical identification of the material absorbing at 260 nm in fractions 151-211 of the Bio-Gel separation step was not pursued further. It was assumed

Figure 30.--Chromatography on a column of Bio-Gel P-2 of a reaction mixture of HEW lysozyme with spin-label glycosides. The peaks labeled I, II, and III represent fractions found to contain respectively the unreacted spin-label TEMPO, β(TEMPO)-GlcNAc, and β(TEMPO)-$(GlcNAc)_2$. Material in peaks I and E was identified by chromatography of lysozyme and TEMPO in a separate experiment. Monitoring of the column effluent 260 nm was initiated just prior to collection of a volume of solvent equal approximately to 5/6 of the void volume of the column. Further details of the chromatography and product identification are provided in the text.

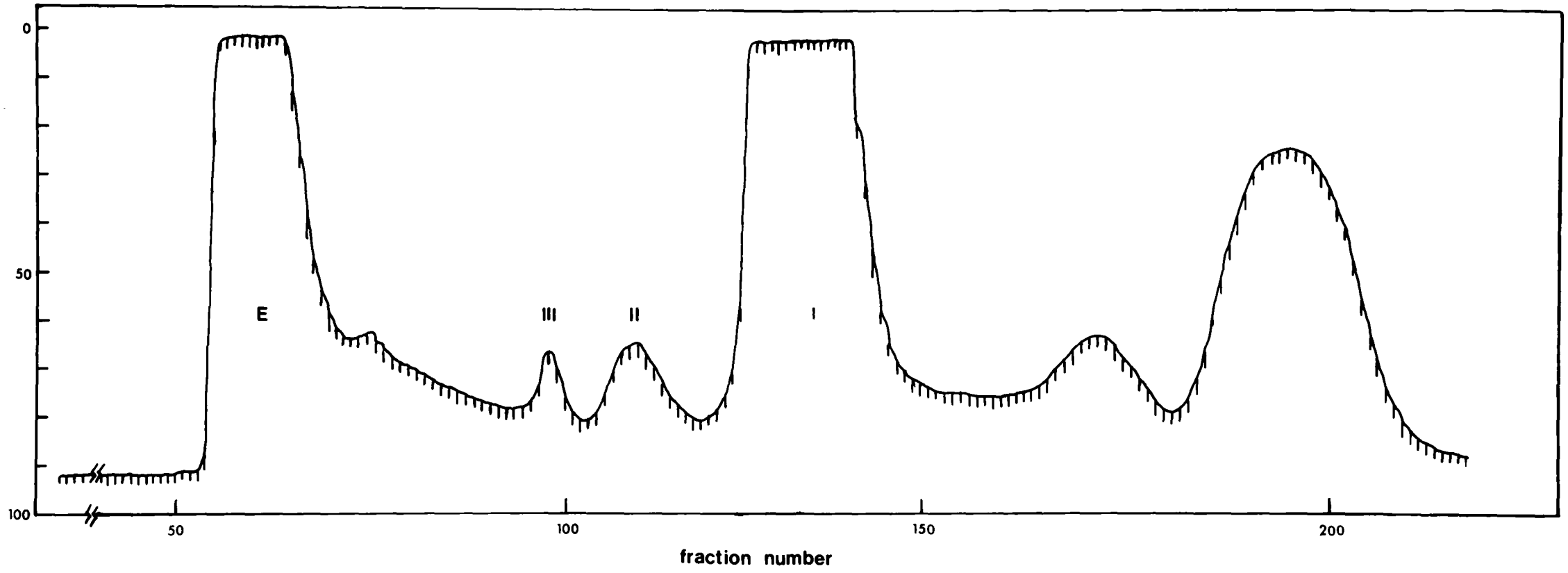
%T
0
50
100
E
III
II
I
50
100
150
200
fraction number

that this material probably represented degradation products of aromatic amino acid residues from direct chemical reaction of the protein with the parent spin-label compound during incubation at 37°C, as suggested by the ultraviolet absorption spectra of corresponding fractions. The lyophilised material corresponding to fractions 95-101 and 103-116 was then redissolved in a 1:1 methanol/water mixture and further purified on a 2 x 50 cm Sephadex LH-20 column with the same solvent. Unreacted spin-label was identified by chromatography of the parent compound in a separate run and proved to elute more slowly than its glycoside derivatives, and separate experiments monitoring the LH-20 column effluent at 220 nm indicated that chitobiose was eluted just prior to both of the synthesised spin-label glycosides.

The material in fractions 103-116 of the Bio-Gel chromatogram was shown by mass spectrometry* to be a glycosidic derivative of GlcNAc. The spectrum indicated a molecular weight of 359 or 16 Daltons less than the theoretically expected value. This exact difference is expected because of the presence of methyl and hydride transfer reactions observed in mass spectrometry of nitroxide free radical derivatives (Morrison and Davies, 1970; Andersson and Fölsch, 1972). A peak corresponding to the lower molecular weight of the expected aglycone less 16 Daltons and one corresponding to the molecular ion of GlcNAc

*Kindly performed by Dr. J. D. Priddle of the Laboratory of Molecular Biophysics.

confirmed the presence of a glycoside of GlcNAc. Unreacted chitobioside was not detected. The material in fractions 103-116 of the Bio-Gel purification step was assumed on this basis to correspond to the spin-label glycoside of GlcNAc in analogy to the synthesis of the β(aryl)-D-glucopyranosyl substrates (see Figure 16). The material corresponding to the higher molecular weight chitobiose analogue (fractions 95-101) was purified and collected but not employed further. Pooled fractions of three separate synthesis runs gave a yield of 0.030 g of β(TEMPO)-GlcNAc as estimated by determination of spin concentration.

2. Precession Photographs of the Lysozyme Spin-label Inhibitor Complex

Binding of the inhibitor to lysozyme in a crystalline phase as required for single crystal ESR studies was demonstrated on the basis of precession photographs of tetragonal crystals of HEW lysozyme soaked with the spin-label inhibitor. A few crystals of tetragonal HEW lysozyme were equilibrated with a solution containing 8% (w/v) NaCl and 0.02 M sodium acetate at pH 4.7 in which β-(TEMPO)-GlcNAc was dissolved. No changes in the distribution of diffracted intensity were observed for crystals equilibrated with 0.01 M spin-label. Changes in the distribution of diffracted intensity in precession photographs were readily observed, however, for crystals soaked with 0.05-0.07 M spin-label, and this concentration range was employed for preparation of spin-label doped lysozyme

crystals for ESR and x-ray studies. Comparison of HKO views of the native and spin-label bound protein crystal is made in Figure 31. HOL views indicated an approximate 1% increase in the axial length of c.

C. ESR and ENDOR Studies of the Lysozyme-Spin-Label Inhibitor Complex

1. The ESR and ENDOR Spectrometer

The ESR spectrometer used in conjunction with ENDOR experiments is described in Chapter IV (Section IV.B.1.). This was operated at a microwave frequency of $9.030 \pm 0.001 \times 10^9$ Hz.

A diagrammatic block illustration of the custom-built ENDOR accessory constructed by Dr. B. A. Coles of the Physical Chemistry Laboratory is given in Figure 32. The radiofrequency oscillator covered a range from 1.2 MHz to 42 MHz. The output was frequency modulated at 10 kHz, and the ESR absorption was phase-sensitive detected at that frequency. The radiofrequency magnetic field amplitude $|\underline{H}_2|$ was estimated to be 1G in the rotating frame. No Zeeman modulation was used for ENDOR experiments since this is not necessary with superheterodyne detection. Frequency modulation at 10 kHz with a maximum deviation of 140 kHz (peak-to-peak) of the radiofrequency was employed. Consideration of the amplifiers employed for ESR and ENDOR signal detection indicated that as little as 1% of the ESR signal intensity could be detected as

Figure 31.--HKO precession photographs of native lysozyme and of its complex with the spin-label β(TEMPO)-GlcNAc. Photograph A illustrates the diffraction pattern of a crystal of lysozyme equilibrated with 8% (w/v) sodium chloride as in Figure 17A. Photograph B illustrates the corresponding diffraction pattern of a crystal equilibrated with 0.05 M β(TEMPO)-GlcNAc under otherwise identical solvent conditions. HOL views indicated a 1% increase in the axial length of c. The limiting resolution of the precession photographs corresponds to 2.5 Å.

A

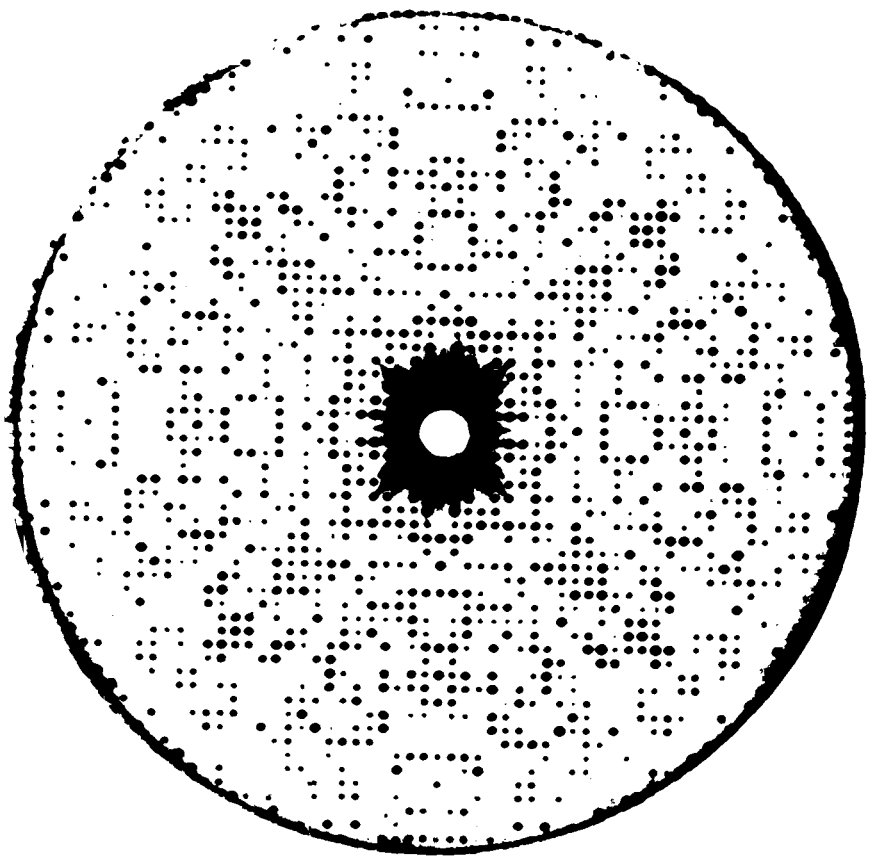

B

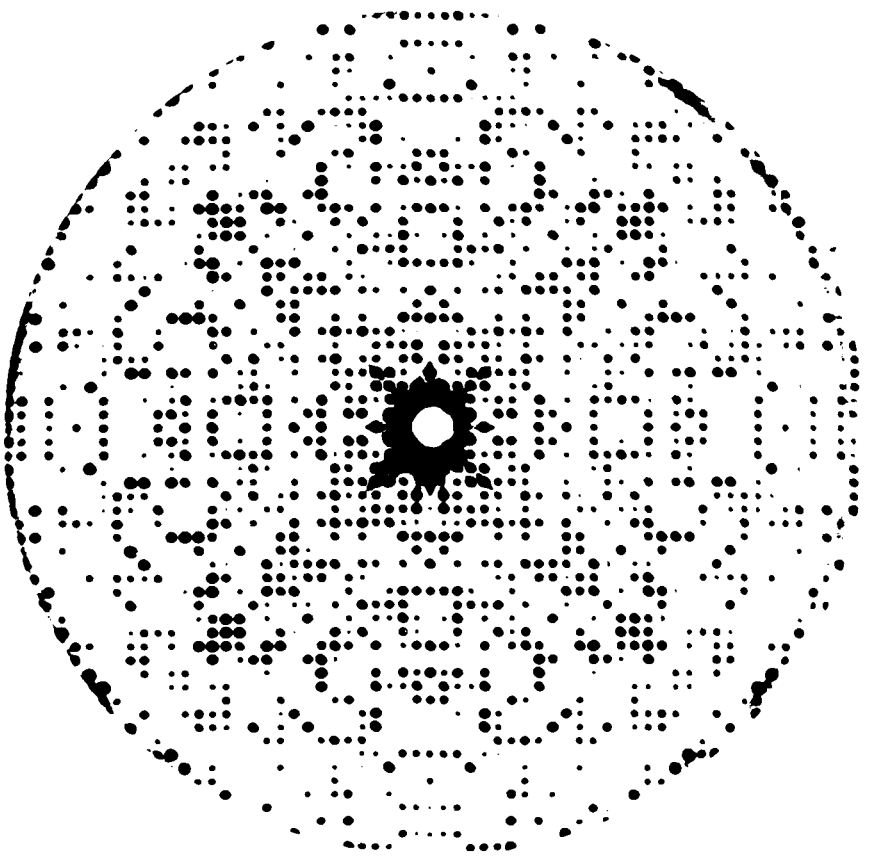

Figure 32.--Schematic block diagram of the ESR and ENDOR spectrometers employed in spin-label studies. A represents the sweep range control and B is the modulation amplitude (frequency deviation) control.

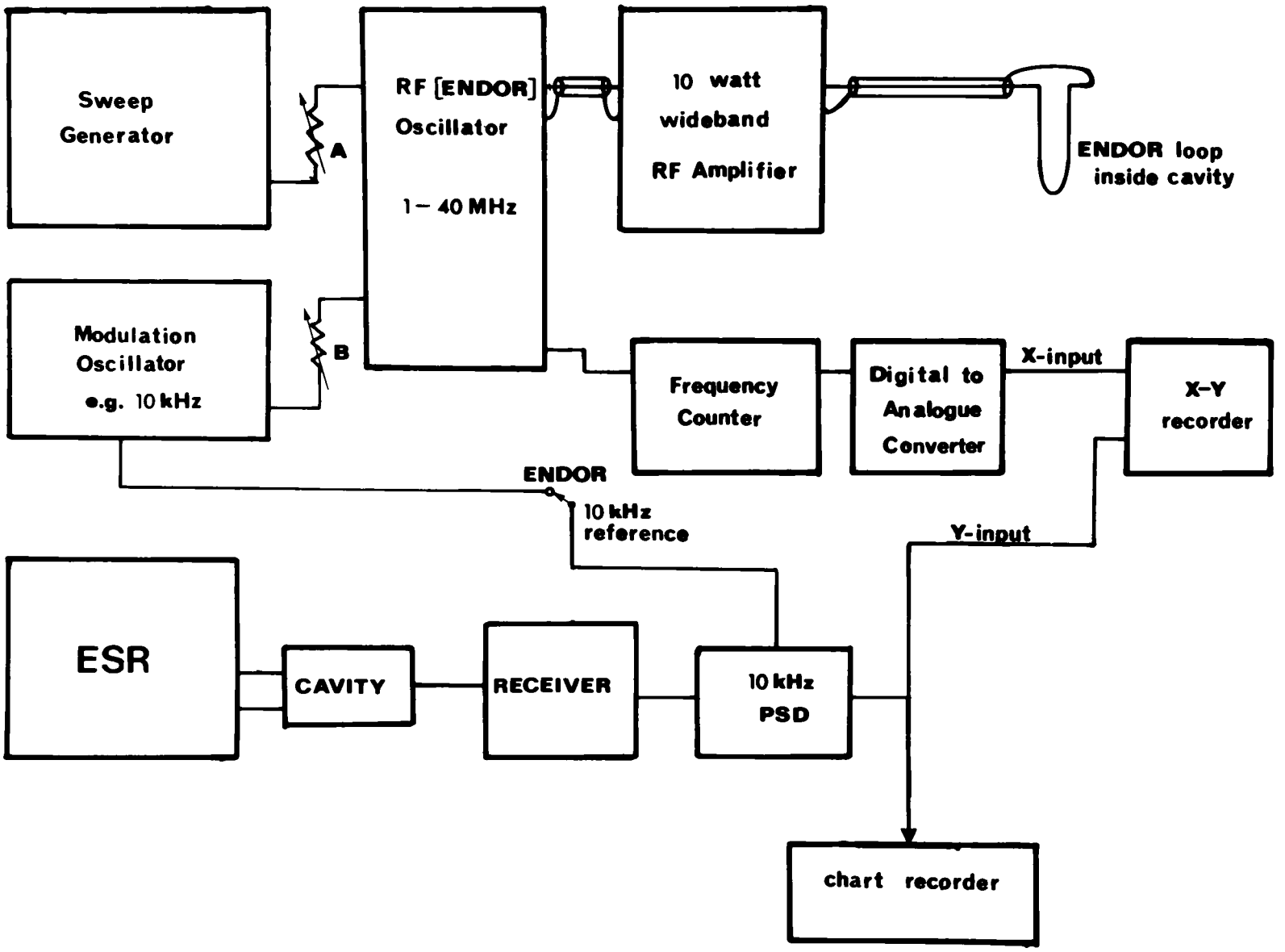
Sweep Generator
A
RF [ENDOR] Oscillator
1 – 40 MHz
10 watt wideband RF Amplifier
ENDOR loop inside cavity
Modulation Oscillator
e.g. 10 kHz
B
Frequency Counter
Digital to Analogue Converter
X-input
X-Y recorder
ENDOR
10 kHz reference
Y-input
ESR
CAVITY
RECEIVER
10 kHz PSD
chart recorder

ENDOR enhancement in the case of phosphorescent triplet state molecules. We have no precise estimate of the corresponding sensitivity of detection in the case of organic free radicals, although in the case of the tetracene free radical cation (see Chapter IV) changes less than 1% were detectable, as estimated on the basis of the ESR and ENDOR absorption spectra at various levels of microwave power incident on the cavity.

For ENDOR experiments with nitroxide free radicals in solution at ambient temperature, the maximum microwave power level available (16 milliwatts) was insufficient to provide appropriate saturation of the ESR signal intensity for ENDOR enhancement. Consequently ENDOR experiments were carried out at cryogenic temperatures where the spin-lattice relaxation of the nitroxide became more favourable for ENDOR. In general, for nitroxide spin-labels in alcohol-aqueous cosolvent mixtures, a temperature near 40°K proved to be optimal for microwave power saturation of the nitroxide free radical signal and for detection of ENDOR enhancement.

2. Crystal Mounting and Orientation

A gonimeter device machined from a Kel-F rod and mounted at the end of a narrow quartz tube was used for mounting single crystals. The crystal could be placed into a small hollow compartment and oriented under examination in a polarising microscope. The crystal was generally

made securely adherent to the inside surface of the compartment by a thin film of solvent whereupon the crystal compartment was sealed to prevent drying of the crystal and solvent film. The goniometer shaft axis was placed parallel to the dewar cylinder in the cavity and rotation was measured with use of a calibrated scale and vernier at the end of the shaft. A narrower quartz rod was placed concentrically within the goniometer shaft which permitted a small (±30°) rotation of the crystal compartment about an axis perpendicular to the goniometer axis.

Large single crystals of HEW lysozyme were selected for ESR studies in order to provide optimal conditions for alignment of the crystal in the goniometer under microscopic examination and to introduce the maximum number of spins possible into the cavity. These crystals were equilibrated with 80% MPD in 0.02 M sodium acetate at pH 4.7 in anticipation of the low temperatures necessary for ENDOR enhancement of the nitroxide free radical signal. Crystals were then soaked in the same solvent containing the β(TEMPO)-GlcNAc inhibitor for at least 24 hr prior to use. Individual crystals were then selected, blotted free of excess solvent with filter paper, and mounted in the goniometer device.

3. Characterisation of the ESR and ENDOR Absorption of the Lysozyme Spin Label Inhibitor Complex

a. ESR Studies

The majority of studies employing spin-label techniques of biological macromolecules are based on considerations of the rotational mobility of the spin-label (Griffith and Waggoner, 1969; Smith, 1972). In such experiments the isotropic motion of the spin-label with respect to the surface of the macromolecule is reflected in the ESR spectrum of a spin-label molecule freely tumbling in solution. The spectrum of the nitroxide radical changes as the reorientation rate is altered (Hamilton and McConnell, 1968; Smith, 1972). The magnetic interactions of the tetramethyl nitroxide radical are characterised according to a defined molecular axis system (Griffith, Cornell, and McConnell, 1965; Libertini and Griffith, 1970) illustrated in Figure 33. A spin-label derivative immobilised in a single crystal which can be oriented at will in the ESR cavity consequently can provide structural information about the orientation of the paramagnetic species with respect to the crystal axis system. Such studies were first carried out with crystals of spin-labeled haemoglobin to define different orientations of the spin-label with respect to the molecular axes (Hamilton and McConnell, 1968), and comparable techniques have been applied to a variety of oriented spin-labeled membranes (Griffith and Waggoner, 1969; Seelig, 1970).

Figure 33.--Schematic illustration of the molecular axis system of nitroxide spin-label compounds. The axis system illustrated indicates that the z-direction is perpendicular to the C-N-C plane. This axis system is employed in describing the magnetic hyperfine interactions of the unpaired electron of the free radical with the nitrogen nucleus of the nitroxide moiety.

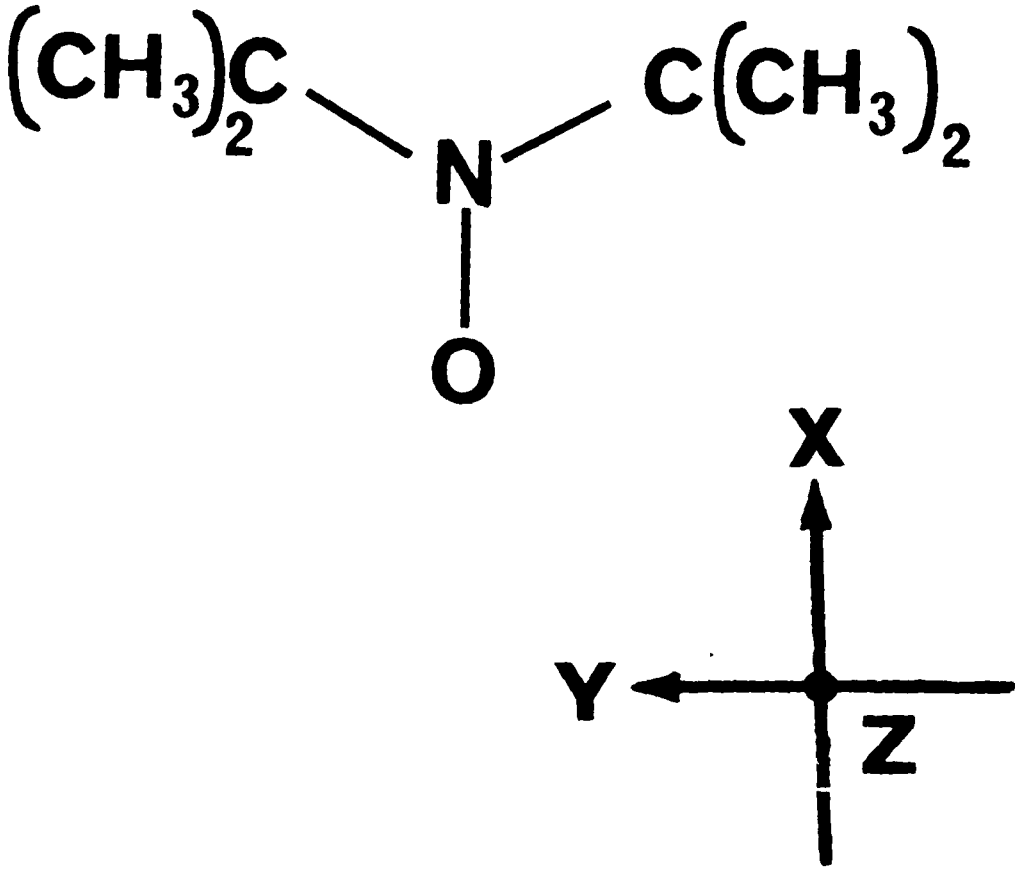
(CH3)2C
N
C(CH3)2
O
X
Y
Z

The spin hamiltonian required to describe an oriented nitroxide radical is

$$\mathcal{H} = +|\beta_e|\underline{H}_0 \cdot \underline{\underline{g}} \cdot \hat{\underline{S}} - |\beta_n| g_n \underline{H}_0 \cdot \hat{\underline{I}} + \hat{\underline{S}} \cdot \underline{\underline{A}} \cdot \hat{\underline{I}} \qquad (5.1)$$

$$\underline{S} = 1/2, \ \underline{I} = 1$$

where $\underline{H}_0$ is the laboratory magnetic field, $|\beta_e|$ is the absolute value of the Bohr magneton, $|\beta_n|$ is the absolute value of the nuclear magneton, g_n the nuclear g value of a nitrogen nucleus, $\hat{\underline{S}}$ the electron spin operator, $\hat{\underline{I}}$ the nuclear spin operator, $\underline{\underline{g}}$ the electron g-value matrix, and $\underline{\underline{A}}$ the electron-nuclear hyperfine interaction tensor. Several other interactions are ignored in Equation 5.1, mainly electron-proton hyperfine interactions and interactions involving the nitrogen nuclear quadrupole moment. This is done since the ESR experiment is designed to determine the relationship of the principal magnetic axes with respect to the crystal axis system.

The representation of each tensor in Equation 5.1 depends upon the choice of coordinate system. It has been determined for spin-label nitroxides that the principal axes of both the hyperfine splitting tensor and the g-value matrix coincide with the molecular axes illustrated in Figure 33 (Griffith et al., 1965). For a coordinate system with principal axes parallel to the molecular axes the hamiltonian may be written as

$$\mathcal{H} = +|\beta_e|\underline{H}_0' \cdot \begin{pmatrix} g'_{xx} & 0 & 0 \\ 0 & g'_{yy} & 0 \\ 0 & 0 & g'_{zz} \end{pmatrix} \cdot \underline{\hat{S}}' - |\beta_n| g_n \underline{H}_0' \cdot \underline{\hat{I}}$$

$$+ \underline{\hat{S}}' \cdot \begin{pmatrix} A'_{xx} & 0 & 0 \\ 0 & A'_{yy} & 0 \\ 0 & 0 & A'_{zz} \end{pmatrix} \cdot \underline{\hat{I}}' \qquad \underline{S} = 1/2, \ \underline{I} = 1$$

where the primes designate the principal values of the tensors and other quantities referred to the molecular axis system. The principal values of the hyperfine splitting tensor and g-value matrix are obtained from the spectra observed with the laboratory magnetic field directed along each respective molecular axis. For instance, with $\underline{H}_0$ parallel to the z-molecular axis, A'_{zz} is the splitting observed between the high field or low field line and the central line of the three line spectrum of a nitroxide free radical. Thus, by appropriately orienting the crystal with respect to the laboratory field, each hyperfine splitting and g-value can be determined in principle.

The ESR absorption characteristics of the spin-label soaked crystals proved to be difficult to analyse for the determination of principal axes, i.e., stationary lines indicating direction of the laboratory magnetic field along a molecular axis. The high concentrations of spin-label not bound to the enzyme but retained in the solvent

channels yielded a broad, generally featureless background absorption reminiscent of those observed for spin-labels undergoing anisotropic tumbling motion in oriented lipid membranes (Devaux and McConnell, 1972; Seelig, 1970). However, with the crystal $\hat{c}$ axis tilted at about 45° from the vertical axis of the goniometer shaft, a position of the crystal could be found which produced a pair of stationary lines separated approximately 32 G (90 MHz) from the center. This spectrum is illustrated in Figure 34. This hyperfine splitting is consistent with the molecular z-axis oriented parallel to H_0 (Libertini et al., 1970). The peak-to-peak width was estimated as approximately 6-8 G for both the low-field and high field transitions. Other stationary lines could not be detected.

b. ENDOR Studies

(1) Physical Basis and Theory of ENDOR

The spin hamiltonian in Equation 5.1 describes an oriented nitroxide radical wherein the electron-nuclear interaction occurs between the unpaired spin of the free radical and the nitrogen nucleus of the nitroxide group. To this must be added the interaction of the unpaired spin with nuclei of neighbouring hydrogen atoms. Such interactions would be considered as the primary origin of the broadening of the ESR lines of an oriented spin-label since their spacing does not exceed their width and their hyperfine splitting is consequently not detected. The ESR lines

Figure 34.--ESR absorption spectrum of a crystal of tetragonal HEW lysozyme equilibrated with β(TEMPO)-GlcNAc. The crystal of the lysozyme-spin-label complex was prepared and mounted in the ESR cavity as described in the text. The spectrometer was operated at a microwave frequency of $9.030 \pm 0.001 \times 10^9$ Hz. With the crystal $\underline{\hat{c}}$ axis tilted about 45° from the vertical axis of the goniometer, rotation of the crystal produced the pair of lines indicated by arrows with a maximum field separation as shown. The lines indicated were the only lines observed as stationary lines and are considered on the basis of their average separation from the centre to correspond to alignment of the z-molecular axis of the nitroxide moiety parallel to $\underline{H}_0$. The spectrum was obtained with the crystal at ambient room temperature.

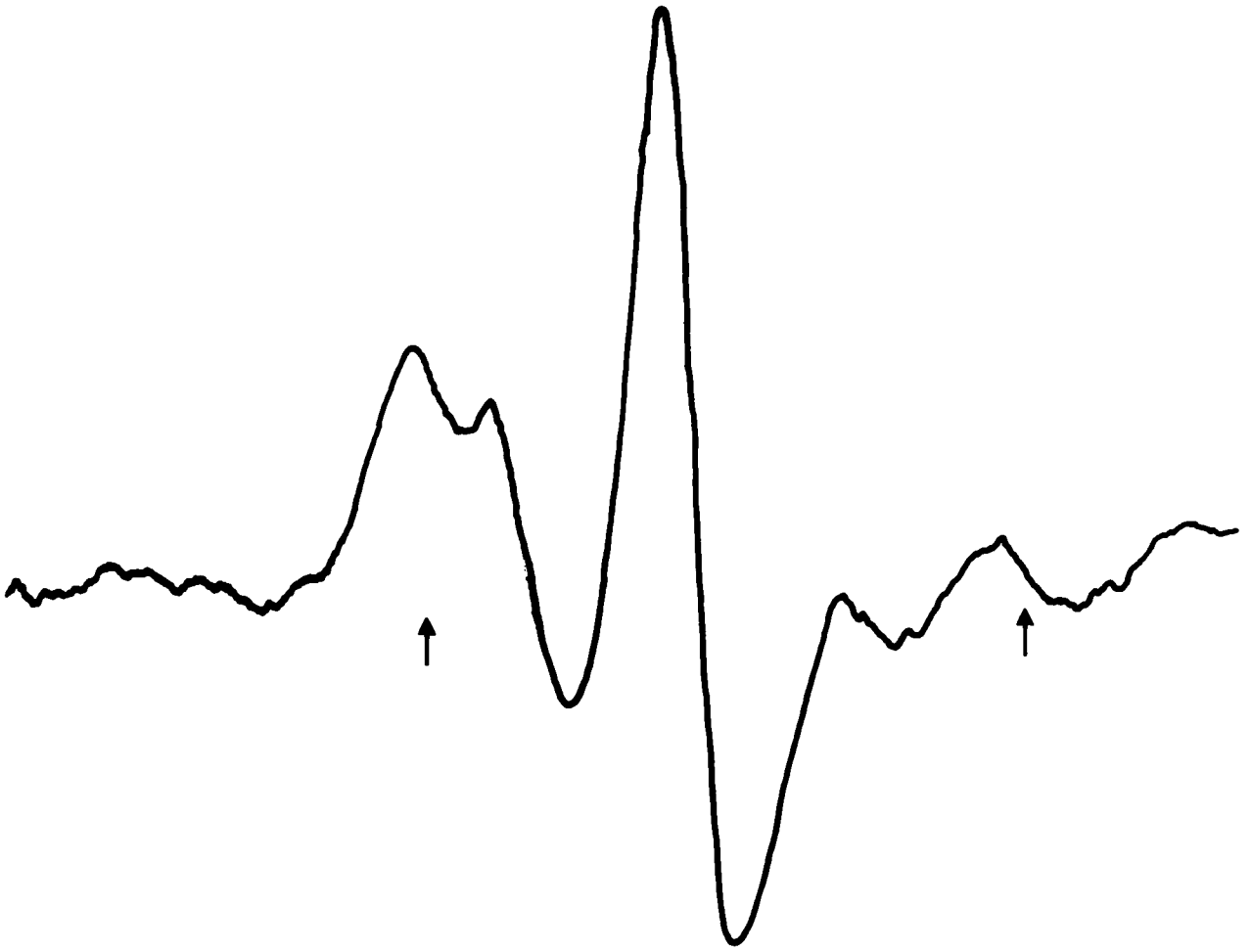

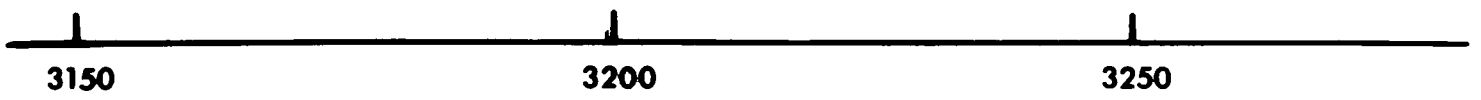

GAUSS

are considered on this basis to be inhomogeneously broadened since hyperfine splitting contributions arise from numerous ^{1}H nuclei in the environment of the unpaired electron and the nature of its interaction with each ^{1}H nucleus will be dependent upon the distance of the ^{1}H nucleus from the paramagnet as well as the various electron and nuclear spin-lattice relaxation times. The detection of electron-nuclear interactions by application of ENDOR techniques (Feher, 1956) in principle can be employed to regain missing details of the hyperfine interactions as well as to evaluate individually the interactions of the unpaired electron with each distinctive type of nucleus in its environment.

A detailed analysis of the ENDOR method has been provided by Abragam and Bleaney (1970), and application of the method to a variety of paramagnetic species has been discussed by others (Hyde, 1965; Allendoerfer and Maki, 1970; Kwiram, 1971). We present here only a brief description of the method to indicate the general physical basis of the phenomenon. The energy level scheme for a system with $\underline{S} = \underline{I} = 1/2$ corresponding to the case of a nitroxide free radical interacting with a ^{1}H nucleus is illustrated in Figure 35. If low lying microwave power is applied to any of the $\Delta m_S = 1$ transitions, the level populations are not significantly disturbed, and the signal intensity is determined primarily by the difference in population between the lower and upper levels.

Figure 35.--The energy level diagram for an $\underline{S} = \underline{I} = 1/2$ system. The contributions of the different interactions are illustrated at the left which correspond to the various parts of the hamiltonian 5.1. The relaxation paths between various levels are indicated and are represented by the appropriate relaxation times (T_1, T_x, T_n, etc.). The relative populations of the states at thermal equilibrium are indicated in (a) for the $\underline{S}_z = +1/2$ manifold by $1 - \epsilon \pm \delta$ where $\epsilon \equiv g|\beta_e||\underline{H}_0|/\underline{k}T$ and $\delta \equiv g_n|\beta_n||\underline{H}_0|/\underline{k}T$. The relative populations in the presence of a saturating microwave field are given in (b). In (c) the relative populations are those which obtain immediately after a population inversion induced by the radiofrequency power at ν_+, one of the ENDOR frequencies. At this instant the ESR transition is again unsaturated causing a change in the rate of microwave power absorption and providing the basis of detection of a nuclear magnetic resonance transition through the change in signal intensity of an ESR transition. Figure from Kwiram (1971).

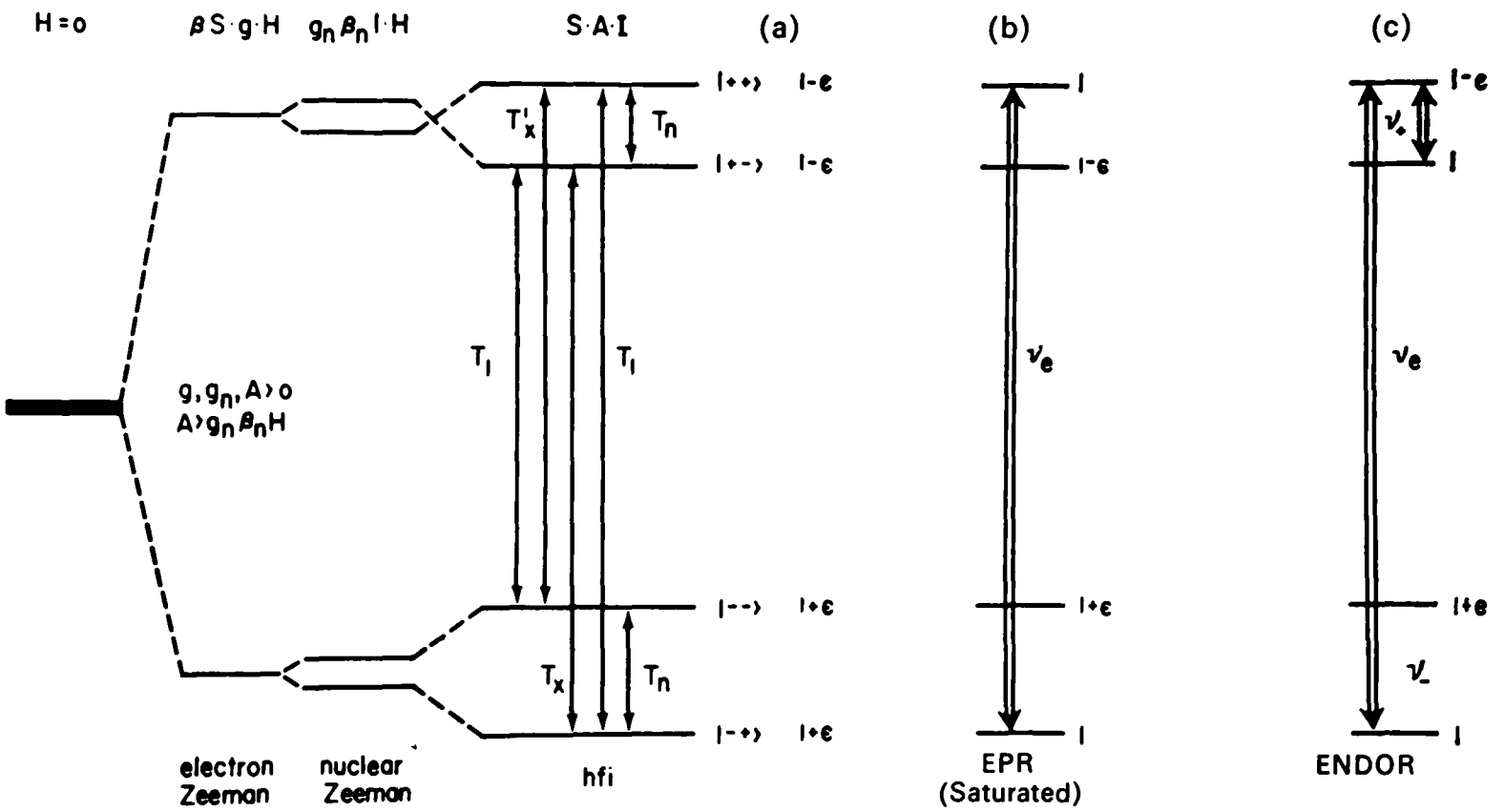
H=o
βS·g·H
gnβnI·H
S·A·I
(a)
(b)
(c)
|+>
|-ε
|->
|-ε
T'x
Tn
T|
T|
g, gn, A>o
A>gnβnH
|-->
|+ε
|+>
|+ε
Tx
Tn
electron Zeeman
nuclear Zeeman
hfi
|
|-ε
|+ε
|
EPR (Saturated)
|-e
ν+
|
ν-
|+e
|
ENDOR

Application of a radiofrequency field of appropriate energy can similarly induce a transition between the nuclear levels, for instance corresponding to the $|{+}{+}\rangle \leftrightarrow |{+}{-}\rangle$ transition, but this signal cannot be detected directly. However, if the $|{+}{+}\rangle \leftrightarrow |{-}{+}\rangle$ ESR transition is saturated with microwave power, the populations of the two levels become equal. If at this point the nuclear spin transition is induced in either of the spin manifolds, the population of, for instance, the $|{+}{+}\rangle$ level will be equalised with respect to the $|{+}{-}\rangle$ level, thus affecting the intensity of the signal of the transition between the $|{+}{+}\rangle$ and $|{-}{+}\rangle$ levels. Such a change in signal intensity corresponds to a change in the rate of microwave power absorption, and will be consequently observed as a change in ESR absorption intensity when the laboratory magnetic field is set to the position of maximum ESR absorption. We consequently see from the diagram that the nuclear radiofrequency power must be strong enough to induce a transition between the $|{+}{+}\rangle$ and $|{+}{-}\rangle$ levels at a rate comparable or faster than that of the relaxation path between the $|{-}{+}\rangle$ and $|{+}{-}\rangle$ levels. The nuclear radiofrequency power must consequently compete with nuclear relaxation times as well as electronic relaxation times.

Although the first description of the ENDOR effect presented an elementary model (Feher, 1956 and 1958), the actual details of the ENDOR mechanism become complex with a variety of relaxation paths involved. In general the

rate of the induced nuclear transition must be at least as fast as $1/T_n$ and $1/T_x$ defined in Figure 35, and T_1 must be long enough so that the ESR transition can be saturated. In practice, as in the study described here, the operating temperature chosen for the experiment which consequently determines the various relaxation times becomes a compromise between available microwave and radiofrequency power and the signal-to-noise ratio. For these reasons it is difficult to specify the constraints which determine the optimal conditions for an ENDOR experiment.

Under the assumption that the magnetic field experienced by a proton at a site $\underline{r}_p$ from the paramagnet will be the vector sum of the laboratory magnetic field $[\underline{H}_0]$ and the field produced at $\underline{r}_p$ by the point dipole of the unpaired electron $[\underline{H}_{e^\pm}(\underline{r}_p)]$, we can evaluate the interaction between the unpaired spin of the nitroxide moiety and neighbouring ^1H nuclei. Since the ^1H atoms of the solvent and protein are not covalently joined to the nitroxide group and the spin on the nitroxide has been demonstrated to be largely confined to the $p\pi$ orbital of the nitrogen (Hamilton and McConnell, 1968), we can expect this interaction to be primarily electric dipole-magnetic dipole in character, and the Fermi contact terms are expected to be negligible. We base this assumption on the ENDOR studies of organic free radicals (Hyde et al., 1968) and of trapped electrons (Helbert, Kevan, and Bales, 1972) in polycrystalline matrices which indicate that the dipole-dipole approximation

adequately describes the electron spin-nuclear spin interaction. We consequently consider the energy of the purely anisotropic dipolar interaction only.

The effective magnetic field at a proton site ($\underline{r}_p$) from the unpaired spin will be

$$\underline{H}_{eff}^{\pm}(\underline{r}_p) \equiv \underline{H}_e^{\pm}(\underline{r}_p) + \underline{H}_0. \tag{5.2}$$

The magnetic field produced by the point dipole of the unpaired spin [$\underline{H}_e^{\pm}(\underline{r}_p)$] is given by the relation

$$\underline{H}_e^{\pm}(\underline{r}_p) = \frac{1}{|\underline{r}_p|^3} \langle \underline{\mu}_e \rangle_{\pm} \cdot \{3\underline{r}_p \cdot \underline{r}_p - \hat{\epsilon}\}$$

in which $\hat{\epsilon}$ is the identity operator and $\langle \underline{\mu}_e \rangle_{\pm}$ is the expectation value of the point dipole of the unpaired electron. From the definition of the electronic magnetic moment we have the general result

$$\langle \underline{\mu}_e \rangle_{\pm} = -|\beta_e| \underline{\underline{g}} \cdot \langle \underline{S} \rangle_{\pm} = -|\beta_e| \frac{1}{g_e} \begin{pmatrix} \ell_1^2 g_{xx}^2 \\ \ell_2^2 g_{yy}^2 \\ \ell_3^2 g_{zz}^2 \end{pmatrix} \cdot \langle \underline{S} \rangle_{\pm}$$

where the ℓ_i are direction cosines of $\underline{H}_0$ in the molecular axis system, g_e is the effective value of $\underline{\underline{g}}$ defined by $g_e = \{\ell_1^2 g_{xx}^2 + \ell_2^2 g_{yy}^2 + \ell_3^2 g_{zz}^2\}^{1/2}$. $\langle \underline{S} \rangle_{\pm}$ is the expectation value of the total spin angular momentum for the system under consideration.

In the case of a nitroxide free radical we shall make the approximation

$$\langle \underline{\mu}_e \rangle_{\pm} = -|\beta_e| \underline{\underline{g}} \cdot \langle \underline{S} \rangle_{\pm} \simeq -2|\beta_e| \langle \underline{S} \rangle$$

Remembering that the spin is polarised in the direction of $g \cdot \underline{H}_0$, we obtain the expression

$$\underline{H}_{eff}{}^{\pm}(\underline{r}_p) = \frac{-2|\beta_e|\langle \underline{S} \rangle_{\pm}}{|\underline{r}_p|^3} \cdot \{3\underline{r}_p \cdot \underline{r}_p - \hat{\epsilon}\} + \underline{H}_0 . \qquad (5.3)$$

To evaluate the ENDOR frequencies, one then simply considers the hamiltonian

$$\mathcal{H}_H = -|\beta_n| g_n \sum \underline{I}_k \cdot \underline{H}_{eff}{}^{\pm}(\underline{r}_p) \quad \underline{I} = 1/2 \qquad (5.4)$$

where $\underline{I}_k$ is the nuclear spin of the kth proton and the summation is carried out over the k proton sites in the crystal. By taking the difference between the eigenvalues of the hamiltonian (5.4) one solves for the ENDOR frequency by the expression

$$\nu_{ENDOR} = h^{-1}\{|\langle \underline{S}_{\pm} \rangle \cdot \underline{\underline{A}}_k - g_n|\beta_n|H_0|\} \qquad (5.5)$$

where

$$\underline{\underline{A}}_k \equiv \frac{2g_n|\beta_e||\beta_n|}{|\underline{r}_p|^3} \begin{pmatrix} 3n_1^2 - 1 & 3n_1n_2 & 3n_1n_3 \\ 3n_1n_2 & 3n_2^2 - 1 & 3n_2n_3 \\ 3n_1n_3 & 3n_2n_3 & 3n_3^2 - 1 \end{pmatrix} ,$$

the n_i being direction cosines of the electric dipole moment of the unpaired spin and consequently also of the nuclear dipole moment of the kth proton in the molecular axis system.

We define the ENDOR shift of the kth proton ($\Delta\nu_k$) as the ENDOR frequency minus the magnitude of the nuclear Zeeman splitting of the proton

$$\Delta\nu_k = \nu_{ENDOR} - \nu_p \qquad (5.6)$$
$$= h^{-1}\{|\langle \underline{S}\rangle_{\pm} \cdot \underline{\underline{A}}_k - h\nu_p|\} - \nu_p$$

where ν_p is the free proton frequency. We thus see that the ENDOR shift can be related directly to the quantity $h^{-1}|\langle \underline{S}\rangle_{\pm} \cdot \underline{\underline{A}}_k|$. In the absence of data for the direction cosines of specific proton positions, we evaluate only an upper limit on the relationship between the ENDOR shift and the closest distance of approach $|\underline{r}_p|$ of the kth proton from the paramagnetic site.

By assuming the simplest model for the nature of the dipole-dipole interaction, i.e., the field "sensed" by the proton is equivalent to a point dipole at the center of the nitrogen nucleus of the nitroxide moiety, we derive the appropriate expression to relate the distance $|\underline{r}_p|$ of a proton from the paramagnetic center. For instance, with $\underline{H}_0$ parallel to the molecular z-axis, $\langle \underline{S}\rangle_{\pm} = \langle \underline{S}_z\rangle_{\pm} = 1/2$ and the distance of a proton from the nitrogen nucleus along the z-axis is given by

$$|\underline{r}_p| = \left[\frac{2g_n|\beta_e||\beta_n|}{h\ \Delta\nu_k}\right]^{1/3}. \qquad (5.7)$$

While in principle the distance of each proton from the paramagnetic centre could be determined by an analysis of the angle dependence of the ESR and ENDOR lines with respect to the set of crystal (and molecular) axes, we elect not to derive these relationships in more detail in view of the difficulty encountered in detecting the principal axes, as explained earlier in the preceding section. It will be evident below that the relationships derived above are adequate to account for the results of our ENDOR studies of the lysozyme-spin-label complex.

(2) Experimental Results

ENDOR signals were observed in general with sample temperatures near 40°K for nitroxide spin-labels dissolved in polycrystalline or glassy matrices or soaked into lysozyme crystals. For the crystal orientation described in Figure 34, with the microwave power set to correspond to a 3 decibel reduction of the extrapolated ESR signal intensity, application of a radiofrequency field to the nitroxide spin-label at 40°K produced a prominent ENDOR signal centered at the free proton frequency position. This signal was most intense when the laboratory magnetic field was set to the low field transition at 3185 G indicated in Figure 34 and was less intense when the field was set to other positions where the unbound spin-label molecules in the solvent channels should make a relatively greater contribution to the ESR absorption. An ENDOR signal of comparable intensity

was also observed when the laboratory magnetic field was set to the central line of the three-line spectrum in Figure 34.

In Figure 36 the ENDOR spectrum of β(TEMPO)-GlcNAc soaked into a tetragonal HEW lysozyme crystal in the orientation described in Figure 34 is compared to that of a nitroxide spin-label dissolved in the glassy matrix of a proton-free perdeuterated cosolvent mixture. The ENDOR line centered at the free proton frequency position is the most prominent transition and displays some structure in the central region. ENDOR transitions of considerably reduced intensity are also observed at approximately ±1.597 (± 0.010) MHz from the free proton frequency line for the spin-label in the HEW lysozyme crystal. No other ENDOR transitions were observed in scans from 1 to 40 MHz, and random orientations of the crystal in the cavity of the spectrometer produced a line at the free proton frequency of less intensity than for the orientation described in Figure 34, with no significant change in peak-to-peak linewidth but with somewhat less pronounced structure in the central portion of the band.

(3) Analysis of ENDOR Results

There are three distinct types of ENDOR lines in the spectrum of Figure 36 which can be analysed on the basis of a dipole-dipole mechanism.

Figure 36.--Comparison of ENDOR spectra of spin-labels in a tetragonal lysozyme crystal and in a deuterated glassy matrix. The crystal spectrum was recorded with the crystal oriented as described in Figure 34. An identical crystal spectrum was observed with the laboratory magnetic field set to 3185 G, the position of maximum ESR absorption for the low field transition in Figure 34. The spectra are shown for comparative purposes with the laboratory magnetic field set to 3217.5 G where spin-labels in both media exhibited absorption lines. The spectrum of the spin-label in the deuterated solvent is shown for a sample dissolved to a concentration of 10^{-4} M directly into the deuterated cosolvent mixture. Spectra for spin-labels in both solvent media were recorded at 40°K with comparable settings for sensitivity and power levels.

ENDOR SPECTRA OF SPIN-LABELS

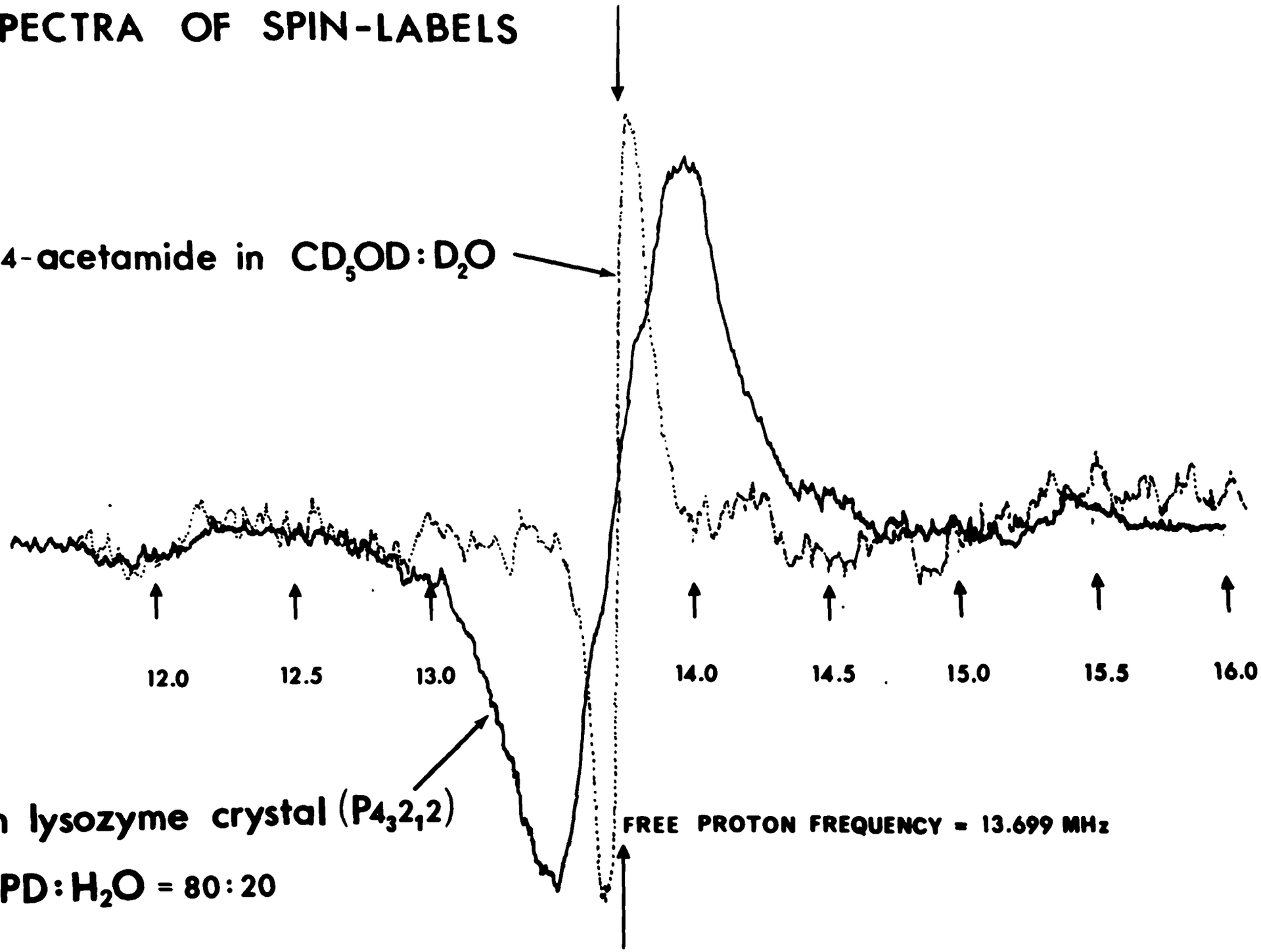

Comparison of the spectrum of the spin-label in a perdeuterated solvent medium to that of the spin-label in the lysozyme crystal indicates that the hydrogens covalently attached to the spin-label piperidinyl ring contribute only to the central region of the broad ENDOR line centered at the free proton frequency. By measurement of an atomic model the methyl protons are ~7 Å distant from the nitrogen nucleus of the nitroxide moiety, and as a first order approximation their average positions are estimated at 60° from the z-molecular axis in either the molecular xz- or yz-planes (see Figure 33). Substitution of the corresponding values into Equations 5.5 and 5.6 suggests that the methyl protons consequently could give rise to an ENDOR shift of approximately 0.17 MHz for the oriented nitroxide group in Figure 34 for which $\underline{H}_0$ is parallel to the molecular z-axis. Careful comparison of the two spectra in Figure 36 indicates that the crystal spectrum demonstrates structure in the central free proton frequency region that is not as prominently detected in the ENDOR spectrum of the randomly oriented spin-label dissolved in a proton-free solvent. The approximate separation of these structured portions of the crystal spectrum from the free proton frequency line is ~0.15 - 0.18 MHz. Conceivably, therefore, the piperidinyl methyl protons could give rise to the added structure observed in the crystal spectrum close to the free proton frequency position above the broad, generally featureless envelope of the most prominent ENDOR line. We expect little further structural

information from the interaction of methyl protons with the paramagnetic centre. In addition, the rotational freedom of methyl groups attached to organic free radicals would be expected to obscure the ENDOR lines arising from each individual class of hydrogen nuclei (Hyde, et al., 1968).

The origin of the broad ENDOR line centered at the free proton frequency has been analysed on the basis of a dipole-dipole mechanism for free radicals (Hyde et al., 1968) and trapped electrons (Helbert et al., 1972) in polycrystalline and glassy matrices. This analysis suggests that the wing portions of the broad line arise from a disordered collection of protons from which the individual ENDOR lines are strongly overlapping and consequently are not resolvable. This can be qualitatively understood on the basis of Equation 5.5 and the definition of $\underline{\underline{A}}_k$. An averaged ENDOR shift for a disordered collection of protons around the nitroxide group between the limits of 0.2 - 0.6 MHz would account for a substantial proportion of the individual protons contributing to the wing portions of the broad line in Figure 36. On the basis of Equations 5.6 and 5.7 we estimate that these contributions must arise from a collection of protons within a 5.1 - 7.0 Å shell from the paramagnetic centre, taking into consideration the nearly isotropic g-value of the nitroxide group. Since precession photographs of the lysozyme-spin-label complex in the crystal (see Figure 31) indicate an ordered lattice structure, we must conclude that only the distribution of hydrogen

nuclei contributing to the wings of the broad ENDOR line resembles that of a disordered solid. Such a disordered distribution of hydrogen nuclei in the vicinity of the nitroxide group must have origin in an isotropic collection of protons from amino acid side chains of the enzyme or from solvent molecules. That this effect must be characteristic of the ordered spin-label groups and not only the disordered molecules in the solvent channels is suggested by the comparable peak-to-peak linewidths of ENDOR lines for on-axis and off-axis crystal orientations.

Binding of the spin-label inhibitor according to the expected configuration associated with the acetamido specificity site in subsite C would be expected to produce an uneven distribution of protons from the enzyme active site cleft on the one hand and exposure to solvent molecules on the other hand. A site-directed orientation of the spin-label into the active site would presumably give rise then to an anisotropic collection of interacting protons with well resolved ENDOR lines. Consequently, it is difficult to conclude that the broad ENDOR line reflects a spin-label buried within a hydrophobic cleft, and a more likely interpretation is that the broad ENDOR line arises from a disordered collection of protons largely from solvent molecules near the surface of the enzyme. We tentatively conclude, therefore, that the β(TEMPO)-GlcNAc inhibitor need not be considered as bound according to the usual (expected) binding pattern and is probably substantially exposed to free solvent molecules.

The pair of well resolved ENDOR lines separated 1.597 (±0.010) MHz from the free proton frequency position deserves special consideration despite their weak intensity. In view of their well resolved features exactly centered around ν_p and in view of the crystal orientation described in Figure 34 with the molecular z-axis parallel to $\underline{H}_0$, we can estimate the precise position of the proton from the nitrogen nucleus as an upper limit of the closest possible distance to the nitrogen nucleus. On the basis of Equation 5.7 this leads to an estimate of

$$|r_p| = \left[\frac{2g_n|\beta_e||\beta_n|}{h \times 1.597 \times 10^6}\right]^{1/3} = 3.7 \times 10^{-8} \text{ cm}$$

or 3.7 Å. Measurement of this distance from the nitrogen nucleus along the molecular z-axis of an atomic model of the spin-label indicates that an approach of a hydrogen atom to within this distance is not incompatible with the steric volume described by the pair of methyl groups on each side of the piperidinyl ring (see Figure 29). This distance is, furthermore, compatible with estimates made for the distance of closest approach of a proton to aromatic nitroxides (Bales, Schwartz, and Kevan, 1973) within the framework of a dipole-dipole model. We consequently expect that a proton should be located along the molecular z-axis approximately 3.7 Å from the nitrogen nucleus. This proton is probably attached to a protein residue, for we know of no reason to assume an oriented solvent molecule to be attracted

to this portion of the spin-label molecule. With an expected C-H bond distance of ~1.0 Å we can safely expect a carbon atom to be located approximately 4.7 Å from the nitrogen nucleus. The stereochemical constraints imposed by the van der Waals radii of likely chemical groups with C-H bonds (Bondi, 1968) approaching the nitrogen nucleus along the molecular z-axis are compatible with this assessment. Further identification of the likely donor residue of the proton unfortunately cannot be made.

Although some estimate of the degree of hydrophilic vs. hydrophobic character of the environment of a free radical can be made from the change in ENDOR signal height upon exchange of the solvent for a fully deuterated solvent (Ehrenberg et al., 1971), such further chemical modification of the spin-label doped lysozyme crystal appeared unwarranted since structural interpretations of higher detail could not be made. The results of these ENDOR studies indicate that the nitroxide moiety, although within van der Waals contact of a protein residue along the molecular z-axis, is nonetheless, largely exposed to a disordered distribution of solvent molecules. We can expect the nitroxide group of the bound spin-label to protrude into the solvent channel of the crystal. Such a structural interpretation implies that the site-directing acetamido specificity site does not orient this spin-label into the active site cleft as in the case of oligomers of GlcNAc (Imoto et al., 1972) or of the inhibitors GlcNAc-Glc and p-nitrophenylchitobioside

(Moult, 1970; Imoto et al., 1972). Binding forces of an unanticipated nature must consequently exist between the spin-label and the enzyme.

In order to further assess the structural origins of the different and rather unexpected binding forces between the spin-label and the lysozyme molecule, the three-dimensional structure of the complex was determined by difference Fourier methods. This more detailed structural study was also motivated by the expectation that the unusual stereochemical binding configuration would provide a better basis to assess in detail the potential use of nitroxide spin-labels to probe specific regions of enzyme active site regions when incorporated into structural analogues of natural inhibitors and substrates.

D. X-ray Crystallographic Determination of the Structure of the Lysozyme-Spin-Label Complex

1. Primary Data Collection and Initial Processing

a. Low Resolution Data

Low resolution data with a minimum interplanar spacing of $d \geq 5.9$ Å were collected on a Hilger and Watts automated four-circle diffractometer controlled by a PDP-8 computer as described in Section III.B.2. Nickel filtered CuK radiation was used from an Elliott Automation fine-focus sealed x-ray tube operated at 40 kV, 30 mA. A NaI scintillation counter with pulse height discrimination served as the detector of diffracted x-rays.

Data collection was carried out for low-resolution data with crystals mounted about $\hat{a}^*$ employing the moving crystal, stationary-counter ordinate analysis procedure of Watson and co-workers (Watson *et al.*, 1970). A scan range of 1.2° on ω was sampled in 60 equal steps with a counting time of 1 sec per step. This range was chosen during the alignment of the crystal, scans of the strongest reflections showing a maximum peak width of ~0.6°. Source and detector collimators had diameters of 2.5 and 3.5 mm respectively, as required by a crystal of approximately 1.5 mm in largest dimension.

Crystal alignment and calculation of orientation matrices were carried out on the three axial reflections 16 0 0, 0 16 0, and 0 0 6 outside of the intended resolution limit. At regular intervals during data collection, the crystal alignment was checked by monitoring the position of two standard reflections 16 0 0 (at $\phi = 0°$ and $\phi = 90°$) and 0 16 0. Diffractometer setting angles were also checked against fixed references; reflections affected by serious missettings were remeasured after correction of faults.

The low resolution data set comprised all reflections having $h \geq 0$ for the limiting interplanar spacing selected. This gave eight equivalents which, separately measured, were subsequently reduced to approximately 400 independent reflections.

For subsequent empirical correction of absorption effects (North *et al.*, 1968), a transmission curve was

measured on the 4 0 0 reflection at 10° intervals in ϕ immediately before data collection. No radiation damage monitor was made for low resolution data.

b. High Resolution Data

High resolution data were collected on a computer controlled Hilger and Watts linear diffractometer (Arndt and Phillips, 1961) adapated to measure five reflections quasi-simultaneously in the flat cone setting (Arndt, North, and Phillips, 1964). The high resolution data set was comprised by the limiting interplanar spacings of ~ 8 Å $\geq d \geq 2.5$ Å. Nickel filtered CuK radiation from an Elliott Automation fine-focus sealed x-ray tube, operated at 40 kV, 16 mA was used. The diffracted x-rays were detected with proportional counters mounted 0.75 cm apart at the end of a helium-filled draw-tube. The crystal-to-counter distance was adjusted to 38.7 cm. The counter positions were frequently checked with vertical and horizontal half-width slits to ensure that the diffracted intensity was equally distributed in the vertical and horizontal halves of each counter.

The high resolution data collection scheme with use of an $\hat{a}^*$ mount of the crystal is illustrated in Figure 37. For tetragonal crystals of lysozyme the $\hat{a}^*$ mount has several advantages over a $\hat{c}^*$ mount:

(1) Reflections near the rotation axis which are inaccessible in the flat cone setting can be measured as accessible equivalent reflections in other parts of reciprocal space.

Figure 37.--High resolution data collection scheme for tetragonal lysozyme crystals using an $\hat{a}^*$ mount. High resolution data are collected in sets of four quintuplets of half-levels $(+h+k\pm\ell)$. Except for the omission of reflections with $h \geq 20$, this data collection scheme yields up to 9000 reflections as Bijvoet-related reflections $hk\ell$ and $hk\bar{\ell}$ and about 5500 reflections equivalent to these on other levels. Reflections in the low resolution region ($d > 6$Å) are separately collected on a four-circle diffractometer. Figure from Snape (1974).

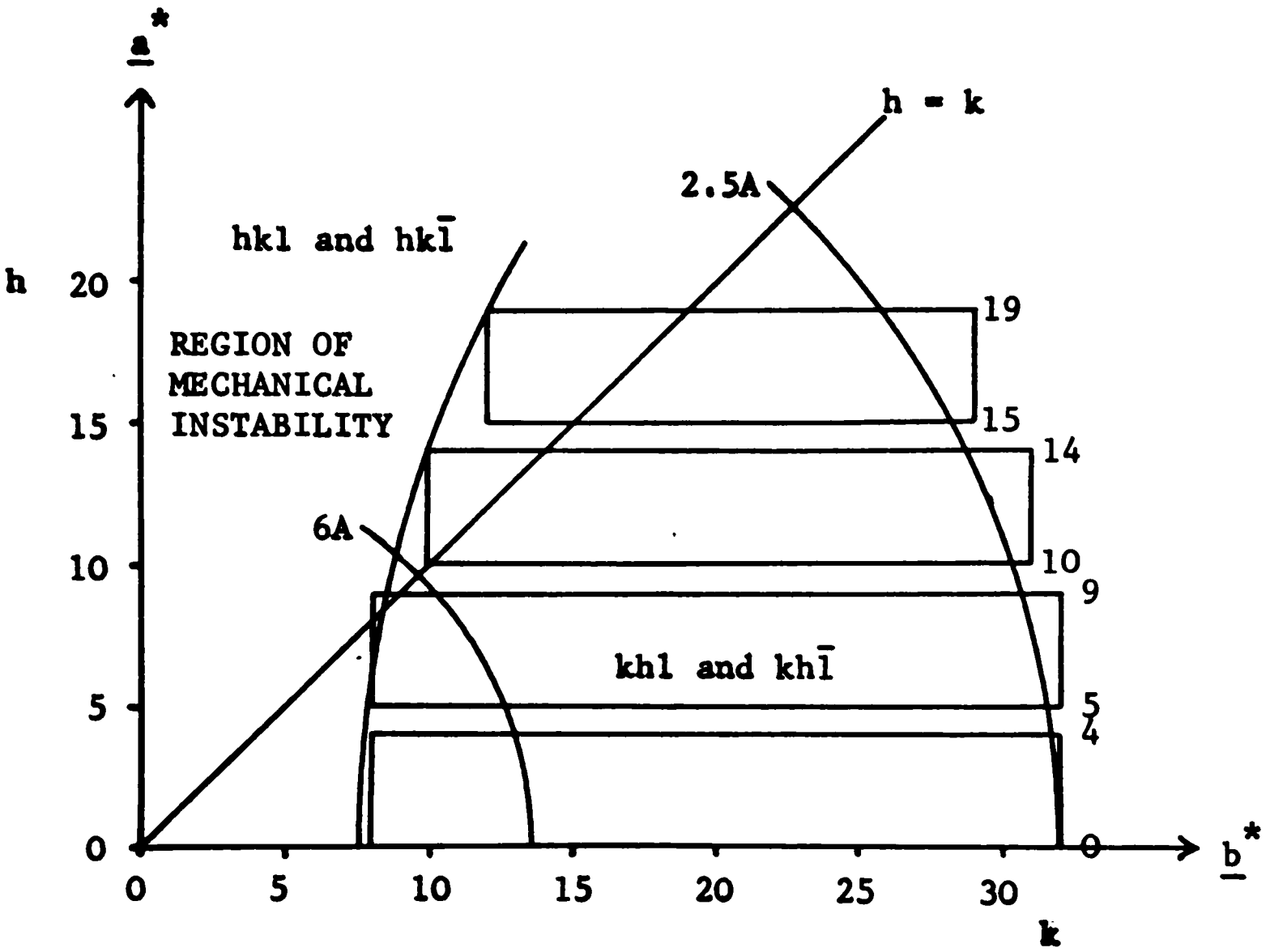
a*
h = k
2.5A
hkl and hkl̄
h
20
REGION OF
MECHANICAL
INSTABILITY
19
15
14
6A
10
10
9
khl and khl̄
5
5
4
0
0
0
5
10
15
20
25
30
b*
k

(2) A large proportion of reflections exist for which equivalent reflections are independently measurable on other reciprocal lattice levels. This large number of intrinsic overlap reflections enables readily the calculation of interlevel scale factors.

(3) The quasi-simultaneous measurement of five adjacent reflections is more exact for $\underline{a}^*$ levels than for the more widely spaced $\underline{c}^*$ levels. This arrangement allows a smaller oscillation range to be used, and for a given oscillation time, yields statistically better data.

With crystals mounted about $\hat{\underline{a}}^*$, data were collected in the background-peak-background mode using a 15 sec stationary count on each background and a 30 sec scan on ϕ with an oscillation range of 1.5°. The data set was comprised by measurement of both components, khl and $kh\bar{l}$, for all reflections from 8 Å to 2.5 Å, and for about two-thirds of these reflections, the equivalent reflections hkl and $hk\bar{l}$ respectively, measured on other levels. The diffractometer was made to scan rows of constant l and stepped onto an adjacent row when the $\hat{\underline{b}}^*$ axis or a preset inner or outer limit switch was met. The outer switch was set just beyond the required 2.5 Å resolution limit.

Preliminary crystal alignment procedures included pulse-height analysis of the five counter outputs, measurement of reciprocal cell dimensions, and determination of the best oscillation angle and the position of the counter assembly at the end of the helium-filled draw tube. Deter-

mination of the unit cell parameters by measurement of axial reflection positions on ϕ indicated that $\underline{a} = \underline{b} = 79.1$ Å, $\underline{c} = 38.2$ Å in good agreement with the lattice constants estimated from precession photographs.

A radiation damage monitor was made as a function of both time of x-ray exposure and of Bragg angle θ. The gross time dependence was monitored by measuring eight quintuplets of reflections before and after data collection and between each quintuplet of actual levels. These monitoring reflections were spread throughout reciprocal space, and their averaged variation was assumed to be representative of the data set as a whole. An approximate 10% decrease in the total average intensity was observed over the entire period of x-ray exposure. The angular dependence of the radiation damage was monitored along $\hat{\underline{b}}^*$ and $\hat{\underline{c}}^*$ by measuring the intensities of ten reflections near each axial reciprocal lattice point between 10 Å and 2.4 Å resolution before and after data collection. Plots of the ratios of the intensities (I_{before}/I_{after}) against the corresponding Miller index for each correspondnng axis yielded parallel straight lines. On this basis an isotropic angular correction was applied as a linear function of $\sin\theta$.

Absorption effects were corrected by the procedure of North _et al_. (1968) from a transmission curve of the 8 0 0 reflection measured at 15° intervals in ϕ immediately before and after data collection. The transmission curve was determined on the linear diffractometer. The highest correction factor was 1.40.

c. Primary Data Reduction

Programs for primary data processing were written by Professor A. T. C. North. The diffractometer data were processed and corrected for Lorentz and polarisation effects (North, 1965) and empirically for absorption effects (North *et al.*, 1968). Monitors of statistical significance and possible crystal and diffractometer missettings were also included. For linear diffractometer data reflections for which the two backgrounds differed by between four and six standard deviations were assigned background counts of twice the lower count. Differences greater than six standard deviations caused rejection of the reflection. Reflections measured to be negative were set to zero. For low resolution data, reflections were rejected if the peak centre departed from the scan centre by more than half the expected peak width.

2. Intermediate Data Processing

In order to determine whether systematic errors due to absorption effects obtained in the data, blocks of Bijvoet-related reflections were compared. Groups of five $\underline{a}^*$ levels were taken together and divided into 24 sectors on ϕ comprising one ξ^2 range each. The ratios ($\langle I^+ \rangle / \langle I^- \rangle$) of the mean intensities of these Bijvoet-related blocks were plotted against ϕ. Significant deviations from unity were observed for the fourth level only, the highest resolution data and most difficult to collect accurately because of the generally

weaker intensities. These ratios demonstrated uncorrected absorption effects in the data. The errors were corrected by making the ratios unity and the averaged data were then used. This procedure does not compensate for absorption errors between unrelated reflections; however, systematic errors due to the generally asymmetric transmission properties of crystals used for high resolution data should be greatly reduced.

In the high resolution data set the large proportion of equivalent reflections which appear in different levels were extracted and used to determine interlevel scale factors by the method of Hamilton, Rollett, and Sparks (1965). This method minimises by a non-linear least squares procedure

$$\Psi = \sum_{hkl} \sum_{i=1}^{N_m} \omega_{m_i} \left(I_{m_i} - G_n I_m\right)^2$$

where I_{m_i} is the ith measurement of reflection m,

ω_{m_i} is the weight associated with that reflection and is the reciprocal of the variance of the reflection,

N_m is the number of measurements of m

G_n is the nth scale factor, and

I_m is the best value of the intensity of reflection m averaged over all equivalent measurements with respect to all scale factors G_n.

Convergence was considered complete when the scale factor shifts were less than 0.5%. The final scale factors were applied to their respective levels and equivalent reflections merged to produce a unique high resolution data set.

The low resolution data set was similarly examined for residual absorption effects in ten ranges of Φ and one range of ξ^2, but no systematic effects were present. The separate high and low resolution data sets were then merged by the Hamilton, Rollett, and Sparks method and reduced to a unique data set. Of the 14680 reflections measured, a unique set of 5910 independent reflections was obtained. The merging R-value was 0.064 where

$$R = \frac{\sum_{hkl}\sum_{i=1}^{n}(I_i - I_{mean})}{\sum_{hkl} nI_{mean}}.$$

The data were scaled to the native lysozyme data set. A list of the resultant structure amplitudes employed in the difference Fourier synthesis of the lysozyme spin-label complex and the phases and figures of merit of the native lysozyme data are provided in Appendix IV.

3. Interpretation of the Difference Electron Density Map

a. Calculation of the Map

A difference Fourier synthesis was computed using as coefficients $\underline{m}(|\underline{F}_{SL}| - |\underline{F}_p|)\exp(i\alpha_p)$ where for each reflection $|\underline{F}_{SL}|$ is the structure amplitude of the protein plus

spin-label inhibitor and $|\underline{F}_p|$ the structure amplitude of the native protein, and α_p is the "best" phase (Blow and Crick, 1959) of the native protein weighted by $\underline{m}$, its associated figure of merit. The factor of two (Luzzati, 1953) was incorporated into the difference Fourier coefficients. The limits of the difference Fourier calculation were

$$-30/120 \leq x \leq 33/120 \text{ in intervals of } \underline{a}/120$$
$$0 \leq y \leq 60/120 \text{ in intervals of } \underline{b}/120$$
$$\text{and} \quad 0 \leq z < 1 \text{ in intervals of } \underline{c}/60$$

corresponding to an approximate 0.67 Å grid spacing for each axis. These limits yield a map, calculated in this case with sections perpendicular to $\hat{z}$ and containing a complete lysozyme molecule approximately in the centre. The difference electron density map was then contoured at a scale of 4 Å/cm on the laboratory Ferranti Argus 500 computer with aid of the Multiweave program of Banyard (1973).

Since difference Fourier syntheses are based on phases of the native protein, there are three likely sources of error contributing to the calculation of difference electron density peaks. They arise from (1) application of the phases of the native enzyme rather than the phases of the derivative; (2) errors in the phases of the native protein determined by the isomorphous replacement method; and (3) errors in the measurement of the structure factor amplitudes (Henderson and Moffat, 1971). The contributions of the

individual sources of error have been estimated in connection with earlier difference Fourier studies of lysozyme complexes (Beddell, 1970; Ford *et al.*, 1974), and the total error arising from such factors has been estimated to range from 0.144 e/Å^3 for the iodine oxidized protein containing no bound inhibitor molecule to 0.202 e/Å^3 for the iodine oxidized lysozyme-chitotriose complex (Beddell, 1970). Complexes with inhibitor molecules of molecular weight comparable to that of the spin-label inhibitor such as the lysozyme-N-acetylglucosaminolactone complex with a merging R-value of 0.07 are associated with an error of about 0.13 e/Å^3 (Beddell, 1970).

A rigorous estimate of the root-mean-square error in a difference electron density map is made difficult because the various sources of error are generally assumed to be independent. Since in the calculation of a variety of difference Fourier maps of lysozyme-inhibitor complexes the same set of structure factor amplitudes, phases, and figures of merit of the native enzyme are employed, it is probably safe to assume that the estimated root-mean-square error of the spin-label difference Fourier map remains comparable to those of other complexes with inhibitors of similar molecular weights and scattering contributions. On this basis we assume that the root-mean-square error in the lysozyme spin-label difference Fourier map is approximately 0.15 e/Å^3. Consequently the lowest contour level chosen corresponded to 0.30 e/Å^3, and the map was contoured at

increments of 0.15 e/Å^3. The highest difference electron density feature contoured corresponded to 1.05 e/Å^3 for positive peaks and -0.60 e/Å^3 for negative peaks. The interpretation of the structure of the complex consequently can be considered at a level of difference electron density features significantly above the random noise level of the Fourier map.

The contoured maps were transferred to transparent acetate sheets and stacked in an interleaving fashion against the corresponding map of the native enzyme contoured to identical grid spacings and at the same electron density levels. Groups of these perpendicularly stacked sheets are viewed in Figure 38 and provide a comparison of the difference electron density features with the electron density features of the native protein.

It is evident that the difference electron density features of the inhibitor molecule are confined to the region of the active site cleft corresponding approximately to subsites A-C in the map of the native molecule. No significant difference electron density features are observed in the solvent channels or between enzyme molecules in anomalous positions. There are small difference electron density features throughout the protein obviously corresponding to movements of amino acid residues and associated solvent molecules. By comparison of the features of this difference electron density map with those of the lysozyme-chitotriose complex (Blake _et al._, 1967) and with the map of the native

Figure 38.--Colour photographs of the difference Fourier map of the lysozyme-spin-label complex minus the native lysozyme structure. The difference map is contoured in red ink. Sections are stacked perpendicular to $\hat{z}$ and are interleaved with sections of the native lysozyme electron density map contoured in black ink for each corresponding level. The lowest contour level of difference electron density features appears at approximately ± 0.30 e/Å^3, and higher contours are drawn at incremental intervals of 0.15 e/Å^3. Positive features in the difference map sections are drawn in solid lines and negative features are in broken lines. The individual photographs correspond to groups of stacked sections as follows (in intervals of z/60): (a) $0 \leq \hat{z} \leq 5$; (b) $6 \leq \hat{z} \leq 13$; (c) $14 \leq \hat{z} \leq 20$; (d) $21 \leq \hat{z} \leq 27$; (e) $28 \leq \hat{z} \leq 34$; (f) $35 \leq \hat{z} \leq 38$. Difference features corresponding to the spin-label molecule or to significant movements of the protein were not observed in sections beyond $\underline{z} = 39/60$. Since sections 35-38 corresponding to subsite D of the active site cleft have no difference electron density features of the spin-label molecule, these maps readily indicate that the spin-label binds in a highly anomalous manner contrary to the expected site directing effect of the acetamido side chain.

a

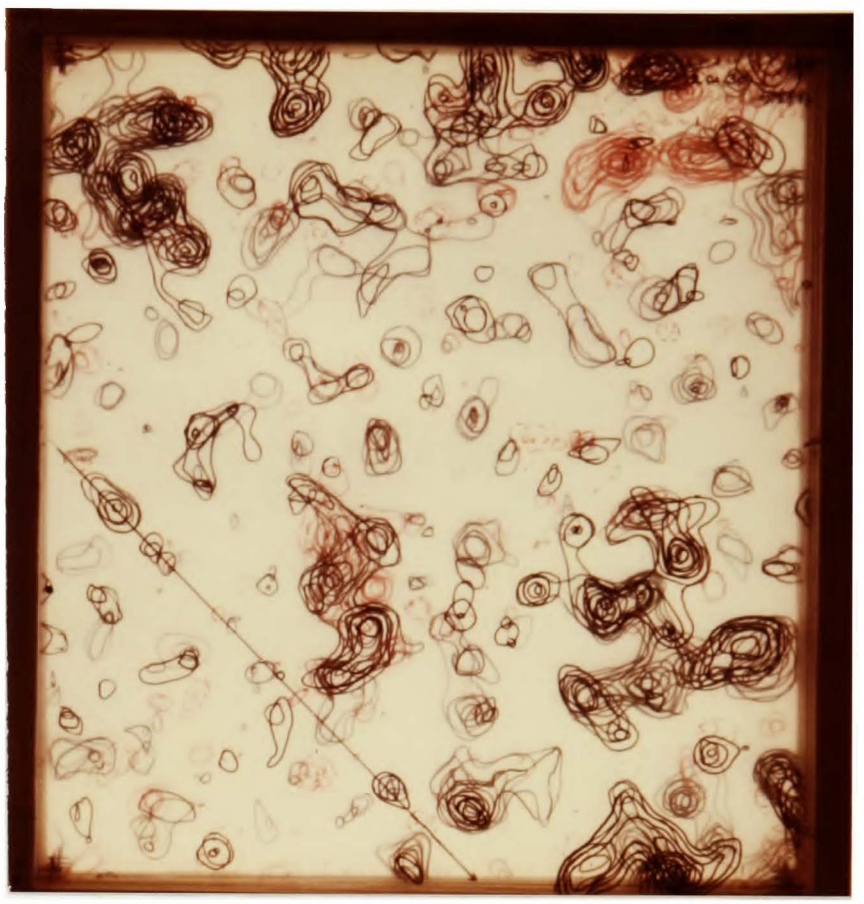

b

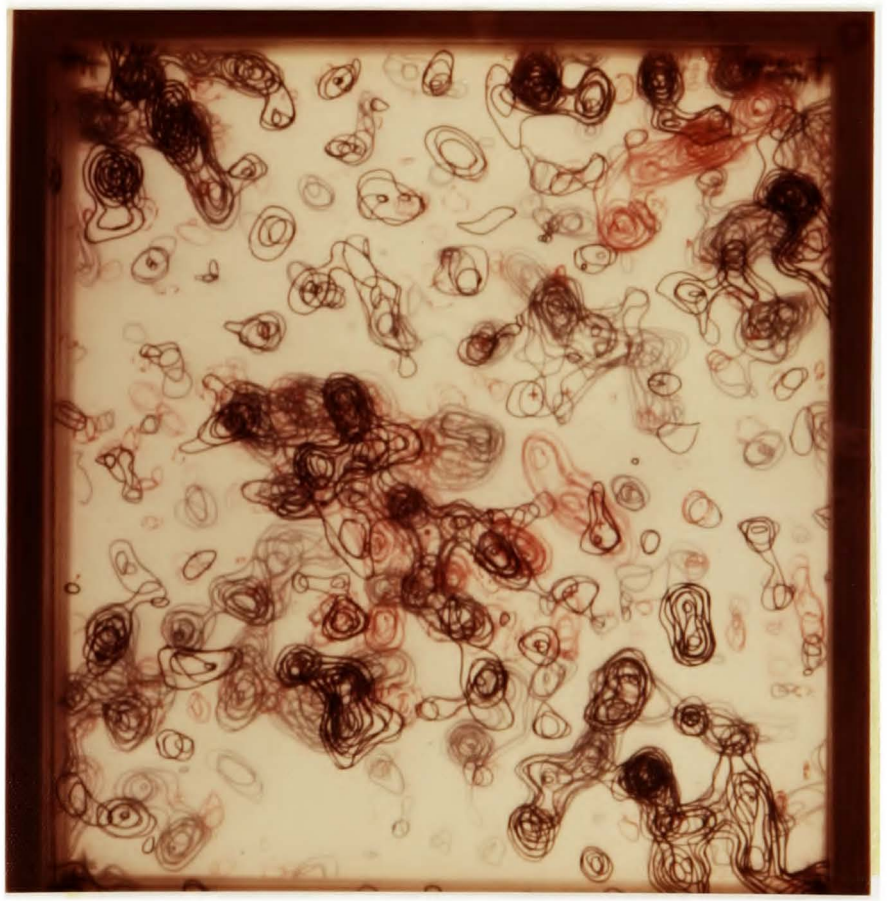

c

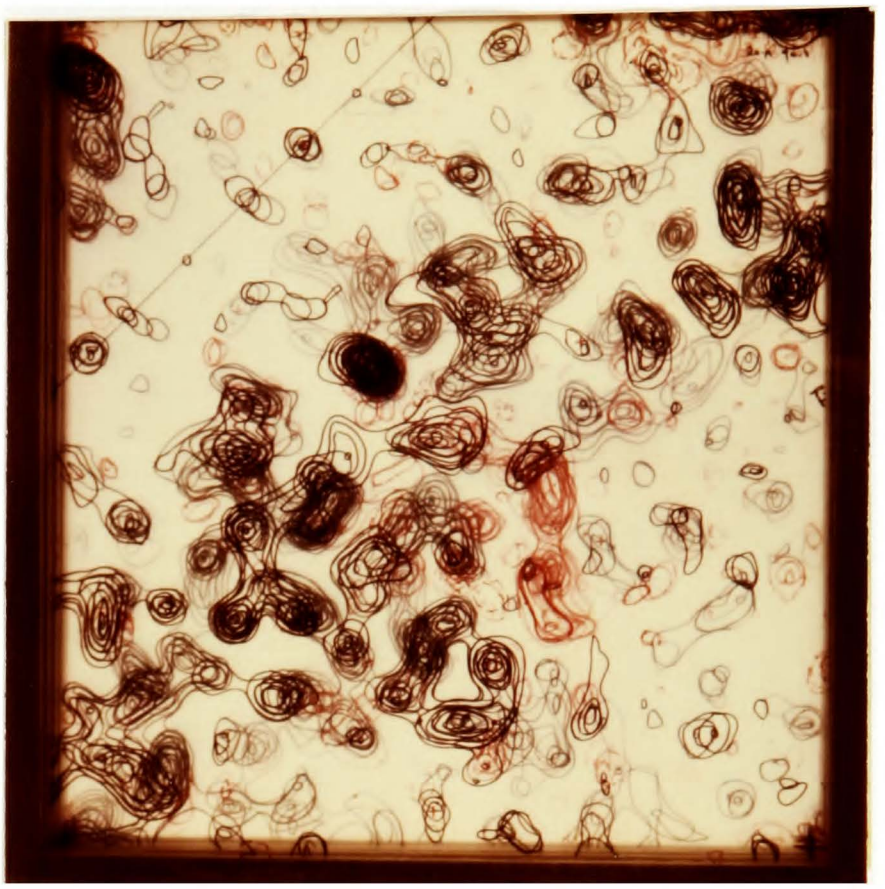

d

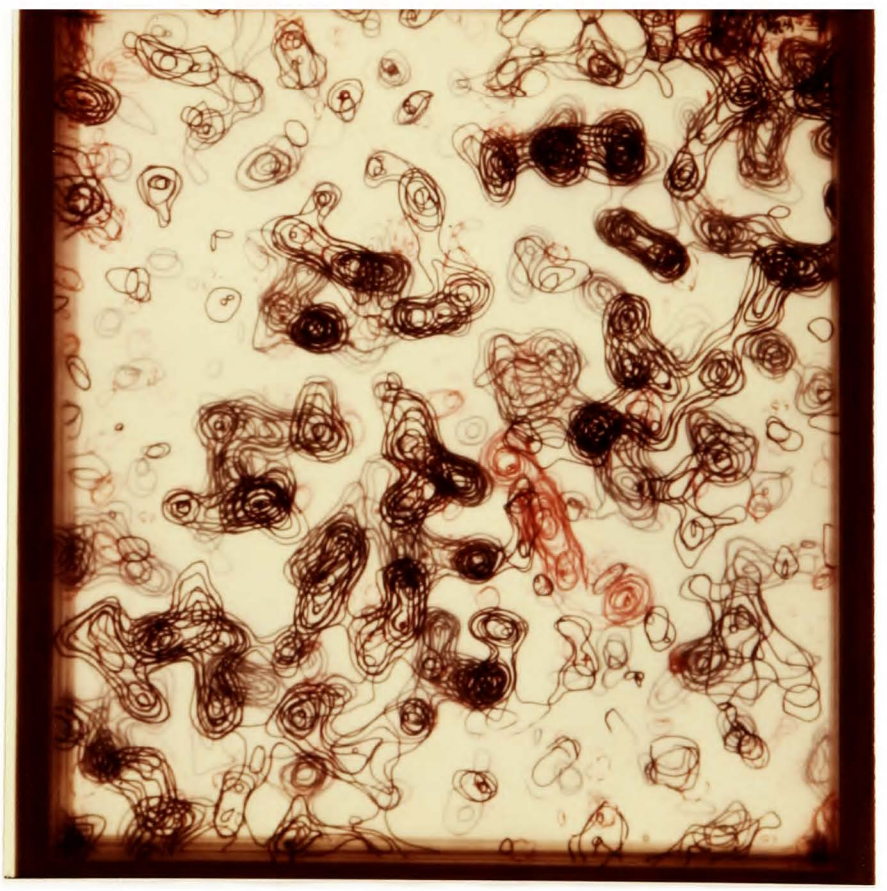

e

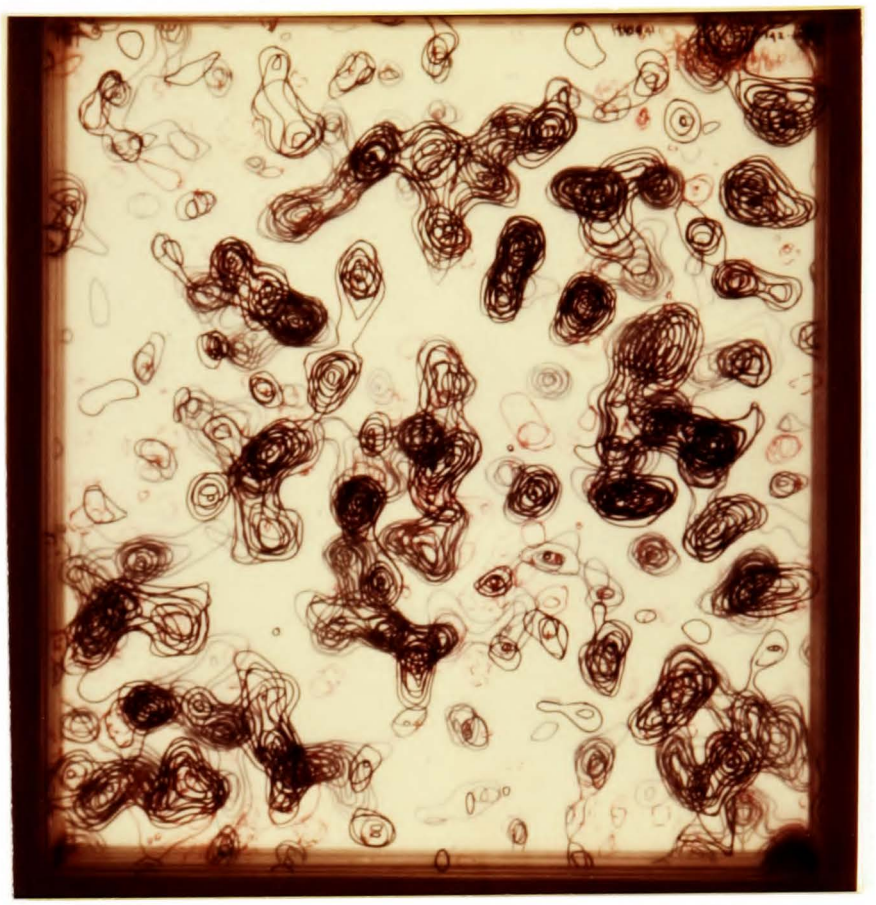

f

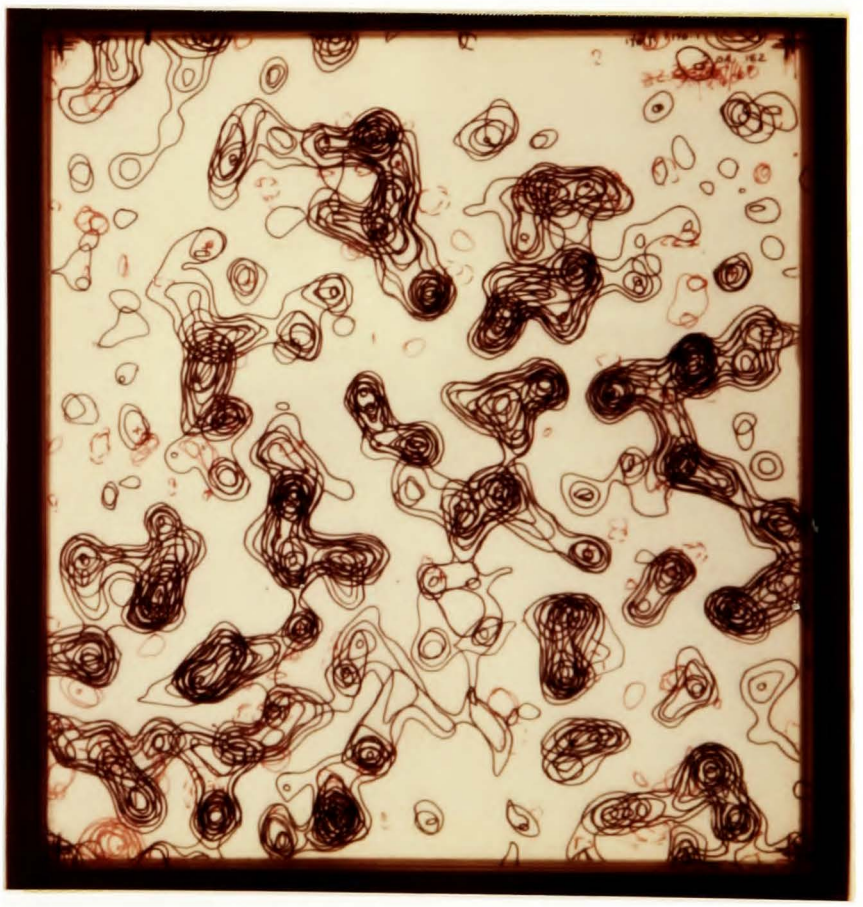

enzyme, close visual study indicated that the spin-label inhibitor binds across subsites B and C. It was possible upon visual inspection to account for difference electron density features corresponding to the piperidinyl ring in subsite B and the acetamido side chain in subsite C, thus providing confirmation of the anomalous binding configuration expected on the basis of the ENDOR results described in Section V.C.3.b. At this point it was decided that a preliminary assessment of the stereochemical features of the binding configuration would be carried out quickly in efforts to explain in more detail the results of ENDOR studies and to try to account for the structural basis of the anomalous binding mode. This was to be carried out with aid of computer model building studies while a detailed examination of fitting a molecular model to the difference Fourier map would be subsequently finished by Dr. K. W. Snape.

b. Computer Aided Model Building Studies

Initial model building studies to fit a molecular model of the spin-label inhibitor to the difference electron density map employed the Laboratory Ferranti Argus 500 computer controlled cathode ray tube display system. Programs for this computer aided method were written by Dr. C. D. Barry and Mr. L. O. Ford and have been described through other publications (Barry and North, 1971 and 1972; Ford et al., 1974).

The input coordinates for the spin-label inhibitor were derived from a model constructed by joining the two separate residues into a β-glycosidic bond on the cathode ray tube screen. For this the atomic coordinates of the structures determined in x-ray diffraction studies of GlcNAc (Johnson, 1964 and 1966) and of TEMPO (Berliner, 1970) were employed. The two residues were linked so as to superimpose the glycosidic oxygen atom of the carbohydrate residue and the alcoholic oxygen atom of the spin-label. The valence bond angle of the glycosidic oxygen was kept at 116° as observed in cellobiose (Chu and Jeffrey, 1968). Since the C-O bond length of the spin-label moiety is 1.421 Å (Berliner, 1970), this bond length was not modified. The distal C-O bond length of alkyl substituted glucopyranosides as listed in Table 21 are consistent with this value. The numerical ordering of the constituent atoms of the inhibitor molecule are indicated in Figure 39.

c. Preliminary Model Building Studies in Interpretation of the Map

The difference electron density features in the immediate region of the inhibitor molecule for purposes of orthonormal projection on the cathode ray tube screen were calculated and contoured at the same grid spacing as for the initial difference Fourier map. In order that the electron density features of the entire inhibitor could be displayed simultaneously with the atomic model of the inhibitor itself, however, the first electron density contour level

Figure 39.--Numerical ordering of constituent atoms of the β(TEMPO)-GlcNAc spin-label inhibitor for purposes of fitting the molecule to the difference map features with the Argus computer controlled cathode ray screen. The atom marked X_{15} serves as a dummy input atom to allow rotation of either spin-label or carbohydrate to alter the glycosidic bond angle if necessary. Free rotation was also permitted around the N_3-C_4, C_0-N_3, C_9-C_{10}, C_{13}-O_{14}, and O_{14}-C_{16} bonds. The acetamido side chain was fixed as planar.

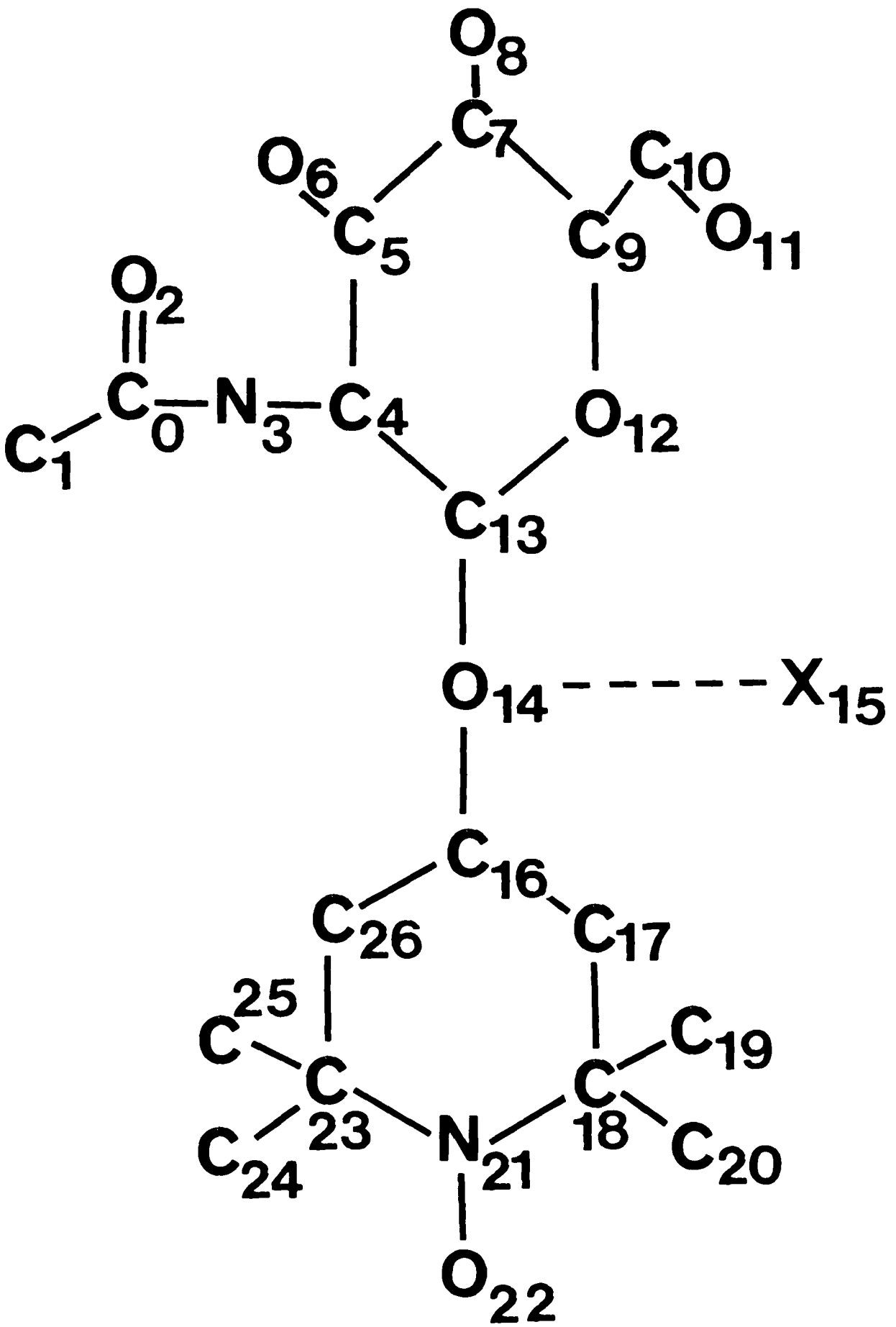
O8
C7
O6
C10
C5
C9
O11
O2
C0
N3
C4
O12
C1
C13
O14
X15
C16
C26
C17
C25
C19
C23
C18
C24
N21
C20
O22

was chosen at a level of 0.35 e/Å^3 rather than 0.30 e/Å^3 because of the limiting computer core storage capacity.

In fitting the model to the difference electron density map with use of the computer controlled visual display system, continual reference was made to the map contoured on transparent plastic sheets. As a result of numerous trial fittings the configuration which appeared to account most adequately for the difference electron density features of the molecule was selected as the most probably correct fit since no configuration would account entirely for the four methyl groups of the nitroxide ring. The binding configuration is characterised by the acetamido side chain binding to the specificity site of the CO and NH groups of residues 107 and 59 but with the nitroxide ring directed into subsite B.

While the computer assisted fitting was carried out, attempts to photograph the best fits displayed in orthonormal projection on the cathode ray screen failed and direct reproduction of these results consequently is not available. The atomic coordinate positions relative to the screen axes were obtained, however, for these trials and on this basis a superposition of the molecule on the difference electron density features of the spin-label inhibitor was drawn and photographed. This superposition is illustrated in Figure 40 and the atomic coordinate positions are listed in Table 30. A more detailed examination of the binding of the spin-label to lysozyme has been subsequently carried out by Dr. K. W.

Figure 40.--Photograph of the density features of the spin-label molecule only in the difference Fourier map of the lysozyme-spin-label complex minus the native lysozyme structure. The sections are contoured essentially as described in Figure 37, but are drawn for sections stacked perpendicularly to x as observed in preliminary molecular fitting trials. The difference map includes mainly positive features corresponding to the spin-label molecule in the active site cleft across subsites C and B. The best fit of the inhibitor molecule obtained by computer aided map fitting studies is superposed on the corresponding density features.

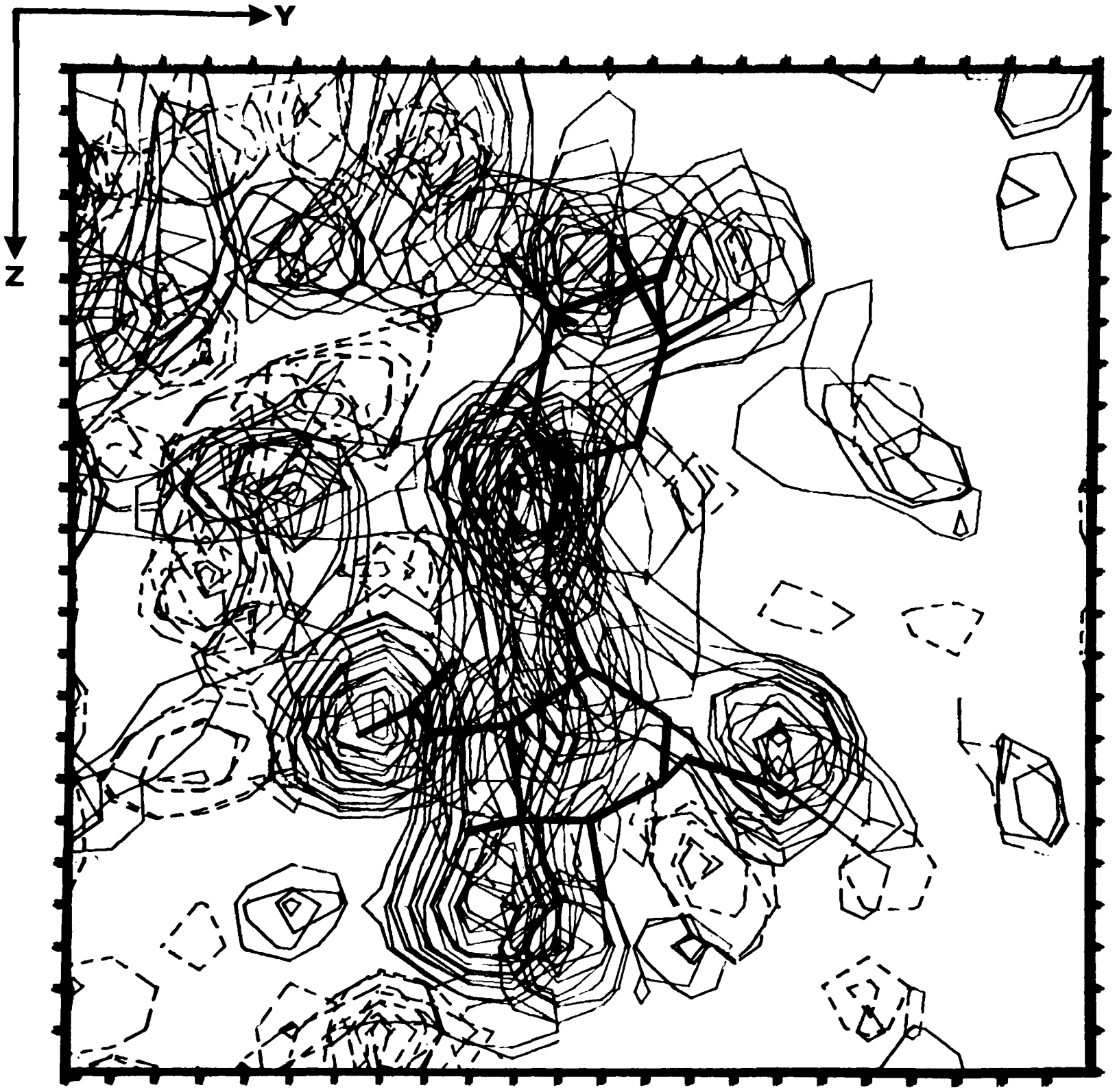
Y
Z

TABLE 30

LISTING OF ATOMIC COORDINATE POSITIONS OF β(TEMPO)-GlcNAc IN THE LYSOZYME-SPIN-LABEL COMPLEX OBTAINED BY COMPUTER AIDED MOLECULAR MODEL BUILDING STUDIES.

Atom*	Atomic Coordinate Position* in Angstroms		
	$\hat{x}$	$\hat{y}$	$\hat{z}$
C_0	-1.62	-0.79	2.55
C_1	-2.02	-1.55	3.82
O_2	-0.86	0.13	2.53
N_3	-2.36	-1.20	1.46
C_4	-2.65	-0.21	0.40
C_5	-2.61	-0.95	-0.95
O_6	-3.78	-1.86	-1.00
C_7	-2.87	0.06	-2.06
O_8	-2.77	-0.63	-3.36
C_9	-1.67	1.07	-2.02
C_{10}	-1.70	2.20	-3.06

O_{11}	-0.48	2.30	-3.70
O_{12}	-1.68	1.73	-0.73
C_{13}	-1.56	0.88	0.44
O_{14}	-1.69	1.63	1.56
C_{16}	-1.22	2.97	1.54
C_{17}	-0.44	3.18	0.47
C_{18}	0.28	4.64	0.33
C_{19}	-0.82	5.45	-0.39
C_{20}	1.60	4.73	-0.44
N_{21}	0.50	5.25	1.68
O_{22}	1.08	6.40	1.70
C_{23}	-0.20	4.84	2.94
C_{24}	0.76	5.07	4.11
C_{25}	-1.46	5.71	3.10
C_{26}	-0.58	3.36	2.88

*Atoms are labeled as in Figure 39. The atomic coordinate positions of the spin-label molecule are given with reference to the coordinate axis system of the computer controlled cathode ray screen. The molecular fit of the inhibitor across subsites C and B is illustrated in Figure 40.

Snape. This more detailed examination has confirmed the essential correctness of the preliminary assessment presented in this chapter (M. W. Makinen, K. W. Snape, and B. A. Coles, manuscript in preparation).

In Figure 40 the salient features of the difference electron density peaks are readily apparent with respect to the structure of the inhibitor molecule. In this view the difference Fourier map was calculated and contoured for sections perpendicular to $\hat{x}$ at the same contour levels and grid intervals as in Figure 37. The acetamido side chain is seen as a prominent difference electron density peak. The appearance of negative density features adjacent to positive features near the O8 and O6 atoms of the carbohydrate moiety may indicate the displacement of solvent molecules from that region of the active site in the native molecule to hydrogen bonded positions adjacent to the carbohydrate hydroxyl groups. The glycosidic oxygen bridge is well accounted for by a central region of difference electron density which merges into features belonging to the C_{16}, C_{17}, and C_{26} atoms of the piperidinyl ring.

Of particular interest here is the orientation of the nitroxide group and the four methyl groups with respect to the protein. Behind the nitroxide ring is visible a prominent positive difference electron density feature associated (upon closer inspection) with a negative difference peak as viewed in projection along $\hat{x}$. These difference peaks are associated with movement of the indole ring of

Tryp-62 towards the four methyl groups of the piperidinyl ring. Orthonormal display of the difference map indicated the corresponding difference electron density peaks of the methyl groups to be immediately adjacent to the positive features of the indole ring. Although the distance between the two ring structures was not estimated, this interaction can be readily rationalised on the basis of hydrophobic interactions between the methyl groups and the indole side chain. The position of the indole side chain, futhermore, is such as to be compatible with placing a proton along a perpendicular to the nitroxide nitrogen atom. The regions of the difference map corresponding to the immediate surroundings of the nitroxide group along its molecular x- and y-axis directions clearly indicate no nearby side chain residues but rather exposure into the solvent channel of the crystal out of the active site cleft. These qualitative structural interpretations of the difference electron density features, thus, confirm the interpretation of the ENDOR results presented earlier and indicate that hydrophobic interactions between the four methyl groups and protein residues are sufficient to perturb the usual binding properties of the GlcNAc residue.

E. A Brief Discussion of Structural Aspects of Synthetic Substrate and Inhibitor Analogues of Lysozyme

Spin-labels in the study of macromolecular structure by magnetic resonance methods have been widely applied to a

variety of monomeric and oligomeric proteins. Nonetheless, only the lysozyme-inhibitor complex described by Berliner (1971), the lysozyme-inhibitor complex described in this chapter, and a covalently formed spin-label derivative of horse methaemoglobin (Moffat, 1971) have been characterised by x-ray diffraction studies.

The immediate importance of the results of the lysozyme-inhibitor studies, especially from the results presented here, is that the lysozyme studies clearly demonstrate binding interactions between the spin-label moiety and the protein which have no resemblance to those observed in complexes of the enzyme with natural inhibitor and substrate molecules. In the case of the β(TEMPO)-GlcNAc complex, the four methyl groups of the nitroxide ring appear to enter into hydrophobic interactions with amino acid side chain residues which must be energetically comparable at least to the hydrogen bonding relationships of the carbohydrate hydroxyl groups required for productive binding modes (Imoto et al., 1972). Furthermore, in the low resolution study of Berliner (1971), it was pointed out that the nitroxide ring may have been bound with the N-O and methyl groups protruding into the active site cleft rather than into the solvent channel through hydrophobic interactions. Since such anomalous binding configurations have no counterpart in the correlation of the interaction of spin-label substrate and inhibitor analogues with enzymes, in comparison to their respective naturally occurring parent compounds, the results clearly emphasise the caution

which must be exercised in the application of spin-label derivatives in the study of macromolecular structure-function relationships. Comparable structural perturbations in the use of spin-labels bound to other types of enzymes and proteins should be consequently anticipated. This precaution is even more emphatically made in light of the results of preliminary model building studies mentioned earlier which indicated that there should be no steric hindrance to the binding of the β(TEMPO)-GlcNAc derivative across subsites C and D.

The results of the x-ray difference Fourier studies, although analysed here only in preliminary form and without a detailed examination of all stereochemical relationships of the spin-label-enzyme binding contacts, provide, nonetheless, structural data in confirmation of the interpretation of the results of ENDOR studies. Although the spin-label inhibitor employed in this investigation proved to have unusual binding relationships to the enzyme, the application of ENDOR methods has demonstrated that such spectroscopic techniques can be employed to characterise detailed stereochemical relationships of enzyme-substrate interactions. Providing that a spin-label probe can be suitably bound into a region of a protein molecule with little exposure to solvent it is possible that the width of the line at the free proton frequency region due to disordered protons would be significantly decreased. This effect would improve the resolution of ENDOR lines. Taking into consideration the

steric constraints imposed by the four methyl groups of nitroxide spin-label derivatives, such spectroscopic probe molecules could be then employed in principle to assess stereochemical configurations in crystalline enzyme complexes on the basis of dipole-dipole interactions of the spin-label with nearby protons of the order of 3.5-7.0 Å distant from the nitroxide nitrogen nucleus. That sufficient resolution in detecting the individual ENDOR lines arising from ordered proton sites can be achieved is readily demonstrated by the results of these studies. Furthermore, the incorporation of a spin-label derivative into a suitable substrate molecule that is catalytically attacked by an enzyme may provide a means to assess, by application of ENDOR techniques, the detailed structural differences of intermediate enzyme-substrate complexes stabilised by low temperature methods in single crystals.

APPENDIX I

PRELIMINARY CRYSTALLOGRAPHIC AND SPECTROSCOPIC STUDIES OF OXYMYGLOBIN

A. The Autoxidation of Oxymyglobin

Haemoglobin and myoglobin, as the transport or storage proteins of oxygen in tissues, are probably the two most widely investigated proteins of all. It is also probably generally agreed that more is known about the chemical structure and function of these proteins than of any other protein or enzyme. Consequently, it is surprising that relatively little is known about the kinetics and binding of the oxygen molecule to the protohaem moiety, and that the stereochemistry of oxygen binding to the haem group in these proteins remains primarily a matter of models suggested on the basis of theoretical considerations of molecular orbital theory. Neither the stereochemistry of the oxygen molecule with respect to the porphyrin plane nor the corresponding d-electron configuration of the iron atom have been firmly established for oxygen-coordinated complexes of haemoglobin or myoglobin. The two hypotheses for the stereochemistry of oxygen binding which remain most attractive are schematically

illustrated in Figure 41 as the Pauling model (Pauling, 1949) and the Griffith model (Griffith, 1956). Pauling suggested on the basis of the electroneutrality principle that oxygen coordination occurred with an oblique stereochemical arrangement (Fe-$\hat{O}$-O angle $\simeq$ 120°) and that the iron remained in the Fe(II) state. Griffith concluded on the basis of molecular orbital theory that bonding could occur with a formally seven-coordinate structure in which the interatomic axis of the oxygen molecule was parallel to the porphyrin plane and was bisected by a perpendicular to the Fe(II) cation.

Clearly, an unambiguous structural determination of the oxygen liganding stereochemistry is desirable. The crystallographic and structural properties of sperm whale myoglobin make this protein an ideal candidate for developing chemical methods to maintain the protein in a reduced, oxygenated state in the crystal for high resolution x-ray diffraction studies. Crystals of sperm whale myoglobin are highly ordered allowing data collection to at least 1.5 Å resolution (Kendrew, 1963), the metmyoglobin structure has been refined at 2.0 Å resolution (Watson, 1968), and crystals of the metmyoglobin species are readily obtained by the procedures originally described by Kendrew and Parrish (1956). Furthermore, the unit cell of the monoclinic crystal employed for x-ray studies contains only one molecule and consequently one haem group per asymmetric unit, and a variety of difference Fourier

Figure 41.--Diagrammatic illustration of the stereochemistry of oxygen binding to the haem iron atom according to the (a) Pauling (1949) and the (b) Griffith (1956) models. The illustration is intended to serve as a comparison of the six-coordinate and seven-coordinate structures only, indicating stereochemical relationships characteristic of each. Electronic bonding structures are not indicated.

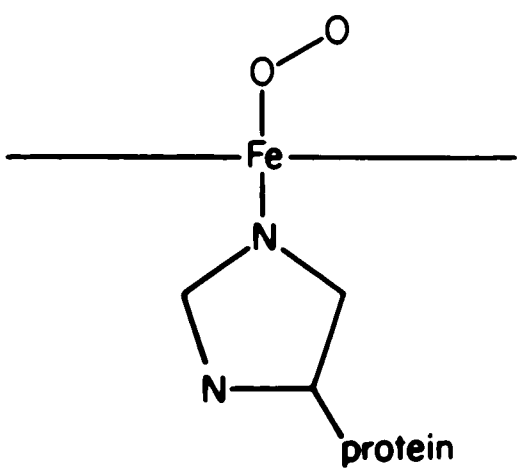

(a)

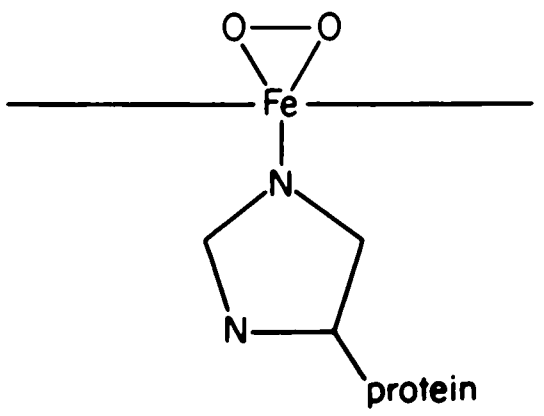

(b)

investigations of high- and low-spin ferric liganded derivatives (Stryer et al., 1964; Watson and Chance, 1966; Bretscher, 1968) and of deoxymyoglobin (Nobbs, Watson, and Kendrew, 1966) provide a thorough structural basis on which to evaluate results of a crystallographic study of the oxymyoglobin species.

An attempt to determine the stereochemistry of the bound oxygen molecule in sperm whale oxymyoglobin by x-ray diffraction methods has been carried out by Watson and Nobbs (1968). They employed oxymyoglobin prepared from fresh muscle tissue (Yamazaki et al., 1964), allowing formation of suitable crystals within 12 hours with high amounts of the oxygenated derivative. A difference Fourier electron-density map of oxymyoglobin versus metmyoglobin at 2.8 Å resolution was calculated in three dimensions. An oblique stereochemical arrangement of the bound oxygen molecule according to the Pauling hypothesis was interpreted as consistent with the difference electron density peaks. However, Watson and Nobbs (1968) pointed out that oxidation of the oxygenated species was promoted by incident x-ray irradiation during data collection. The high pH (~8) employed to stabilise the oxymyoglobin derivative, furthermore, implies conditions under which a mixture of the oxidised species aquometmyoglobin, metmyoglobin hydroxide, and the metmyoglobin ammonia complex would be formed. No monitor was employed of the relative initial and final concentrations of oxygenated species in the crystal or of

the time dependent change in oxyhaem concentration due to x-ray exposure. Although the interpretation may be basically correct, the rigorousness with which the results can be held are consequently difficult to assess. Thus, a detailed high resolution structural elucidation of the oxyhaem stereochemistry in oxymyoglobin is required for clarifying the chemical bonding of the iron-oxygen bond in a manner consistent with its known diamagnetism and spectroscopic properties.

B. Chemical and Crystallographic Studies of Oxymyoglobin

1. Stabilisation of Oxymyoglobin in Solution

In general the stabilisation of oxymyoglobin for x-ray studies can be expected to require control of the autoxidation from two sources: the autoxidation intrinsic to the chemical nature of oxymyoglobin which can be controlled through a suitable choice of pH, temperature, and oxygen partial pressure (Brown and Mebine, 1969) and the autoxidation promoted by the incident x-ray irradiation. The autoxidation of oxymyoglobin (Watson and Nobbs, 1968) promoted by incident x-rays can be considered a general phenomenon in the study of Fe(II) containing proteins. This factor has prevented the determination of the structure of oxyhaemoglobin (Perutz, 1970) and has contributed to the x-ray investigation of the structures of reduced iron-sulfur proteins (Carter et al., 1971). An adjunct chemical method to maintain the oxymyoglobin content of

crystals at high levels must thus counteract the time dependent x-ray induced autoxidation effect and incorporate the chemical and physical conditions known to stabilise oxymyoglobin in solution. In general, the conditions known to stabilise oxymyoglobin may be summarised as: high oxygen partial pressures, an optimal pH in the 8-9 region, and low temperatures to counteract the high Q_{10} of oxymyoglobin in solution (Brown and Mebine, 1969). Of these, clearly the control of pH and temperature of the crystal during x-ray exposure can be readily carried out for crystallographic investigations.

Although oxymyoglobin can be prepared from skeletal muscle as described by Yamazaki *et al*. (1964), the procedure requires a suitable source of freshly obtained muscle tissue. A more generally applicable method obviously would be to generate oxymyoglobin from commercially available metmyoglobin through use of a suitable reducing reagent. This is not a simple chemical requirement since most reducing reagents are associated with damaging affects on haem and protein structure, as evidenced by the formation of choleglobin (Lemberg and Legge, 1949), or immediately cause complete removal of dissolved molecular oxygen with generation of peroxides and harmful free radicals.

Hill and Holden (1927), however, successfully determined the oxygen binding capacity of methaemoglobin reduced with ferrous tartrate in an alkaline medium. This

reducing medium has been known as Stokes' solution (Keilin, 1966) and appears to reduce the ferric form of haem derivatives without complete removal of dissolved oxygen from the solution. In addition to its kinetically sluggish behaviour towards dissolved oxygen, the alkaline conditions required to poise the corresponding Fe(III)/Fe(II) half-cell potentials to reduce a ferric haem derivative (Hill and Holden, 1927) would appear especially advantageous in the case of generating oxymyoglobin: The oxidation of oxymyoglobin is markedly retarded under alkaline pH conditions (see Yamazaki et al., 1964).

For investigation of suitable conditions for generation of oxymyoglobin with use of Stokes' reagent, sperm whale metmyoglobin obtained from Sigma Chemical Co., Ltd., was used without further purification. Stokes' solution is essentially comprised of a mixture of ferrous tartrate formed by addition of ferrous ammonium sulphate to sodium D(+)-tartrate in a medium made sufficiently alkaline by addition of concentrated ammonia (Hill and Holden, 1927). Figure 42 compares the visible absorption spectrum of sperm whale myoglobin under various solvent conditions at room temperature. The addition of concentrated ammonia resulting in bringing the solution to pH 10 has clearly converted the (aquo)metmyoglobin to the ferrimyoglobin ammonia complex (Eaton and Hochstrasser, 1968). No perturbation is observed by the presence of D(+)-tartrate. Addition of the amount of $FeSO_4 \cdot (NH_4)_2SO_4$ to the cuvette

Figure 42.--Comparison of absorption spectra of myoglobin derivatives under different solvent conditions. Lyophilised sperm whale metmyoglobin was dissolved in 0.05 M phosphate buffer at pH 6.5 to a concentration of approximately 10^{-3} M in haem. Aliquots of this solution were then used for spectral studies. The spectrum of acid metmyoglobin at pH 6.5 is illustrated by the solid line (——). Identical dilutions of metmyoglobin were made to simulate solvent conditions for formation of alkaline ferrous tartrate. The spectrum (—— · ——) was obtained by dissolving a solution of metmyoglobin to the same haem concentration in 8% (w/v) sodium D(+)-tartrate in 1.5 M ammonium sulphate buffered to ~pH 9 by addition of concentrated ammonia solution. The spectrum (—— ——) was obtained by addition of ferrous ammonium sulphate to a metmyoglobin solution to an Fe(II) : haem ratio of 10:1 in the presence of 8% (w/v) sodium D(+)-tartrate under alkaline conditions. Spectra were obtained at ambient temperature (~20°C) with a Unicam 800 recording spectrophotometer. Identical spectra were obtained with use of 0.01 M sodium tetraborate at pH 9.2 as the buffering agent.

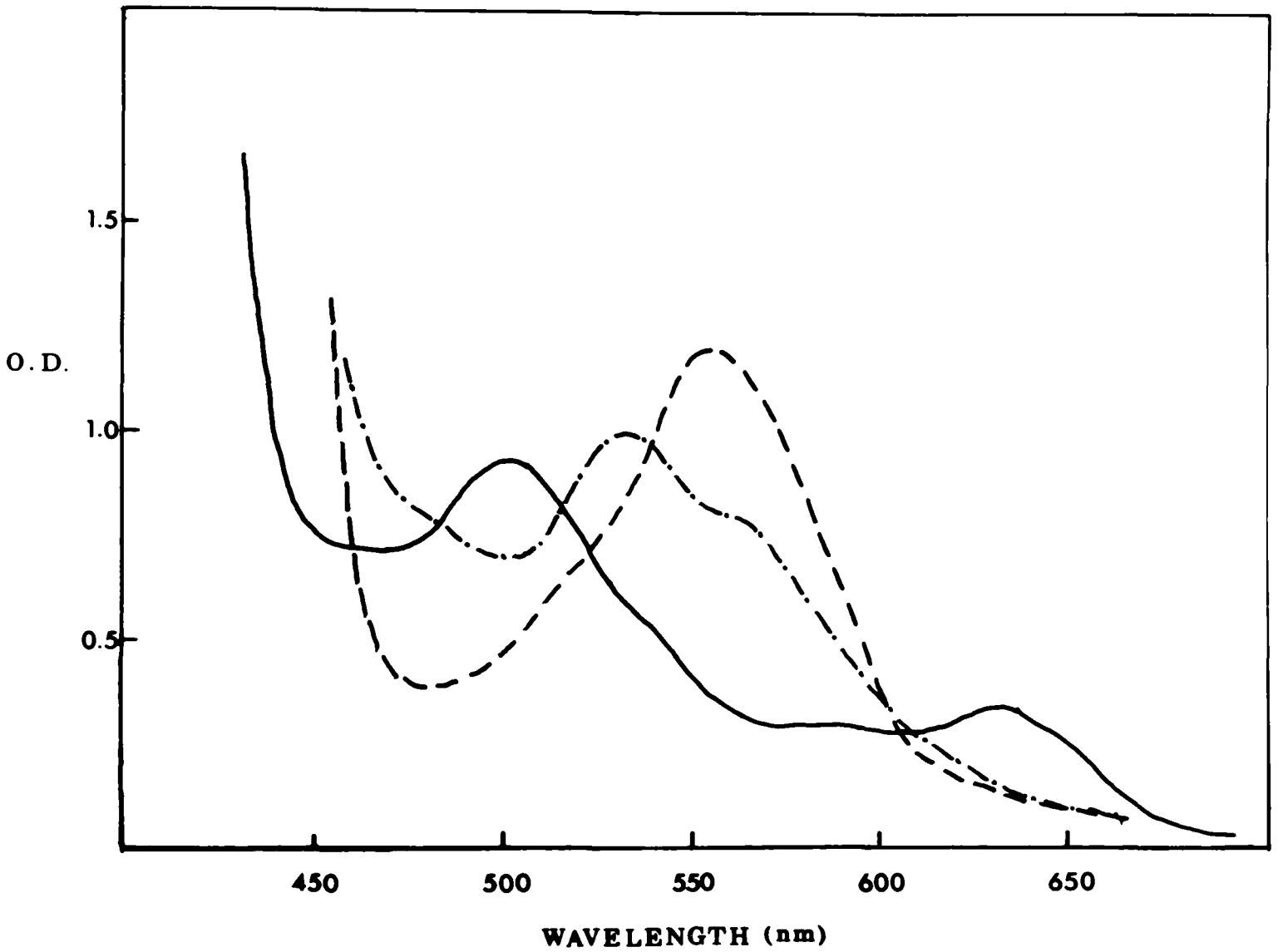
O.D.
1.5
1.0
0.5
450
500
550
600
650
WAVELENGTH (nm)

after addition of D(+)-tartrate in proportion to the concentrations suggested by Hill and Holden (1927), however, resulted in the appearance of a deoxymyoglobin spectrum. Aeration of the solution produced no further change. However, by allowing the solution of deoxymyoglobin to remain at 0°C overnight in the presence of the ferrous tartrate complex, the spectrum of the solution indicated complete loss of the deoxymyoglobin species with the appearance of absorption bands characteristic of an oxygenated ferrous haem protein. These preliminary results indicated that a careful evaluation of optimal conditions for introducing the alkaline ferrous tartrate complex into myoglobin crystals may provide a means of generating crystalline oxymyoglobin.

Under the assumption that all added $FeSO_4 \cdot (NH_4)_2SO_4$ is converted to the ferrous tartrate complex, providing that at least an approximate 1:10 ratio of concentrations of $FeSO_4 \cdot (NH_4)_2SO_4$ and tartrate is maintained (Hill and Holden, 1927), the optimal ratio of concentrations of ferrous tartrate to haem for generating a stable oxymyoglobin complex was determined. In order to provide a sufficiently alkaline but well buffered medium, sodium tetraborate buffer was used in all further experiments. This buffer provides a well stabilised control of hydrogen ion concentration near pH 9 largely insensitive to high ionic strength (Bates, 1973) and meets the requirement of stabilisation of oxymyoglobin above pH 8 (Yamazaki *et al.*,

1964). In Figure 43 are compared the visible absorption spectra of metmyoglobin solution (haem concentration 6.7×10^{-5} M) after standing at 0°C for 20 hours in the presence of various concentrations of ferrous tartrate. A further increase in absorption at 541 and 580 nm was not observed with Fe(II)-tartrate : myoglobin ratios greater than 10:1. These spectra remained without change over approximately another 10 hr period and were then observed to begin slow deterioration. Comparable results were obtained for metmyoglobin dissolved in solutions in the absence of ammonium sulphate.

2. Preliminary Crystallographic Studies on Myoglobin Single Crystals

a. Precession Photographs of Myoglobin Derivatives

Sperm whale metmyoglobin was crystallised from strong ammonium sulphate as described by Kendrew and Parrish (1956). These crystals grew generally with a well developed {001} face and were elongated along $\hat{b}$. The crystals belong to space group $P2_1$ and have unit cell parameters of $a = 64.6$ Å, $b = 31.1$ Å, $c = 34.8$ Å with $\beta = 105.5°$ (Watson, 1968).

Preliminary studies for determining the liganding stereochemistry of the haem-oxygen complex at sub-zero temperatures were directed first toward determining possible effects of the ferrous tartrate complex on the crystal

Figure 43.--Comparison of absorption spectra of myoglobin derivatives under varying concentrations of Stokes' reagent. Metmyoglobin was dissolved as described in Figure 42 and aliquots were used to prepare mixtures buffered at pH 9 with 0.01 M sodium tetraborate in 1.5 M ammonium sulphate. Stokes' reagent was prepared at various Fe(II) : haem ratios with identical haem concentrations. Solutions were maintained at 0°C for 20 hrs prior to spectral recording. Spectra A, B, and C correspond to ferrous tartrate : haem ratios of 2.0, 6.0, and 10.0 respectively. No aeration of the solutions occurred upon transfer of the cold solutions to spectrophotometer cuvettes. The spectra were recorded as in Figure 42 but immediately upon transfer of the cold solution into the cuvette.

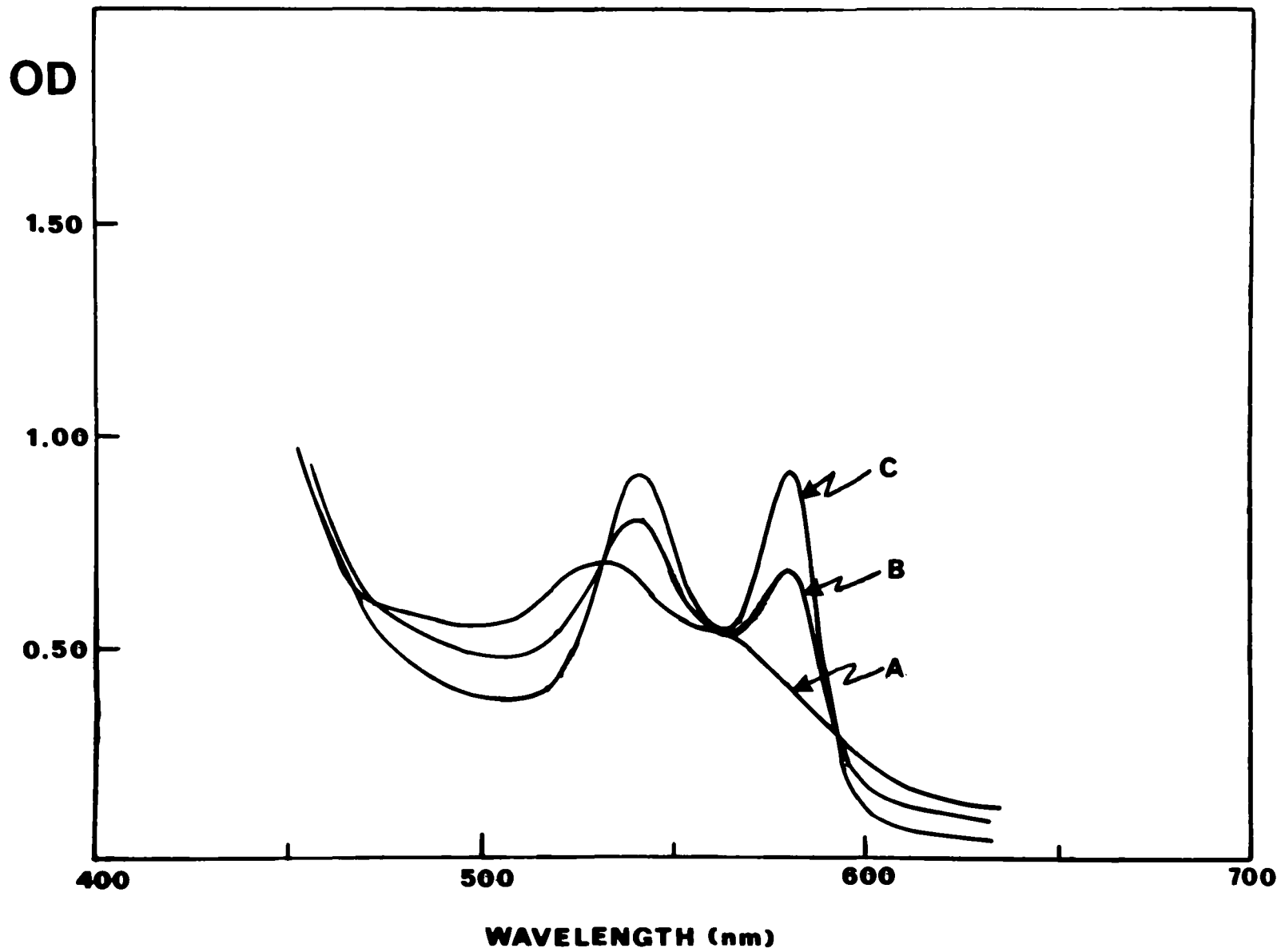
OD
1.50
1.00
0.50
C
B
A
400
500
600
700
WAVELENGTH (nm)

structure. Figure 44 compares the HOL views of precession photographs of sperm whale metmyoglobin in 75% ammonium sulphate buffered with 0.05 M phosphate at pH 6.5 and with 0.05 M sodium tetraborate at pH 9.0 in the presence of 10% (w/v) sodium D(+)-tartrate. Comparison of these photographs as well as of the corresponding OKL views indicated no change in unit cell parameters as a result of introduction of tartrate. Furthermore, the precession photographs of metmyoglobin at pH 9.0 were identical in the absence of tartrate suggesting no specific binding of the carboxylic acid derivative to the protein. Careful inspection of the HOL patterns in Figure 44 indicates small changes in the distribution of diffracted intensity as a result of the pH change as expected by the difference Fourier studies of Watson and Chance (1966).

Figure 45 compares the HOL patterns of deoxymyoglobin crystals sealed in capillary tubes. In Figure 45 one crystal was prepared by soaking it for several hours in a drop of ammonium sulphate solution containing sodium dithionite at pH 9 while the other had been previously soaked overnight in the identical tartrate containing alkaline ammonium sulphate solution but with added 0.005 M $FeSO_4 \cdot (NH_4)_2SO_4$. The crystal at pH 9.0 was kept at about 4°C for equilibration with ferrous tartrate but the precession photograph was obtained with the crystal at room temperature. The photographs with their corresponding OKL views demonstrated that the presence of ferrous tartrate

Figure 44.--Comparison of HOL precession photographs of sperm whale metmyoglobin crystals. Photograph A corresponds to a crystal maintained in 75% ammonium sulphate at pH 6.5. Photograph B corresponds to a crystal maintained at pH 9 in the presence of 10% (w/v) sodium D(+)-tartrate. No change in unit cell dimensions is observed. See text for discussion. The limiting resolution of precession photographs is 2.5 Å.

A

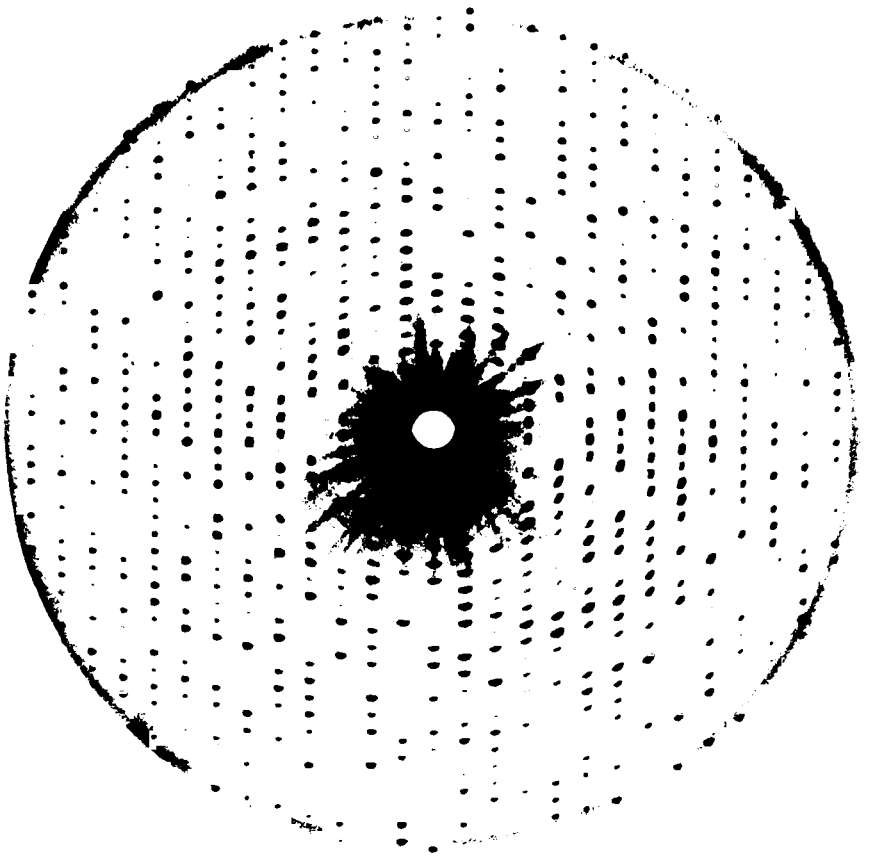

B

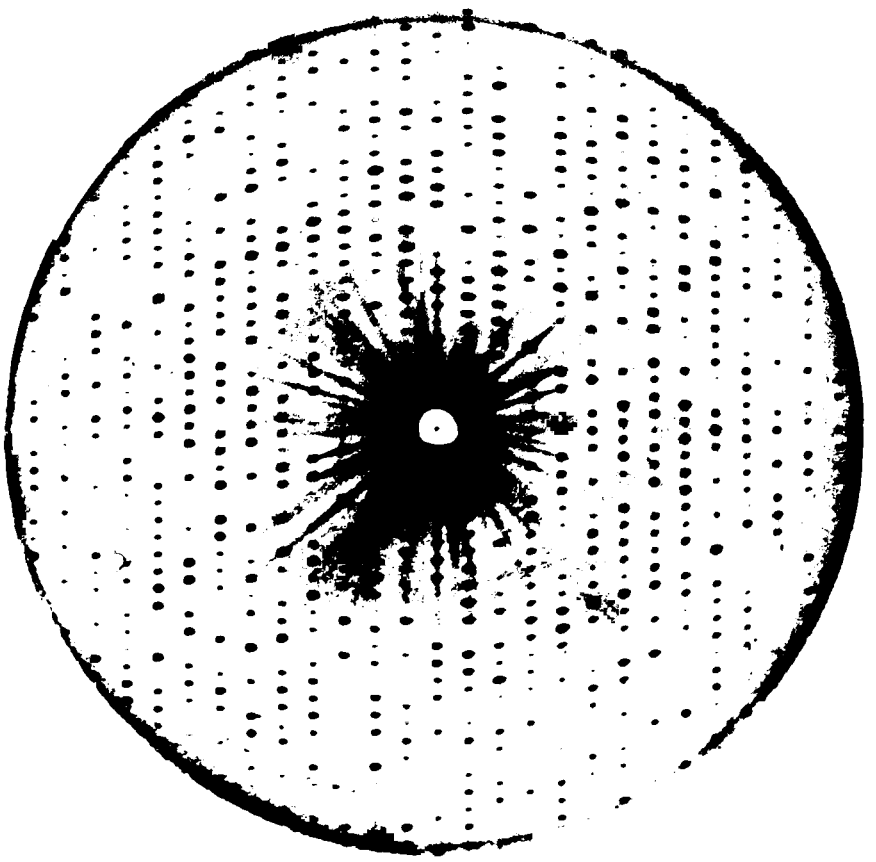

Figure 45.--Comparison of HOL precession photographs of sperm whale deoxymyoglobin crystals. Photograph A is of a crystal at pH 9 as in Figure 44B but reduced by addition of sodium dithionite. Photograph B is of a crystal equilibrated overnight in an identical tartrate containing medium but to which 0.005 M $FeSO_4 \cdot (NH_4)_2SO_4$ had been added. See text for discussion. The limiting resolution of precession photographs is 2.5 Å.

A

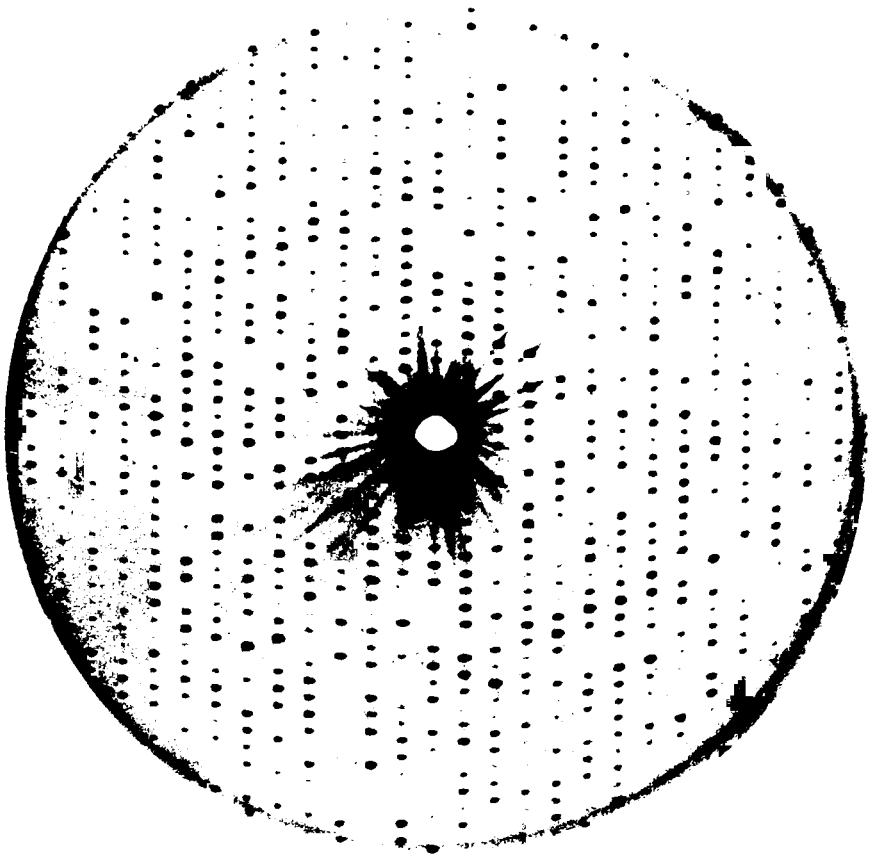

B

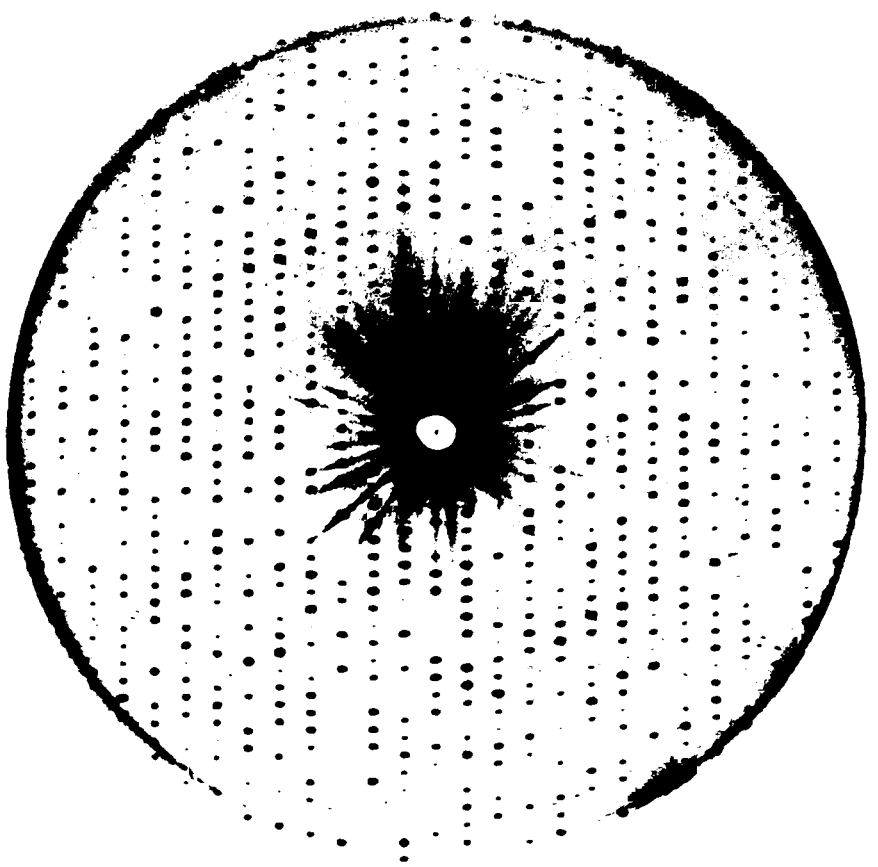

did not alter the unit cell parameters. The pattern of diffracted intensity from the ferrous tartrate treated crystal is similar to that of deoxymyoglobin. Since spectral studies indicated that the presence of ferrous tartrate generates only deoxymyoglobin at room temperature we can expect during x-ray exposure little or no oxymyoglobin to be present under these conditions. No facilities were present at this time to determine by spectroscopic methods the chemical species in the crystal after equilibration with ferrous tartrate. We assume in accordance with previous investigations by others (Eaton and Hochstrasser, 1968) that in Figure 44 the myoglobin species are the (aquo)-metmyoglobin and metmyoglobin ammonia complex and in Figure 45 the deoxymyoglobin derivative. The similar intensity patterns for the dithionite reduced deoxymyoglobin crystal and of the ferrous tartrate soaked crystal in Figure 45 suggests that the ferrous tartrate has brought about chemical reduction of the ferric haem protein. Reduction by ferrous tartrate at 0°C or even lower would be expected to result in stabilisation of the oxygenated derivative as for the protein in solution.

b. Flow Cell Modifications and Evaluation of Conditions for Automatic Data Collection

Preliminary x-ray diffraction studies were also carried out with metmyoglobin crystals at sub-zero temperatures on a five-circle diffractometer (Banner, 1972;

Evans, 1973). For these experiments metmyoglobin crystals were mounted in a flow-cell system (Wyckoff et al., 1967) designed for maintenance of crystals and solvent at low temperatures during data collection (G. A. Petsko, D. C. Phillips, M. Pickford, and P. S. Rivers, unpublished observations).

Crystals were mounted with the $\hat{b}$ axis nearly parallel to the long axis of capillaries of 1.3 mm inside diameter (0.01 mm wall thickness) milled from polystyrene. The crystal was stabilised in a bed of Sephadex beads (50% G-25 course, 50% G-200 fine) which had been previously equilibrated with the buffered ammonium sulphate followed by decantation of the fines. The Sephadex bed was packed between plugs of cotton wool at both ends of the capillary, and the capillary was sealed with Bostik Quick Set epoxy adhesive to polyethylene tubing. A flow of buffered 75% ammonium sulphate through the capillary and consequently around the crystal was controlled by gravity and was generally maintained at a rate of 0.5-1.0 ml/hr. The capillary and connected tubing were mounted in a double walled cryostat assembly constructed of Perspex and fastened to a standard goniometer head, and the crystal was maintained at ambient temperature of $-4.0 \pm 0.2°C$ with aid of the low-temperature compressed air cooling device designed in this laboratory (Marsh and Petsko, 1973). Crystals were aligned in a general setting. For crystals maintained at pH 6.5 or pH 9.0 in 75% ammonium sulphate at $-4.0°C$, no

indication of alteration of the unit cell axes was evident from the Bragg angles of axial reflections as compared to those at normal temperatures.

In order to estimate the length of time required for completion of chemical changes in the crystal by solvent flow, changes in the intensity of appropriate low order reflections were monitored which appeared from precession photographs to be sensitive to solvent changes. In this manner, one could expect to determine at least the appropriate length of time required to exchange the solvent in the crystal channels during the introduction or exchange of different buffers and reducing agents. Figure 46 illustrates the change in the integrated intensity of the 3 0 0 reflection of a crystal of metmyoglobin at pH 9.0 after introduction of 75% ammonium sulphate buffered at pH 6.5 at a flow rate of approximately 1 ml/hr. The onset of the decrease in intensity after 25 min corresponds closely to the time expected for displacement of the solvent in the entrance tubing and bead-filled capillary (approximately 0.4 ml). While the change from pH 9.0 to pH 6.5 required approximately 4 hours for completion, back-titration to pH 9.0 was completed within 30 min. On the other hand, introduction of ferrous tartrate [approximately 0.005 M in Fe(II)] to the crystal at pH 9 caused a monotonic decrease in the intensity of the 3 0 0 reflection to a constant level of 8200 counts within 50 min.

Figure 46.--Time dependent change in the integrated intensity of the 3 0 0 reflection of a sperm whale metmyoglobin crystal during introduction of solvent changes by flow methods. The crystal was initially maintained at pH 9.0 in 75% ammonium sulphate and an ammonium sulphate solution buffered to pH 6.5 was introduced at a flow rate of 1.0 ml/hr. The ammonium sulphate solution contained 10% (w/v) sodium D(+)-tartrate. See text for discussion.

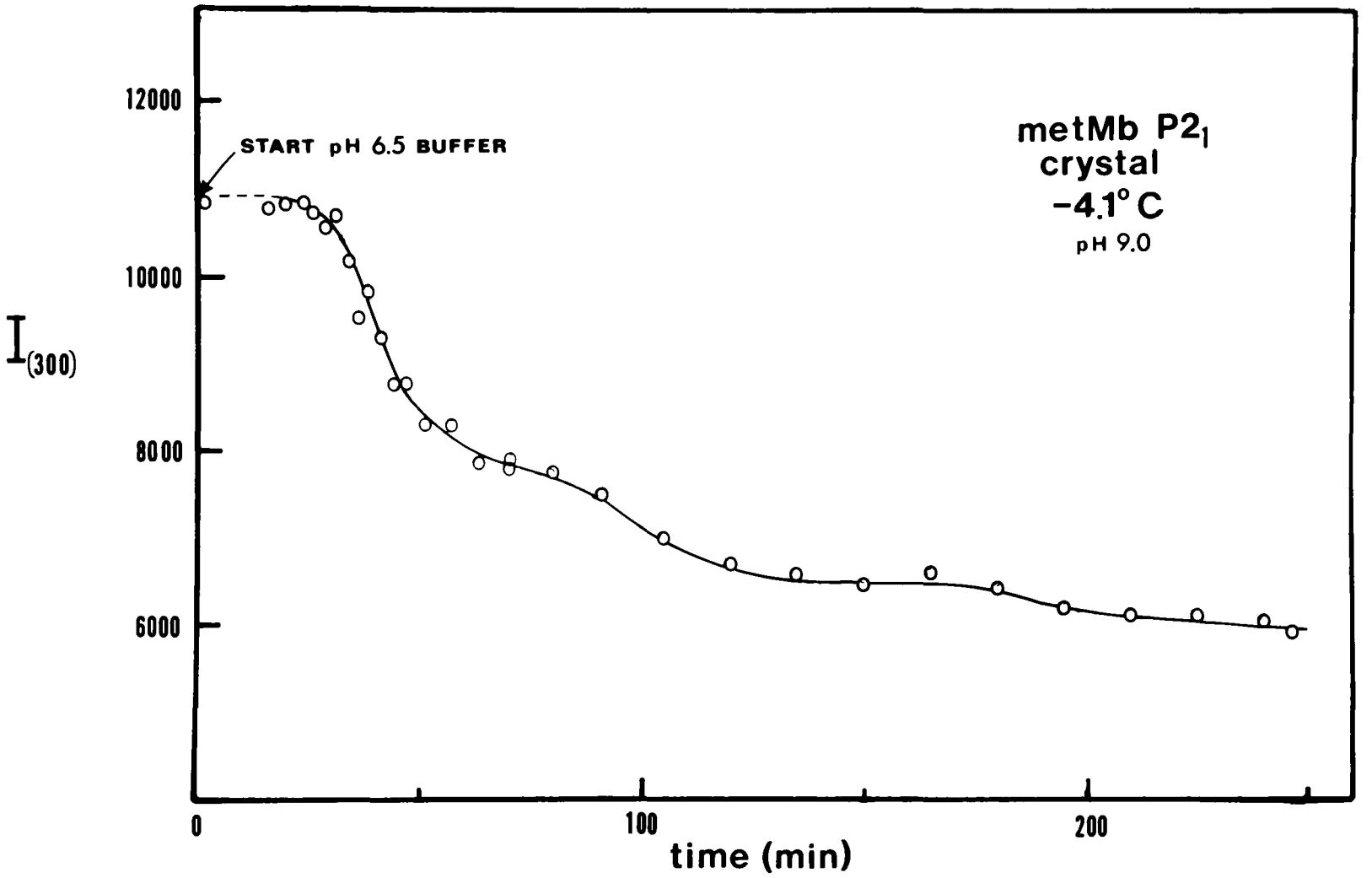
12000
10000
8000
6000
$I_{(300)}$
START pH 6.5 BUFFER
metMb $P2_1$
crystal
-4.1° C
pH 9.0
0
100
200
time (min)

It is safe to assume that the chemical change associated with iron reduction and ligand binding proceeds considerably faster than the diffusion process. The time required for exchange of solvent components in the crystal, as monitored by the intensity of the 3 0 0 reflection, thus, served as a suitable estimate of the maximum time required for change in the oxidation and ligand state of the haem iron. It would be expected, however, on the basis of the solution spectra of regenerated oxymyoglobin that several hours further of perfusion of the crystal with solvent would be required to assure an adequately high occupancy of iron binding sites by molecular oxygen. These preliminary experiments, thus, help to establish conditions under which high resolution structural investigations can be carried out in order to determine the stereochemistry of the haem-oxygen complex in oxymyoglobin by x-ray diffraction methods.

APPENDIX II

LOW FREQUENCY RAMAN SPECTRA OF LYSOZYME (WITH L. GENZEL, F. KEILMANN, T. P. MARTIN, G. WINTERLING, Y. YACOBY, AND H. FRÖHLICH).

Copy of manuscript accepted for publication in Biopolymers.

Figure 47.--Picture of a typical orthorhombic HEW lysozyme crystal employed for low frequency Raman spectral studies. Crystals (space group $P2_12_12_1$, $\underline{z} = 4$ molecules/unit cell) were grown routinely from buffered 5% (w/v) sodium chloride at 37°C as described by Jollès and Berthou (1972) and employed in Raman studies as described in the accompanying manuscript.

Low Frequency Raman Spectra of Lysozyme

L. Genzel, F. Keilmann, T. P. Martin,
G. Winterling, Y. Yacoby,[+]

Max-Planck-Institut für Festkörperforschung,
Stuttgart, Federal Republic of Germany

H. Fröhlich

Department of Electrical Engineering,
University of Salford,
Salford, England

and

Marvin W. Makinen[X]

Laboratory of Molecular Biophysics
Department of Zoology, Oxford University
South Parks Road, Oxford, England

ABSTRACT

New techniques in laser Raman spectroscopy are used to obtain spectra of aqueous solutions of lysozyme for frequency shifts as small as $5cm^{-1}$. In addition, Raman measurements are made on two crystalline forms of hen egg white lysozyme. The spectra obtained from the solution and from the crystal are found to be similar for frequencies above $100cm^{-1}$. However, a low frequency band at $25cm^{-1}$ observed in crystalline lysozyme is not found in the solution, indicating that this band cannot be attributed to an internal molecular vibration.

3.

RUNNING TITLE: Raman Spectra of Lysozyme

4.

INTRODUCTION

It has been suggested that long range forces are of importance in biological systems[1,2] and that such forces may be created by dipoles induced by very low frequency vibrational modes.[3] Recently, Raman bands at frequencies smaller than 100 cm^{-1} have been observed in solid proteins, such as films of native and chemically modified α-chymotrypsin.[4] The observation was made possible by discriminating against the strong elastic Rayleigh scattering. The Raman bands were interpreted to arise from low frequency internal vibrations of the protein molecule.[4] In the solid state, low frequency vibrations can also arise from the linking forces between neighboring macromolecules. Thus, it was desirable to search for the existence of these vibrational modes in aqueous solution in order to establish whether the vibrations arise from internal motions within the macromolecule or from collective motions of many macromolecules.

In aqueous solution, on the other hand, contributions to the inelastic light scattering can arise from the reorientation of molecules with anisotropic polarizability. The spectral width of this anisotropy scattering depends on the magnitude of the rotational diffusion constant; for lysozyme the spectral width was found[5] to be as small as $\sim 10^{-3}$ cm^{-1}. Water molecules, however, reorient much faster due to their smaller dimensions; their anisotropy scattering extending up to frequency shifts of ~ 50 cm^{-1} makes it difficult to observe the low frequency Raman scattering of the lysozyme molecule. Iodine filter techniques or the use of a triple grating spectrometer[4] cannot improve the experimental situation in this case.

In this paper, we report the application of new methods to overcome the above difficulty and we present Raman spectra of aqueous solutions

of lysozyme. These spectra are compared with results obtained for orthorhombic and triclinic crystal form of lysozyme.

EXPERIMENTAL METHODS

1. Raman Techniques

Raman spectra were recorded with a cw Argon laser and a double monochromator. The signal from the photomultiplier was processed using standard pulse shaping and photon counting techniques.

The spectra of aqueous solutions were, in general, not readily reproducible using the conventional Raman techniques alone. Slow fluctuations of the scattered intensity were observed which could mask the presence of weak Raman bands or could give rise to misinterpretations. These flucturations seem to arise from macroscopic optical inhomogeneities driven by thermal gradients due to laser beam heating.

To analyse the influence of the fluctuations on the recorded spectra, we denote the unperturbed Raman intensity by $I_R(\nu)$, where ν is the Raman frequency shift. Introducing $f(t)$ to represent the intensity variations arising from macroscopic fluctuations, we get for the intensity actually measured $I(t) = [1+f(t)]I_R(\nu)$. The spectrum is recorded by changing ν at scanning speed ν_s, thus giving

$$I(t) = [1+f(t)]\ I_R(\nu_s t). \qquad (1)$$

The scattered intensity $I_R(\nu)$ can be divided into two components

$$I_R(\nu) = I_{RB}(\nu) + I_{RS}(\nu) \qquad (2)$$

where $I_{RB}(\nu)$ is a background intensity and $I_{RS}(\nu)$ represents the lines varying relatively fast with frequency ν. $I(t)$ will then have three components

6.

$$I(t) = I_R(v_s t) * f(t)I_{RB}(v_s t)\ f(t)I_{RS}(v_s t)\ . \qquad (3)$$

The second and third terms represent the noise arising from macroscopic fluctuations which is usually small since $|f(t)|<<1$. If, however, the background $I_{RB}(\nu)$ is large compared to $I_{RS}(\nu)$, the second term may give rise to components comparable in size to the lines in the spectrum; in particular, these components may have a shape similar to a line of the true spectrum if the characteristic fluctuation time τ_o is comparable to the time τ_s it takes to scan such a line.

There are several ways to reduce the noise arising from the macroscopic fluctuations:

a) The heating effects of the laser beam can be appreciably reduced and the apparent fluctuation time τ_o shortened by using a cylindrical cell and rotating it at high speed. In this case, the second and third terms of Eq. (3) introduce noise only at high frequencies ($\tau_o<<\tau_s$) which can be filtered out.

b) The time τ_s can be made shorter by using faster scanning speeds. In the limit $\tau_s<<\tau_o$, the structures produced by the second term in Eq. (3) are much broader than the true structures and can thus be ignored. Averaging over many scans further reduces the effect of the noise terms in Eq. (3).

c) It is possible to reduce the background contribution by directly measuring the derivative dI_R of the Raman intensity with respect to energy displacement $d\nu$. The recorded signal is then given by

7.

$$I(t) = [1+f(t)]\left[\frac{dI_{RS}}{d\nu} + \frac{dI_{RB}}{d\nu}\right]. \qquad (4)$$

In general, the background I_{RB} varies much less with frequency than the signal I_{RS} so that noise associated with $\frac{dI_{RB}}{d\nu}$ $f(t)$ is reduced in comparison to the signal.

The technique of differentiation has been described in detail elsewhere.[6] It is achieved by vibrating a glass plate near the exit slit of the monochromator, leading to an optical frequency peak to peak variation of 3 cm^{-1} at 14.5 Hz. The detector signal is then fed into a lock-in amplifier and recorded.

A more direct study of the contribution of lysozyme to the Raman spectrum of an aqueous solution was made in the following way: a rotating cell[7] (obtained from W. Zeh, Duisberg, Germany) was divided into two equal parts. One half was filled with pure solvent and the other half with a concentrated lysozyme solution. By subtracting the corresponding signals using a lock-in amplifier the difference between the two Raman spectra was obtained in a reproducible way.

2. Preparation of Protein Solutions and Crystals

Hen egg white lysozyme (three times crystallized and lyophilized) was obtained from Sigma Chemical Company or from Boehringer-Mannheim A. G., and used without further purification. Orthorhombic crystals (space group $P2_12_12_1$) were prepared from solutions containing 5% (w/v)NaCl, 5% (w/v) protein, and 0.02M acetate buffer, pH 4.7, at 37°C as described by Jolles and Berthou.[8] Triclinic crystals[9] (space group P1) were obtained with 1% (w/v) lysozyme and 2% (w/v) $NaNO_3$ buffered at

pH 4.5. Crystals were placed into cuvettes and oriented under microscopic examination. The large dimensions of the crystals, generally at least 1-3 mm in the longest direction, allowed identification of crystal faces to be readily made on the basis of clinographic projections. The crystals were then blotted free of excess solvent, and a drop of solvent was placed in the bottom of the cuvette not in contact with the crystal. Upon sealing the cuvette, this provided for the crystal an ambient atmosphere of vapor pressure equal to that of the mother liquor and prevented drying of the crystal with resultant loss of crystallinity.

Solutions of lysozyme were prepared by slowly dissolving the lyophilized protein into a solution of 0.02 M sodium acetate at pH 4.7 under gentle stirring. The solution was then filtered prior to spectral studies.

All reagents were of analytical reagent grade and deionized distilled water was used throughout.

RESULTS AND DISCUSSION

The low frequency Raman spectra obtained for crystals of lysozyme show several relatively broad peaks superimposed on a broad background as illustrated in Figure 1. This background is probably due to reorientation scattering of the unbound water known to exist in lysozyme crystals. Comparison of the various polarization configurations demonstrate that each crystal form is associated with peaks at the same frequency positions 25, 75, 115 and 160 cm^{-1}. However, as shown in Figure 2, the Raman spectrum of a 300 mg/ml aqueous solution of lysozyme in a stationary cell shows only one band at 75 cm^{-1}. More sensitive measurements on solutions using the rotating cell (Figure 3) and differential Raman techniques (Figure 4) demonstrate that the 115 and 160 cm^{-1} bands exist also in lysozyme solutions; however, these measurements contain no indication

of the low frequency band at 25 cm^{-1}. For the pH conditions employed in this study, hen egg white lysozyme has been demonstrated to be essentially in a monodisperse form with little dimer formation.[10,11] Therefore, we conclude that the peak at 25 cm^{-1} arises from intermolecular vibrations which are, of course, absent in a solution of free enzyme molecules.

The low frequency Raman bands observed in all forms of lysozyme most probably correspond to bending and rotational motion of the peptide chain. Such modes are expected to be more sensitive to the configuration of the chain than to the peptide sequence. Therefore, it is not unreasonable for us to compare our results with the calculated eigenfrequencies of polypeptides.[12] The normal modes of polyglycine have been calculated for both the α and the β configuration. Lysozyme is known to contain both configurations of the peptide chain.[13] The α helix of polyglycine II has Raman active modes at 76, 79 and 126 cm^{-1}. The extended β form has Raman active modes at 91, 146 and 173 cm^{-1}. After comparison of these calculated frequencies with our observed bands, we can make the following assignments. The low frequency line at 75 cm^{-1} is due to a torsional motion of a peptide chain with α configuration. The weaker experimentally observed band near 160 cm^{-1} is due to bending motion in a peptide chain with β configuration. This same band has been seen in the Raman spectrum of polyglycine I.[14]

The use of a rotating cell and differential Raman technique is clearly seen to provide a suitable means of detecting low frequency peaks of macromolecules in solution and avoids the difficulties otherwise introduced by Rayleigh scattering of the solvent. As evident through the results of this study, the comparison of a single crystal spectrum

to that of the enzyme in solution may be employed to identify Raman peaks diagnostic of various structural and functional states of the macromolecule. On this basis, it is possible to relate at least one band of the lysozyme spectrum to intermolecular vibration modes associated with the lattice packing arrangement of the enzyme, and to assign others to internal molecular vibrations.

ACKNOWLEDGEMENT

We thank Professor D. C. Phillips for helpful discussions and support.

11.

REFERENCES

1. Parsigian, A. V. (1973), Ann. Rev. Biophys. Bioeng. 2, 221-255.

2. Israelachvili, J. N. (1974), Quat. Rev. Biophys. 6, 341-387.

3. Fröhlich, H. (1968), Intern. J. Quant. Chem. 2, 641-649.

4. Brown, K. G., Erfurth, S. C., Small, E. W. and Peticolas, W. L. (1972), Proc. Natl. Acad. Sci. (U.S.) 69, 1467-1469.

5. Dubin, S. B., Clark, N. A. and Benedek, G. B. (1971), J. Chem. Phys. 54, 5158-5164.

6. Yacoby, Y. and Linz, A. (1974), Phys. Rev. B9, 2723-2742.

7. Kiefer, W. and Bernstein, H. J. (1971), Appl. Spectrosc. 25, 500-501.

8. Jolles, P. and Berthou, J. (1972). FEBS Letters 23, 21-23.

9. Steinrauf, L. K. (1959), Acta Cryst. 12, 77-79.

10. Sophianopoulos, A. J. and Van Holde, K. E. (1964), J. Biol. Chem. 239, 2516-2524.

11. Gordon, J. A. (1968), J. Biol. Chem. 243, 4615-4625.

12. Gupta, V. D., Trevino, S. and Boutin, H. (1968), J. Chem. Phys. 48, 3008-3015.

13. Imoto, T., Johnson, L. N., North, A. C. T., Phillips, D. C. and Rupley, J. A. (1972), The Enzymes, VII (edit. by P. D. Boyer), pp. 745-873, 3rd edition, Academic Press, New York.

14. Small, E. W., Fanconi, B. and Peticolas, L. (1970), J. Chem. Phys. 52, 4369-4379.

FOOTNOTES

+Permanent address: Racah Institute of Physics, Hebrew University, Jerusalem, Israel

xSupported by a Special Fellowship of the National Institute of General Medical Sciences (1 F03 GM50802), National Institutes of Health, Bethesda, Maryland 20014, U.S.A. Present address: Department of Biophysics and Theoretical Biology, University of Chicago, 920 E. 58th Street, Chicago, Illinois 60637 U.S.A.

13.

FIGURE LEGENDS

Figure 1: Raman spectra of triclinic (curves 1-4) and orthorhombic (curves 5-8) lysozyme crystals oriented with the wavevector k_L of the incident beam parallel to the 010 and 100 crystallographic directions, respectively. The direction of polarization of the incident and scattered light are indicated by the first and second coordinates in parentheses.

Figure 2: Comparison of the Raman spectra of orthorhombic crystalline lysozyme, of a 300 mg/ml aqueous solution of lysozyme and of water. The solution spectrum was obtained by averaging several runs with a fixed cell.

Figure 3: Raman spectrum of 300 mg/ml lysozyme in a 0.02 M acetate buffer solution with pH 4.7. This spectrum was obtained using a divided, rotating cell by subtracting electronically the signal of the buffer solution in one half of the cell from that of the lysozyme solution in the other half.

Figure 4: Differential Raman spectra obtained by wavelength modulation using a rotating cell. The four solutions measured are: (a) 0.02 M acetate buffer, pH 4.7; (b) 300 mg/ml lysozyme in buffer solution; (c) 300 mg/ml lysozyme in water.

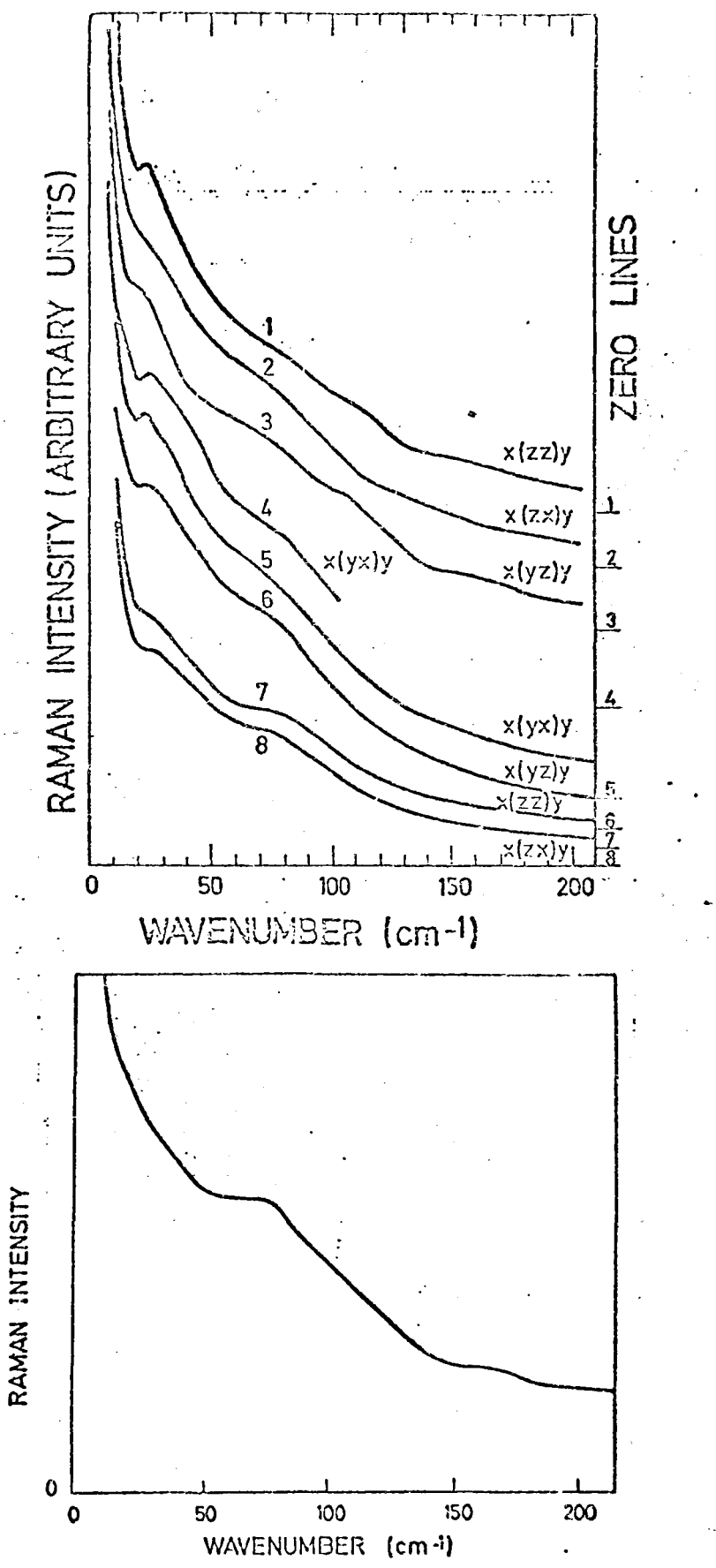
RAMAN INTENSITY (ARBITRARY UNITS)
ZERO LINES
1
2
3
4
5
6
7
8
x(zz)y
x(zx)y
x(yz)y
x(yx)y
x(yz)y
x(zz)y
x(zx)y
0
50
100
150
200
WAVENUMBER (cm-1)
RAMAN INTENSITY
0
0
50
100
150
200
WAVENUMBER (cm-1)

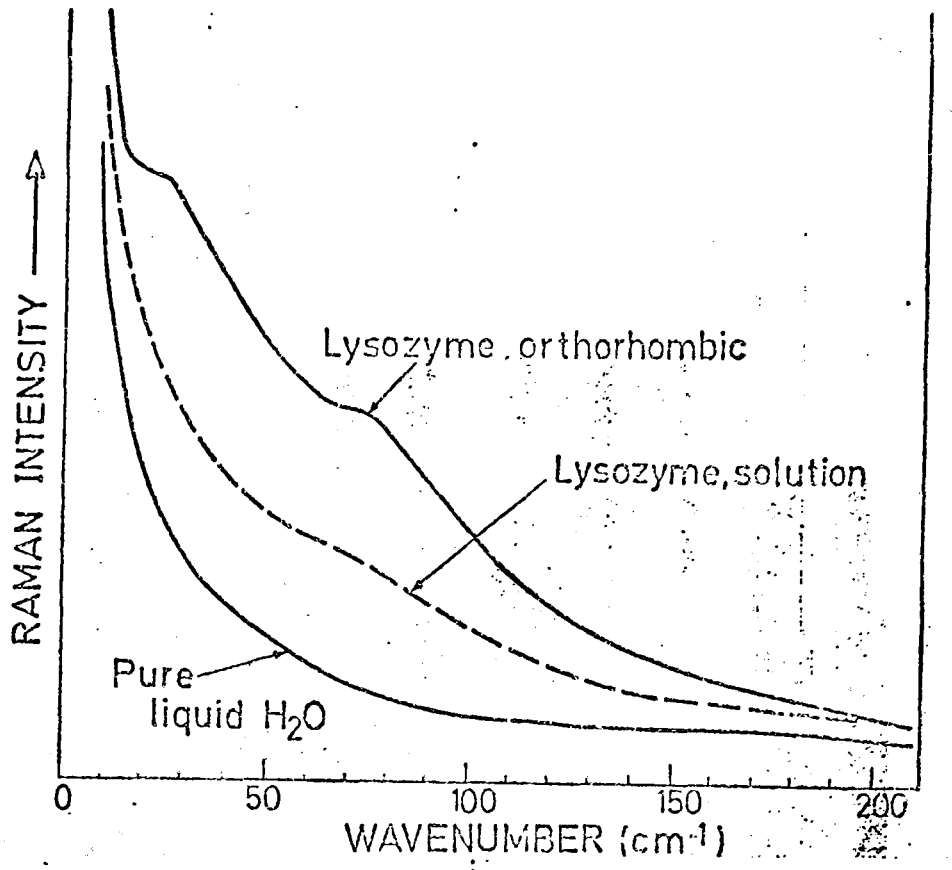
RAMAN INTENSITY
Lysozyme, orthorhombic
Lysozyme, solution
Pure liquid H_2O
0
50
100
150
200
WAVENUMBER (cm^{-1})

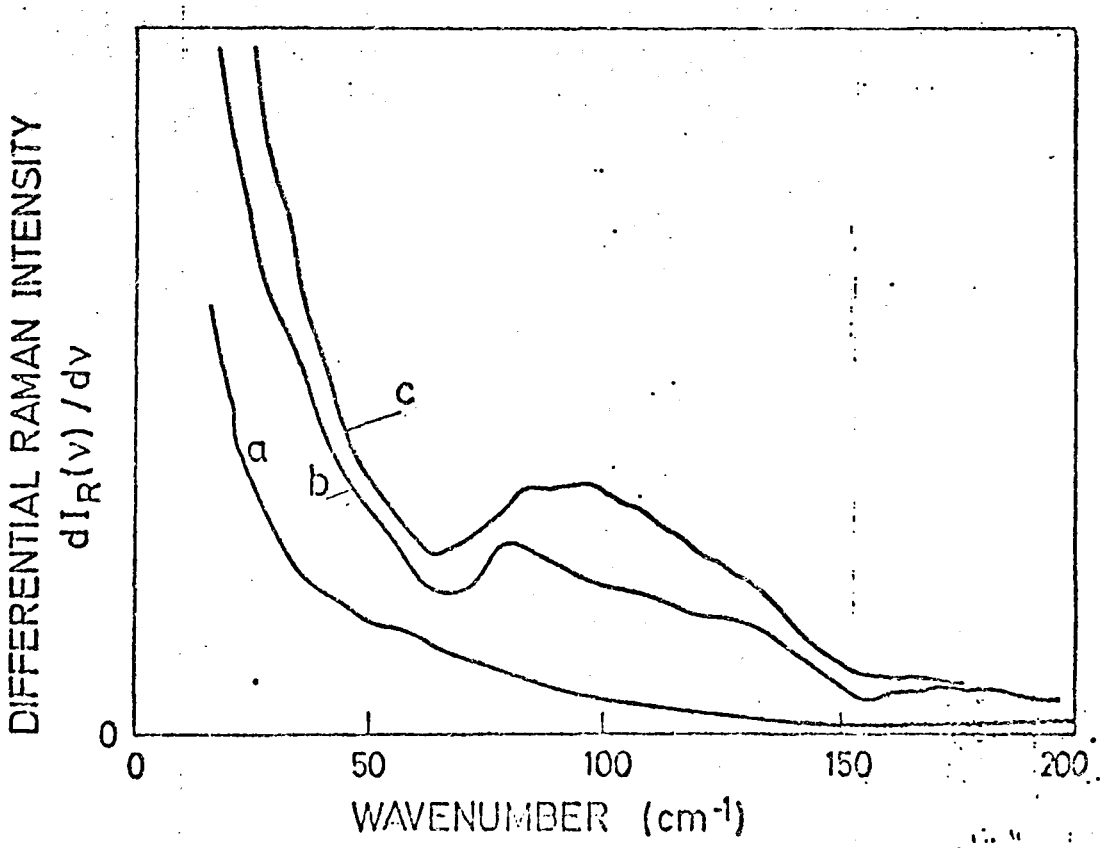
DIFFERENTIAL RAMAN INTENSITY
$dI_R(\nu)/d\nu$
a
b
c
0
0
50
100
150
200
WAVENUMBER (cm^{-1})

APPENDIX III

A. TABLE OF OBSERVED AND CALCULATED STRUCTURE AMPLITUDES AND PHASES OF β(1-NAPHTHYL)-D-GLUCOPYRANOSIDE-2',3',4',6'-TETRA-O-ACETATE.

The table on the following pages provides a complete listing of all observed data. Reflections not included in the refinement with $I_o < 3\sigma(I_o)$ are marked with a star (*). Reflections removed from the refinement on the basis of secondary extinction effects are indicated by a closed circle (•). The phase angle is indicated in degrees.

H	K	L	/F0/	/FC/	PHASE	H	K	L	/F0/	/FC/	PHASE	H	K	L	/F0/	/FC/	PHASE
2	0	0	13.6	15.7	0.0	7	3	0	7.6	4.9	-90.0	2	6	0	10.0	11.0	-180.0
4	0	0●	84.6	104.7	-180.0	8	3	0	20.0	20.6	-180.0	3	6	0	38.0	42.7	-90.0
6	0	0	34.5	34.0	-180.0	9	3	0	23.8	23.5	-90.0	4	6	0	16.0	15.4	0.0
8	0	0	55.9	55.0	-180.0	10	3	0	19.6	17.4	-180.0	5	6	0	41.5	40.4	90.0
10	0	0	15.9	15.9	-180.0	11	3	0*	2.5	0.5	-90.0	6	6	0	11.5	13.1	-180.0
12	0	0	28.8	29.4	-180.0	12	3	0	11.3	10.0	0.0	7	6	0	33.0	31.0	-90.0
14	0	0	8.8	9.8	-180.0	13	3	0	3.5	4.2	90.0	8	6	0	7.5	4.5	0.0
16	0	0*	2.6	2.0	-180.0	14	3	0	10.0	10.1	0.0	9	6	0	11.5	13.0	90.0
18	0	0	6.6	6.5	0.0	15	3	0	7.1	6.9	90.0	10	6	0	16.5	15.4	-180.0
20	0	0	2.8	2.9	-180.0	16	3	0*	3.1	3.0	-180.0	11	6	0	8.1	7.7	90.0
1	1	0	41.8	49.5	90.0	17	3	0*	3.2	2.7	-90.0	12	6	0	8.4	7.9	0.0
2	1	0●	84.6	122.9	0.0	18	3	0*	2.2	0.7	-180.0	13	6	0*	3.2	2.4	-90.0
3	1	0	44.3	48.6	-90.0	19	3	0*	1.7	0.5	-90.0	14	6	0	4.9	4.0	0.0
4	1	0●	74.9	90.1	0.0	20	3	0*	1.3	0.0	0.0	15	6	0	8.4	9.1	-90.0
5	1	0●	113.8	145.2	90.0	0	4	0	39.3	44.8	-180.0	16	6	0	4.1	3.3	0.0
6	1	0*	2.5	3.0	-180.0	1	4	0●	59.3	67.9	-90.0	17	6	0*	2.5	1.9	-90.0
7	1	0	50.7	50.4	90.0	2	4	0	26.7	28.1	0.0	18	6	0*	2.2	0.6	0.0
8	1	0	49.8	50.4	0.0	3	4	0	54.9	59.3	-90.0	19	6	0*	1.6	0.2	90.0
9	1	0	19.6	17.9	-90.0	4	4	0	16.4	18.8	0.0	20	6	0*	1.3	0.9	0.0
10	1	0*	2.3	0.9	0.0	5	4	0	64.7	68.7	90.0	1	7	0	30.5	30.2	-90.0
11	1	0	5.8	6.2	90.0	6	4	0	8.8	9.7	-180.0	2	7	0	21.0	20.9	0.0
12	1	0	3.8	3.1	0.0	7	4	0	28.0	27.3	90.0	3	7	0	31.6	30.9	-90.0
13	1	0	7.6	7.9	-90.0	8	4	0	14.6	14.7	0.0	4	7	0	36.5	35.0	0.0
14	1	0	14.3	14.6	-180.0	9	4	0	12.0	10.7	-90.0	5	7	0	11.7	11.5	90.0
15	1	0*	2.9	2.3	90.0	10	4	0	4.8	5.5	0.0	6	7	0	5.8	5.8	-180.0
16	1	0	5.4	5.6	-180.0	11	4	0	6.4	7.2	90.0	7	7	0	4.7	3.7	-90.0
17	1	0*	3.1	3.1	-90.0	12	4	0	19.0	20.0	-180.0	8	7	0	13.3	12.7	0.0
18	1	0*	2.3	0.0	-180.0	13	4	0	4.6	3.3	-90.0	9	7	0	15.3	14.3	90.0
19	1	0*	2.0	0.5	-90.0	14	4	0	5.8	6.4	0.0	10	7	0	31.6	31.8	-180.0
20	1	0*	1.3	0.2	0.0	15	4	0	4.2	4.9	90.0	11	7	0	4.5	4.5	90.0
0	2	0	2.2	1.1	-180.0	16	4	0*	3.8	5.9	0.0	12	7	0*	2.6	1.1	0.0
1	2	0●	71.3	97.3	-90.0	17	4	0*	2.3	0.5	-90.0	13	7	0	12.2	12.8	-90.0
2	2	0	12.4	13.6	0.0	18	4	0*	2.6	2.1	-180.0	14	7	0	10.4	11.6	-180.0
3	2	0	51.2	55.3	-90.0	19	4	0*	1.7	0.8	90.0	15	7	0	7.8	6.8	-90.0
4	2	0	21.5	25.5	0.0	20	4	0	2.4	2.7	0.0	16	7	0*	3.6	3.2	0.0
5	2	0	22.1	21.4	90.0	1	5	0	42.9	45.1	90.0	17	7	0*	2.4	1.1	90.0
6	2	0	15.6	17.1	0.0	2	5	0	20.5	23.4	-180.0	18	7	0	2.9	1.8	0.0
7	2	0	27.6	30.2	90.0	3	5	0	47.0	52.8	90.0	19	7	0*	1.7	1.1	90.0
8	2	0	26.8	25.6	-180.0	4	5	0●	58.9	64.7	0.0	0	8	0	9.4	9.4	-180.0
9	2	0	27.4	29.2	90.0	5	5	0	9.9	10.5	-90.0	1	8	0	9.5	7.8	90.0
10	2	0	9.7	9.5	-180.0	6	5	0	24.1	23.4	-180.0	2	8	0	9.7	8.5	-180.0
11	2	0	14.0	12.4	90.0	7	5	0	11.5	10.3	-90.0	3	8	0	8.8	10.1	90.0
12	2	0	5.8	6.3	0.0	8	5	0	8.4	6.0	0.0	4	8	0	20.8	21.4	-180.0
13	2	0*	2.7	1.8	90.0	9	5	0	6.6	5.5	-90.0	5	8	0	26.4	27.6	90.0
14	2	0	7.2	7.2	0.0	10	5	0	17.0	16.2	-180.0	6	8	0	12.1	12.4	-180.0
15	2	0	6.2	6.8	-90.0	11	5	0	6.9	6.1	-90.0	7	8	0	19.8	19.3	-90.0
16	2	0	5.5	4.6	-180.0	12	5	0	7.7	8.2	-180.0	8	8	0	4.2	3.7	-180.0
17	2	0	4.4	4.9	90.0	13	5	0*	2.8	2.6	-90.0	9	8	0	15.8	14.7	90.0
18	2	0*	2.2	1.5	-180.0	14	5	0	14.0	14.4	0.0	10	8	0	16.8	16.5	0.0
19	2	0	3.2	2.1	90.0	15	5	0	6.5	6.4	-90.0	11	8	0	16.3	16.5	-90.0
20	2	0*	1.4	1.0	-180.0	16	5	0	3.9	3.3	0.0	12	8	0	9.3	9.9	0.0
1	3	0	14.0	13.5	-90.0	17	5	0	5.3	4.5	90.0	13	8	0	9.1	9.6	90.0
2	3	0	7.4	4.2	-180.0	18	5	0*	2.4	0.6	0.0	14	8	0	4.3	4.5	0.0
3	3	0	63.7	69.3	90.0	19	5	0*	2.0	0.3	-90.0	15	8	0	3.9	3.9	-90.0
4	3	0	42.5	43.3	-180.0	20	5	0*	0.8	0.8	-180.0	16	8	0	7.5	8.4	-180.0
5	3	0	31.2	33.7	90.0	0	6	0●	91.5	113.9	-180.0	17	8	0*	2.4	2.8	-90.0
6	3	0	47.2	48.5	0.0	1	6	0	35.5	37.3	90.0	18	8	0*	1.6	0.5	-180.0

H	K	L	/F0/	/FC/	PHASE	H	K	L	/F0/	/FC/	PHASE	H	K	L	/F0/	/FC/	PHASE
19	8	0*	1.6	0.2	90.0	18	11	0*	1.2	0.3	0.0	2	15	0	10.8	9.2	-180.0
1	9	0	13.5	13.2	90.0	0	12	0	50.5	53.0	0.0	3	15	0	12.7	13.2	-90.0
2	9	0*	2.7	3.0	-180.0	1	12	0	41.4	40.5	-90.0	4	15	0	19.6	19.9	0.0
3	9	0*	2.2	1.4	-90.0	2	12	0*	3.7	4.1	-180.0	5	15	0	8.9	9.4	-90.0
4	9	0	30.2	30.9	0.0	3	12	0	32.4	31.9	90.0	6	15	0*	2.2	2.0	0.0
5	9	0	47.0	47.7	-90.0	4	12	0	4.3	3.5	0.0	7	15	0	20.9	19.6	-90.0
6	9	0	7.8	6.4	-180.0	5	12	0	12.2	12.5	90.0	8	15	0	9.1	9.3	-180.0
7	9	0*	3.1	0.2	90.0	6	12	0*	2.3	0.6	-180.0	9	15	0	12.7	13.1	90.0
8	9	0	5.1	4.5	0.0	7	12	0	5.4	5.7	90.0	10	15	0	11.4	11.5	-180.0
9	9	0	5.6	5.1	-90.0	8	12	0	8.8	7.2	0.0	11	15	0	9.1	10.1	90.0
10	9	0	5.9	5.3	-180.0	9	12	0*	1.8	0.7	-90.0	12	15	0*	3.1	1.4	0.0
11	9	0*	2.5	0.1	90.0	10	12	0	3.9	2.6	-180.0	13	15	0*	2.8	2.1	-90.0
12	9	0	9.0	9.2	-180.0	11	12	0	13.8	13.8	-90.0	14	15	0	6.9	4.8	0.0
13	9	0*	3.5	0.0	90.0	12	12	0	20.4	20.8	-180.0	15	15	0*	2.2	0.4	90.0
14	9	0	4.6	4.9	0.0	13	12	0	3.8	3.5	90.0	16	15	0*	1.8	0.6	0.0
15	9	0*	2.9	0.4	-90.0	14	12	0	6.6	6.3	-180.0	17	15	0*	1.6	0.6	90.0
16	9	0	5.3	5.1	-180.0	15	12	0	6.3	6.5	90.0	0	16	0	19.8	20.3	-180.0
17	9	0*	2.1	0.5	90.0	16	12	0	7.8	7.4	0.0	1	16	0	13.8	13.1	90.0
18	9	0*	2.0	0.5	0.0	17	12	0*	1.6	1.2	90.0	2	16	0	10.4	10.7	-180.0
19	9	0*	1.8	1.7	90.0	18	12	0*	1.8	1.7	0.0	3	16	0	28.4	26.2	-90.0
0	10	0	54.3	54.4	-180.0	1	13	0	11.6	9.7	-90.0	4	16	0	6.6	6.5	0.0
1	10	0	20.3	19.3	-90.0	2	13	0	46.4	45.0	0.0	5	16	0	9.9	8.9	90.0
2	10	0	17.5	17.5	-180.0	3	13	0	9.0	7.0	90.0	6	16	0	7.1	6.8	0.0
3	10	0	27.8	27.4	90.0	4	13	0	34.4	34.2	0.0	7	16	0	6.6	5.4	-90.0
4	10	0	17.5	17.6	0.0	5	13	0	9.1	8.7	-90.0	8	16	0	13.9	14.4	0.0
5	10	0	16.4	14.8	90.0	6	13	0*	1.9	3.7	-180.0	9	16	0*	1.9	1.6	-90.0
6	10	0	11.2	12.2	-180.0	7	13	0	4.0	3.3	90.0	10	16	0*	2.3	1.7	-180.0
7	10	0	20.6	19.9	90.0	8	13	0*	2.6	0.9	0.0	11	16	0	4.5	4.7	90.0
8	10	0	5.0	4.8	-180.0	9	13	0	5.0	3.6	90.0	12	16	0*	2.8	1.9	0.0
9	10	0	9.7	8.9	-90.0	10	13	0*	3.1	2.6	-180.0	13	16	0*	2.4	1.6	90.0
10	10	0	7.6	7.5	0.0	11	13	0	6.7	7.7	-90.0	14	16	0*	2.8	2.6	0.0
11	10	0	8.0	7.0	90.0	12	13	0	6.5	5.7	0.0	15	16	0*	2.2	1.5	90.0
12	10	0	4.8	4.6	0.0	13	13	0	5.0	5.4	-90.0	16	16	0*	1.8	1.9	-180.0
13	10	0	21.8	21.7	-90.0	14	13	0	7.2	7.0	-180.0	1	17	0	13.1	14.2	90.0
14	10	0*	2.3	1.4	-180.0	15	13	0*	2.8	1.1	90.0	2	17	0*	2.2	0.7	-180.0
15	10	0*	3.4	1.1	-90.0	16	13	0*	2.3	0.2	-180.0	3	17	0	12.0	11.5	-90.0
16	10	0*	2.9	1.6	0.0	17	13	0*	2.6	2.6	90.0	4	17	0*	2.6	0.8	0.0
17	10	0	4.8	3.9	-90.0	18	13	0*	1.3	0.4	0.0	5	17	0	10.4	9.3	-90.0
18	10	0*	2.1	0.3	0.0	0	14	0	63.6	63.3	-180.0	6	17	0	14.4	13.8	-180.0
19	10	0	2.7	3.2	90.0	1	14	0	20.8	20.7	-90.0	7	17	0	3.9	3.1	-90.0
1	11	0	38.9	38.6	90.0	2	14	0	7.1	4.0	-180.0	8	17	0	7.5	8.4	0.0
2	11	0	55.7	53.4	-180.0	3	14	0	19.1	16.5	-90.0	9	17	0	14.3	14.8	90.0
3	11	0	28.2	27.2	-90.0	4	14	0	3.5	3.0	0.0	10	17	0	4.6	5.0	0.0
4	11	0	20.3	20.0	-180.0	5	14	0*	2.6	0.0	-90.0	11	17	0	4.2	4.2	90.0
5	11	0	12.0	12.1	-90.0	6	14	0	15.9	14.3	0.0	12	17	0	4.3	3.5	0.0
6	11	0	28.6	25.9	0.0	7	14	0*	2.6	0.9	90.0	13	17	0	5.4	4.4	-90.0
7	11	0	6.2	4.8	-90.0	8	14	0	3.8	1.7	-180.0	14	17	0	3.5	2.6	-180.0
8	11	0	18.3	18.9	-180.0	9	14	0	23.7	23.6	90.0	15	17	0	4.4	4.3	-90.0
9	11	0	3.1	0.9	-90.0	10	14	0	7.4	6.7	0.0	16	17	0*	1.7	1.1	-180.0
10	11	0*	2.5	0.2	-180.0	11	14	0	13.0	13.7	90.0	0	18	0*	2.4	2.1	-180.0
11	11	0	7.8	8.3	-90.0	12	14	0	11.0	12.4	0.0	1	18	0	4.0	3.2	90.0
12	11	0	12.2	11.9	-180.0	13	14	0*	2.4	0.5	-90.0	2	18	0	9.5	8.9	-180.0
13	11	0	11.7	13.3	90.0	14	14	0	4.5	4.6	-180.0	3	18	0*	3.0	3.5	-90.0
14	11	0	5.8	6.4	0.0	15	14	0	4.9	4.3	-90.0	4	18	0	15.3	15.1	0.0
15	11	0	11.1	10.2	90.0	16	14	0	4.4	2.8	-180.0	5	18	0*	2.8	4.0	90.0
16	11	0*	2.4	0.7	-180.0	17	14	0*	1.7	0.8	-90.0	6	18	0*	2.6	0.5	0.0
17	11	0	7.1	6.9	-90.0	1	15	0	37.7	37.0	-90.0	7	18	0	7.9	8.2	-90.0

H	K	L	/Fo/	/Fc/	PHASE	H	K	L	/Fo/	/Fc/	PHASE	H	K	L	/Fo/	/Fc/	PHASE
8	18	0*	2.6	1.4	-180.0	7	22	0*	3.0	2.5	-90.0	13	0	1	8.1	8.3	-90.0
9	18	0*	3.8	3.6	90.0	8	22	0	4.5	3.7	0.0	14	0	1	7.7	8.0	-90.0
10	18	0*	2.6	1.7	-180.0	9	22	0	3.3	2.6	-90.0	15	0	1	1.8	1.4	-90.0
11	18	0	3.6	2.9	-90.0	10	22	0*	1.7	2.1	-180.0	16	0	1	5.8	5.7	90.0
12	18	0*	2.5	1.0	-180.0	11	22	0	3.3	3.0	90.0	17	0	1*	3.2	2.9	90.0
13	18	0*	2.0	1.0	-90.0	12	22	0*	1.6	1.6	0.0	18	0	1	3.3	3.0	90.0
14	18	0*	1.5	0.1	-180.0	1	23	0	7.0	6.7	-90.0	19	0	1	5.0	4.7	90.0
15	18	0*	1.5	2.0	-90.0	2	23	0	5.1	5.8	0.0	20	0	1*	1.4	0.7	-90.0
1	19	0	5.9	6.6	90.0	3	23	0	3.7	3.6	-90.0	0	1	1	31.3	34.7	-90.0
2	19	0*	2.0	0.8	-180.0	4	23	0*	2.4	2.3	0.0	1	1	1	10.2	9.1	-117.4
3	19	0	3.8	5.0	90.0	5	23	0*	2.4	2.3	90.0	2	1	1	39.4	43.0	45.0
4	19	0*	2.2	1.0	-180.0	6	23	0	3.7	2.7	-180.0	3	1	1●	82.7	94.1	100.9
5	19	0	4.4	4.5	90.0	7	23	0	2.5	2.1	-90.0	4	1	1	45.6	51.4	175.7
6	19	0*	3.6	4.8	0.0	8	23	0*	1.7	1.4	-180.0	5	1	1	50.8	54.5	-95.5
7	19	0	7.9	7.9	90.0	9	23	0	4.8	4.0	-90.0	6	1	1	6.4	6.0	-125.9
8	19	0	17.6	17.3	0.0	10	23	0*	2.0	1.2	-180.0	7	1	1	34.3	34.1	-97.1
9	19	0*	2.7	1.2	-90.0	11	23	0*	1.4	0.0	-90.0	8	1	1	6.4	4.3	-54.7
10	19	0	3.6	3.5	0.0	0	24	0*	2.5	1.0	0.0	9	1	1	20.1	19.6	96.8
11	19	0	5.0	4.0	90.0	1	24	0	5.0	4.5	90.0	10	1	1	32.6	32.1	172.7
12	19	0*	1.9	1.3	-180.0	2	24	0*	1.8	0.0	-180.0	11	1	1	5.9	4.2	-22.9
13	19	0	5.1	4.8	90.0	3	24	0	4.0	3.5	-90.0	12	1	1	8.1	7.8	32.6
14	19	0	7.9	10.0	-180.0	4	24	0	5.3	4.2	-180.0	13	1	1	6.9	7.6	173.7
0	20	0	17.4	18.6	-180.0	5	24	0*	1.5	0.0	-90.0	14	1	1	10.4	10.5	33.8
1	20	0	4.7	5.3	-90.0	6	24	0	2.7	2.3	0.0	15	1	1	3.7	3.0	-82.6
2	20	0	5.5	4.5	0.0	7	24	0*	1.8	0.1	90.0	16	1	1	4.2	5.6	-120.0
3	20	0	4.0	4.0	-90.0	8	24	0*	1.8	1.9	0.0	17	1	1*	2.2	1.0	101.8
4	20	0*	1.4	1.0	-180.0	9	24	0	2.2	1.5	-90.0	18	1	1	2.4	2.5	32.3
5	20	0	10.3	11.3	-90.0	1	25	0	5.5	4.8	-90.0	19	1	1*	2.6	1.5	35.6
6	20	0	6.2	7.0	0.0	2	25	0*	1.7	1.9	-180.0	20	1	1*	1.6	0.5	44.8
7	20	0*	3.5	3.0	90.0	3	25	0*	1.4	1.5	-90.0	0	2	1●	115.5	179.2	-180.0
8	20	0*	3.4	2.7	0.0	4	25	0	6.5	6.4	-180.0	1	2	1●	70.5	84.4	-45.0
9	20	0	6.3	5.5	90.0	5	25	0*	2.5	2.8	-90.0	2	2	1	42.1	41.8	0.5
10	20	0*	2.3	0.8	-180.0	6	25	0	4.9	6.0	-180.0	3	2	1●	80.8	96.2	33.3
11	20	0	4.4	3.2	-90.0	7	25	0*	1.2	0.9	90.0	4	2	1	56.9	59.0	-39.3
12	20	0	2.8	2.2	0.0	8	25	0*	1.4	2.1	0.0	5	2	1	64.8	67.8	111.8
13	20	0	4.5	5.6	90.0	0	26	0*	2.7	2.6	-180.0	6	2	1	17.8	19.2	54.7
14	20	0*	1.3	0.5	-180.0	1	26	0	2.4	1.0	90.0	7	2	1	17.8	19.3	161.2
1	21	0	10.4	11.0	-90.0	2	26	0*	1.4	1.6	0.0	8	2	1	41.1	39.7	-67.5
2	21	0*	3.4	3.0	0.0	3	26	0*	1.0	1.1	90.0	9	2	1	31.2	30.1	-41.7
3	21	0*	3.1	2.5	90.0	4	26	0*	2.2	1.0	0.0	10	2	1	17.1	16.9	163.8
4	21	0	5.0	4.5	-180.0	5	26	0*	1.0	1.5	90.0	11	2	1	6.1	6.5	9.7
5	21	0	7.4	7.2	-90.0	6	26	0*	1.7	1.9	-180.0	12	2	1	12.1	11.1	156.9
6	21	0	9.4	8.4	0.0	1	27	0*	1.1	0.0	-90.0	13	2	1	3.5	2.9	-87.7
7	21	0	6.0	5.9	-90.0	2	27	0	4.9	5.5	-180.0	14	2	1	6.1	6.1	70.0
8	21	0	4.4	3.5	0.0	3	27	0*	1.2	1.4	-90.0	15	2	1	10.5	10.5	-159.4
9	21	0*	1.8	0.9	-90.0	1	0	1	22.2	24.1	-90.0	16	2	1*	2.6	3.1	-43.5
10	21	0	5.3	4.2	0.0	2	0	1	11.6	12.4	-90.0	17	2	1*	2.6	1.5	-67.0
11	21	0*	1.7	1.1	-90.0	3	0	1	51.8	53.8	-90.0	18	2	1*	2.2	1.3	72.2
12	21	0*	1.6	1.1	0.0	4	0	1●	112.0	143.8	-90.0	19	2	1*	2.5	2.3	143.3
13	21	0*	1.0	0.6	90.0	5	0	1	50.8	53.4	90.0	20	2	1	2.6	3.3	9.7
0	22	0	7.2	6.9	0.0	6	0	1	60.1	63.3	-90.0	0	3	1●	94.2	119.6	90.0
1	22	0	3.8	4.1	90.0	7	0	1	21.8	20.9	90.0	1	3	1●	83.5	96.5	166.1
2	22	0*	3.0	2.0	0.0	8	0	1	42.5	41.7	90.0	2	3	1●	86.7	106.2	-104.1
3	22	0	5.7	6.0	90.0	9	0	1	21.2	19.6	90.0	3	3	1	60.4	65.2	-166.3
4	22	0	11.9	11.9	-180.0	10	0	1	11.8	6.3	-90.0	4	3	1●	83.3	96.6	-51.2
5	22	0	8.5	8.6	-90.0	11	0	1	15.7	17.3	-90.0	5	3	1	49.7	53.4	-23.5
6	22	0*	2.0	0.1	-180.0	12	0	1*	2.2	1.9	90.0	6	3	1*	3.0	0.5	154.0

H	K	L	/Fo/	/Fc/	PHASE	H	K	L	/Fo/	/Fc/	PHASE	H	K	L	/Fo/	/Fc/	PHASE
7	3	1	32.7	33.5	96.1	1	6	1	24.7	24.6	9.0	18	8	1*	2.0	0.3	-102.9
8	3	1	44.8	42.9	99.6	2	6	1	33.2	34.5	48.3	19	8	1	3.1	3.0	79.9
9	3	1	27.0	26.4	22.3	3	6	1	6.7	7.3	-113.5	0	9	1	25.3	26.0	90.0
10	3	1	26.2	24.6	133.1	4	6	1	27.1	26.7	50.1	1	9	1	16.2	16.0	-171.0
11	3	1	9.0	7.7	-13.8	5	6	1	32.3	32.3	-160.4	2	9	1	14.3	14.1	106.2
12	3	1	10.3	10.1	-142.3	6	6	1	27.6	27.7	131.0	3	9	1	35.1	36.9	40.2
13	3	1	20.1	20.6	2.4	7	6	1	17.5	17.5	143.1	4	9	1	11.1	10.5	94.4
14	3	1	7.9	8.6	61.3	8	6	1	21.2	18.6	104.9	5	9	1	20.8	20.9	-69.1
15	3	1	7.1	7.1	-151.6	9	6	1	14.9	14.4	39.8	6	9	1	26.1	24.8	-35.1
16	3	1	4.4	3.8	0.6	10	6	1	6.1	4.6	-171.1	7	9	1	22.3	22.5	-65.5
17	3	1*	2.6	1.4	93.7	11	6	1	7.9	7.3	-59.6	8	9	1	14.9	14.0	-99.2
18	3	1*	2.2	1.5	57.8	12	6	1	6.4	6.7	50.7	9	9	1	5.5	5.4	48.2
19	3	1*	1.7	0.8	-76.6	13	6	1*	3.1	2.5	81.8	10	9	1	13.6	13.1	-20.7
20	3	1*	2.1	2.6	-119.7	14	6	1	8.0	8.7	-95.1	11	9	1	9.2	9.5	-113.4
0	4	1●	74.6	85.5	-180.0	15	6	1*	2.2	2.6	-97.5	12	9	1	5.9	6.0	126.1
1	4	1●	97.1	118.4	145.3	16	6	1	4.8	3.2	179.9	13	9	1	7.8	7.6	65.5
2	4	1	49.6	53.6	-98.7	17	6	1*	2.6	0.6	41.5	14	9	1	5.4	5.8	-13.9
3	4	1	44.1	46.3	-91.9	18	6	1	3.7	2.9	-72.9	15	9	1	5.6	6.0	141.8
4	4	1	23.1	24.6	-61.0	19	6	1*	1.6	1.5	-60.8	16	9	1	4.1	4.4	-148.0
5	4	1	58.0	60.8	166.8	0	7	1	10.5	9.6	-90.0	17	9	1	4.4	3.5	-124.5
6	4	1	44.4	45.1	-70.8	1	7	1	13.8	14.1	7.6	18	9	1*	2.5	2.4	-166.6
7	4	1	50.4	50.5	-109.7	2	7	1	27.8	27.6	86.5	19	9	1	2.5	2.7	-158.2
8	4	1	50.7	50.2	-73.1	3	7	1	41.3	41.5	-45.9	0	10	1	39.6	38.3	-180.0
9	4	1	18.5	18.1	61.8	4	7	1	40.4	40.7	-67.1	1	10	1	52.1	51.7	-119.9
10	4	1	24.7	25.1	70.8	5	7	1	31.5	30.3	-122.1	2	10	1	22.0	20.8	-159.0
11	4	1	6.5	5.8	99.0	6	7	1	6.2	5.7	35.0	3	10	1	30.8	31.6	99.4
12	4	1	5.2	4.6	-75.1	7	7	1	12.7	11.3	149.2	4	10	1	25.1	24.1	67.4
13	4	1	5.9	4.5	-37.9	8	7	1	24.3	23.7	-13.1	5	10	1	30.3	31.3	-167.8
14	4	1	10.3	10.0	158.9	9	7	1	20.7	19.6	77.4	6	10	1	14.1	14.3	30.1
15	4	1	3.8	3.7	-14.1	10	7	1	6.6	6.6	12.0	7	10	1	14.0	14.0	30.8
16	4	1	6.6	6.0	70.3	11	7	1	14.8	14.0	33.3	8	10	1	14.8	14.3	29.2
17	4	1*	3.3	3.8	-26.2	12	7	1	5.4	4.8	174.7	9	10	1	3.4	1.9	3.6
18	4	1*	2.3	1.4	56.2	13	7	1	9.5	9.7	-164.2	10	10	1	7.1	7.3	-163.0
19	4	1*	1.7	0.5	-148.8	14	7	1	7.2	7.2	166.0	11	10	1	6.3	6.4	6.2
20	4	1*	1.4	0.2	-7.2	15	7	1*	2.8	1.9	20.2	12	10	1	10.9	11.1	135.5
0	5	1●	63.9	70.0	90.0	16	7	1*	2.6	1.8	142.3	13	10	1	10.5	11.0	0.4
1	5	1	28.9	30.5	-178.5	17	7	1*	2.7	2.0	-101.7	14	10	1	3.9	3.9	117.5
2	5	1	28.4	27.1	172.3	18	7	1*	2.0	2.0	-54.1	15	10	1	4.6	3.7	62.0
3	5	1	25.0	25.2	144.8	19	7	1*	1.9	1.1	136.9	16	10	1	4.5	4.6	-3.2
4	5	1	55.2	60.3	27.9	0	8	1	28.9	29.1	-180.0	17	10	1*	2.2	1.0	159.9
5	5	1	30.8	30.5	-54.1	1	8	1	35.3	34.5	-29.3	18	10	1	2.7	1.7	-37.5
6	5	1	35.2	36.7	-178.7	2	8	1	12.7	13.2	28.3	19	10	1*	2.0	2.4	-156.0
7	5	1	20.2	17.9	31.3	3	8	1	17.0	18.7	-119.7	0	11	1	29.2	27.9	90.0
8	5	1	17.8	17.1	-126.7	4	8	1	7.3	6.6	87.8	1	11	1	60.7	59.4	-31.5
9	5	1	26.7	24.9	75.7	5	8	1	21.3	22.9	4.1	2	11	1	26.3	24.3	-49.8
10	5	1	22.4	20.6	-71.0	6	8	1	11.3	10.6	-101.2	3	11	1	14.1	11.9	-73.5
11	5	1	5.4	5.5	-142.1	7	8	1	12.5	12.2	18.4	4	11	1	6.3	5.7	170.6
12	5	1	6.2	5.8	-72.1	8	8	1	22.0	20.5	89.8	5	11	1	5.9	6.2	146.3
13	5	1	3.4	1.3	22.4	9	8	1	4.7	5.7	-1.7	6	11	1	7.4	8.5	-26.3
14	5	1*	2.8	2.7	148.8	10	8	1	8.6	8.4	17.6	7	11	1	9.9	9.7	-79.5
15	5	1	9.0	9.7	-53.0	11	8	1	7.3	7.3	-174.0	8	11	1	5.9	6.0	-72.9
16	5	1*	3.5	3.1	22.6	12	8	1	6.1	6.5	-64.6	9	11	1	23.7	22.3	-179.1
17	5	1*	3.0	2.1	-158.3	13	8	1	5.7	5.0	-145.2	10	11	1	10.2	9.8	-135.9
18	5	1*	2.3	1.5	72.7	14	8	1	7.2	8.0	141.6	11	11	1*	3.4	2.9	-174.4
19	5	1*	2.1	0.7	118.9	15	8	1	4.2	4.0	68.1	12	11	1	11.5	11.0	-34.5
20	5	1*	1.2	1.5	-77.6	16	8	1*	3.2	2.4	-130.5	13	11	1	8.4	9.7	-175.6
0	6	1*	2.0	1.0	-180.0	17	8	1	3.9	3.1	179.9	14	11	1	6.9	6.9	123.8

H	K	L	/F0/	/FC/	PHASE	H	K	L	/F0/	/FC/	PHASE	H	K	L	/F0/	/FC/	PHASE
8	18	0*	2.6	1.4	-180.0	7	22	0*	3.0	2.5	-90.0	13	0	1	8.1	8.3	-90.0
9	18	0*	3.8	3.6	90.0	8	22	0	4.5	3.7	0.0	14	0	1	7.7	8.0	-90.0
10	18	0*	2.6	1.7	-180.0	9	22	0	3.3	2.6	-90.0	15	0	1	1.8	1.4	-90.0
11	18	0	3.6	2.9	-90.0	10	22	0*	1.7	2.1	-180.0	16	0	1	5.8	5.7	90.0
12	18	0*	2.5	1.0	-180.0	11	22	0	3.3	3.0	90.0	17	0	1*	3.2	2.9	90.0
13	18	0*	2.0	1.0	-90.0	12	22	0*	1.6	1.6	0.0	18	0	1	3.3	3.0	90.0
14	18	0*	1.5	0.1	-180.0	1	23	0	7.0	6.7	-90.0	19	0	1	5.0	4.7	90.0
15	18	0*	1.5	2.0	-90.0	2	23	0	5.1	5.8	0.0	20	0	1*	1.4	0.7	-90.0
1	19	0	5.9	6.6	90.0	3	23	0	3.7	3.6	-90.0	0	1	1	31.3	34.7	-90.0
2	19	0*	2.0	0.8	-180.0	4	23	0*	2.4	2.3	0.0	1	1	1	10.2	9.1	-117.4
3	19	0	3.8	5.0	90.0	5	23	0*	2.4	2.3	90.0	2	1	1	39.4	43.0	45.0
4	19	0*	2.2	1.0	-180.0	6	23	0	3.7	2.7	-180.0	3	1	1●	82.7	94.1	100.9
5	19	0	4.4	4.5	90.0	7	23	0	2.5	2.1	-90.0	4	1	1	45.6	51.4	175.7
6	19	0*	3.6	4.8	0.0	8	23	0*	1.7	1.4	-180.0	5	1	1	50.8	54.5	-95.5
7	19	0	7.9	7.9	90.0	9	23	0	4.8	4.0	-90.0	6	1	1	6.4	6.0	-125.9
8	19	0	17.6	17.3	0.0	10	23	0*	2.0	1.2	-180.0	7	1	1	34.3	34.1	-97.1
9	19	0*	2.7	1.2	-90.0	11	23	0*	1.4	0.0	-90.0	8	1	1	6.4	4.3	-54.7
10	19	0	3.6	3.5	0.0	0	24	0*	2.5	1.0	0.0	9	1	1	20.1	19.6	96.8
11	19	0	5.0	4.0	90.0	1	24	0	5.0	4.5	90.0	10	1	1	32.6	32.1	172.7
12	19	0*	1.9	1.3	-180.0	2	24	0*	1.8	0.0	-180.0	11	1	1	5.9	4.2	-22.9
13	19	0	5.1	4.8	90.0	3	24	0	4.0	3.5	-90.0	12	1	1	8.1	7.8	32.6
14	19	0	7.9	10.0	-180.0	4	24	0	5.3	4.2	-180.0	13	1	1	6.9	7.6	173.7
0	20	0	17.4	18.6	-180.0	5	24	0*	1.5	0.0	-90.0	14	1	1	10.4	10.5	33.8
1	20	0	4.7	5.3	-90.0	6	24	0	2.7	2.3	0.0	15	1	1	3.7	3.0	-82.6
2	20	0	5.5	4.5	0.0	7	24	0*	1.8	0.1	90.0	16	1	1	4.2	5.6	-120.0
3	20	0	4.0	4.0	-90.0	8	24	0*	1.8	1.9	0.0	17	1	1*	2.2	1.0	101.8
4	20	0*	1.4	1.0	-180.0	9	24	0	2.2	1.5	-90.0	18	1	1	2.4	2.5	32.3
5	20	0	10.3	11.3	-90.0	1	25	0	5.5	4.8	-90.0	19	1	1*	2.6	1.5	35.6
6	20	0	6.2	7.0	0.0	2	25	0*	1.7	1.9	-180.0	20	1	1*	1.6	0.5	44.8
7	20	0*	3.5	3.0	90.0	3	25	0*	1.4	1.5	-90.0	0	2	1●	115.5	179.2	-180.0
8	20	0*	3.4	2.7	0.0	4	25	0	6.5	6.4	-180.0	1	2	1●	70.5	84.4	-45.0
9	20	0	6.3	5.5	90.0	5	25	0*	2.5	2.8	-90.0	2	2	1	42.1	41.8	0.5
10	20	0*	2.3	0.8	-180.0	6	25	0	4.9	6.0	-180.0	3	2	1●	80.8	96.2	33.3
11	20	0	4.4	3.2	-90.0	7	25	0*	1.2	0.9	90.0	4	2	1	56.9	59.0	-39.3
12	20	0	2.8	2.2	0.0	8	25	0*	1.4	2.1	0.0	5	2	1	64.8	67.8	111.8
13	20	0	4.5	5.6	90.0	0	26	0*	2.7	2.6	-180.0	6	2	1	17.8	19.2	54.7
14	20	0*	1.3	0.5	-180.0	1	26	0	2.4	1.0	90.0	7	2	1	17.8	19.3	161.2
1	21	0	10.4	11.0	-90.0	2	26	0*	1.4	1.6	0.0	8	2	1	41.1	39.7	-67.5
2	21	0*	3.4	3.0	0.0	3	26	0*	1.0	1.1	90.0	9	2	1	31.2	30.1	-41.7
3	21	0*	3.1	2.5	90.0	4	26	0*	2.2	1.0	0.0	10	2	1	17.1	16.9	163.8
4	21	0	5.0	4.5	-180.0	5	26	0*	1.0	1.5	90.0	11	2	1	6.1	6.5	9.7
5	21	0	7.4	7.2	-90.0	6	26	0*	1.7	1.9	-180.0	12	2	1	12.1	11.1	156.9
6	21	0	9.4	8.4	0.0	1	27	0*	1.1	0.0	-90.0	13	2	1	3.5	2.9	-87.7
7	21	0	6.0	5.9	-90.0	2	27	0	4.9	5.5	-180.0	14	2	1	6.1	6.1	70.0
8	21	0	4.4	3.5	0.0	3	27	0*	1.2	1.4	-90.0	15	2	1	10.5	10.5	-159.4
9	21	0*	1.8	0.9	-90.0	1	0	1	22.2	24.1	-90.0	16	2	1*	2.6	3.1	-43.5
10	21	0	5.3	4.2	0.0	2	0	1	11.6	12.4	-90.0	17	2	1*	2.6	1.5	-67.0
11	21	0*	1.7	1.1	-90.0	3	0	1	51.8	53.8	-90.0	18	2	1*	2.2	1.3	72.2
12	21	0*	1.6	1.1	0.0	4	0	1●	112.0	143.6	-90.0	19	2	1*	2.5	2.3	143.3
13	21	0*	1.0	0.6	90.0	5	0	1	50.8	53.4	90.0	20	2	1	2.6	3.3	9.7
0	22	0	7.2	6.9	0.0	6	0	1	60.1	63.3	-90.0	0	3	1●	94.2	119.6	90.0
1	22	0	3.8	4.1	90.0	7	0	1	21.8	20.9	90.0	1	3	1●	83.5	96.5	166.1
2	22	0*	3.0	2.0	0.0	8	0	1	42.5	41.7	90.0	2	3	1●	86.7	106.2	-104.1
3	22	0	5.7	6.0	90.0	9	0	1	21.2	19.6	90.0	3	3	1	60.4	65.2	-166.3
4	22	0	11.9	11.9	-180.0	10	0	1	11.8	6.3	-90.0	4	3	1●	83.3	96.6	-51.2
5	22	0	8.5	8.6	-90.0	11	0	1	15.7	17.3	-90.0	5	3	1	49.7	53.4	-23.5
6	22	0*	2.0	0.1	-180.0	12	0	1*	2.2	1.9	90.0	6	3	1*	3.0	0.5	154.0

H	K	L	/F0/	/FC/	PHASE	H	K	L	/F0/	/FC/	PHASE	H	K	L	/F0/	/FC/	PHASE
7	3	1	32.7	33.5	96.1	1	6	1	24.7	24.6	9.0	18	8	1*	2.0	0.3	-102.9
8	3	1	44.8	42.9	99.6	2	6	1	33.2	34.5	48.3	19	8	1	3.1	3.0	79.9
9	3	1	27.0	26.4	22.3	3	6	1	6.7	7.3	-113.5	0	9	1	25.3	26.0	90.0
10	3	1	26.2	24.6	133.1	4	6	1	27.1	28.7	60.1	1	9	1	16.2	16.0	-171.0
11	3	1	9.0	7.7	-13.8	5	6	1	32.3	32.3	-160.4	2	9	1	14.3	14.1	106.2
12	3	1	10.3	10.1	-142.3	6	6	1	27.6	27.7	131.0	3	9	1	35.1	36.9	40.2
13	3	1	20.1	20.6	2.4	7	6	1	17.5	17.5	143.1	4	9	1	11.1	10.5	94.4
14	3	1	7.9	8.6	61.3	8	6	1	21.2	18.6	104.8	5	9	1	20.8	20.9	-69.1
15	3	1	7.1	7.1	-151.6	9	6	1	14.9	14.4	39.8	6	9	1	26.1	24.8	-35.1
16	3	1	4.4	3.8	0.6	10	6	1	6.1	4.6	-171.1	7	9	1	22.3	22.5	-65.5
17	3	1*	2.6	1.4	93.7	11	6	1	7.9	7.3	-59.6	8	9	1	14.9	14.0	-99.2
18	3	1*	2.2	1.5	87.8	12	6	1	6.4	6.7	50.7	9	9	1	5.5	5.4	48.2
19	3	1*	1.7	0.8	-76.6	13	6	1*	3.1	2.5	81.8	10	9	1	13.6	13.1	-20.7
20	3	1*	2.1	2.6	-119.7	14	6	1	8.0	8.7	-95.1	11	9	1	9.2	9.5	-113.4
0	4	1●	74.6	85.5	-180.0	15	6	1*	2.2	2.6	-97.5	12	9	1	5.9	6.0	126.1
1	4	1●	97.1	118.4	145.3	16	6	1	4.8	3.2	179.9	13	9	1	7.8	7.6	65.5
2	4	1	49.6	53.6	-98.7	17	6	1*	2.6	0.6	41.5	14	9	1	5.4	5.8	-13.9
3	4	1	44.1	46.3	-91.9	18	6	1	3.7	2.9	-72.9	15	9	1	5.6	6.0	141.8
4	4	1	23.1	24.6	-61.0	19	6	1*	1.6	1.5	-60.8	16	9	1	4.1	4.4	-148.0
5	4	1	58.0	60.8	166.8	0	7	1	10.5	9.6	-90.0	17	9	1	4.4	3.5	-124.5
6	4	1	44.4	45.1	-70.8	1	7	1	13.8	14.1	7.6	18	9	1*	2.5	2.4	-166.6
7	4	1	50.4	50.5	-109.7	2	7	1	27.8	27.6	86.5	19	9	1	2.5	2.7	-158.2
8	4	1	50.7	50.2	-73.1	3	7	1	41.3	41.5	-45.9	0	10	1	39.6	38.3	-180.0
9	4	1	18.5	18.1	61.8	4	7	1	40.4	40.7	-67.1	1	10	1	52.1	51.7	-119.9
10	4	1	24.7	25.1	70.8	5	7	1	31.5	30.3	-122.1	2	10	1	22.0	20.8	-159.0
11	4	1	6.5	5.8	99.0	6	7	1	6.2	5.7	35.0	3	10	1	30.8	31.6	99.4
12	4	1	5.2	4.6	-75.1	7	7	1	12.7	11.3	149.2	4	10	1	25.1	24.1	67.4
13	4	1	5.9	4.5	-37.9	8	7	1	24.3	23.7	-13.1	5	10	1	30.3	31.3	-167.8
14	4	1	10.3	10.0	158.9	9	7	1	20.7	19.6	77.4	6	10	1	14.1	14.3	30.1
15	4	1	3.8	3.7	-14.1	10	7	1	6.6	6.6	12.0	7	10	1	14.0	14.0	30.8
16	4	1	6.6	6.0	70.3	11	7	1	14.8	14.0	33.3	8	10	1	14.8	14.3	29.2
17	4	1*	3.3	3.8	-26.2	12	7	1	5.4	4.8	174.7	9	10	1	3.4	1.9	3.6
18	4	1*	2.3	1.4	56.2	13	7	1	9.5	9.7	-164.2	10	10	1	7.1	7.3	-163.0
19	4	1*	1.7	0.5	-148.8	14	7	1	7.2	7.2	166.0	11	10	1	6.3	6.4	6.2
20	4	1*	1.4	0.2	-7.2	15	7	1*	2.8	1.9	20.2	12	10	1	10.9	11.1	135.5
0	5	1●	63.9	70.0	90.0	16	7	1*	2.6	1.8	142.3	13	10	1	10.5	11.0	0.4
1	5	1	28.9	30.5	-178.5	17	7	1*	2.7	2.0	-101.7	14	10	1	3.9	3.9	117.5
2	5	1	28.4	27.1	172.3	18	7	1*	2.0	2.0	-54.1	15	10	1	4.6	3.7	82.0
3	5	1	25.0	25.2	144.8	19	7	1*	1.9	1.1	136.9	16	10	1	4.5	4.6	-3.2
4	5	1	55.2	60.3	27.9	0	8	1	28.9	29.1	-180.0	17	10	1*	2.2	1.0	159.9
5	5	1	30.8	30.5	-54.1	1	8	1	35.3	34.5	-29.3	18	10	1	2.7	1.7	-37.5
6	5	1	35.2	36.7	-178.7	2	8	1	12.7	13.2	28.3	19	10	1*	2.0	2.4	-156.0
7	5	1	20.2	17.9	31.3	3	8	1	17.0	18.7	-119.7	0	11	1	29.2	27.9	90.0
8	5	1	17.8	17.1	-126.7	4	8	1	7.3	6.6	87.8	1	11	1	60.7	59.4	-31.5
9	5	1	26.7	24.9	75.7	5	8	1	21.3	22.9	4.1	2	11	1	26.3	24.3	-49.8
10	5	1	22.4	20.6	-71.0	6	8	1	11.3	10.6	-101.2	3	11	1	14.1	11.9	-73.5
11	5	1	5.4	5.5	-142.1	7	8	1	12.5	12.2	18.4	4	11	1	6.3	5.7	170.6
12	5	1	6.2	5.8	-72.1	8	8	1	22.0	20.5	89.8	5	11	1	5.9	6.2	146.3
13	5	1	3.4	1.3	22.4	9	8	1	4.7	5.7	-1.7	6	11	1	7.4	8.5	-26.3
14	5	1*	2.8	2.7	148.8	10	8	1	8.6	8.4	17.6	7	11	1	9.9	9.7	-79.5
15	5	1	9.0	9.7	-53.0	11	8	1	7.3	7.3	-174.0	8	11	1	5.9	6.0	-72.9
16	5	1*	3.5	3.1	22.6	12	8	1	6.1	6.5	-64.6	9	11	1	23.7	22.3	-179.1
17	5	1*	3.0	2.1	-158.3	13	8	1	5.7	5.0	-145.2	10	11	1	10.2	9.8	-135.9
18	5	1*	2.3	1.5	72.7	14	8	1	7.2	8.0	141.6	11	11	1*	3.4	2.9	-174.4
19	5	1*	2.1	0.7	118.9	15	8	1	4.2	4.0	69.1	12	11	1	11.5	11.0	-34.5
20	5	1*	1.2	1.5	-77.6	16	8	1*	3.2	2.4	-130.5	13	11	1	8.4	9.7	-175.6
0	6	1*	2.0	1.0	-180.0	17	8	1	3.9	3.1	179.9	14	11	1	6.9	6.9	123.8

H	K	L	/FØ/	/FC/	PHASE	H	K	L	/FØ/	/FC/	PHASE	H	K	L	/FØ/	/FC/	PHASE
15	11	1	3.1	3.0	62.4	16	14	1	3.0	2.3	-142.5	4	18	1	22.0	22.2	93.1
16	11	1	5.6	4.3	61.5	17	14	1*	1.5	0.5	30.7	5	18	1	15.2	15.1	-126.2
17	11	1	4.0	3.0	7.4	0	15	1	12.0	13.1	90.0	6	18	1	6.9	6.7	68.7
18	11	1*	1.8	2.1	53.4	1	15	1	13.4	12.2	176.7	7	18	1	5.9	6.6	168.5
0	12	1	41.4	43.5	-180.0	2	15	1	11.5	10.9	-169.4	8	18	1	6.4	6.9	131.4
1	12	1	15.6	15.9	114.9	3	15	1	15.0	14.5	-111.5	9	18	1*	2.6	2.1	10.0
2	12	1	20.8	19.7	103.0	4	15	1	18.9	20.0	-142.1	10	18	1	7.8	7.7	-164.8
3	12	1	15.2	13.4	-127.5	5	15	1	8.1	7.6	129.1	11	18	1	4.8	4.5	-89.2
4	12	1	9.2	7.5	170.4	6	15	1	10.0	8.7	-130.1	12	18	1	4.5	3.6	122.7
5	12	1	22.4	22.1	-70.9	7	15	1	19.5	19.8	127.4	13	18	1*	2.4	1.7	149.2
6	12	1	17.6	16.5	24.4	8	15	1	19.9	19.3	39.5	14	18	1	3.6	4.2	-59.6
7	12	1	9.1	9.2	-51.5	9	15	1	15.4	15.7	3.8	15	18	1*	1.3	1.5	108.1
8	12	1	5.5	5.8	47.2	10	15	1	5.4	4.9	37.0	0	19	1	6.8	7.5	-90.0
9	12	1	19.7	18.3	56.2	11	15	1*	3.0	0.8	-61.8	1	19	1	5.9	4.7	-48.1
10	12	1	6.0	5.4	-75.0	12	15	1	6.1	5.5	-147.8	2	19	1	7.0	8.5	51.1
11	12	1*	3.4	3.0	-133.3	13	15	1	6.9	6.7	-1.4	3	19	1	17.6	18.6	70.9
12	12	1	5.7	4.8	14.7	14	15	1	5.7	4.7	-178.9	4	19	1	8.6	9.3	92.2
13	12	1*	3.8	4.7	95.0	15	15	1	4.7	4.3	-77.1	5	19	1	8.5	9.0	83.0
14	12	1	6.4	6.2	-139.2	16	15	1*	2.0	2.1	89.2	6	19	1	4.5	4.6	2.6
15	12	1*	3.4	3.4	135.7	17	15	1*	1.5	1.3	-67.6	7	19	1	4.4	3.9	-135.2
16	12	1*	1.8	0.3	-84.1	0	16	1	12.2	12.4	0.0	8	19	1	5.1	4.5	-54.3
17	12	1*	2.4	2.1	0.7	1	16	1	27.2	28.4	144.9	9	19	1	13.0	11.5	-156.0
18	12	1*	1.6	1.4	11.3	2	16	1	7.1	7.4	103.4	10	19	1	6.8	6.5	-64.5
0	13	1	21.2	20.2	-90.0	3	16	1	11.8	11.6	-127.6	11	19	1*	2.9	2.0	-7.0
1	13	1	34.0	32.2	-45.8	4	16	1	6.1	4.6	-155.2	12	19	1	4.3	3.9	-144.0
2	13	1	7.7	6.6	31.3	5	16	1	8.9	8.0	-134.0	13	19	1*	2.2	2.1	25.6
3	13	1	5.5	4.1	-179.5	6	16	1	9.9	9.4	-95.5	14	19	1	2.6	2.5	122.2
4	13	1	6.8	6.3	-155.3	7	16	1	17.7	18.0	167.8	0	20	1*	2.2	2.0	0.0
5	13	1	21.9	19.9	-98.7	8	16	1	9.9	9.9	-79.6	1	20	1	5.4	6.3	-149.9
6	13	1	9.7	9.2	-163.9	9	16	1	12.7	12.4	-179.1	2	20	1	8.2	9.2	9.8
7	13	1	19.6	17.0	-119.6	10	16	1	5.2	4.4	-12.5	3	20	1	4.6	4.1	102.9
8	13	1	9.6	8.3	-142.6	11	16	1*	3.3	1.9	-78.0	4	20	1	10.2	11.3	124.5
9	13	1	16.0	15.8	69.5	12	16	1*	2.8	1.0	27.0	5	20	1	6.3	6.1	-56.1
10	13	1	9.5	10.6	101.9	13	16	1*	2.8	2.5	21.4	6	20	1	5.1	4.9	133.5
11	13	1	11.9	11.8	149.5	14	16	1	3.9	2.6	172.7	7	20	1	10.0	9.8	3.3
12	13	1	6.7	8.1	21.2	15	16	1	5.0	4.9	2.0	8	20	1*	2.2	0.9	16.9
13	13	1	5.7	5.6	-79.3	16	16	1*	1.6	0.7	78.4	9	20	1	9.1	7.8	-163.2
14	13	1*	2.1	1.2	40.7	0	17	1	19.6	19.2	90.0	10	20	1*	2.8	2.2	60.2
15	13	1	6.9	6.3	-113.0	1	17	1	15.4	15.2	61.1	11	20	1	7.1	6.7	158.0
16	13	1*	1.8	0.2	-148.3	2	17	1	13.4	13.8	110.9	12	20	1	3.6	3.5	-52.7
17	13	1	2.5	2.7	105.4	3	17	1	9.4	8.5	140.9	13	20	1	2.9	3.6	44.4
0	14	1	7.6	6.7	-180.0	4	17	1	23.6	23.2	138.6	0	21	1	3.8	2.9	90.0
1	14	1	29.0	26.9	63.4	5	17	1	5.3	5.3	109.7	1	21	1	7.6	9.9	-47.6
2	14	1	14.1	13.7	-97.3	6	17	1	6.3	6.5	-161.8	2	21	1	8.3	9.2	-63.2
3	14	1	10.3	8.2	-28.2	7	17	1	13.1	13.0	29.6	3	21	1*	2.8	0.6	-26.2
4	14	1	7.0	6.7	-89.3	8	17	1	9.2	10.0	-78.6	4	21	1	7.8	7.5	73.7
5	14	1	6.2	5.5	122.2	9	17	1	9.2	10.0	-126.8	5	21	1	7.4	6.2	125.6
6	14	1	26.5	25.4	84.8	10	17	1	11.7	11.1	-23.0	6	21	1*	2.8	0.9	19.8
7	14	1	14.7	14.9	-132.5	11	17	1*	3.4	2.1	-153.6	7	21	1*	2.7	1.0	-51.9
8	14	1	7.5	7.0	-91.7	12	17	1	7.7	6.1	-61.6	8	21	1	5.6	5.8	163.9
9	14	1	16.0	14.7	-65.4	13	17	1	7.6	6.7	108.6	9	21	1*	2.3	1.6	-65.7
10	14	1	8.8	8.1	-162.3	14	17	1	7.1	6.9	-129.3	10	21	1*	2.6	2.6	145.7
11	14	1	10.9	11.9	34.2	15	17	1	3.3	3.4	-18.9	11	21	1*	2.3	2.3	-128.2
12	14	1	9.3	11.2	-65.5	0	18	1	13.1	12.8	0.0	12	21	1*	1.0	1.3	23.0
13	14	1	4.9	4.5	93.0	1	18	1	6.9	6.9	86.7	0	22	1	9.2	9.7	0.0
14	14	1	8.5	7.9	62.4	2	18	1	9.6	9.7	-13.7	1	22	1	3.8	2.0	177.9
15	14	1	4.5	4.4	-128.6	3	18	1	8.5	9.9	127.0	2	22	1	4.8	3.7	-59.4

H	K	L	/FØ/	/FC/	PHASE	H	K	L	/FØ/	/FC/	PHASE	H	K	L	/FØ/	/FC/	PHASE
3	22	1	6.8	6.8	-27.8	11	0	2	6.5	5.0	0.0	6	3	2	27.2	27.0	163.6
4	22	1	4.1	3.7	-128.7	12	0	2	26.7	29.0	-180.0	7	3	2	24.5	24.4	87.4
5	22	1*	2.8	0.8	105.9	13	0	2	9.0	9.3	0.0	8	3	2	36.0	35.0	-126.2
6	22	1	5.6	5.2	-111.4	14	0	2	5.0	6.8	-180.0	9	3	2	8.4	6.2	-21.6
7	22	1	2.9	2.7	30.6	15	0	2	9.0	11.7	-180.0	10	3	2	11.1	11.1	-22.5
8	22	1	3.5	2.6	130.8	16	0	2*	2.3	0.9	-180.0	11	3	2	11.3	11.3	-26.1
9	22	1*	1.7	1.0	-78.5	17	0	2*	3.0	2.9	0.0	12	3	2	12.8	13.0	49.6
10	22	1*	1.4	0.3	-174.4	18	0	2	7.3	5.9	0.0	13	3	2	10.1	10.5	46.9
11	22	1*	1.4	1.1	136.4	19	0	2*	1.9	0.6	-180.0	14	3	2*	3.1	2.2	176.9
0	23	1*	2.2	0.9	90.0	20	0	2	2.4	2.7	0.0	15	3	2	4.4	3.2	14.0
1	23	1*	1.8	0.5	31.8	0	1	2	7.3	7.3	-90.0	16	3	2*	3.3	1.7	-176.7
2	23	1*	3.2	2.2	68.1	1	1	2	25.0	27.7	22.0	17	3	2	3.8	4.2	-27.1
3	23	1*	2.4	2.3	-27.5	2	1	2	50.6	55.2	-93.3	18	3	2	2.9	2.1	172.3
4	23	1*	1.8	0.8	-127.0	3	1	2	46.1	48.2	175.5	19	3	2*	1.9	1.7	-119.5
5	23	1*	1.6	1.4	-134.1	4	1	2	51.3	50.6	-45.5	0	4	2	19.0	15.8	-180.0
6	23	1*	1.3	0.8	-167.1	5	1	2	35.6	34.5	73.1	1	4	2	38.2	36.6	71.2
7	23	1*	1.6	1.4	130.4	6	1	2	37.6	37.6	-50.5	2	4	2	30.6	32.1	-26.8
8	23	1	3.6	3.6	-48.8	7	1	2	15.9	14.4	60.9	3	4	2	17.5	16.8	-135.8
9	23	1*	2.4	2.6	164.1	8	1	2	40.6	40.1	78.2	4	4	2	28.3	30.2	133.1
10	23	1*	1.7	0.8	-99.6	9	1	2	26.0	24.3	55.7	5	4	2	37.8	36.6	-83.8
0	24	1*	2.2	2.1	-180.0	10	1	2	16.8	17.9	59.6	6	4	2	28.7	26.8	85.5
1	24	1	8.4	6.8	-30.0	11	1	2	13.1	13.5	174.6	7	4	2	17.4	16.6	74.2
2	24	1	4.4	4.4	96.7	12	1	2	8.3	7.5	-126.3	8	4	2	10.3	10.0	106.0
3	24	1*	1.8	1.9	-152.4	13	1	2	8.3	9.2	-53.0	9	4	2	6.7	5.7	-164.5
4	24	1	2.0	2.0	35.2	14	1	2	18.1	20.9	118.9	10	4	2	33.9	30.5	-91.0
5	24	1	3.2	3.5	51.4	15	1	2	3.6	3.0	-86.1	11	4	2	9.8	9.3	-164.0
6	24	1	2.8	2.4	148.3	16	1	2	4.5	5.2	-16.7	12	4	2	10.3	9.1	-21.1
7	24	1	3.2	2.9	112.2	17	1	2	4.1	3.1	-71.7	13	4	2*	2.9	2.3	-137.7
8	24	1*	1.6	1.8	-168.5	18	1	2*	2.9	2.8	-165.1	14	4	2*	3.4	3.5	130.8
9	24	1*	1.6	1.0	-142.3	19	1	2*	1.8	1.7	-174.1	15	4	2	4.3	6.0	57.8
0	25	1	10.6	10.2	-90.0	20	1	2	2.4	2.1	-131.7	16	4	2	4.0	3.5	-14.1
1	25	1	4.5	3.5	57.3	0	2	2	26.1	27.1	-180.0	17	4	2	4.3	4.0	179.3
2	25	1	3.1	4.1	-147.6	1	2	2	20.0	18.5	177.2	18	4	2	4.8	4.2	-142.7
3	25	1*	1.9	0.6	-120.9	2	2	2	9.3	7.6	-50.7	19	4	2*	1.8	1.5	-32.3
4	25	1	3.9	4.0	-128.7	3	2	2	59.1	63.5	-14.7	0	5	2	26.5	28.1	90.0
5	25	1*	1.9	2.4	-63.0	4	2	2	18.1	17.8	2.1	1	5	2	41.2	40.7	61.7
6	25	1	4.5	5.6	69.4	5	2	2	56.1	55.6	-143.0	2	5	2	23.8	23.6	146.6
7	25	1*	1.7	0.3	154.6	6	2	2	16.5	15.2	-76.7	3	5	2	41.3	42.0	128.7
8	25	1	3.7	3.7	109.7	7	2	2	26.3	25.4	-69.1	4	5	2	63.1	63.7	-156.3
0	26	1*	1.8	1.0	0.0	8	2	2	27.2	26.4	-81.3	5	5	2	30.9	30.0	-165.1
1	26	1	3.7	3.6	14.1	9	2	2	52.2	53.7	28.1	6	5	2	24.2	22.2	80.0
2	26	1	4.0	4.7	-132.9	10	2	2	4.7	6.0	64.6	7	5	2	25.4	24.4	-40.0
3	26	1	2.4	2.0	53.0	11	2	2	23.4	24.0	87.2	8	5	2	16.3	16.7	-7.7
4	26	1*	1.5	2.1	-63.1	12	2	2	11.6	11.8	-130.4	9	5	2	15.1	13.7	63.0
5	26	1*	1.5	1.3	2.5	13	2	2	14.4	14.8	99.9	10	5	2	15.4	15.2	-13.3
0	27	1*	1.5	1.5	90.0	14	2	2	7.3	7.8	105.2	11	5	2	11.5	12.1	10.3
0	0	2	69.3	77.7	0.0	15	2	2	7.1	6.8	-115.1	12	5	2	9.7	10.0	162.5
1	0	2	12.9	13.4	0.0	16	2	2*	3.6	1.9	138.6	13	5	2	10.8	10.6	-178.3
2	0	2	51.2	53.7	0.0	17	2	2*	2.9	2.8	-88.0	14	5	2	4.0	4.8	-122.9
3	0	2	15.4	17.6	0.0	18	2	2	4.4	3.0	-25.2	15	5	2	7.6	8.8	-57.7
4	0	2	38.1	34.9	0.0	19	2	2	3.5	3.6	-117.6	16	5	2*	2.3	1.9	-27.0
5	0	2	22.3	22.3	-180.0	0	3	2*	75.0	85.0	90.0	17	5	2*	2.3	1.8	-118.3
6	0	2	6.7	4.7	-180.0	1	3	2	45.9	47.4	-122.6	18	5	2	4.1	3.4	-25.9
7	0	2	19.8	19.1	0.0	2	3	2	27.6	28.4	-107.7	19	5	2	4.6	4.6	161.3
8	0	2	18.0	15.0	0.0	3	3	2	31.7	34.3	-153.6	0	6	2	29.0	30.4	0.0
9	0	2	10.4	12.4	0.0	4	3	2	27.5	30.7	-7.7	1	6	2	12.0	10.1	-59.5
10	0	2	39.7	39.7	-180.0	5	3	2	34.9	36.4	-139.7	2	6	2	16.6	17.0	-167.7

H	K	L	/FO/	/FC/	PHASE
3	6	2	32.2	31.2	160.0
4	6	2	8.2	8.3	17.3
5	6	2	27.0	26.6	97.2
6	6	2	29.6	28.2	-120.4
7	6	2	15.7	15.4	170.1
8	6	2	24.8	23.9	132.8
9	6	2	6.8	6.2	-54.7
10	6	2	16.7	16.5	-78.4
11	6	2	14.7	15.1	-65.5
12	6	2	11.9	12.7	32.0
13	6	2	4.4	3.5	93.9
14	6	2	4.0	3.8	130.9
15	6	2	3.6	2.2	-86.8
16	6	2*	2.2	2.5	-166.5
17	6	2*	2.6	0.8	172.1
18	6	2*	2.2	1.5	75.5
19	6	2*	1.0	1.0	91.9
0	7	2	31.2	30.2	90.0
1	7	2	24.0	22.6	-54.5
2	7	2	35.8	34.5	87.5
3	7	2	48.1	47.8	18.4
4	7	2	21.3	21.6	95.1
5	7	2	41.4	40.4	153.9
6	7	2	8.9	8.3	-134.1
7	7	2	11.5	10.6	140.0
8	7	2	31.0	30.3	-54.0
9	7	2	16.5	15.7	161.5
10	7	2	15.8	16.5	-172.1
11	7	2	5.4	5.1	-109.4
12	7	2	6.7	7.4	-37.5
13	7	2	7.7	7.3	-48.1
14	7	2	7.1	7.3	-120.3
15	7	2*	3.0	1.6	-130.1
16	7	2	4.3	4.2	144.7
17	7	2*	2.7	2.1	69.0
18	7	2	2.7	2.5	-172.9
19	7	2*	1.5	0.7	-114.8
0	8	2	38.0	38.5	-160.0
1	8	2	44.2	45.1	-155.8
2	8	2	6.8	6.8	19.2
3	8	2	19.0	18.1	99.2
4	8	2	45.5	48.8	101.7
5	8	2	10.9	9.1	9.2
6	8	2	24.7	23.7	-9.5
7	8	2	7.2	7.5	-115.6
8	8	2*	2.7	2.0	10.6
9	8	2	16.9	16.8	166.2
10	8	2	6.4	6.1	149.3
11	8	2*	3.2	1.6	137.9
12	8	2	5.2	5.7	-116.8
13	8	2	4.3	4.2	109.6
14	8	2*	3.1	2.3	131.4
15	8	2	3.7	2.8	-150.1
16	8	2*	3.2	2.8	-11.2
17	8	2	2.9	2.3	-49.3
18	8	2*	1.5	1.2	96.6
19	8	2*	1.2	0.7	-123.1
0	9	2	11.0	12.0	90.0
1	9	2	32.9	30.7	-24.8
2	9	2	25.1	23.2	-38.3
3	9	2	30.1	20.1	32.9
4	9	2	34.0	33.4	91.0
5	9	2	7.0	6.7	-142.2
6	9	2	26.1	25.2	-26.5
7	9	2	19.4	19.2	-64.5
8	9	2	13.3	13.1	168.2
9	9	2	18.0	16.3	-118.9
10	9	2	5.4	4.1	112.0
11	9	2	9.3	10.4	156.3
12	9	2	5.8	5.0	-91.4
13	9	2	4.8	4.1	99.8
14	9	2*	2.2	2.0	26.7
15	9	2	4.9	4.6	105.0
16	9	2*	2.1	1.3	-110.9
17	9	2*	2.6	2.1	-165.8
18	9	2*	1.7	1.3	134.6
0	10	2	20.3	18.8	-180.0
1	10	2	25.8	23.1	101.0
2	10	2	16.1	15.6	136.5
3	10	2	12.9	11.4	57.9
4	10	2	12.0	11.7	58.7
5	10	2	22.9	21.9	-131.4
6	10	2	11.9	10.3	85.2
7	10	2*	2.9	0.8	-9.4
8	10	2	6.6	4.7	-27.4
9	10	2	9.3	7.8	-80.1
10	10	2	9.9	8.4	-79.0
11	10	2	6.3	5.7	105.4
12	10	2	7.5	7.7	122.7
13	10	2	7.1	7.3	-53.2
14	10	2*	3.2	2.2	14.8
15	10	2	4.3	3.7	143.4
16	10	2*	2.5	1.8	61.5
17	10	2*	2.0	2.3	-14.4
18	10	2*	1.6	0.9	26.8
0	11	2	23.5	24.4	-90.0
1	11	2	12.5	12.2	-4.3
2	11	2	12.6	10.1	134.2
3	11	2	19.2	18.6	-66.8
4	11	2	9.8	9.8	179.1
5	11	2*	2.0	2.6	-175.1
6	11	2	4.5	3.3	-13.2
7	11	2	13.0	11.5	157.7
8	11	2	13.0	11.2	152.6
9	11	2	9.9	9.9	78.4
10	11	2	6.2	5.3	32.6
11	11	2*	2.4	1.6	-141.9
12	11	2	4.1	3.8	-122.0
13	11	2	5.1	5.4	-58.7
14	11	2*	3.2	1.9	35.5
15	11	2*	2.6	1.5	-104.5
16	11	2*	2.2	0.3	108.8
17	11	2*	2.1	1.7	92.2
18	11	2*	1.5	0.5	85.4
0	12	2	33.7	33.5	0.0
1	12	2	8.2	5.9	3.2
2	12	2	10.3	12.1	-3.5
3	12	2	15.4	15.0	-150.5
4	12	2	6.6	6.4	92.3
5	12	2	11.4	9.7	-39.9
6	12	2	22.8	21.4	119.1
7	12	2	4.7	3.9	146.5
8	12	2	8.8	7.9	-114.0
9	12	2	18.0	17.2	-147.2
10	12	2	9.6	9.5	172.3
11	12	2	11.1	10.7	96.8
12	12	2	7.0	6.5	-105.2
13	12	2	7.9	8.6	61.8
14	12	2	5.4	4.7	70.0
15	12	2*	2.4	1.9	-47.4
16	12	2*	1.8	1.3	-57.0
17	12	2*	1.5	0.9	29.7
0	13	2	27.1	27.7	-90.0
1	13	2	19.6	19.3	28.6
2	13	2	6.8	7.1	26.5
3	13	2	8.3	7.8	-109.9
4	13	2	4.1	3.4	-178.5
5	13	2	11.9	12.1	-162.4
6	13	2	12.4	12.2	-13.1
7	13	2	7.9	7.9	67.0
8	13	2	21.9	22.3	36.9
9	13	2	10.7	10.9	-31.3
10	13	2	8.2	8.2	0.4
11	13	2	9.0	9.8	-168.4
12	13	2*	3.5	3.1	-157.5
13	13	2	4.7	4.5	-8.2
14	13	2	8.5	8.2	-177.1
15	13	2	3.6	2.9	-64.9
16	13	2*	2.6	1.7	-127.7
17	13	2*	1.8	1.1	177.2
0	14	2	9.2	7.2	0.0
1	14	2	18.3	18.2	-85.4
2	14	2	5.4	5.5	-119.3
3	14	2	17.7	16.5	-48.2
4	14	2	19.1	18.2	176.2
5	14	2	14.0	12.6	13.7
6	14	2	9.2	8.1	-137.3
7	14	2	9.0	8.9	118.1
8	14	2	5.0	3.8	150.3
9	14	2	10.9	10.3	116.6
10	14	2	12.4	13.2	3.4
11	14	2	5.9	6.0	61.7
12	14	2	7.8	7.9	6.0
13	14	2	7.0	6.7	130.4
14	14	2*	2.5	1.3	31.5
15	14	2	2.9	2.9	-34.3
16	14	2*	1.8	1.0	164.8
17	14	2*	1.5	1.4	-27.0
0	15	2	15.6	14.9	-90.0
1	15	2	11.4	10.4	-135.8
2	15	2	5.6	4.7	151.9

H	K	L	/FO/	/FC/	PHASE
3	15	2	14.2	13.6	-158.5
4	15	2	18.4	19.0	84.8
5	15	2	4.7	3.8	-37.9
6	15	2*	2.9	2.3	-64.6
7	15	2	9.2	9.3	7.3
8	15	2	10.6	10.4	-66.4
9	15	2	17.0	17.2	-112.9
10	15	2	3.9	4.0	-43.6
11	15	2	14.7	14.8	-21.6
12	15	2*	2.1	1.0	158.9
13	15	2	7.1	6.6	95.1
14	15	2	5.8	5.1	-111.0
15	15	2	5.3	4.8	103.9
16	15	2	2.8	3.6	166.2
0	16	2	4.4	3.7	-180.0
1	16	2	13.9	14.5	156.1
2	16	2	14.9	14.5	-143.9
3	16	2	5.3	4.2	-142.5
4	16	2	14.5	14.4	95.3
5	16	2	19.3	19.3	-65.8
6	16	2	8.3	7.0	52.8
7	16	2	6.4	7.0	93.0
8	16	2	7.9	7.7	39.5
9	16	2	10.3	11.0	126.0
10	16	2	9.1	9.5	-85.5
11	16	2*	3.2	2.5	-129.4
12	16	2	6.7	6.3	56.4
13	16	2	6.0	4.8	-71.3
14	16	2	5.2	5.0	-41.2
15	16	2*	2.5	3.3	36.6
0	17	2	5.0	5.5	-90.0
1	17	2	23.6	25.1	93.9
2	17	2	13.3	13.1	-45.3
3	17	2	16.2	16.8	100.7
4	17	2	5.6	5.4	-48.3
5	17	2*	3.3	3.2	105.9
6	17	2	11.8	11.5	128.9
7	17	2	20.5	21.6	-65.4
8	17	2	8.2	9.0	132.0
9	17	2	12.7	12.1	-157.7
10	17	2*	2.8	2.7	-74.5
11	17	2	5.7	5.8	52.6
12	17	2	4.1	2.8	-23.3
13	17	2	3.4	3.0	177.7
14	17	2*	2.0	1.0	-5.5
15	17	2*	1.7	1.6	99.0
0	18	2*	3.4	3.5	0.0
1	18	2	16.8	16.8	-31.9
2	18	2	3.6	3.3	-174.5
3	18	2	10.3	10.7	48.6
4	18	2	10.2	10.9	-34.4
5	18	2	11.1	12.0	85.6
6	18	2	17.6	18.9	-98.4
7	18	2	10.8	13.1	-29.1
8	18	2	6.1	6.2	-178.3
9	18	2*	2.9	2.4	-134.3
10	18	2	6.9	6.2	89.9
11	18	2	6.5	5.5	-118.2
12	18	2*	2.4	1.2	80.5
13	18	2*	1.8	2.0	45.8
14	18	2*	2.4	2.3	-30.8
0	19	2*	3.0	2.6	90.0
1	19	2	14.0	15.4	-148.8
2	19	2*	3.5	2.8	-17.3
3	19	2	4.3	4.0	0.2
4	19	2	11.6	13.9	26.2
5	19	2	6.6	6.4	71.5
6	19	2	5.9	5.6	14.7
7	19	2	7.8	7.3	119.5
8	19	2	6.8	6.8	-61.0
9	19	2	4.0	3.6	50.7
10	19	2	9.2	8.8	-148.3
11	19	2*	1.7	0.5	73.7
12	19	2	4.7	4.0	141.8
13	19	2	3.3	3.4	-57.5
14	19	2*	1.8	1.4	4.7
0	20	2*	1.5	0.8	-180.0
1	20	2	4.3	4.7	-91.7
2	20	2	4.8	5.3	-9.8
3	20	2	7.7	8.8	-61.6
4	20	2	4.4	5.1	-132.0
5	20	2*	3.1	2.2	166.8
6	20	2*	2.7	2.1	-145.7
7	20	2	4.3	4.2	69.0
8	20	2*	2.4	0.2	-119.7
9	20	2*	2.3	0.8	95.7
10	20	2	3.7	3.5	11.9
11	20	2	4.1	4.1	131.1
12	20	2*	2.1	2.5	-95.0
13	20	2*	1.3	1.2	38.8
0	21	2*	3.0	2.2	90.0
1	21	2	8.8	8.2	-137.7
2	21	2	6.2	6.2	-46.6
3	21	2	7.8	8.6	-53.4
4	21	2	7.5	7.4	-58.6
5	21	2	6.8	7.0	-101.0
6	21	2	6.8	6.8	48.1
7	21	2*	2.5	2.1	-175.8
8	21	2	3.3	2.8	105.3
9	21	2	3.5	3.1	50.2
10	21	2	3.0	3.0	59.1
11	21	2*	1.9	1.4	116.2
12	21	2*	1.5	1.1	100.0
0	22	2*	3.2	0.6	-180.0
1	22	2	8.1	7.1	-4.7
2	22	2*	3.1	3.2	175.1
3	22	2	3.7	2.8	-157.3
4	22	2	9.7	8.8	-96.5
5	22	2	5.5	4.0	72.0
6	22	2	6.9	6.4	-71.3
7	22	2	3.9	3.7	144.0
8	22	2*	1.9	0.8	-10.6
9	22	2	3.1	2.7	-97.9
10	22	2*	1.7	0.3	89.3
11	22	2*	1.3	1.4	9.9
0	23	2	6.1	6.7	-90.0
1	23	2	5.5	4.8	101.4
2	23	2	8.5	8.1	120.7
3	23	2	3.3	2.5	-128.3
4	23	2	4.6	3.7	-142.5
5	23	2	4.6	4.1	-55.9
6	23	2*	2.1	1.2	107.7
7	23	2*	1.8	0.5	17.4
8	23	2*	2.0	2.3	70.4
9	23	2*	1.5	1.5	45.1
10	23	2*	1.5	1.7	-51.0
0	24	2*	2.0	0.2	-180.0
1	24	2	3.1	2.5	9.8
2	24	2*	1.9	0.5	156.0
3	24	2	5.6	5.5	175.1
4	24	2	2.8	2.5	-63.8
5	24	2	3.8	3.1	-175.5
6	24	2	2.6	2.3	35.7
7	24	2*	2.3	2.5	-117.1
8	24	2*	1.6	1.4	62.6
0	25	2	2.8	2.2	90.0
1	25	2*	2.4	1.5	84.8
2	25	2*	2.2	1.5	85.2
3	25	2	3.3	2.8	49.3
4	25	2*	2.3	2.1	-139.9
5	25	2*	1.7	0.7	101.1
6	25	2*	1.7	0.9	139.2
0	26	2*	2.2	1.5	-180.0
1	26	2*	1.6	1.2	-101.5
2	26	2*	0.8	2.2	78.4
3	26	2*	1.9	2.3	28.5
4	26	2*	1.5	1.4	162.7
1	0	3	24.2	25.6	90.0
2	0	3	10.5	11.2	-90.0
3	0	3	14.1	11.5	-90.0
4	0	3	57.3	57.9	-90.0
5	0	3	21.7	21.4	-90.0
6	0	3	17.3	16.4	-90.0
7	0	3	8.2	9.2	-90.0
8	0	3*	2.0	1.7	90.0
9	0	3	3.6	3.4	-90.0
10	0	3*	2.3	3.8	-90.0
11	0	3	6.7	7.0	90.0
12	0	3	13.6	13.8	-90.0
13	0	3	16.6	18.2	90.0
14	0	3*	1.7	0.3	90.0
15	0	3*	2.7	1.2	-90.0
16	0	3	3.4	3.0	90.0
17	0	3	3.4	1.9	-90.0
18	0	3*	1.8	2.0	-90.0
19	0	3	2.9	2.9	-90.0
0	1	3	29.1	31.1	-90.0
1	1	3	30.8	31.0	-23.6
2	1	3	43.9	43.8	-126.8
3	1	3	24.8	21.6	60.3
4	1	3	30.7	30.7	-170.4

H	K	L	/Fo/	/Fc/	PHASE
5	1	3	48.7	47.3	-132.7
6	1	3	28.7	28.3	103.6
7	1	3	5.5	6.0	39.7
8	1	3	9.3	10.5	-112.2
9	1	3	9.5	8.4	82.6
10	1	3	16.2	16.4	137.5
11	1	3	8.5	8.3	-126.3
12	1	3	14.8	14.7	71.8
13	1	3	5.4	5.8	-83.8
14	1	3	5.4	6.5	-14.5
15	1	3*	2.3	1.5	-22.1
16	1	3	3.7	3.9	-55.6
17	1	3	4.8	4.0	90.3
18	1	3	3.5	3.3	-146.2
19	1	3*	1.7	1.3	134.0
0	2	3*	2.8	0.3	-180.0
1	2	3	38.6	38.2	11.6
2	2	3	44.8	46.3	-32.3
3	2	3	37.3	35.8	52.6
4	2	3	48.0	48.0	162.2
5	2	3	33.2	32.0	19.4
6	2	3	11.3	8.3	-73.7
7	2	3	18.1	17.7	-77.4
8	2	3	10.8	9.2	-133.4
9	2	3	3.6	3.6	-127.1
10	2	3	11.9	11.1	-74.3
11	2	3	7.1	6.0	129.9
12	2	3	14.2	14.6	5.2
13	2	3*	3.6	3.6	-24.2
14	2	3	11.4	12.0	90.1
15	2	3	7.2	6.0	-69.7
16	2	3*	3.3	3.5	29.3
17	2	3	6.8	6.3	-152.6
18	2	3	3.6	3.4	-176.5
19	2	3	2.2	2.1	109.7
0	3	3	16.7	19.3	-90.0
1	3	3	8.4	8.0	-148.1
2	3	3	4.3	3.5	-84.7
3	3	3	41.9	41.4	119.2
4	3	3	22.4	20.1	-113.8
5	3	3	13.1	13.9	-144.2
6	3	3	12.9	12.1	175.4
7	3	3	15.4	14.3	74.2
8	3	3	3.6	2.7	70.0
9	3	3	9.8	8.7	1.2
10	3	3	8.6	8.4	40.9
11	3	3	10.5	9.5	-16.7
12	3	3	9.4	9.1	121.4
13	3	3	13.1	14.7	63.9
14	3	3	5.7	6.7	-118.5
15	3	3	6.8	6.9	-80.3
16	3	3*	2.6	1.9	144.3
17	3	3*	2.3	1.5	-36.8
18	3	3	4.1	4.2	47.7
19	3	3	3.8	4.0	-169.6
0	4	3	19.1	21.1	-180.0
1	4	3*	3.2	3.5	-162.1
2	4	3	19.0	16.4	161.7
3	4	3*	2.8	0.3	178.2
4	4	3	23.9	23.9	-46.4
5	4	3	20.4	19.2	81.2
6	4	3	15.0	13.4	-69.6
7	4	3	12.5	12.0	26.5
8	4	3	18.2	17.2	-155.2
9	4	3	20.9	19.9	-157.0
10	4	3	18.4	18.2	-51.3
11	4	3	18.4	19.6	-73.5
12	4	3	21.0	21.9	17.5
13	4	3	7.0	6.1	-55.2
14	4	3	5.3	6.1	142.9
15	4	3	6.8	7.1	102.3
16	4	3*	2.4	1.2	170.4
17	4	3	6.4	5.4	42.1
18	4	3	3.9	3.8	122.3
19	4	3*	1.0	0.5	-14.6
0	5	3	37.5	37.6	-90.0
1	5	3	40.6	40.1	112.5
2	5	3	33.9	32.9	179.7
3	5	3	21.0	20.3	56.0
4	5	3	33.1	33.4	95.3
5	5	3	9.2	9.0	168.6
6	5	3	10.7	10.2	-124.7
7	5	3	9.3	8.9	-11.4
8	5	3	9.7	9.3	31.5
9	5	3	15.1	15.6	156.1
10	5	3	13.3	13.8	-140.6
11	5	3	12.5	12.7	-28.1
12	5	3	14.4	14.8	-59.8
13	5	3	8.7	9.2	-67.4
14	5	3*	1.5	1.1	-146.3
15	5	3	3.5	2.7	13.7
16	5	3	4.3	4.1	67.9
17	5	3	4.5	4.3	122.7
18	5	3*	2.1	1.6	73.9
0	6	3	4.4	2.5	0.0
1	6	3	6.8	5.4	-158.0
2	6	3	27.6	25.7	51.2
3	6	3	7.8	6.1	158.2
4	6	3	22.0	18.6	43.4
5	6	3	24.9	25.7	30.1
6	6	3	22.3	19.2	-95.8
7	6	3	5.8	7.2	-126.4
8	6	3	13.8	14.0	86.1
9	6	3	12.8	13.0	136.1
10	6	3	5.3	5.5	-164.3
11	6	3	10.9	11.2	-52.9
12	6	3	12.4	11.7	161.2
13	6	3*	3.2	2.1	-133.3
14	6	3	8.0	8.5	-92.2
15	6	3	6.2	6.4	-93.0
16	6	3*	2.2	1.8	-10.4
17	6	3	4.2	3.8	5.9
18	6	3	2.9	3.7	50.1
0	7	3	58.9	60.1	-90.0
1	7	3	13.2	11.9	-114.1
2	7	3	49.5	48.8	2.6
3	7	3	7.5	8.6	62.0
4	7	3	26.2	25.2	25.4
5	7	3	10.6	10.3	157.7
6	7	3	13.7	13.0	12.2
7	7	3	3.7	3.8	-120.0
8	7	3	6.4	5.0	162.3
9	7	3	3.2	1.5	-86.4
10	7	3	5.2	5.7	81.8
11	7	3	8.0	7.6	58.3
12	7	3*	2.6	2.7	9.1
13	7	3*	2.8	2.8	29.5
14	7	3	3.9	3.4	-93.1
15	7	3	5.3	5.7	125.3
16	7	3*	2.1	1.7	166.5
17	7	3	2.5	2.2	-119.8
18	7	3*	1.5	1.4	149.3
0	8	3	27.4	26.9	-180.0
1	8	3	8.9	7.8	44.6
2	8	3	10.5	8.2	-100.1
3	8	3	19.4	16.4	-65.4
4	8	3	23.3	21.7	-40.4
5	8	3	28.8	28.3	-61.6
6	8	3*	2.8	0.7	-41.8
7	8	3	10.3	11.3	83.4
8	8	3	12.5	12.0	-77.9
9	8	3	15.6	15.9	-118.7
10	8	3	4.0	3.4	-135.2
11	8	3	14.6	14.3	107.2
12	8	3	11.0	11.6	169.9
13	8	3*	2.4	1.7	-55.2
14	8	3	5.3	5.1	36.4
15	8	3	6.4	6.4	60.3
16	8	3*	2.4	1.8	24.2
17	8	3*	2.4	1.7	96.5
18	8	3*	1.3	0.9	73.8
0	9	3*	4.2	3.8	90.0
1	9	3	17.3	18.0	141.2
2	9	3	9.1	9.4	73.7
3	9	3	20.9	19.3	-108.9
4	9	3	10.7	9.3	8.4
5	9	3	12.2	11.8	-36.5
6	9	3	15.4	14.8	7.1
7	9	3	8.6	8.0	-54.9
8	9	3	7.2	7.1	153.5
9	9	3	4.2	3.5	18.1
10	9	3	19.4	19.6	-22.0
11	9	3*	2.6	1.5	139.9
12	9	3	9.1	10.1	-175.9
13	9	3	6.6	7.5	-79.4
14	9	3	4.3	3.8	-56.2
15	9	3*	2.6	1.2	-37.6
16	9	3*	1.4	2.1	-83.5
17	9	3*	1.7	1.5	64.4
18	9	3*	1.0	1.5	95.6
0	10	3	11.4	12.0	0.0

H	K	L	/Fo/	/Fc/	PHASE
1	10	3	19.6	17.0	-59.9
2	10	3	10.1	8.7	-108.2
3	10	3	6.8	5.6	-114.1
4	10	3	6.0	4.8	-85.0
5	10	3	6.5	5.2	-109.0
6	10	3	13.5	13.6	-166.2
7	10	3	8.9	8.3	-176.3
8	10	3	5.9	5.7	-159.9
9	10	3	13.7	13.0	169.5
10	10	3	4.2	3.7	103.3
11	10	3	15.2	16.2	90.2
12	10	3	4.1	5.0	23.8
13	10	3*	2.7	2.8	33.9
14	10	3	3.3	2.3	55.0
15	10	3	6.7	6.0	-8.7
16	10	3*	2.3	1.2	157.7
17	10	3*	1.8	0.9	-75.7
0	11	3	4.5	4.6	-90.0
1	11	3	7.9	8.4	-73.0
2	11	3	20.2	18.7	105.0
3	11	3	13.3	11.4	-97.5
4	11	3	5.6	6.0	98.6
5	11	3	6.9	6.3	-115.8
6	11	3	11.9	11.4	9.6
7	11	3	6.5	6.7	-5.2
8	11	3	8.3	8.2	-17.6
9	11	3	6.9	6.7	-45.4
10	11	3	10.8	11.2	-88.1
11	11	3	5.6	5.7	-166.4
12	11	3	4.2	4.8	-46.0
13	11	3	5.8	5.6	147.4
14	11	3	5.4	5.1	-145.0
15	11	3	3.1	3.0	-87.6
16	11	3*	2.2	2.0	102.2
17	11	3*	2.1	1.5	152.2
0	12	3	8.8	8.6	-180.0
1	12	3	20.4	19.5	-105.8
2	12	3	11.7	11.3	-153.8
3	12	3	19.2	17.6	-168.3
4	12	3	17.3	17.2	143.9
5	12	3	4.6	3.8	-57.7
6	12	3	4.4	3.1	16.8
7	12	3	11.4	11.7	153.0
8	12	3	9.6	9.3	113.5
9	12	3	14.5	15.1	98.9
10	12	3	8.6	8.7	47.1
11	12	3	6.1	6.7	-80.2
12	12	3	8.9	8.5	-15.1
13	12	3	6.5	6.9	103.5
14	12	3	5.2	4.9	-80.6
15	12	3	5.1	5.0	20.7
16	12	3*	1.7	1.2	-44.5
17	12	3*	1.9	1.7	-6.4
0	13	3	25.9	25.6	-90.0
1	13	3	11.4	11.2	11.8
2	13	3	17.6	17.1	153.3
3	13	3	10.7	9.2	62.1
4	13	3	9.3	7.3	132.3
5	13	3	15.1	14.5	-68.1
6	13	3	12.5	12.1	140.7
7	13	3	8.1	8.1	-102.1
8	13	3	9.6	9.3	-24.6
9	13	3	11.6	10.8	-140.7
10	13	3	5.5	6.1	169.9
11	13	3*	3.5	3.4	-82.2
12	13	3*	2.9	3.0	31.0
13	13	3	5.5	4.6	-171.5
14	13	3*	2.3	2.6	-123.2
15	13	3	3.3	3.0	135.9
16	13	3	2.0	0.9	140.6
0	14	3	5.8	5.3	0.0
1	14	3	12.4	11.1	51.2
2	14	3	11.3	10.4	-81.6
3	14	3	4.7	3.9	116.3
4	14	3	16.6	16.5	-138.5
5	14	3	11.4	11.7	55.9
6	14	3	9.8	9.6	95.4
7	14	3	7.1	7.3	-82.2
8	14	3	7.7	7.6	52.0
9	14	3	4.1	4.4	128.4
10	14	3*	3.2	3.2	118.3
11	14	3*	3.6	3.4	-78.4
12	14	3*	3.2	1.9	-32.1
13	14	3	5.2	4.7	-111.2
14	14	3*	1.6	1.4	-30.3
15	14	3*	1.3	1.6	-81.2
16	14	3*	0.7	0.3	142.8
0	15	3	17.4	17.4	90.0
1	15	3	8.7	8.0	143.1
2	15	3	25.8	25.2	-3.8
3	15	3	15.3	15.8	140.1
4	15	3	10.9	11.2	-27.6
5	15	3	24.1	25.0	55.8
6	15	3	14.0	13.8	-179.6
7	15	3*	2.7	2.2	17.6
8	15	3	5.2	5.6	138.2
9	15	3	3.7	3.5	-40.9
10	15	3	4.4	3.8	-100.0
11	15	3	4.5	4.0	-25.7
12	15	3	3.2	2.5	-169.0
13	15	3*	2.7	3.3	146.7
14	15	3*	1.6	1.2	-87.4
15	15	3*	1.9	2.3	173.2
0	16	3	6.6	6.6	-180.0
1	16	3	9.5	10.5	39.2
2	16	3	16.2	16.1	142.0
3	16	3	6.8	6.8	-86.9
4	16	3	19.1	19.1	-10.6
5	16	3	20.0	20.6	-174.6
6	16	3	7.8	7.8	-54.8
7	16	3	6.7	7.3	81.7
8	16	3	4.3	3.6	175.3
9	16	3	5.6	5.6	155.6
10	16	3	5.4	4.0	91.3
11	16	3	7.2	5.6	-96.2
12	16	3	3.2	3.2	84.4
13	16	3	5.7	5.4	-8.7
14	16	3	2.7	1.7	-76.0
15	16	3*	1.3	0.9	116.0
0	17	3	16.8	17.8	90.0
1	17	3	9.5	9.8	153.2
2	17	3	9.1	8.8	134.6
3	17	3	12.7	12.8	-11.3
4	17	3	5.0	5.2	-69.6
5	17	3	8.2	8.8	4.9
6	17	3*	2.5	1.5	17.0
7	17	3*	3.4	3.3	88.8
8	17	3*	3.0	2.3	-134.4
9	17	3	6.8	5.8	135.5
10	17	3	9.8	9.2	-139.0
11	17	3	7.4	7.0	124.7
12	17	3*	2.0	1.3	-60.1
13	17	3	2.7	2.6	-120.9
14	17	3*	1.3	2.2	-5.7
0	18	3	17.8	20.1	0.0
1	18	3	6.3	6.6	27.8
2	18	3	19.4	20.0	32.8
3	18	3	5.9	5.6	178.5
4	18	3	8.8	9.6	-179.4
5	18	3	7.3	7.1	146.1
6	18	3*	2.5	2.6	92.6
7	18	3*	2.7	1.4	-38.7
8	18	3	5.5	5.5	82.3
9	18	3	7.2	6.2	-50.5
10	18	3	8.0	6.5	129.3
11	18	3*	1.6	0.8	-161.9
12	18	3	5.6	6.7	-171.4
13	18	3*	1.6	0.6	168.4
0	19	3*	3.1	2.3	-90.0
1	19	3	14.3	17.1	-89.7
2	19	3	9.9	12.1	-11.7
3	19	3	6.2	7.0	-4.0
4	19	3	5.6	5.2	-8.6
5	19	3*	3.7	3.1	39.2
6	19	3	5.8	4.9	32.5
7	19	3	9.9	10.4	130.2
8	19	3	4.8	4.5	-85.1
9	19	3	7.2	6.5	76.4
10	19	3	8.0	8.1	10.6
11	19	3	4.3	3.7	-172.9
12	19	3*	2.4	3.2	148.0
0	20	3	9.1	9.7	-180.0
1	20	3	6.1	5.5	-156.3
2	20	3	5.0	4.6	-37.8
3	20	3	4.4	4.2	-76.9
4	20	3	7.2	7.3	-70.7
5	20	3	6.5	7.3	-35.0
6	20	3	5.4	4.5	52.9
7	20	3	5.4	4.9	102.3
8	20	3*	2.8	1.9	102.6
9	20	3	4.8	5.0	-12.3

H	K	L	/FO/	/FC/	PHASE	H	K	L	/FO/	/FC/	PHASE	H	K	L	/FO/	/FC/	PHASE
10	20	3*	2.4	1.6	161.7	11	0	4	9.9	9.8	-180.0	11	3	4	8.9	8.2	17.8
11	20	3	3.9	4.6	80.8	12	0	4	7.6	7.5	0.0	12	3	4	4.0	4.2	-132.8
12	20	3*	1.2	0.5	-60.1	13	0	4	8.5	9.9	0.0	13	3	4	4.4	4.9	29.5
0	21	3*	3.8	3.2	90.0	14	0	4	6.0	5.7	-180.0	14	3	4	8.5	8.6	-160.7
1	21	3*	3.0	1.4	119.3	15	0	4	2.9	2.2	0.0	15	3	4*	2.7	2.0	21.6
2	21	3	8.2	8.0	171.1	16	0	4	4.7	4.0	-180.0	16	3	4*	2.1	0.7	145.0
3	21	3*	2.5	2.2	-151.0	17	0	4*	1.6	1.2	-180.0	17	3	4*	2.0	1.8	79.8
4	21	3	7.6	6.8	-144.6	18	0	4*	1.6	0.2	0.0	18	3	4	2.4	2.8	35.9
5	21	3	4.1	3.9	-112.1	0	1	4	27.4	26.1	-90.0	0	4	4	22.5	20.1	-180.0
6	21	3	4.1	3.7	-54.1	1	1	4	15.0	14.7	-22.6	1	4	4	18.0	16.9	85.3
7	21	3*	2.2	0.8	-95.0	2	1	4	27.6	26.1	-91.1	2	4	4	14.8	14.4	-168.5
8	21	3	3.0	3.1	28.9	3	1	4	29.0	26.7	140.5	3	4	4	20.1	20.4	112.9
9	21	3	4.0	3.5	-28.1	4	1	4	10.5	10.3	-34.3	4	4	4	19.5	17.2	-9.4
10	21	3*	1.8	2.1	34.7	5	1	4	9.9	10.8	-125.9	5	4	4	5.9	5.5	2.9
11	21	3*	1.4	0.8	-15.4	6	1	4	18.6	17.4	153.4	6	4	4	8.5	8.0	20.3
0	22	3	4.8	3.5	0.0	7	1	4	8.1	6.6	32.7	7	4	4	7.3	6.7	40.9
1	22	3*	3.2	2.3	-152.1	8	1	4	6.8	6.8	97.4	8	4	4	14.9	14.4	77.7
2	22	3*	2.2	0.5	-30.9	9	1	4	16.4	16.9	40.5	9	4	4	12.6	12.1	-161.2
3	22	3	3.0	2.8	-150.9	10	1	4	11.8	12.6	77.3	10	4	4	7.4	7.3	-64.5
4	22	3*	2.8	2.4	-105.9	11	1	4	7.8	8.9	-126.9	11	4	4	13.7	14.5	-100.9
5	22	3*	2.5	2.0	121.8	12	1	4	9.2	8.6	33.7	12	4	4	5.8	7.5	131.3
6	22	3*	2.0	0.6	-55.1	13	1	4	4.7	4.6	-123.3	13	4	4	6.1	6.5	-135.5
7	22	3*	2.0	1.9	-93.7	14	1	4	4.0	3.6	179.6	14	4	4	6.0	6.5	-118.6
8	22	3*	1.5	1.0	-54.6	15	1	4	4.3	3.9	-85.6	15	4	4*	2.9	2.7	101.7
9	22	3*	1.5	1.5	44.6	16	1	4*	2.8	1.7	168.4	16	4	4*	2.3	1.3	-88.5
0	23	3*	2.6	0.4	90.0	17	1	4*	2.4	2.1	-10.0	17	4	4*	2.1	2.2	5.9
1	23	3	3.7	3.1	99.9	18	1	4*	1.0	0.8	125.9	0	5	4	34.0	31.3	-90.0
2	23	3*	1.5	1.7	67.7	0	2	4	43.9	26.8	-180.0	1	5	4	4.4	5.1	118.3
3	23	3	3.1	2.7	139.3	1	2	4	17.8	16.7	-15.6	2	5	4	25.4	24.5	76.9
4	23	3*	2.6	1.9	178.2	2	2	4	16.3	16.6	64.8	3	5	4	3.0	2.2	96.4
5	23	3*	1.7	0.7	-110.1	3	2	4	32.0	29.0	-1.1	4	5	4	25.3	22.5	-156.0
6	23	3	2.4	1.8	-91.8	4	2	4	32.9	30.3	-75.8	5	5	4	19.8	18.3	95.7
7	23	3*	1.8	2.2	-32.3	5	2	4	8.5	2.3	98.5	6	5	4	12.9	12.4	117.3
8	23	3*	1.1	2.2	-41.7	6	2	4	4.7	4.8	24.3	7	5	4	17.0	16.4	7.5
0	24	3	4.3	4.7	-180.0	7	2	4	4.5	4.8	58.0	8	5	4	14.1	12.5	139.6
1	24	3	2.5	1.9	-122.0	8	2	4	15.4	13.5	171.5	9	5	4	7.4	8.0	123.7
2	24	3*	1.5	1.8	164.0	9	2	4	22.9	24.1	81.0	10	5	4	10.8	10.8	-117.9
3	24	3	3.5	3.6	132.7	10	2	4	9.2	9.2	-177.9	11	5	4	3.6	3.2	6.8
4	24	3*	2.3	1.9	91.0	11	2	4	10.9	11.7	-96.7	12	5	4	5.2	5.0	-99.1
5	24	3	2.8	2.5	-132.2	12	2	4*	3.2	4.8	-36.4	13	5	4	8.3	8.2	-152.8
6	24	3*	1.9	1.8	-171.2	13	2	4	6.7	7.0	-112.3	14	5	4	3.8	3.5	-34.6
0	25	3*	1.8	0.6	-90.0	14	2	4*	3.1	2.7	67.7	15	5	4	3.2	2.7	172.2
1	25	3*	2.2	1.8	31.0	15	2	4*	2.9	3.2	129.3	16	5	4*	1.8	0.8	143.6
2	25	3*	0.9	1.3	125.8	16	2	4	4.9	4.4	-36.2	17	5	4	3.1	3.7	-133.3
3	25	3*	1.6	1.2	-48.8	17	2	4*	2.0	2.2	38.9	0	6	4	25.7	23.5	0.0
4	25	3*	1.0	1.1	-175.9	18	2	4*	1.4	1.3	142.5	1	6	4	32.4	32.5	46.0
0	0	4	19.7	19.3	-180.0	0	3	4	12.8	12.8	-90.0	2	6	4	15.2	14.4	-23.8
1	0	4	4.4	3.8	-180.0	1	3	4	37.2	34.2	158.8	3	6	4	13.7	13.1	-167.4
2	0	4	27.0	25.9	0.0	2	3	4	20.3	17.9	-22.2	4	6	4	11.4	9.1	-21.4
3	0	4	8.3	9.1	0.0	3	3	4	9.9	9.5	133.4	5	6	4	24.1	22.9	-49.9
4	0	4	14.2	13.6	-180.0	4	3	4	16.7	14.6	79.3	6	6	4*	3.4	3.2	-13.9
5	0	4	28.4	29.5	0.0	5	3	4	19.4	20.8	-64.3	7	6	4	8.5	7.8	129.4
6	0	4	28.5	28.1	-180.0	6	3	4	13.8	12.5	-171.5	8	6	4*	3.2	2.5	78.7
7	0	4	7.0	5.9	0.0	7	3	4	7.4	8.3	-139.2	9	6	4	4.4	3.8	-112.3
8	0	4	5.3	4.7	0.0	8	3	4	9.7	9.7	77.2	10	6	4	17.4	18.0	158.5
9	0	4	15.7	16.9	-180.0	9	3	4	5.7	5.0	-62.4	11	6	4	6.4	7.5	78.8
10	0	4	8.2	10.3	0.0	10	3	4	5.1	4.2	-75.7	12	6	4	11.1	11.4	167.5

H	K	L	/FO/	/FC/	PHASE	H	K	L	/FO/	/FC/	PHASE	H	K	L	/FO/	/FC/	PHASE
13	6	4*	3.5	2.1	133.9	10	9	4*	2.1	1.6	158.3	6	13	4*	3.8	3.4	-167.7
14	6	4	2.2	2.6	-53.3	0	10	4	4.5	2.6	0.0	7	13	4	6.1	6.4	-29.6
15	6	4	5.0	4.0	-35.9	1	10	4	5.0	5.1	-180.0	8	13	4	8.1	6.9	-9.0
16	6	4*	2.5	2.6	20.6	2	10	4	3.6	3.6	-39.6	9	13	4	10.2	10.2	-18.7
17	6	4	2.5	2.7	-162.9	3	10	4	5.0	4.0	90.8	10	13	4*	2.9	2.0	-119.0
0	7	4	10.8	9.2	0.0	4	10	4	23.2	22.3	-123.6	11	13	4	5.2	5.0	-163.0
1	7	4*	2.1	1.8	-90.0	5	10	4	12.4	11.7	-163.0	12	13	4*	2.2	1.9	104.2
2	7	4	18.7	19.5	67.2	6	10	4	5.4	5.5	2.3	13	13	4*	1.5	1.1	-46.4
3	7	4	5.7	3.4	43.0	7	10	4*	2.8	2.7	-164.2	14	13	4*	1.8	1.0	44.6
4	7	4	8.1	5.6	-6.1	8	10	4*	1.3	1.8	81.9	15	13	4	2.6	2.6	98.8
5	7	4	13.8	13.0	42.2	9	10	4	8.7	9.1	25.2	0	14	4	4.4	3.8	-180.0
6	7	4	5.6	5.8	-39.9	10	10	4	6.6	6.8	105.2	1	14	4	8.8	9.2	37.0
7	7	4	15.3	16.0	88.4	11	10	4	4.2	3.2	-48.9	2	14	4	5.0	4.7	164.3
8	7	4	5.4	4.5	-108.3	12	10	4	5.8	6.2	22.1	3	14	4	15.9	15.0	-66.6
9	7	4	6.3	6.0	64.5	13	10	4*	2.8	1.9	111.4	4	14	4	10.7	10.6	-120.6
10	7	4	11.4	12.6	-10.3	14	10	4*	2.4	1.9	-63.9	5	14	4	21.7	23.0	-152.9
11	7	4	10.6	11.0	174.3	15	10	4*	1.8	0.9	24.4	6	14	4*	2.4	1.9	160.7
12	7	4	9.9	10.0	176.7	16	10	4*	1.6	0.8	46.5	7	14	4	6.6	6.3	93.2
13	7	4	5.3	5.0	-142.4	0	11	4	4.0	2.9	90.0	8	14	4	6.1	6.1	-42.8
14	7	4	5.2	6.1	-137.3	1	11	4	10.1	9.5	143.7	9	14	4	6.3	5.7	59.8
15	7	4	4.8	4.8	-104.7	2	11	4*	3.6	2.8	-35.9	10	14	4*	3.3	2.6	31.5
16	7	4	2.7	2.0	-62.5	3	11	4	20.5	19.2	107.0	11	14	4	5.2	4.7	41.8
17	7	4	2.7	2.1	-21.0	4	11	4	10.8	11.4	-174.7	12	14	4*	1.6	1.0	-156.6
0	8	4	16.2	17.8	0.0	5	11	4	19.4	20.1	44.2	13	14	4*	1.9	1.1	-7.9
1	8	4	14.8	14.8	-118.4	6	11	4	6.4	6.3	45.6	14	14	4*	2.2	2.7	18.3
2	8	4	16.5	14.6	-30.9	7	11	4	8.5	9.3	-141.6	0	15	4	26.9	27.1	90.0
3	8	4	15.5	14.0	-53.7	8	11	4	13.6	14.3	-34.9	1	15	4	15.7	16.2	174.3
4	8	4	7.9	9.9	147.1	9	11	4	5.1	5.6	-63.7	2	15	4	16.1	16.4	16.6
5	8	4*	2.7	1.9	-164.8	10	11	4*	3.4	3.3	105.2	3	15	4	11.0	11.3	-62.4
6	8	4	4.0	4.1	88.2	11	11	4	5.8	6.1	-26.7	4	15	4	6.4	5.7	47.7
7	8	4	6.3	5.9	141.3	12	11	4*	2.7	0.9	93.7	5	15	4	8.3	8.2	-76.0
8	8	4	11.5	11.3	169.1	13	11	4*	2.7	0.4	-139.5	6	15	4	10.4	11.7	-49.5
9	8	4*	3.1	3.7	158.8	14	11	4	3.8	3.2	142.6	7	15	4*	3.6	3.1	-60.1
10	8	4	9.9	10.4	68.9	15	11	4*	2.3	1.6	150.3	8	15	4	7.4	7.4	-124.9
11	8	4	16.1	17.2	90.3	16	11	4*	1.1	1.3	87.3	9	15	4	4.9	4.5	-110.2
12	8	4	4.8	4.3	0.3	0	12	4	7.8	7.8	0.0	10	15	4*	2.6	1.9	-70.2
13	8	4	3.8	3.6	126.7	1	12	4	20.9	20.4	-108.3	11	15	4	5.1	4.7	20.1
14	8	4	4.0	3.6	161.1	2	12	4	4.6	3.6	-117.6	12	15	4*	2.5	2.6	-133.0
15	8	4*	1.7	0.8	-43.7	3	12	4	27.0	28.7	-155.4	13	15	4*	1.7	2.4	20.2
16	8	4*	1.9	1.9	-137.7	4	12	4	10.1	10.1	-98.7	14	15	4*	1.2	0.7	-83.7
17	8	4*	2.0	2.0	-79.4	5	12	4	12.6	12.3	105.7	0	16	4	4.4	3.7	-180.0
0	9	4	5.8	5.8	90.0	6	12	4	8.0	7.7	131.4	1	16	4	6.6	7.5	-169.5
1	9	4	12.9	12.6	-68.3	7	12	4	6.3	5.8	66.0	2	16	4	10.7	10.7	166.8
2	9	4	17.3	15.8	-150.7	8	12	4	5.8	6.1	-26.0	3	16	4	10.3	11.6	130.8
3	9	4	8.9	8.0	-29.9	9	12	4	4.0	3.7	110.2	4	16	4	9.8	10.7	104.1
4	9	4	10.8	10.6	7.1	10	12	4	5.2	4.8	107.8	5	16	4	5.0	5.6	-134.1
5	9	4	17.4	15.8	-40.9	11	12	4	4.5	4.5	-152.0	6	16	4*	3.6	2.9	-22.6
6	9	4	13.8	12.7	-6.4	12	12	4	3.1	3.3	-131.2	7	16	4*	2.7	0.8	143.9
7	9	4	4.3	2.9	138.1	13	12	4	4.9	4.5	37.7	8	16	4	5.5	5.1	67.8
8	9	4*	2.8	0.2	82.9	14	12	4*	2.0	1.5	4.4	9	16	4*	3.1	3.1	-94.7
9	9	4	3.9	3.3	-74.7	15	12	4*	1.9	1.7	33.9	10	16	4	5.5	6.2	-43.8
10	9	4	5.0	5.0	-1.3	0	13	4	3.9	4.4	90.0	11	16	4*	2.2	2.2	178.1
11	9	4	5.9	6.0	144.6	1	13	4	11.2	10.7	-81.0	12	16	4	3.0	3.2	82.1
12	9	4*	3.1	2.7	96.9	2	13	4	19.0	18.0	6.7	13	16	4*	1.7	1.7	-17.7
13	9	4	8.9	9.6	147.2	3	13	4	19.2	19.3	-158.9	0	17	4	4.4	4.8	90.0
14	9	4	3.3	2.4	151.0	4	13	4	14.1	14.8	-14.7	1	17	4	7.3	7.7	-74.4
15	9	4*	2.5	2.1	-120.6	5	13	4	8.9	9.2	61.4	2	17	4	7.6	8.2	161.4

H	K	L	/FO/	/FC/	PHASE
3	17	4	9.5	10.3	-44.2
4	17	4	6.8	7.0	-132.7
5	17	4	7.2	7.5	-154.9
6	17	4*	1.7	0.1	-176.4
7	17	4*	2.9	2.2	81.1
8	17	4	4.0	3.9	-163.4
9	17	4*	1.8	1.1	78.7
10	17	4	2.9	2.8	-36.4
11	17	4*	2.5	2.1	-151.7
12	17	4	1.6	1.2	-55.8
0	18	4*	2.6	0.1	-180.0
1	18	4	5.3	5.9	149.9
2	18	4	5.2	5.6	20.7
3	18	4*	2.8	0.3	39.3
4	18	4	7.3	7.0	-125.5
5	18	4	4.2	3.3	-0.7
6	18	4	4.2	3.3	-91.0
7	18	4*	2.5	0.9	51.2
8	18	4*	2.5	1.1	10.1
9	18	4	5.5	5.9	-19.5
10	18	4	2.9	3.0	150.7
11	18	4*	2.0	1.8	45.3
12	18	4*	1.5	1.9	-102.8
0	19	4	4.3	4.6	90.0
1	19	4	5.5	5.0	39.7
2	19	4	7.0	6.4	-176.4
3	19	4	6.4	6.6	111.7
4	19	4	6.8	6.9	137.0
5	19	4	5.0	4.5	-150.0
6	19	4*	3.0	3.1	-71.3
7	19	4	3.7	3.2	-159.2
8	19	4	6.1	6.0	-51.4
9	19	4*	1.8	1.8	-53.5
10	19	4*	2.2	2.2	22.6
11	19	4*	1.4	0.5	-122.9
0	20	4*	2.9	1.0	0.0
1	20	4	6.1	6.0	-130.5
2	20	4*	2.8	1.7	-77.6
3	20	4*	2.9	2.0	8.4
4	20	4	3.6	3.8	50.0
5	20	4	6.4	6.5	101.1
6	20	4*	2.3	1.8	95.7
7	20	4*	2.6	2.2	-141.7
8	20	4	5.4	6.3	-149.7
9	20	4	3.2	4.0	-13.6
10	20	4	3.2	3.4	-50.3
0	21	4*	1.6	1.2	-90.0
1	21	4	4.2	4.0	75.8
2	21	4	3.8	2.7	-136.9
3	21	4*	2.5	0.8	-78.2
4	21	4	4.9	4.3	-54.0
5	21	4*	2.5	2.5	-66.0
6	21	4	2.8	3.0	0.6
7	21	4	3.2	2.8	159.6
8	21	4*	2.0	2.8	83.0
9	21	4	2.5	4.2	-143.3
0	22	4	2.9	1.7	-180.0
1	22	4*	2.6	2.0	48.1
2	22	4	3.4	3.5	129.9
3	22	4	4.1	3.9	127.0
4	22	4*	1.5	0.4	117.3
5	22	4*	2.1	2.2	-48.2
6	22	4	2.6	4.1	-127.8
7	22	4	2.0	1.7	-64.1
0	23	4	3.5	4.7	-90.0
1	23	4*	2.2	3.4	93.3
2	23	4*	2.4	2.9	72.7
3	23	4	2.9	2.5	124.0
4	23	4*	1.3	0.8	175.3
5	23	4*	1.6	2.0	95.8
0	24	4*	1.5	1.4	0.0
1	24	4	2.8	3.3	-76.2
2	24	4*	1.5	2.1	28.1
1	0	5	4.6	4.8	90.0
2	0	5	10.3	10.6	-90.0
3	0	5	20.4	20.5	-90.0
4	0	5*	3.0	1.1	-90.0
5	0	5	12.0	13.0	-90.0
6	0	5	35.9	37.1	90.0
7	0	5*	3.5	3.4	90.0
8	0	5	14.4	15.0	90.0
9	0	5	15.5	17.4	90.0
10	0	5	5.5	5.5	-90.0
11	0	5*	3.7	5.3	-90.0
12	0	5	4.9	5.8	-90.0
13	0	5*	1.8	0.2	-90.0
14	0	5*	2.1	0.9	-90.0
15	0	5	3.4	3.5	90.0
16	0	5	3.1	2.7	-90.0
0	1	5	10.9	11.8	-90.0
1	1	5	4.3	4.9	-32.8
2	1	5	9.0	7.1	-95.2
3	1	5	12.9	12.2	111.2
4	1	5	17.7	16.8	-90.3
5	1	5	8.9	9.3	-91.6
6	1	5	11.0	9.4	138.8
7	1	5	12.3	11.7	-83.4
8	1	5	11.8	11.6	72.9
9	1	5	13.5	13.1	-30.1
10	1	5	6.8	7.4	57.2
11	1	5	4.6	4.5	125.0
12	1	5*	3.1	2.2	26.1
13	1	5	3.7	3.6	-163.8
14	1	5*	2.5	2.1	-155.8
15	1	5*	2.3	1.8	-82.3
16	1	5*	2.0	1.8	56.4
0	2	5	16.2	15.5	-180.0
1	2	5	12.0	13.7	-20.2
2	2	5	12.7	12.1	178.3
3	2	5	11.2	10.9	88.5
4	2	5	22.6	21.0	-128.0
5	2	5	6.9	7.2	14.2
6	2	5	22.1	21.8	-30.7
7	2	5	5.5	4.9	12.7
8	2	5	8.0	6.2	-17.8
9	2	5	8.2	8.7	-55.0
10	2	5	7.0	6.5	112.1
11	2	5*	2.8	1.8	-35.8
12	2	5	5.0	5.3	94.8
13	2	5*	2.4	1.7	148.3
14	2	5	4.2	3.2	27.3
15	2	5*	2.0	1.9	131.6
16	2	5	3.2	3.9	10.3
0	3	5	16.9	17.7	-90.0
1	3	5	23.9	21.9	-133.5
2	3	5	20.2	18.4	78.4
3	3	5	9.7	9.8	-105.8
4	3	5	18.3	16.2	158.4
5	3	5	14.0	13.8	61.9
6	3	5	13.0	11.6	-86.6
7	3	5	11.2	10.8	-7.2
8	3	5	7.8	8.0	-111.7
9	3	5	4.7	5.8	-89.5
10	3	5	7.0	7.6	-44.6
11	3	5	4.5	3.6	-31.4
12	3	5*	3.2	2.6	-173.8
13	3	5*	2.5	1.0	-168.0
14	3	5*	2.4	0.5	20.6
15	3	5*	2.0	1.6	83.1
16	3	5*	1.8	0.4	121.0
0	4	5*	1.2	0.0	0.0
1	4	5	19.7	18.7	89.8
2	4	5	15.4	15.5	-133.5
3	4	5	15.9	15.7	176.9
4	4	5	5.1	4.5	148.9
5	4	5	14.3	14.3	-83.0
6	4	5	7.8	7.7	-148.9
7	4	5	8.9	9.5	-19.2
8	4	5	7.1	7.1	0.4
9	4	5	4.5	4.6	-95.9
10	4	5*	3.5	4.3	-76.0
11	4	5	4.5	4.9	78.4
12	4	5	7.0	6.2	58.4
13	4	5*	3.2	1.9	22.7
14	4	5	3.3	2.9	8.8
15	4	5*	1.8	2.3	-47.3
16	4	5*	1.7	1.7	92.7
0	5	5	4.5	3.8	90.0
1	5	5	7.1	5.9	-154.0
2	5	5	11.2	10.5	141.3
3	5	5	9.3	8.5	-74.8
4	5	5	6.1	5.3	-165.0
5	5	5*	1.9	0.4	59.8
6	5	5	8.6	8.7	-79.4
7	5	5	6.3	7.4	-50.6
8	5	5	6.0	5.4	-114.8
9	5	5	3.7	4.2	-134.8
10	5	5	4.1	4.1	-122.1
11	5	5*	3.2	3.2	-91.1
12	5	5*	2.0	1.3	-65.0
13	5	5*	2.7	2.6	154.3
14	5	5*	2.3	2.1	113.4
15	5	5*	2.1	1.0	104.8
16	5	5*	1.8	0.5	68.4
0	6	5	9.6	11.1	0.0
1	6	5	24.9	22.5	136.0
2	6	5	4.6	3.9	-0.7
3	6	5	6.6	6.1	62.0
4	6	5	9.8	9.4	-179.4
5	6	5*	2.9	1.6	-24.5
6	6	5	12.9	11.9	-105.8
7	6	5	7.6	7.2	-149.5
8	6	5	4.2	3.7	176.1
9	6	5	6.1	7.0	-63.4
10	6	5	6.5	6.6	60.0
11	6	5	4.2	3.6	-37.1
12	6	5*	3.4	2.5	-51.9
13	6	5*	2.9	2.7	10.3
14	6	5	2.8	2.1	1.8
15	6	5*	2.2	1.6	-68.6
16	6	5*	1.4	0.2	-45.6
0	7	5	14.3	12.8	90.0
1	7	5	5.1	4.7	84.5
2	7	5	12.8	13.1	-111.3
3	7	5	7.6	6.5	107.8
4	7	5	7.3	6.8	153.4
5	7	5	5.5	4.1	-119.0
6	7	5	3.8	3.5	-51.5
7	7	5	9.2	8.2	105.1
8	7	5	8.6	9.3	-90.4
9	7	5	5.2	5.8	-78.0
10	7	5	7.3	7.1	49.0
11	7	5*	3.0	1.3	103.5
12	7	5	3.9	3.5	102.6
13	7	5*	2.3	0.8	-52.7
14	7	5*	1.9	1.7	126.7
15	7	5*	2.1	1.9	-151.2
0	8	5	20.5	20.8	0.0
1	8	5	10.9	11.8	-147.0
2	8	5	6.8	6.3	-52.0
3	8	5	7.5	4.5	123.6
4	8	5	18.2	17.7	-117.0
5	8	5	8.5	7.3	-146.8
6	8	5	3.6	2.4	-177.1
7	8	5	4.7	5.4	122.7
8	8	5	10.2	10.5	-148.7
9	8	5	5.9	7.0	-8.8
10	8	5*	2.4	1.4	-6.5
11	8	5	4.4	4.2	52.7
12	8	5*	3.0	2.9	-0.6
13	8	5*	2.7	1.7	-67.3
14	8	5*	1.6	0.7	69.5
15	8	5*	1.2	0.4	31.7
0	9	5	16.5	17.2	90.0
1	9	5	9.5	9.8	125.6
2	9	5	9.6	9.2	-7.8
3	9	5	15.3	15.6	153.4
4	9	5	6.3	7.5	-155.3
5	9	5	13.8	13.8	36.6
6	9	5	4.7	4.8	37.0
7	9	5	15.2	15.1	-130.8
8	9	5	5.2	5.0	-107.2
9	9	5	9.7	10.0	-84.3
10	9	5*	3.0	2.0	-18.6
11	9	5	7.3	6.7	10.7
12	9	5*	3.0	1.5	102.2
13	9	5	4.4	4.7	29.3
14	9	5*	1.4	1.1	23.8
15	9	5*	1.5	1.1	80.8
0	10	5	10.0	10.6	0.0
1	10	5	14.5	14.1	-117.1
2	10	5	7.8	7.9	120.9
3	10	5	15.4	15.1	172.6
4	10	5	12.7	13.3	-42.0
5	10	5	9.7	10.6	147.9
6	10	5*	3.6	4.2	-132.1
7	10	5	6.8	7.6	107.5
8	10	5	6.8	8.5	-105.6
9	10	5	5.2	4.4	-157.3
10	10	5	6.0	6.1	172.3
11	10	5*	3.1	2.1	-145.1
12	10	5*	2.4	0.6	140.4
13	10	5	3.6	3.6	9.9
14	10	5*	2.2	2.7	3.5
0	11	5*	3.0	3.9	90.0
1	11	5*	2.9	4.0	120.0
2	11	5	16.5	16.2	78.0
3	11	5	6.2	6.8	-127.4
4	11	5	13.3	14.3	47.9
5	11	5	12.3	13.6	107.5
6	11	5	4.4	3.5	-17.0
7	11	5	7.1	7.4	6.4
8	11	5	11.1	10.9	-69.7
9	11	5	5.4	5.3	-37.1
10	11	5	9.9	8.9	-123.6
11	11	5	3.7	3.1	-150.3
12	11	5*	2.4	1.7	-113.6
13	11	5*	1.5	1.8	-57.3
14	11	5*	1.8	1.6	-16.3
0	12	5*	3.2	2.5	0.0
1	12	5	5.0	4.0	-38.4
2	12	5	4.2	3.2	-122.0
3	12	5	21.0	21.7	-138.7
4	12	5	17.2	17.8	106.2
5	12	5	13.2	13.7	168.3
6	12	5	10.5	11.3	115.5
7	12	5*	3.5	2.6	167.2
8	12	5	6.3	5.3	20.7
9	12	5	6.6	6.9	92.8
10	12	5	5.7	6.4	-36.9
11	12	5*	2.4	1.5	47.7
12	12	5	4.3	4.1	-140.4
13	12	5*	2.1	0.8	53.2
14	12	5*	1.5	1.2	7.5
0	13	5	9.0	9.8	90.0
1	13	5	7.1	6.9	15.4
2	13	5	5.9	6.6	47.1
3	13	5	10.6	12.0	7.0
4	13	5	9.6	11.4	-22.7
5	13	5	7.4	9.9	-131.9
6	13	5	7.3	5.2	-150.9
7	13	5	6.0	5.0	148.5
8	13	5	6.2	7.0	150.0
9	13	5	4.6	3.3	151.1
10	13	5*	2.6	1.4	157.4
11	13	5*	2.5	1.4	-144.3
12	13	5	2.9	2.4	-72.3
13	13	5*	2.3	2.5	-94.1
0	14	5*	2.5	0.1	-180.0
1	14	5	5.5	5.7	-115.5
2	14	5	6.3	5.9	81.1
3	14	5	10.4	11.7	37.8
4	14	5	5.4	5.6	69.0
5	14	5*	3.2	1.8	14.3
6	14	5	4.9	4.9	-87.7
7	14	5*	3.4	2.9	-131.1
8	14	5	4.7	4.5	94.4
9	14	5*	2.1	0.9	-142.4
10	14	5*	1.8	0.2	14.2
11	14	5	3.9	4.0	122.8
12	14	5*	2.0	2.3	163.9
13	14	5*	1.5	0.9	-82.5
0	15	5	7.2	7.1	90.0
1	15	5*	2.4	1.1	21.0
2	15	5*	3.5	2.4	154.9
3	15	5	8.9	9.3	-38.1
4	15	5	4.2	4.4	79.1
5	15	5	7.6	7.7	126.3
6	15	5	5.3	5.0	-34.1
7	15	5	6.6	6.3	68.7
8	15	5	4.4	3.7	-65.4
9	15	5	3.3	3.4	136.1
10	15	5*	2.1	1.3	-39.4
11	15	5*	2.2	1.5	-10.1
12	15	5*	1.4	1.4	-164.5
0	16	5	4.8	3.7	0.0
1	16	5*	2.2	1.1	-99.1
2	16	5*	3.3	1.9	96.8
3	16	5*	3.2	2.9	-78.9
4	16	5	5.2	5.4	59.6
5	16	5	4.0	3.2	144.2
6	16	5*	2.0	2.0	-166.4
7	16	5*	2.1	1.5	-52.8
8	16	5*	2.2	2.1	134.4
9	16	5*	2.4	2.0	57.9
10	16	5*	1.5	0.3	-175.8
11	16	5*	1.9	1.8	-94.5
0	17	5*	3.3	1.6	90.0
1	17	5	6.5	5.7	14.9
2	17	5	3.9	4.5	-172.6
3	17	5	9.0	7.7	63.3
4	17	5	3.5	3.7	-21.3

H	K	L	/FO/	/FC/	PHASE	H	K	L	/FO/	/FC/	PHASE	H	K	L	/FO/	/FC/	PHASE
5	17	5*	2.3	1.2	65.7	0	1	6	4.4	4.5	-90.0	12	4	6*	2.2	2.1	14.9
6	17	5	3.3	2.7	-8.2	1	1	6	7.3	6.7	-116.7	13	4	6*	2.7	3.2	-83.3
7	17	5	6.2	5.9	-164.8	2	1	6	9.2	9.3	142.3	14	4	6	2.4	3.0	2.4
8	17	5	3.4	3.1	21.4	3	1	6	10.0	10.3	59.0	0	5	6	15.2	14.0	90.0
9	17	5	2.6	2.7	144.7	4	1	6*	2.5	0.3	-152.4	1	5	6	13.6	14.6	44.0
10	17	5	2.9	3.5	-142.9	5	1	6	9.3	10.2	61.8	2	5	6	6.9	7.6	-174.9
0	18	5*	1.5	0.9	0.0	6	1	6	4.4	5.8	-6.1	3	5	6	10.8	10.9	27.1
1	18	5	4.2	3.8	-119.1	7	1	6*	3.4	1.5	169.8	4	5	6	7.9	8.8	-120.9
2	18	5	7.5	7.2	61.8	8	1	6*	3.3	3.1	-85.3	5	5	6	5.9	5.8	102.9
3	18	5*	2.2	2.1	-48.3	9	1	6*	3.2	4.0	-93.1	6	5	6*	3.6	3.8	28.4
4	18	5	3.8	2.9	94.7	10	1	6	5.5	5.7	151.2	7	5	6	4.9	3.6	142.7
5	18	5	3.5	3.9	64.7	11	1	6*	3.2	2.5	-140.5	8	5	6*	3.4	2.7	-114.6
6	18	5	3.6	3.8	40.8	12	1	6*	2.5	1.4	149.4	9	5	6	5.7	5.4	-163.0
7	18	5*	2.4	2.2	161.2	13	1	6*	2.7	2.5	-70.7	10	5	6	3.6	3.0	172.4
8	18	5*	2.2	1.5	-157.6	14	1	6*	1.4	0.6	-14.5	11	5	6*	2.1	1.7	98.8
9	18	5*	1.3	1.8	12.6	0	2	6	16.7	14.5	0.0	12	5	6*	2.9	2.7	-118.5
0	19	5	7.5	8.5	-90.0	1	2	6	8.8	9.2	136.5	13	5	6*	1.8	0.8	62.4
1	19	5	6.0	5.6	39.1	2	2	6	13.5	13.7	87.7	14	5	6	1.4	0.5	-73.2
2	19	5	6.0	6.3	-53.5	3	2	6	5.1	5.5	-143.7	0	6	6	28.1	30.3	0.0
3	19	5	4.2	3.5	96.4	4	2	6	13.0	12.8	132.0	1	6	6	11.7	11.6	-77.1
4	19	5*	2.5	2.9	-51.9	5	2	6	3.0	1.8	-70.3	2	6	6	13.1	12.4	29.4
5	19	5	4.4	4.9	-57.9	6	2	6	7.2	7.7	-110.3	3	6	6	4.0	3.3	-10.7
6	19	5	5.3	5.2	63.5	7	2	6	5.6	6.0	-16.2	4	6	6	5.3	5.0	96.4
7	19	5	2.3	2.0	160.1	8	2	6*	3.4	1.4	-84.1	5	6	6	7.6	8.1	21.6
8	19	5	2.8	3.3	48.2	9	2	6*	3.6	3.1	114.2	6	6	6	6.9	7.4	137.7
0	20	5	2.9	3.6	-180.0	10	2	6	3.9	4.1	88.1	7	6	6	9.1	8.8	94.6
1	20	5	5.4	6.1	-43.6	11	2	6	3.7	3.5	95.4	8	6	6	7.1	7.1	168.2
2	20	5*	1.7	1.5	72.3	12	2	6*	2.7	1.0	-166.8	9	6	6	3.6	4.0	12.4
3	20	5	2.8	2.5	50.5	13	2	6*	2.1	0.3	64.7	10	6	6	5.0	5.6	128.0
4	20	5*	2.6	2.4	-52.4	14	2	6*	2.2	1.8	-45.1	11	6	6*	2.2	0.6	-84.9
5	20	5*	2.6	3.8	5.8	0	3	6	5.9	5.3	-90.0	12	6	6*	2.6	3.0	-151.5
6	20	5*	2.5	2.6	-151.0	1	3	6	8.9	8.4	113.7	13	6	6*	1.9	2.4	-102.4
7	20	5*	1.9	1.4	-12.0	2	3	6	13.0	13.8	-7.0	14	6	6	2.0	1.9	-110.5
0	21	5	3.3	4.7	-90.0	3	3	6	8.3	9.7	-20.7	0	7	6	4.6	4.3	-90.0
1	21	5*	2.5	2.8	-161.2	4	3	6	14.9	15.5	50.8	1	7	6	9.7	9.5	31.6
2	21	5	2.8	3.8	22.7	5	3	6	4.7	3.1	-139.4	2	7	6	13.9	14.6	-9.5
3	21	5	3.4	4.4	-117.1	6	3	6	5.4	6.1	-131.5	3	7	6	8.6	9.1	156.4
4	21	5*	2.5	3.7	-26.1	7	3	6*	3.1	2.6	-62.5	4	7	6	12.2	13.5	-26.3
5	21	5*	1.7	1.5	-77.4	8	3	6*	2.8	2.0	-77.2	5	7	6	8.3	8.7	39.6
0	22	5	2.9	3.9	-180.0	9	3	6	3.7	3.4	-119.0	6	7	6	7.0	6.2	31.9
1	22	5*	1.2	1.9	14.5	10	3	6*	1.7	1.6	-112.2	7	7	6	3.8	4.1	140.7
2	22	5	2.2	2.1	-168.8	11	3	6*	2.0	1.6	-31.7	8	7	6*	3.6	3.0	131.6
0	0	6	17.2	16.8	-180.0	12	3	6	3.9	3.7	110.4	9	7	6*	2.2	1.0	-124.8
1	0	6*	2.4	0.7	-180.0	13	3	6*	2.2	0.7	146.2	10	7	6*	2.6	2.4	15.6
2	0	6*	3.2	1.6	-180.0	14	3	6*	1.9	2.3	152.0	11	7	6*	2.3	0.6	-94.0
3	0	6	8.6	9.5	-180.0	0	4	6	4.0	3.7	0.0	12	7	6*	2.1	1.4	168.0
4	0	6*	2.5	1.8	-180.0	1	4	6	8.6	8.3	115.7	13	7	6*	1.6	2.5	-61.6
5	0	6	6.7	7.6	0.0	2	4	6	7.1	8.3	-96.6	0	8	6	5.9	6.7	-180.0
6	0	6	5.6	5.0	0.0	3	4	6	5.2	5.3	61.7	1	8	6	17.6	20.1	-68.2
7	0	6	4.9	5.9	-180.0	4	4	6	12.0	12.4	55.9	2	8	6	10.3	10.6	101.9
8	0	6	3.8	3.4	-180.0	5	4	6	6.0	5.4	133.2	3	8	6	6.8	7.1	-97.4
9	0	6*	2.6	0.2	0.0	6	4	6	7.0	6.7	172.6	4	8	6	8.7	9.2	-56.8
10	0	6*	2.5	1.2	-180.0	7	4	6	4.5	4.8	-137.8	5	8	6	6.9	6.1	141.9
11	0	6*	2.1	0.2	-180.0	8	4	6	7.2	6.7	132.6	6	8	6	6.0	5.6	53.8
12	0	6	3.5	3.4	0.0	9	4	6*	2.6	1.4	-136.8	7	8	6	9.7	9.1	66.2
13	0	6*	2.0	1.4	0.0	10	4	6	3.3	2.0	22.0	8	8	6*	2.6	0.5	-155.4
14	0	6*	1.1	0.3	0.0	11	4	6*	2.7	2.1	-61.6	9	8	6	6.8	6.9	89.7

H	K	L	/FO/	/FC/	PHASE	H	K	L	/FO/	/FC/	PHASE	H	K	L	/FO/	/FC/	PHASE
10	8	6*	2.6	2.3	161.5	1	13	6	5.3	4.7	-140.9	2	19	6*	1.4	0.6	23.3
11	8	6	4.9	5.3	68.8	2	13	6	6.2	5.4	-167.0	3	19	6*	2.1	2.4	-129.7
12	8	6*	1.3	0.5	23.2	3	13	6	5.9	4.9	-152.8	1	0	7*	2.8	0.9	90.0
13	8	6*	1.8	0.7	-32.4	4	13	6	4.8	3.3	29.2	2	0	7	3.7	4.0	90.0
0	9	6	12.0	13.2	-90.0	5	13	6*	2.9	1.6	64.2	3	0	7	9.1	10.0	-90.0
1	9	6*	3.7	2.3	-119.5	6	13	6	4.3	3.9	-7.9	4	0	7*	2.4	2.7	90.0
2	9	6*	2.3	2.0	-50.5	7	13	6*	2.7	2.0	119.7	5	0	7*	3.2	1.9	90.0
3	9	6	4.8	4.7	-26.2	8	13	6	3.3	2.8	-46.5	6	0	7*	3.3	2.7	90.0
4	9	6	9.5	9.3	18.2	9	13	6	4.3	4.7	50.3	7	0	7*	1.5	2.7	-90.0
5	9	6	4.9	5.2	-36.4	10	13	6*	1.7	1.4	167.7	8	0	7*	2.7	1.5	-90.0
6	9	6	5.1	4.7	-27.1	11	13	6	2.4	2.8	35.1	9	0	7	3.1	3.7	90.0
7	9	6	6.3	5.4	-117.7	0	14	6	7.1	6.3	0.0	10	0	7*	1.3	1.2	90.0
8	9	6*	3.1	2.0	135.2	1	14	6	4.5	4.4	-163.2	11	0	7*	1.1	0.5	-90.0
9	9	6*	3.1	2.7	-155.5	2	14	6*	2.2	2.0	164.8	12	0	7*	1.1	0.1	-90.0
10	9	6	4.4	5.0	-172.8	3	14	6*	3.3	3.4	-28.8	0	1	7*	3.1	2.1	90.0
11	9	6*	1.9	2.0	140.0	4	14	6	3.3	3.1	-143.4	1	1	7	6.8	7.7	-176.0
12	9	6	2.4	1.9	91.4	5	14	6	6.9	7.3	-176.1	2	1	7*	3.3	3.4	-31.7
13	9	6	2.2	2.7	106.1	6	14	6*	2.8	3.4	-82.7	3	1	7	4.2	4.8	-70.5
0	10	6	5.0	6.1	-180.0	7	14	6	3.2	4.3	167.4	4	1	7	7.8	9.1	-11.9
1	10	6	4.9	5.3	-48.4	8	14	6	3.2	3.2	-49.4	5	1	7	3.8	3.8	-63.0
2	10	6	5.2	5.3	-129.6	9	14	6*	2.1	1.9	150.9	6	1	7*	2.3	0.4	110.7
3	10	6	5.3	4.3	-114.9	10	14	6*	1.3	1.0	79.8	7	1	7*	1.6	2.2	160.2
4	10	6	5.0	3.7	109.8	0	15	6	3.8	3.7	90.0	8	1	7*	3.2	3.2	33.6
5	10	6	6.0	5.6	50.4	1	15	6*	2.4	1.1	173.3	9	1	7	3.8	3.2	-45.2
6	10	6	3.7	3.5	-64.1	2	15	6	5.1	4.6	25.8	10	1	7*	2.1	2.3	-140.2
7	10	6	6.1	6.0	-11.6	3	15	6*	3.1	2.8	-67.2	11	1	7*	2.0	2.0	15.8
8	10	6	6.0	6.4	-15.2	4	15	6	4.7	5.6	80.7	0	2	7*	2.4	0.8	0.0
9	10	6*	1.8	1.9	79.2	5	15	6	3.4	3.7	-99.1	1	2	7*	2.1	0.6	85.5
10	10	6	4.8	5.6	-71.5	6	15	6*	2.2	1.4	50.0	2	2	7	5.5	5.5	-155.8
11	10	6	2.6	3.1	-125.2	7	15	6	2.8	2.6	-130.2	3	2	7*	3.1	3.3	-58.1
12	10	6	2.2	2.9	170.4	8	15	6	2.9	3.4	8.2	4	2	7	6.0	5.9	-147.8
0	11	6*	2.7	0.8	-90.0	9	15	6*	1.5	1.4	133.1	5	2	7*	3.1	2.2	-17.0
1	11	6	7.2	7.8	-163.8	0	16	6	6.3	7.6	-180.0	6	2	7	7.4	6.7	-100.6
2	11	6*	3.3	3.4	45.6	1	16	6*	2.8	1.9	78.0	7	2	7*	2.0	1.4	146.1
3	11	6	4.7	4.6	-64.4	2	16	6*	2.1	2.0	-104.7	8	2	7	3.2	2.1	-11.4
4	11	6	9.7	10.4	-34.2	3	16	6*	2.7	2.9	127.0	9	2	7*	2.7	3.1	153.9
5	11	6	7.9	7.9	-170.8	4	16	6*	2.1	1.3	-21.4	10	2	7	3.6	3.0	16.8
6	11	6	6.6	7.2	151.3	5	16	6*	1.8	1.5	-173.8	11	2	7*	1.7	0.4	97.7
7	11	6	6.1	6.7	71.1	6	16	6*	2.2	3.2	51.0	0	3	7	10.2	12.0	90.0
8	11	6*	3.0	2.9	48.9	7	16	6*	1.9	2.1	-140.7	1	3	7	3.5	2.0	93.5
9	11	6	5.1	5.5	45.3	8	16	6*	1.9	1.8	109.5	2	3	7	8.1	8.7	72.6
10	11	6*	2.3	2.4	-164.5	0	17	6*	2.5	3.1	90.0	3	3	7	5.0	5.0	-149.6
11	11	6	2.5	2.9	-66.8	1	17	6*	2.3	1.6	-55.9	4	3	7	3.6	2.2	-162.8
12	11	6*	1.7	1.4	-54.0	2	17	6	2.9	3.1	74.3	5	3	7	3.5	3.0	-148.2
0	12	6	10.0	9.8	-180.0	3	17	6	2.9	3.4	90.8	6	3	7*	1.4	0.9	-164.5
1	12	6*	2.5	0.4	-63.7	4	17	6	3.0	4.2	-123.8	7	3	7*	2.1	8.0	-49.5
2	12	6*	2.8	1.5	-109.9	5	17	6*	2.4	2.9	-41.2	8	3	7	5.7	5.1	-131.3
3	12	6	3.8	2.9	-71.6	6	17	6*	1.6	1.0	50.8	9	3	7	3.2	2.5	-50.3
4	12	6	4.9	4.5	-49.1	7	17	6	2.2	1.7	-48.9	10	3	7*	2.6	2.9	-55.7
5	12	6	4.5	3.5	86.1	0	18	6	3.7	3.4	-180.0	11	3	7*	1.4	1.3	10.6
6	12	6	5.0	4.8	-90.2	1	18	6	2.7	2.1	-31.1	0	4	7*	3.1	2.2	-180.0
7	12	6	5.6	6.6	-144.0	2	18	6	3.9	5.4	55.9	1	4	7	10.8	10.9	-70.1
8	12	6*	2.5	1.8	-94.5	3	18	6*	1.8	1.0	-154.7	2	4	7	3.8	3.9	-121.2
9	12	6	3.5	3.7	96.1	4	18	6*	1.9	1.0	44.3	3	4	7	8.1	7.0	107.4
10	12	6*	2.1	2.6	67.8	5	18	6*	1.5	1.1	-29.9	4	4	7*	2.4	0.8	-70.0
11	12	6*	1.8	2.0	161.9	0	19	6	4.1	5.7	-90.0	5	4	7	7.7	8.0	143.4
0	13	6	10.9	11.1	90.0	1	19	6*	1.3	2.5	-25.7	6	4	7*	1.6	5.3	163.8

H	K	L	/Fo/	/Fc/	PHASE
7	4	7*	2.5	8.8	152.6
8	4	7*	2.6	2.3	24.7
9	4	7	3.2	3.7	-33.7
10	4	7*	1.6	0.9	102.6
11	4	7	2.6	2.5	-45.8
0	5	7	7.0	7.0	90.0
1	5	7	9.4	8.9	-82.9
2	5	7*	3.4	3.3	95.8
3	5	7	9.8	10.3	-80.5
4	5	7*	3.3	2.1	-67.9
5	5	7	5.7	4.8	-14.8
6	5	7*	2.1	3.5	81.6
7	5	7	3.4	3.4	179.4
8	5	7	3.9	3.4	-145.8
9	5	7	3.8	4.7	-173.5
10	5	7*	2.5	4.4	-116.0
11	5	7*	2.0	2.1	-111.4
0	6	7	9.5	9.0	-180.0
1	6	7	6.2	6.0	91.1
2	6	7	5.5	4.9	115.8
3	6	7	4.7	5.0	-167.9
4	6	7	5.8	5.1	-128.5
5	6	7*	2.0	4.4	175.8
6	6	7*	2.5	4.8	30.6
7	6	7*	2.4	3.4	38.8
8	6	7	3.2	3.8	29.7
9	6	7*	2.0	0.8	85.4
10	6	7*	1.8	1.4	43.9
11	6	7	2.2	2.9	-122.5
0	7	7*	3.2	2.9	-90.0
1	7	7	3.6	4.0	-9.1
2	7	7*	2.8	1.0	-31.1
3	7	7	6.1	6.0	74.1
4	7	7*	2.5	1.9	72.0
5	7	7*	2.1	6.1	-76.8
6	7	7	4.7	5.6	-152.4
7	7	7*	2.5	2.8	147.4
8	7	7	3.2	4.2	145.3
9	7	7*	2.6	2.1	69.3
10	7	7*	1.3	1.8	167.3
0	8	7	6.4	6.9	-180.0
1	8	7*	2.9	2.1	-92.8
3	8	7*	2.2	3.6	76.5
4	8	7*	2.3	0.7	32.7
5	8	7*	2.1	2.4	122.0
6	8	7	6.4	6.7	6.8
7	8	7	3.4	4.4	-19.8
8	8	7*	2.6	2.2	-90.1
9	8	7*	1.2	0.9	-132.6
10	8	7	2.9	3.5	-171.9
0	9	7*	3.0	0.8	-90.0
1	9	7*	2.7	7.6	-150.8
2	9	7*	1.5	2.7	-93.2
3	9	7*	2.2	5.7	-96.4
4	9	7*	1.9	3.7	-157.3
5	9	7*	2.6	1.6	144.4
6	9	7*	3.0	0.8	-118.2

H	K	L	/Fo/	/Fc/	PHASE
7	9	7*	2.9	3.7	48.6
8	9	7	2.8	3.1	32.3
9	9	7	3.3	4.9	36.2
0	10	7*	1.7	1.6	0.0
1	10	7*	1.9	5.4	111.4
2	10	7*	2.1	2.9	-108.5
3	10	7*	3.2	2.5	-145.0
4	10	7	3.7	5.1	-14.4
5	10	7	3.4	3.5	-146.1
6	10	7	3.8	4.3	-102.3
7	10	7	4.8	5.6	-153.4
8	10	7	2.9	3.8	-78.1
9	10	7*	1.4	1.7	87.9
0	11	7	7.1	7.3	90.0
1	11	7*	2.3	1.0	107.4
2	11	7	6.2	6.8	150.8
3	11	7*	2.5	2.5	-153.5
4	11	7	3.2	2.2	43.6
5	11	7*	2.5	2.3	81.1
6	11	7*	1.6	1.0	4.6
7	11	7*	1.5	1.3	159.3
8	11	7	3.5	4.5	-51.5
0	12	7	3.7	4.1	0.0
1	12	7*	2.7	2.7	174.5
2	12	7*	2.1	1.7	37.1
3	12	7*	2.2	2.3	-63.4
4	12	7*	2.3	1.7	129.6
5	12	7*	1.5	1.7	-167.3
6	12	7	3.4	4.3	92.1
7	12	7*	2.2	2.7	-139.3
0	13	7	3.2	3.7	90.0
1	13	7*	1.7	1.1	83.0
2	13	7*	2.0	2.5	-85.3
3	13	7*	1.8	2.0	97.0
4	13	7*	1.5	2.0	176.5
5	13	7*	1.4	0.3	79.0
6	13	7*	1.7	2.4	10.3
0	14	7*	1.0	0.6	0.0
1	14	7*	1.7	2.1	-131.1
2	14	7*	1.7	1.6	-6.0
3	14	7*	1.5	0.6	51.8
4	14	7*	1.6	0.9	-102.8
5	14	7	2.5	2.9	-75.9
0	15	7*	1.2	0.5	-90.0
1	15	7*	1.6	1.8	-9.1
2	15	7*	1.9	2.9	31.7
3	15	7*	1.9	2.1	128.1
4	15	7*	2.0	1.8	143.8
4	0	8*	1.5	2.5	-180.0
5	0	8*	1.8	4.3	0.0
6	0	8*	2.2	1.4	-180.0
7	0	8*	1.7	1.3	-180.0
4	1	8*	2.3	2.6	-41.7
5	1	8*	2.1	3.1	124.8
6	1	8	3.1	4.7	6.9
7	1	8	2.8	2.9	83.9
4	2	8*	1.8	0.3	154.9

H	K	L	/Fo/	/Fc/	PHASE
5	2	8*	1.7	0.9	-119.2
6	2	8*	1.9	1.6	9.6
7	2	8	2.4	3.0	101.1
4	3	8*	2.1	1.5	32.5
5	3	8*	1.4	1.2	-33.8
6	3	8*	2.3	3.0	-2.0
7	3	8	2.3	2.7	-37.9
3	4	8*	1.6	0.9	137.9
4	4	8*	1.4	0.4	-0.7
5	4	8	3.9	5.8	157.2
6	4	8*	1.6	1.4	-36.1
7	4	8	2.6	3.8	-24.6
2	5	8*	1.5	1.8	-87.1
3	5	8*	1.9	3.9	-16.6
4	5	8*	1.3	1.7	37.3
5	5	8*	1.6	0.7	-104.3
6	5	8*	1.5	1.5	-132.9
0	6	8*	1.4	0.7	-180.0
1	6	8*	1.7	1.4	-155.5
2	6	8*	2.1	1.9	27.4
3	6	8*	1.8	2.5	-94.0
4	6	8	3.5	4.5	24.5
5	6	8	2.7	4.9	-61.3
6	6	8	2.4	3.7	29.8
0	7	8*	2.0	0.9	-90.0
1	7	8*	1.5	0.3	110.4
2	7	8*	1.6	1.2	-84.9
3	7	8*	2.2	3.0	-168.9
4	7	8*	1.4	2.1	-94.4
5	7	8*	1.7	1.2	-97.9
0	8	8*	1.7	0.2	-180.0
1	8	8*	2.3	2.5	-77.7
2	8	8	2.6	3.7	154.6
3	8	8*	1.7	2.0	-24.7
4	8	8*	1.4	1.7	155.0
0	9	8*	1.1	0.4	-90.0
1	9	8*	1.8	2.0	152.7
2	9	8*	1.7	1.5	174.6
3	9	8*	2.0	2.6	-77.7
0	10	8*	1.5	0.4	-180.0
1	10	8*	1.5	2.2	94.4

B. LIST OF COMPUTER PROGRAMS FOR SOLVING AND REFINING THE STRUCTURE OF NGTA

Calculation	Program	Author
Lorentz, Polarisation and Absorption Corrections	PDP-8RUN	D. Watkins
Data Reduction	X-RAYRUN	R. H. Carruthers
Direct Methods Programs for Calculation of |E| Triplet Relationships, with Tangent Formula Extension of Phases	ECALC	S. M. W. Motherwell and A. K. Larsen
Structure Factor Calculation	X-RAY 70	J. Stewart
Least Squares Refinement and Difference Fourier Calculations	X-RAYRUN	R. H. Carruthers
Chebyshev Polynomial Weighting Scheme	X-RAYRUN	R. H. Carruthers
Bond Distances and Angles	X-RAYRUN	R. H. Carruthers
Hydrogen Placing	X-RAYRUN	R. H. Carruthers
Least Squares Planes	X-RAYRUN	R. H. Carruthers
Model Figure Drawing	PLUTO	S. M. W. Motherwell
Conformation Angles	PLUTO	S. M. W. Motherwell
Least Squares Determation of Best Unit Cell Parameters		N. W. Isaacs

APPENDIX IV

TABLE OF OBSERVED STRUCTURE AMPLITUDES OF THE DIFFERENCE FOURIER SYNTHESIS OF THE LYSOZYME-β(TEMPO)-GlcNAc COMPLEX.

For each reflection the following quantities are provided in sets of six columns of figures each:

$h\ k\ \ell$ $\quad\quad$ ΔF $\quad\quad$ α_p $\quad\quad$ $\underline{m}$

where

$hk\ell$ are the Miller indices of a reflection.

ΔF is the difference structure amplitude ≡ $(|\underline{F}_{SL}| - |\underline{F}_p|)$ where $|\underline{F}_{SL}|$ is the observed structure amplitude of the complex and $|\underline{F}_p|$ is the observed structure amplitude of the native tetragonal HEW lysozyme molecule of the corresponding reflection.

α_p is the "best" parent phase angle in degrees.

$\underline{m}$ is the figure of merit x 100.

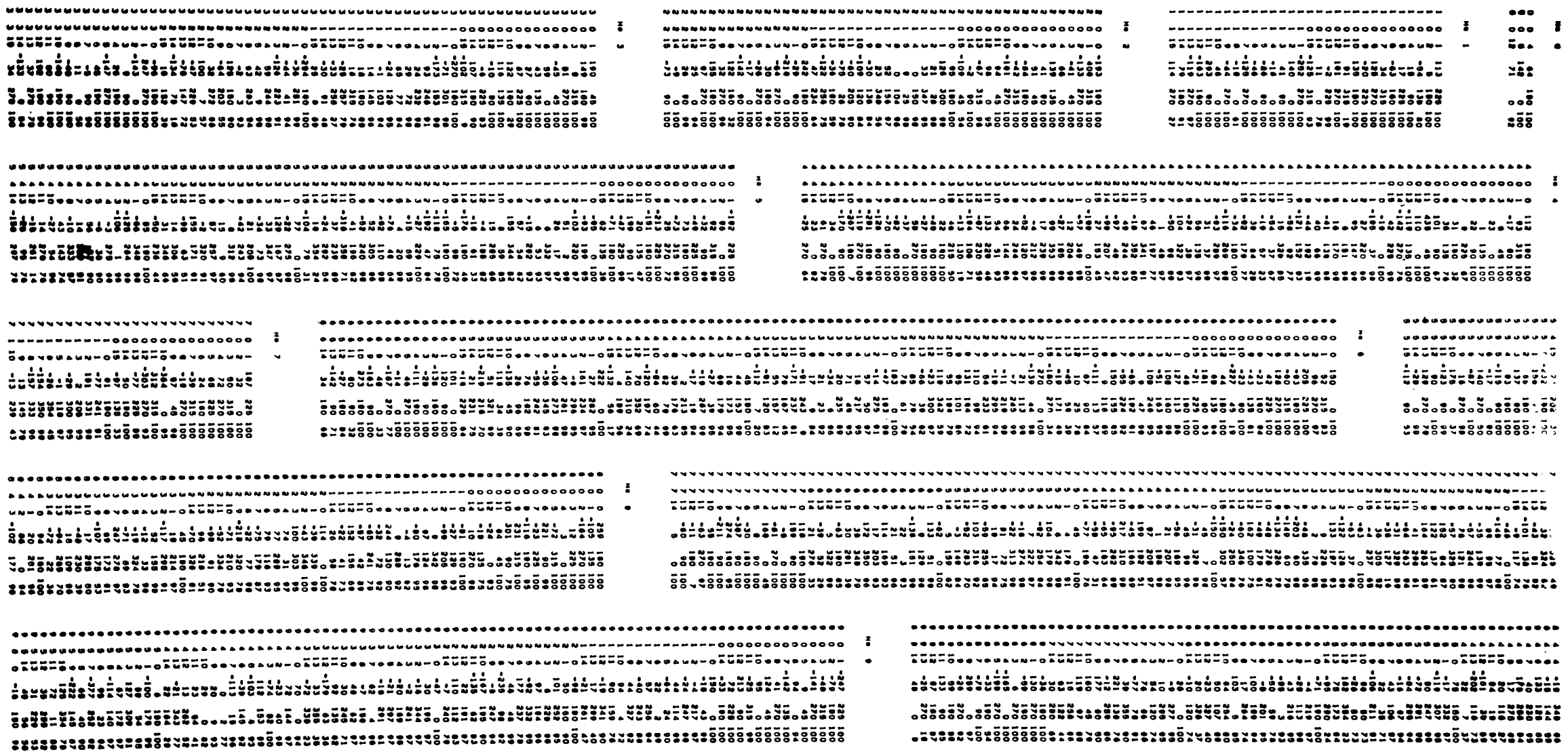

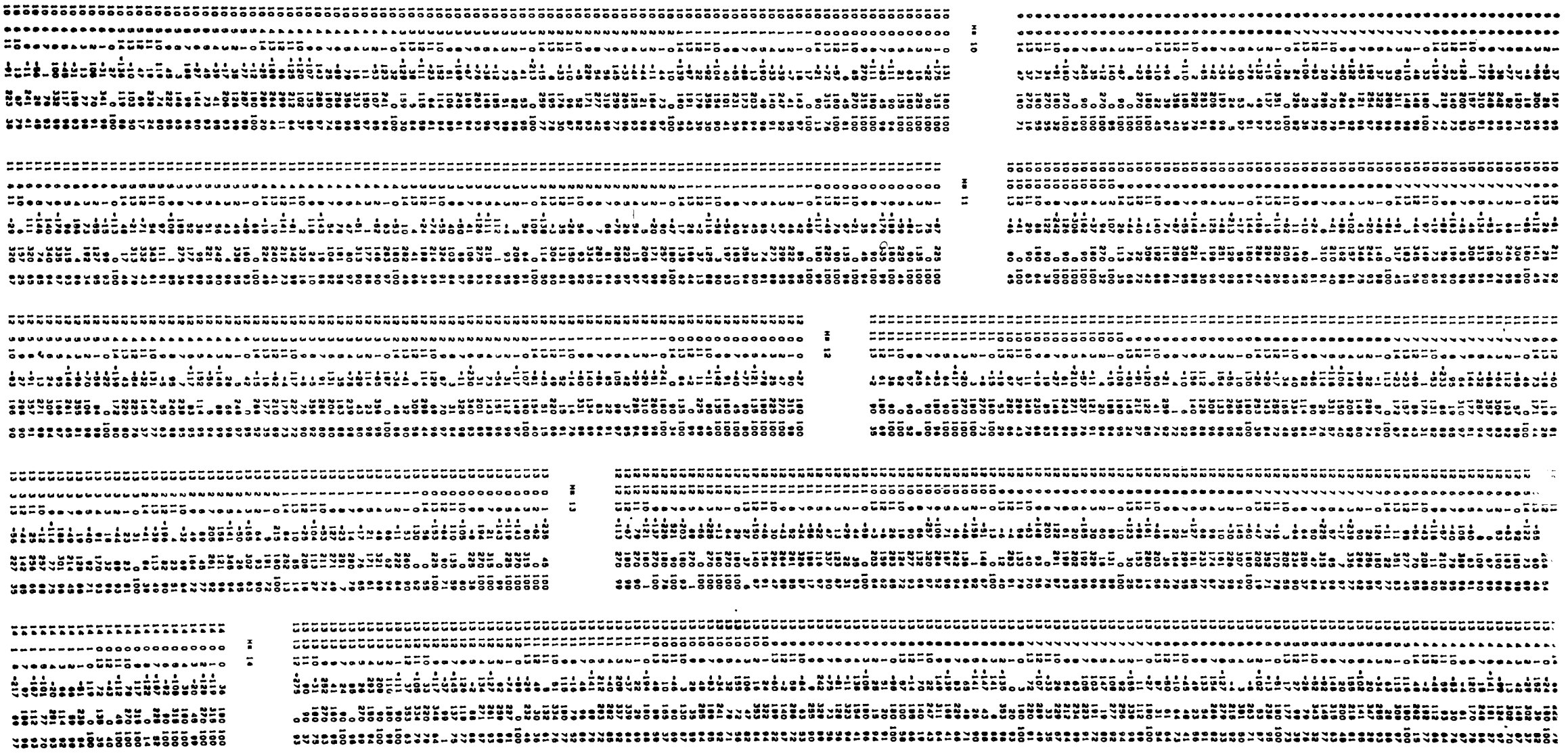

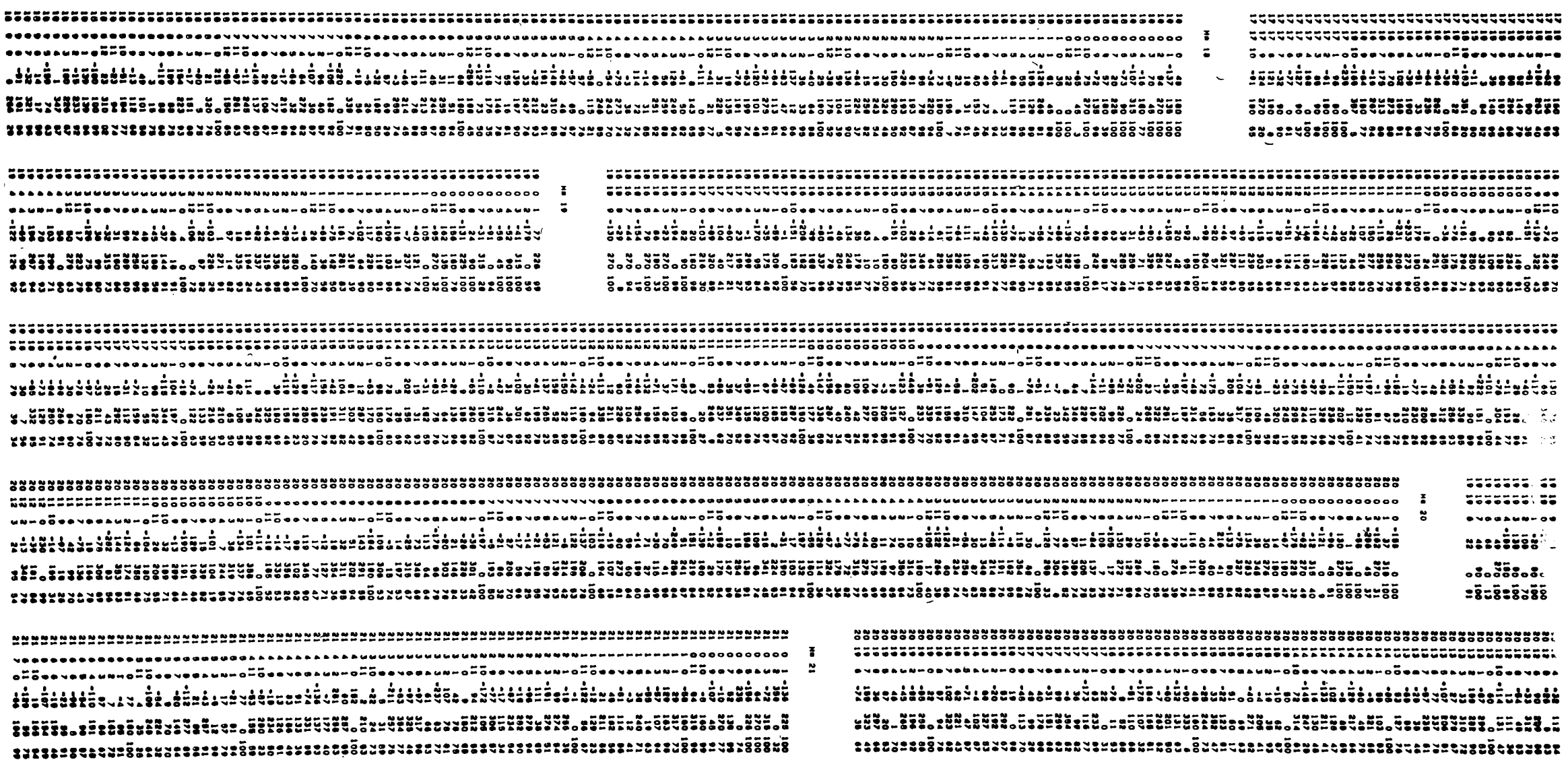

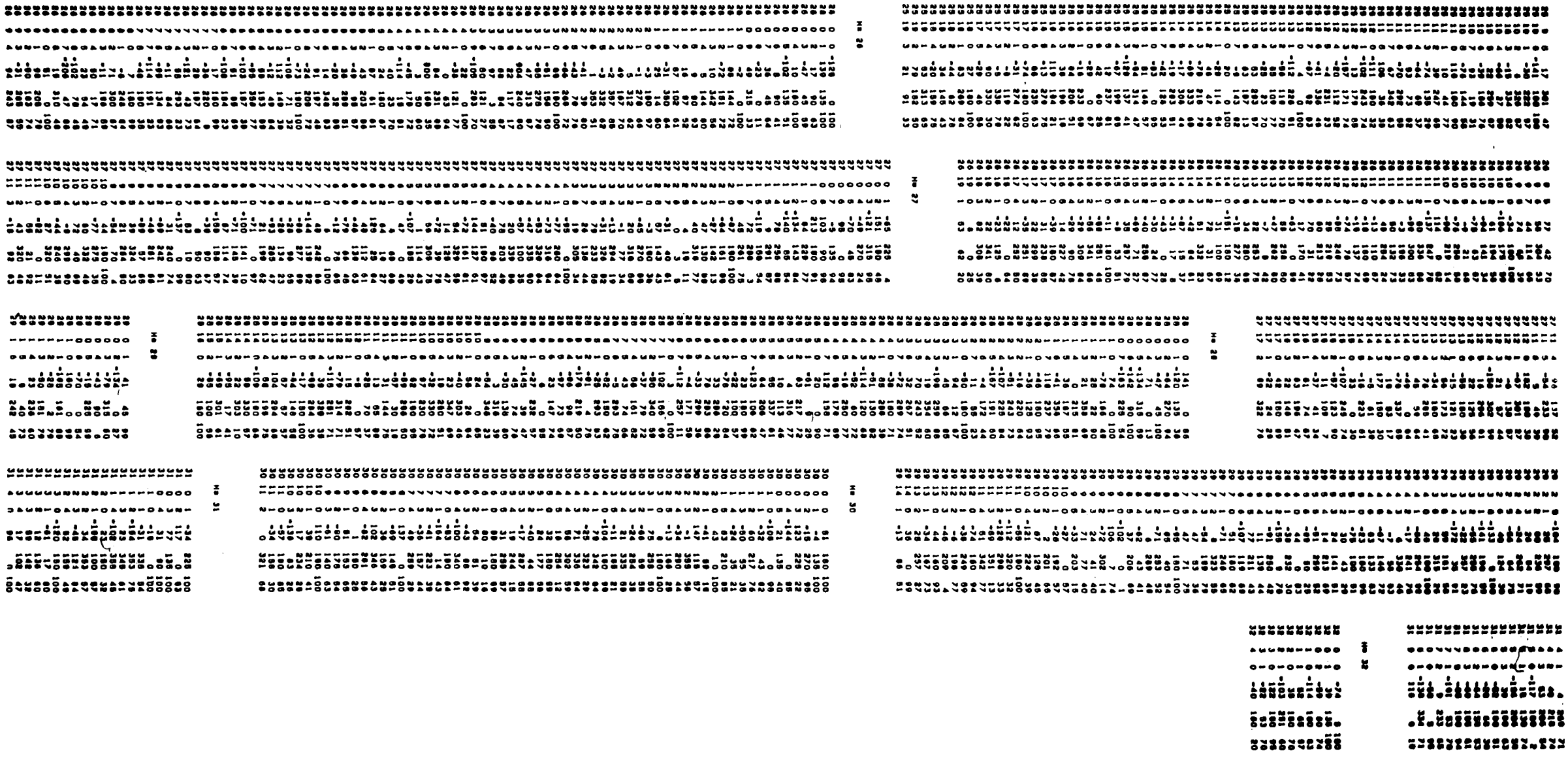

REFERENCES

Abragam, A. and Bleaney, B. (1970), Electron Paramagnetic Resonance of Transition Ions (Clarendon Press, Oxford) Chap. 4, p. 217.

Allendoerfer, R. D. and Maki, A. H. (1970), J. Magn. Res. 3, 396.

Andersson, B. Å. and Fölsch, G. (1972), Chemica Scripta 2, 21.

Arndt, U. W., North, A. C. T., and Phillips, D. C. (1964), J. Sci. Instrum. 41, 421.

Arndt, U. W. and Phillips, D. C. (1961), Acta Cryst. 14, 807.

Arnone, A. (1972), Nature 237, 146.

Arnone, A. Bier, C. J., Cotton, F. A., Hazen, Jr., E. E., Richardson, D. C., and Richardson, J. S. (1969), Proc. Natl. Acad. Sci. (U.S.) 64, 420.

Bales, B. L., Schwartz, R. N., and Kevan, L. (1973), Chem. Phys. Letters 22, 13.

Banerjee, R., Douzou, P., and Lombard, A. (1968), Nature 217, 23.

Banner, D. (1972), D. Phil. Thesis, Oxford University.

Banyard, S. H. (1973), D. Phil. Thesis, Oxford University.

Barry, C. D. and North, A. C. T. (1971), Cold Spring Harbor Symp. Quant. Biol. 36, 577.

Barry, C. D. and North, A. C. T. (1972), FEBS Proceedings: Analysis and Simulation of Biochemical Systems (North-Holland Publishers, Amsterdam), p. 411.

Bates, R. (1973), Determination of pH (Wiley-Interscience, New York), p. 80.

Beddell, C. R. (1970), D. Phil. Thesis, Oxford University.

Bello, J. and Nowoswiat, E. F. (1965), Biochim. Biophys. Acta 105, 325.

Bender, M. L. (1962), J. Am. Chem. Soc. 84, 2582.

Berliner, L. (1970), Acta Cryst. B26, 1198.

Berliner, L. (1971), J. Mol. Biol. 61, 189.

Berman, H. M., Chu, S. C. and Jeffrey, G. A. (1967), Science 157, 1576.

Berman, H. M. and Kim, S. H. (1967), Acta Cryst. B24, 897.

Bernhard, S. A. and Lau, S. J. (1971), Cold Spring Harbor Symp. Quant. Biol. 36, 75.

Bishop, W. H. and Richards, F. M. (1968), J. Mol. Biol. 38, 315.

Blake, C. C. F., Koenig, D. F., Mair, G. A., North, A. C. T., Phillips, D. C., and Sarma, V. R. (1967), Proc. Roy. Soc. B167, 378.

Blake, C. C. F. and Swan, I. D. A. (1971), Nature 232, 12.

Blow, D. M. and Steitz, T. A. (1970), Ann. Rev. Biochem. 39, 63.

Blundell, T. L., Cutfield, J. F., Dodson, E. J., Dodson, G. G., Hodgkin, D. C., and Mercola, D. A. (1971), Cold Spring Harbor Symp. Quant. Biol. 36, 233.

Bondi, A. (1968), Molecular Crystals, Liquids, and Gases (John Wiley & Sons, Inc., New York).

Booth, J. and Boyland, E. (1958), Biochem. J. 70, 681.

Bragg, W. L. and Perutz, M. F. (1952), Acta Cryst. 5, 277.

Bränden, C. I. (1965), Arch. Biochem. Biophys. 112, 215.

Brandt, K. G., Himoe, A., and Hess, G. P. (1967), J. Biol. Chem. 242, 3973.

Brehm, L. and Moult, J. (1975), Proc. Roy. Soc. B118, 425.

Bretscher, P. (1968), Ph.D. Thesis, Cambridge University.

Bretschneider, H. and Beran, K. (1949), Monatsh. 80, 262.

Brown, G. M. and Levy, H. A. (1965), Science 147, 1038.

Brown, W. D. and Mebine, L. B. (1969), J. Biol. Chem. 244, 6696.

Carlisle, C. H., Palmer, R. A., Mazumdar, S. K., Gorinsky, B. A., and Yeates, D. G. R. (1974), J. Mol. Biol. 85, 1.

Carter, Jr., C. W., Freer, S. T., Xuong, Ng. H., Alden, R. A., and Kraut, J. (1971), Cold Spring Harbor Symp. Quant. Biol. 36, 381.

Chan, I. Y., Schmidt, J., and van der Waals, J. H. (1969), Chem. Phys. Letters 4, 269.

Chan, I. Y., van Dorp, W. G., Schaafsma, T. J., and van der Waals, J. H. (1971), Mol. Phys. 22, 741.

Chance, B. and Ravilly, A. (1966), J. Mol. Biol. 21, 195.

Chance, B., Ravilly, A., and Rumen, N. (1966), J. Mol. Biol. 17, 525.

Charney, E. and Bernhard, S. A. (1967), J. Am. Chem. Soc. 89, 2726.

Chu, S. S. C. and Jeffrey, G. A. (1967), Acta Cryst. 23, 1038.

Chu, S. S. C. and Jeffrey, G. A. (1968), Acta Cryst. B24, 830.

Cohn, M. and Reuben, J. (1971), Accts. Chem. Res. 4, 6.

Coles, B. A. (1972), J. Phys. E5, 287.

Crank, J. (1956), The Mathematics of Diffusion (Clarendon Press, Oxford).

Crick, F. H. C. and Blow, D. M. (1959), Acta Cryst. 12, 794.

Crick, F. H. C. and Kendrew, J. C. (1957), Adv. Prot. Chem. 12, 134.

Cruickshank, D. W. J. and Sparks, R. A. (1960), Proc. Roy. Soc. A258, 270.

Dahlquist, F. W., Borders, Jr., C. L., Jacobson, G., and Raftery, M. A. (1969), Biochemistry 8, 694.

Davis, L. A. and Hess, G. P. (1974), J. Mol. Biol. 82, 27.

Debey, P. (1970), Ph.D. Thesis, University of Paris.

Debey, P., Hui Bon Hou, G., and Douzou, P. (1973), FEBS Letters 32, 227.

Devaux, P. and McConnell, H. M. (1972), J. Am. Chem. Soc. 94, 4475.

Doscher, M. S. and Richards, F. M. (1963), J. Biol. Chem. 238, 2399.

Douzou, P. (1971a), Biochimie 53, 17.

Douzou, P. (1971b), Biochimie 53, 1135.

Douzou, P. (1975), Mol. Cell. Biochem. 1, 15.

Douzou, P., Sireix, R., and Travers, F. (1970), Proc. Natl. Acad. Sci. (U.S.) 66, 787.

Drenth, J., Jansonius, J. N., Koekoek, R., and Wolthers, B. G. (1971), Adv. Prot. Chem. 25, 79.

Eaton, W. A. and Hochstrasser, R. M. (1968), J. Chem. Phys. 49, 985.

Ehrenberg, A., Eriksson, E. G., and Hyde, J. S. (1971), in Flavins and Flavoproteins, edit. by H. Kamin (University Park Press, Baltimore, Maryland), p. 141.

Ehrenberg, M. (1965), Acta Cryst. 19, 698.

Ehret, P. and Wolf, H. C. (1968), Z. Naturforsch. 23, 1740.

El-Sayed, M. A. and Siegel, S. (1966), J. Chem. Phys. 44, 1416.

Evans, P. (1973), D. Phil. Thesis, Oxford University.

Eyring, H. (1935), J. Chem. Phys. 3, 107.

Feather, M. S. and Harris, J. M. (1965), J. Chem. Soc. 1965, 153.

Feher, G. (1956), Phys. Rev. 103, 834.

Feher, G. (1958), Physica 24, 580.

Fife, T. H., Rikihisa, T., and Benjamin, B. M. (1971), Biochemistry 10, 3875.

Fink, A. L. (1973), Biochemistry 12, 1736.

Fink, A. L. and Good, N. E. (1974), Biochem. Biophys. Res. Commun. 58, 126.

Ford, L. O., Johnson, L. N., Machin, P. A., Phillips, D. C., and Tjian, R. (1974), J. Mol. Biol. 88, 349.

Freer, S. T., Kraut, J., Robertus, J. D., Wright, H. T., and Xuong, Ng. H. (1970), Biochemistry 9, 1997.

Garen, A. and Levinthal, C. (1960), Biochim. Biophys. Acta 38, 470.

Geschwind, S. (1972), in Electron Paramagnetic Resonance, edit. by S. Geschwind (Plenum Press, New York), Chap. 5, p. 353.

Gougoutas, J. Z. (1971), Pure Appl. Chem. 27, 305.

Griffith, J. S. (1956), Proc. Roy. Soc. A235, 23.

Griffith, O. H., Cornell, D. W., and McConnell, H. M. (1965), J. Chem. Phys. 43, 2902.

Griffith, O. H. and Waggoner, A. S. (1969), Accts. Chem. Res. 2, 17.

Gutfreund, H. and Sturtevant, J. M. (1956), Proc. Natl. Acad. Sci. (U.S.) 42, 719.

Haas, D. J. (1968), Acta Cryst. B24, 604.

Haas, D. J. and Rossmann, M. G. (1970), Acta Cryst. B26, 998.

Ham, J. T. and Williams, D. G. (1970), Acta Cryst. B26, 1373.

Hamilton, C. L. and McConnell, H. M. (1968), in Structural Chemistry and Molecular Biology, edit. by A. Rich and N. Davidson (W. H. Freeman, San Francisco, California), p. 115.

Hamilton, W. C. (1965), Acta Cryst. 18, 502.

Hamilton, W. C., Rollett, J. S., and Sparks, R. A. (1965), Acta Cryst. 18, 129.

Harrison, G. R. (1939), Massachusetts Institute of Technology Wavelength Tables (John Wiley & Sons, New York).

Hauptman, H. and Karle, J. (1965), Acta Cryst. 9, 45.

Hayaishi, O. (1963), in The Enzymes, edit. by P. D. Boyer, H. Lardy, and K. Myrbäck (Academic Press, New York), Vol. VIII, Second Edition, p. 366.

Hayaishi, O., Rothberg, S., Mehler, A. H., and Saito, Y. (1957), J. Biol. Chem. 229, 889.

Helbert, J., Kevan, L., and Bales, B. L. (1972), J. Chem. Phys. 57, 723.

Henderson, R. and Moffat, J. K. (1971), Acta Cryst. B27, 1414.

Hill, R. and Holden, H. F. (1927), Biochem. J. 21, 625.

Holler, E., Rupley, J. A., and Hess, G. P. (1975), Biochemistry 14, 1088.

Hoogenstraaten, W. and Sleuyterman, L. A. (1969), Biochim. Biophys. Acta 171, 284.

Howell, L. G. and Massey, V. (1971), in Flavins and Flavoproteins, edit. by H. Kamin (University Park Press, Baltimore, Maryland), p. 499.

Hutchison Jr., C. A. (1967), in The Triplet State, edit. by A. Zahlan (Cambridge University Press, Cambridge), p. 63.

Hutchison Jr., C. A. (1971), Pure Appl. Chem. 27, 327.

Hutchison Jr., C. A. and Mangum, B. W. (1961), J. Chem. Phys. 34, 908.

Hui Bon Hoa, G. and Douzou, P. (1973), J. Biol. Chem. 248, 4649.

Hui Bon Hoa, G., Douzou, P., and Petsko, G. A. (1975), J. Mol. Biol. 96, 367.

Hyde, J. S. (1965), J. Chem. Phys. 43, 1806.

Hyde, J. S., Rist, G. H., and Eriksson, L. E. G. (1968), J. Phys. Chem. 72, 4269.

Ikeda, K. and Hamaguchi, K. (1970), J. Biochem. 68, 785.

Ikeda, K. and Hamaguchi, K. (1973), J. Biochem. 73, 307.

Imoto, T., Johnson, L. N., North, A. C. T., Phillips, D. C., and Rupley, J. A. (1972), in The Enzymes, edit. by P. D. Boyer (Academic Press, New York), Vol. VII, Third Edition, p. 665.

International Tables for X-ray Crystallography (1962), edit. by C. H. Macgillavry and G. D. Ruck (The Kynoch Press, Birmingham), Vol. III, pp. 201-227.

Jacobs, J. W., McFarland, J. T., Wainer, I., Jeanmaier, D., Ham, C., Hamm, K., Wuuk, M., and Lam, M. (1974), Biochemistry 13, 60.

James, M. and Hall, D. (1969), Acta Cryst. A25, S196.

Jencks, W. P. (1969), Catalysis in Chemistry and Enzymology (McGraw-Hill, New York).

Johnson, L. N. (1964), Ph.D. Thesis, University of London.

Johnson, L. N. (1966), Acta Cryst. 21, 885.

Johnson, L. N., Phillips, D. C., and Rupley, J. A. (1968), Brookhaven Symp. Biol. 21, 120.

Jollès, P. and Berthou, J. (1972), FEBS Letters 23, 21.

Kallos, J. (1964), Biochim. Biophys. Acta 89, 364.

Karle, I. L., Dragonette, K. S., and Brenner, S. A. (1965), Acta Cryst. 19, 713.

Karle, I. L. and Karle, J. (1964), Acta Cryst. 17, 835.

Karle, J. and Karle, I. L. (1966), Acta Cryst. 21, 849.

Karle, I. L. and Karle, J. (1970), Acta Cryst. B26, 1276.

Kasha, M. (1948), J. Opt. Soc. Am. 38, 929.

Kaufman, S. (1963), in The Enzymes, edit. by P. D. Boyer, H. Lardy, and K. Myrbäck (Academic Press, New York), Vol. VIII, Second Edition, p. 373.

Keilin, D. (1966), The History of Cytochromes and Respiratory Pigments (Cambridge University Press, Cambridge), p. 99.

Kempster, C. J. E. and Lipson, H. (1972), Acta Cryst. B28, 3674.

Kendrew, J. C. (1963), Science 139, 1259.

Kendrew, J. C. and Parrish, R. G. (1956), Proc. Roy. Soc. A238, 305.

Kennard, O., Isaacs, N. W., Motherwell, W. D. S., Coppola, J. C., Wampler, D. L., Larson, A. C., and Watson, D. G. (1971), Proc. Roy. Soc. A325, 401.

Kevan, L. (1965), J. Am. Chem. Soc. 87, 1481.

Kĕzdy, F. and Kaiser, E. T. (1970), Methods in Enzymology 19, 3.

Klyne, W. and Prelog, V. (1960), Experientia 16, 521.

Kottis, P. and Lefebvre, R. (1963), J. Chem. Phys. 39, 393.

Kraicsovits, F. and Douzou, P. (1973), Biochimie 55, 1007.

Krimm, S., Kuriowa, K., and Relune, T. (1967), in Conformation of Biopolymers, edit. by G. N. Ramachandran (Academic Press, New York), Vol. II, p. 439.

Kuramitsu, S., Ikeda, K., and Hamaguchi, K. (1973), J. Biochem. (Tokyo) 74, 143.

Kwiram, A. L. (1971), Adv. Phys. Chem. 22, 133.

Kwiram, A. L. (1972), M.T.P. Intern. Rev. Science, Magnetic Resonance, edit. by C. A. McDowell (Butterworths, London), Vol. IV, Chap. 8, p. 221.

Laidler, K. J. (1972), J. Chem. Educ. 49, 343.

Laidler, K. J. and Bunting, P. S. (1973), The Chemical Kinetics of Enzyme Action (Clarendon Press, Oxford), Second Edition.

Lalitha, S. and Haug, A. (1972), Biochemistry 11, 1590.

Larsson, L. O., Hagman, L. O., Kierkegaard, P., and Yonetani, T. (1970), J. Biol. Chem. 245, 902.

Laval, F. and Michelson, A. M. (1970), Compte Rendus Acad. Sci. (Paris) 270, 2126.

Leiserowitz, L. and Schmidt, G. M. J. (1965), Acta Cryst. 18. 1058.

Lemberg, R. and Legge, J. W. (1949), Hematin Compounds and Bile Pigments (Interscience, New York), p. 228.

Lemieux, R. U. and Huber, G. (1956), J. Am. Chem. Soc. 78, 4117.

Levine, D., Reid, J. W., and Wilson, I. B. (1969), Biochemistry 8, 2375.

Lewis, G. N. and Kasha, M. (1944), J. Am. Chem. Soc. 66, 2100.

Lewis, G. N. and Kasha, M. (1945), J. Am. Chem. Soc. 67, 994.

Lhoste, J. M., Haug, A., and Hemmerich, P. (1966), Biochemistry 5, 3290.

Libertini, L. J. and Griffith, O. H. (1970), J. Chem. Phys. 53, 1359.

Lienhard, G. E., Secemski, I. I., Koehler, K. A., and Lindquist, R. N. (1971), Cold Spring Harbor Symp. Quant. Biol. 36, 45.

Lipscomb, W. N. (1973), Proc. Natl. Acad. Sci. (U.S.) 70, 3797.

Loew, G. H. and Thomas, D. D. (1972), J. Theor. Biol. 36, 89.

Lonsdale, K. (1969), in Physics of the Solid State, edit. by S. Balakrishna, M. Krishnamurthi, and B. Ramachandran RAO (Academic Press, New York) p. 43.

Lovrien, R. (1969), J. Theor. Biol. 24, 247.

Luzzati, V. (1953), Acta Cryst. 6, 142.

Maatman, R. W. (1970), J. Catalysis 19, 64.

Maatman, R. W. (1973), Catalysis Rev. 8, 6.

Makinen, M. W. and Eaton, W. A. (1973), Ann. N. Y. Acad. Sci. 206, 210.

Makinen, M. W. and Eaton, W. A. (1976), in The Porphyrins, edit. by D. Dolphin (Academic Press, New York), Vol. I, in preparation.

Malhotra, O. P. and Bernhard, S. A. (1968), J. Biol. Chem. 243, 1243.

Marsh, D. J. and Petsko, G. A. (1973), J. Appl. Cryst. 6, 76.

Mathieson, A. McL. and Welsh, H. K. (1965), Acta Cryst. 18, 953.

Mavridis, A., Tulinsky, A., and Liebman, M. N. (1974), Biochemistry 13, 3661.

McGlynn, S. P., Azumi, T., and Kinoshita, M. (1969), Molecular Spectroscopy of the Triplet State (Prentice Hall, Inc., Englewood Cliffs, New Jersey).

Moffat, J. K. (1971), J. Mol. Biol. 55, 135.

Morrison, A. and Davies, A. P. (1970), Org. Mass. Spectrom. 3, 353.

Moult, J. (1970), D. Phil. Thesis, Oxford University.

Murdock, A. L. (1967), Fed. Proc. Am. Soc. Exptl. Biol. 26, 385.

Naqvi, K. R., Behr, J. P., and Chapman, D. (1974), Chem. Phys. Letters 26, 440.

Nebert, D. W. and Kon, H. (1973), J. Biol. Chem. 248, 169.

Nobbs, C. L., Watson, H. C., and Kendrew, J. C. (1966), Nature 209, 339.

North, A. C. T. (1965), Acta Cryst. 18, 212.

North, A. C. T., Phillips, D. C., and Mathews, F. S. (1968), Acta Cryst. A24, 351.

O'Sullivan, D. G. (1955), Bull. Math. Biophys. 17, 243.

Parkhurst, L. J. and Gibson, Q. H. (1967), J. Biol. Chem. 242, 5762.

Pauling, L. (1946), Chem. Eng. News 24, 1375.

Pauling, L. (1949), in Haemoglobin, edit. by F. J. W. Roughton and J. C. Kendrew (Butterworths, London), p. 57.

Perutz, M. F. (1970), Nature 228, 726.

Petsko, G. A. (1975), J. Mol. Biol. 96, 381.

Phillips, D. C. (1967), Proc. Natl. Acad. Sci. (U.S.) 57, 484.

Pinnock, P. R., Taylor, C. A., and Lipson, H. (1956), Acta Cryst. 9, 173.

Pocker, Y. and Storm, D. R. (1968), Biochemistry 7, 1202.

Poland, D. and Scheraga, H. A. (1967), Biochemistry 6, 3791.

Quiocho, F. A., McMurray, C. H., and Lipscomb, W. N. (1972), Proc. Natl. Acad. Sci. (U.S.) 69, 2850.

Quiocho, F. A. and Richards, F. M. (1966), Biochemistry 5, 4062.

Raftery, M. A. and Rand-Meir, T. (1968), Biochemistry 7, 3281.

Raftery, M. A., Rand-Meir, T., Dahlquist, F. W., Parsons, S. M., Borders, Jr., C. L., Wolcott, R. G., Beranek, Jr., W., and Jao, L. (1969), Anal. Biochem. 30, 427.

Ramachandran, G. N., Ramakrishnan, G., and Venkatachalam, C. M. (1967), in Conformation of Biopolymers, edit. by G. N. Ramachandran (Academic Press, New York), Vol. II, p. 429.

Rand-Meir, T., Dahlquist, F. W., and Raftery, M. A. (1969), Biochemistry 8, 4206.

Reeves, R. E. (1950), J. Am. Chem. Soc. 72, 1499.

Richardson, D. C., Bier, C. J., and Richardson, J. S. (1972), J. Biol. Chem. 247, 6368.

Robbins, P. W. (1963), in The Enzymes, edit. by P. Boyer, H. Lardy, and K. Myrbäck (Academic Press, New York), Vol. VI, Second Edition, p. 363.

Rollett, J. S. (1965), in Computing Methods in Crystallography, edit. by J. S. Rollett (Pergamon Press, Oxford), p. 175.

Rossi, G. L. and Bernhard, S. A. (1971), J. Mol. Biol. 55, 215.

Roughton, F. J. W. (1952), Proc. Roy. Soc. B110, 203.

Rupley, J. A. (1964), Biochem. Biophys. Acta 83, 245.

Rupley, J. A. (1969), in Structure and Stability of Biological Macromolecules, edit. by S. N. Timasheff and G. D. Fasman (Marcel Dekker, Inc., New York), p. 291.

Rupley, J. A., Gates, V., and Bilbrey, R. (1968), J. Am. Chem. Soc. 90, 5633.

Schmidt, J. (1971), Ph.D. Thesis, University of Leiden.

Schmidt, J., Antheunis, D. A., and van der Waals, J. H. (1971), Mol. Phys. 22, 1.

Schmidt, J. Hesselman, A. M., de Groot, M. S., and van der Waals, J. H. (1967), Chem. Phys. Letters 1, 434.

Schmidt, J. and van der Waals, J. H. (1968), Chem. Phys. Letters 2, 640.

Seelig, J. (1970), J. Am. Chem. Soc. 92, 3881.

Seligman, A. M., Nachlas, M. M., Manheimer, L. H., Friedman, O. M., and Wolf, G. (1949), Ann. Surg. 130, 333.

Sharnoff, M. (1967), J. Chem. Phys. 46, 3263.

Sharon, N. and Seifter, S. (1964), J. Biol. Chem. 239, PC2398.

Shiga, T., Layani, M., and Douzou, P. (1968), in Flavins and Flavoproteins, edit. by K. Yagi (University Park Press, Baltimore, Maryland), p. 140.

Shotton, D. M., White, N. J., and Watson, H. C. (1971), Cold Spring Harbor Symp. Quant. Biol. 36, 91.

Shugar, D. (1952), Biochim. Biophys. Acta 8, 302.

Siegel, S. and Goldstein, L. (1966), J. Chem. Phys. 44, 2780.

Sigler, P. B., Jeffrey, B. A., Matthews, B. W., and Blow, D. M. (1966), J. Mol. Biol. 15, 175.

Sireix, R., Canva, J., and Douzou, P. (1970), Compte Rendus Acad. Sci. (Paris) 270, 577.

Sleuyterman, L. A. E., and de Graaf, M. J. M. (1969), Biochim. Biophys. Acta 171, 277.

Smith, I. C. P. (1972), in Biological Applications of Electron Spin Resonance, edit. by H. M. Schwartz, J. R. Bolton, and D. C. Borg (Wiley-Interscience, New York), p. 483.

Smith, D. W. and Williams, R. J. W. (1970), Structure and Bonding 7, 1.

Snape, K. W. (1974), D. Phil. Thesis, Oxford University.

Stauffer, C. E. and Zeffren, E. (1970), J. Biol. Chem. 245, 3282.

Stewart, R. F., Davidson, E. R., and Simpson, W. T. (1965), J. Chem. Phys. 42, 3175.

Stout, G. H. and Jensen, L. H. (1968), X-ray Structure Determination (The Macmillan Company, Ltd., London).

Strahs, G. (1970), Adv. Carbohydrate Res. 25, 53.

Stryer, L., Kendrew, J. C., and Watson, H. C. (1964), J. Mol. Biol. 8, 96.

Theorell, H., Chance, B., and Yonetani, T. (1966), J. Mol. Biol. 17, 513.

Thiele, E. W. (1939), Ind. Eng. Chem. 31, 916.

Travers, P. and Douzou, P. (1970), J. Phys. Chem. 74, 2243.

Travers, P. and Douzou, P. (1974), Biochimie 56, 509.

van der Waals, J. H. and de Groot, M. S. (1959), Mol. Phys. 2, 333.

van Egmond, J. (1973), Ph.D. Thesis, University of Leiden.

Wampler, J. E. and Churchich, J. E. (1969), J. Biol. Chem. 244, 1477.

Wasserman, E., Snyder, L. C., and Yager, W. A. (1964), J. Chem. Phys. 41, 1763.

Watson, H. C. (1968), Prog. Stereochem. 4, 299.

Watson, H. C. and Chance, B., in Hemes and Hemoproteins, edit. by B. Chance, R. W. Estabrook, and T. Yonetani (Academic Press, New York), p. 149.

Watson, H. C. and Nobbs, C. L. (1968), in Biochemie des Sauerstoffs, edit. by B. Hess and H. Staudinger (Springer Verlag, Berlin), p. 57.

Watson, H. C., Shotton, D. M., Cox, J. M., and Muirhead, H. (1970), Nature 225, 506.

Weisz, P. B. (1973), Science 179, 433.

Wertz, J. E. and Bolton, J. R. (1972), Electron Spin Resonance (McGraw-Hill, New York).

Wheatley, P. J. (1964), J. Chem. Soc. 1964, 6036.

Wien, R. W., Morrisett, J. D., and McConnell, H. M. (1972), Biochemistry 11, 3707.

Wilson, A. J. C. (1942), Nature 150, 152.

Wolfenden, R. (1969), Nature 223, 704.

Wolfenden, R. (1972), Accts. Chem. Res. 5, 10.

Wyckoff, H. W., Doscher, M., Tsernoglou, D., Inagami, T., Johnson, L. N., Hardman, K. D., Allewell, N. M., Kelly, D. M., and Richards, F. M. (1967), J. Mol. Biol. 27, 563.

Wynne-Jones, W. F. K. and Eyring, H. (1935), J. Chem. Phys. 3, 492.

Yagi, K. (1965), Adv. Enzymol. 27, 1.

Yamazaki, I., Yokota, K. and Shikama, K. (1964), J. Biol. Chem. 239, 4151.

Yasuoka, N., Ando, T., and Kurijabashi, S. (1967), Bull. Chem. Soc. (Japan) 40, 270.

Yonetani, T., Chance, B., and Kajiwara, S. (1966), J. Biol. Chem. 241, 2981.

Zeppezauer, E., Söderberg, B. O., Brändén, C. I., Åkesson, Å., and Theorell, H. (1967), Acta Chem. Scand. 21, 1099.